

## INFORMATION TO USERS

This manuscript has been reproduced from the microfilm master. UMI films the text directly from the original or copy submitted. Thus, some thesis and dissertation copies are in typewriter face, while others may be from any type of computer printer.

**The quality of this reproduction is dependent upon the quality of the copy submitted.** Broken or indistinct print, colored or poor quality illustrations and photographs, print bleedthrough, substandard margins, and improper alignment can adversely affect reproduction.

In the unlikely event that the author did not send UMI a complete manuscript and there are missing pages, these will be noted. Also, if unauthorized copyright material had to be removed, a note will indicate the deletion.

Oversize materials (e.g., maps, drawings, charts) are reproduced by sectioning the original, beginning at the upper left-hand corner and continuing from left to right in equal sections with small overlaps. Each original is also photographed in one exposure and is included in reduced form at the back of the book.

Photographs included in the original manuscript have been reproduced xerographically in this copy. Higher quality 6" x 9" black and white photographic prints are available for any photographs or illustrations appearing in this copy for an additional charge. Contact UMI directly to order.

# UMI

A Bell & Howell Information Company  
300 North Zeeb Road, Ann Arbor MI 48106-1346 USA  
313/761-4700 800/521-0600



**THERMALLY ENHANCED BIOVENTING OF  
PETROLEUM HYDROCARBONS IN COLD REGIONS**

**A  
THESIS**

**Presented to the Faculty  
of the University of Alaska Fairbanks  
in Partial Fulfillment of the Requirements  
for the Degree of**

**DOCTOR OF PHILOSOPHY**

**By**

**Dennis M. Filler, B.S., M.S.E.**

**Fairbanks, Alaska**

**August 1997**

**UMI Number: 9804922**

---

**UMI Microform 9804922**  
**Copyright 1997, by UMI Company. All rights reserved.**  
**This microform edition is protected against unauthorized**  
**copying under Title 17, United States Code.**

---

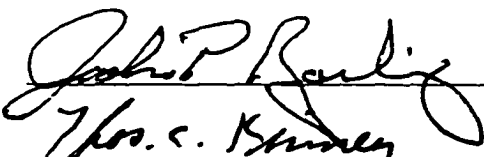
**UMI**  
**300 North Zeeb Road**  
**Ann Arbor, MI 48103**

THERMALLY ENHANCED BIOVENTING OF  
PETROLEUM HYDROCARBONS IN COLD REGIONS

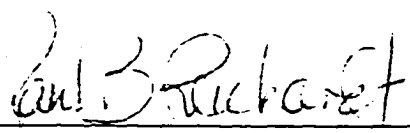
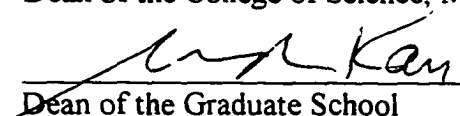
By

Dennis M. Filler

RECOMMENDED:

  
\_\_\_\_\_  
Thos. C. Bunday  
\_\_\_\_\_  
Steph. D. J. [unclear]  
\_\_\_\_\_  
[unclear]  
\_\_\_\_\_  
Robert H. Gauer  
Advisory Committee Chair  
\_\_\_\_\_  
[unclear]  
Department Head

APPROVED:

  
\_\_\_\_\_  
Dean of the College of Science, Mathematics and Engineering  
  
\_\_\_\_\_  
Dean of the Graduate School  
7-30-47  
\_\_\_\_\_  
Date

## ABSTRACT

Petroleum-based contamination of the environment has and will likely continue to be a problem as long as oil and natural gas supply much of the world energy demands. In cold regions, where vast quantities of these fuels are extracted and used, climate and frozen soils limit remedial efforts to a few technologies. Bioventing has shown promise as a viable method for the remediation of spilled petroleum-based fuels in cold regions.

An *in situ* study of bioventing with soil warming was conducted at a Fairbanks, Alaska site. The main purpose of this research effort was to compare the effectiveness of thermal enhancement techniques applied to bioventing. Objectives included (1) developing a suitable thermal insulation system(s) that would provide year-round bioventing of petroleum contaminated soils, (2) modeling of the thermal regime below three treatment areas, (3) relating monitoring and testing data to thermally enhanced biodegradation, and (4) presenting the information in a way that is useful to engineers, biologists and environmental scientists.

Active soil warming with electrical heat tape beneath polystyrene insulation and sand and gravel overburden raised subsurface soil temperatures from the ground surface to the water table by as much as 15°F. The actively warmed test plot was successfully heated year-round, preventing soil freezing and enhancing microbial activity. Soil gas, microbiological, and geochemical sampling data evidenced correlation between increased bioactivity and soil warming. Passively treated soils evidenced some winter increase in temperatures, although some periodic soil freezing did occur. Overall, biodegradation within both passively treated and untreated contaminated test plots was noticeably slower than within the actively warmed plot.

Thermally enhanced bioventing successfully remediated hydrocarbon contamination in vadose zone soils at a subarctic site within two years. After oxygen, temperature appears to be the most important factor affecting microbial activity and biodegradation. Variable and low moisture contents did not seem detrimental to bioactivity.

## Table of Contents

1.0 Introduction .....	1
2.0 Background .....	5
2.1 Bioventing .....	5
2.1.1 Bioventing Applicability .....	7
2.1.2 Microbiology, Geochemistry and Environmental Considerations .....	9
2.1.3 Geotechnical Considerations .....	12
2.2 Enhanced Bioventing .....	13
3.0 Bioventing System and Thermal Insulation System (TIS) Designs .....	14
3.1 Site Description .....	14
3.1.1 Climate .....	15
3.1.2 History .....	15
3.1.3 Contamination Assessment .....	16
3.2 Summary of Bioventing System Design .....	17
3.2.1 Soil Stratigraphy .....	20
3.2.1a Darcy Flow Theory and Site Specific Permeability .....	20
3.2.1b Variable Permeability and Velocity Profiling .....	26
3.2.2 Thermal Insulation System Design .....	28
3.2.2a ELSYM-5 Stress-Strain Analysis on TISs .....	28
3.2.2b BERG-2 Freeze-Thaw Analysis .....	35
3.2.2c Thermocouple Installations .....	40

4.0 Heat Transfer Theory and Biovented Soils . . . . .	42
4.1 General Equations of Transfer . . . . .	42
4.2 The Heat Transfer Problem . . . . .	43
4.3 Convection and Soil Venting . . . . .	43
4.4 Heat Diffusion Analysis . . . . .	47
4.5 About TDHC . . . . .	50
4.6 The Zone II Heat Conduction Problem Defined . . . . .	52
4.6.1 Site Specific Geotechnical Parameters . . . . .	53
4.6.2 Heat Tape Energy Contribution . . . . .	54
4.6.3 Polystyrene Insulation Thermal Conductivity . . . . .	58
4.6.4 Boundary Conditions . . . . .	60
4.6.4a Surface Boundary Condition . . . . .	63
4.6.4b Other Boundary Conditions . . . . .	65
4.6.4c Initial Temperature Conditions . . . . .	66
4.6.5 The Zone II Heat Conduction Problem Summarized . . . . .	66
4.7 The Zone I and Zone III Heat Transfer Problems . . . . .	67
4.7.1 Boundary Conditions . . . . .	69
4.7.2 The Zone I Heat Conduction Problem Summarized . . . . .	70
4.7.3 The Zone III Heat Conduction Problem Summarized . . . . .	71
4.8 Zone II Boundary Analysis . . . . .	72
5.0 Monitoring and Testing Methods . . . . .	74
5.1 Thermal Monitoring . . . . .	74
5.2 Soil Gas Monitoring . . . . .	75
5.2.1 Background Levels and Operating Injection Flow Rate . . . . .	75
5.3 Biodegradation Rates . . . . .	77
5.4 Microbiology and Geochemistry . . . . .	77
5.4.1 Enumeration Assays . . . . .	80
5.4.2 Activity Measurements . . . . .	81



5.4.3	Groundwater Sampling	82
5.4.4	Statistics	82
5.5	Bioventing Optimization Test	83
5.6	TDHC Heat Transfer Modeling	84
6.0	Analyses and Results	87
6.1	Thermal Comparisons	87
6.1.1	Whiplash Curves	87
6.1.2	Time Variance Temperature Profiles	91
6.1.3	Model and Field Temperature Comparisons	94
6.1.3a	Zone II	94
6.1.3b	Zone I	98
6.1.3c	Zone III	101
6.2	Soil Gas Comparisons	103
6.3	Biodegradation Rates	108
6.4	Microbiology and Geochemistry Analyses	109
6.4.1	Microbial Populations	110
6.4.2	Temperature, Moisture and Bioactivity	112
6.4.3	July 1995 and 1996 Geochemical Results	119
6.5	Historical Soil Analytical Results	121
7.0	Economic Analyses	122
7.1	Electrical Heat Tape	123
7.2	Insulation	124
7.3	Heat Loss and Power Considerations	128
7.4	Bioventing Treatment Cost Comparisons	129
7.4.1	Present Worth Analysis	131
8.0	Conclusions and Recommendations	135

References .....	140
APPENDIX A: Sample Permeability and Reynolds Number Calculations, D-1 Specifications, and Bioventing Case Studies .....	147
APPENDIX B: Moduli of Elasticity Calculations and Typical Values for Soil Elastic Modulus and Poisson's Ratio .....	155
APPENDIX C: ELSYM-5 Stress-Strain Analysis .....	157
APPENDIX D: BERG-2 Freeze-Thaw Analyses .....	163
APPENDIX E: Mass Transport Equations .....	166
APPENDIX F: Surface Boundary Conditions .....	169
APPENDIX G: TDHC Input File and Additional Thermal Comparison Plots .....	172
APPENDIX H: Summary of Soil Analytical Results and Theoretical Temperature Calculations (Figures 6-1a and b) .....	180
APPENDIX I: A "How To" Guide to Bioventing in Cold Regions .....	184
I.1 Bioventing Organization Chart .....	184
I.2 Soil and Groundwater Sampling .....	188
I.3 Monitoring Points .....	189
I.4 Vent Well Construction .....	190
I.5 Blowers .....	191
I.6 Air Quality Monitoring .....	192
I.7 TIS Materials .....	192
I.8 Maintenance Items .....	193

## List of Figures

Figure 2-1. Physicochemical properties of common hydrocarbon compounds and their bioventing potential . . . . .	9
Figure 3-1. General site location map . . . . .	14
Figure 3-2. UAF Physical Plant bioventing system site plan . . . . .	19
Figure 3-3. Example soil profile and input parameters for ELSYM-5 analysis . . . . .	29
Figure 3-4. Critical load points for ELSYM-5 stress-strain analysis . . . . .	32
Figure 3-5. (a) Cross-sectional view of Zone I and Zone II thermally enhanced bioventing treatment design, and (b) plan view of Zone II electrical heat tape installations . . . . .	34
Figure 3-6. Typical individual layer geotechnical parameters for BERG-2 analysis . . . . .	37
Figure 3-7. BERG-2 freeze-thaw at VW-3 for (a) snow cover and (b) without snow cover surface conditions . . . . .	38
Figure 4-1. (a) Convective heat transfer and (b) conceptual velocity distribution at a vent well . . . . .	44
Figure 4-2. Heat transfer through a volumetric unit of Zone II unsaturated soil . . . . .	49
Figure 4-3. Experimental heat tape output versus operating temperature range . . . . .	57
Figure 4-4. Foamular 400 thermal conductivity rating curve . . . . .	58
Figure 4-5. Soil column for TDHC analysis . . . . .	62
Figure 4-6. Dirac delta function applied to soil latent heat . . . . .	69
Figure 4-7. Freeze-thaw isotherm within a soil finite element . . . . .	69
Figure 4-8. Soil columns for (a) Zone I and (b) Zone III TDHC analyses . . . . .	70
Figure 4-9. Zone II finite element region for TDHC boundary analysis . . . . .	73
Figure 5-1. July 1995 and June 1996 soil sampling locations . . . . .	78

Figure 5-2. Typical TDHC finite element mesh for 1D analysis . . . . .	85
Figure 5-3. Boundary problem finite element mesh . . . . .	85
Figure 6-1. (a) TC-2, (b) TC-4 and (c) MP-10 vadose zone whiplash curves . . . . .	89
Figure 6-2. Comparison of actual and TDHC based subsurface temperatures at TC-2 . . . . .	90
Figure 6-3. Subsurface temperatures at the contamination level versus time at three test plots and background area . . . . .	92
Figure 6-4. Subsurface temperatures at the 10-foot depth versus time at three test plots . . . . .	92
Figure 6-5. Subsurface temperatures versus time near the groundwater table in two test plots and background area . . . . .	93
Figure 6-6. Subsurface temperatures at the contamination level versus time in the area of highest contamination and background area . . . . .	93
Figure 6-7. Comparison of TDHC model output and measured Zone II temperatures at (a) TC-2 (2.834 ft.), (b) TC-2 (8.134 ft.), and (c) TC-2 (10.534 ft.) . . . . .	95
Figure 6-8. Comparison of subsurface temperatures across a Zone II perimeter boundary at (a) 6.08 feet, and (b) 8.03 feet in depth . . . . .	97
Figure 6-9. Comparison of TDHC model output and measured Zone I temperatures at (a) MP-14 (2.3 ft.), (b) MP-14 (5.8 ft.) and (c) MP-14 (10.8 ft.) . . . . .	98
Figure 6-10. Comparison of TDHC model output and measured Zone I temperatures at (a) MP-13 (3.8 ft.), (b) MP-13 (9.3 ft.) and (c) MP-13 (11.3 ft.) . . . . .	100
Figure 6-11. Comparison of TDHC model output and measured Zone III temperatures at (a) MP-10 (4.8 ft.), (b) MP-10 (9.0 ft.) and (c) MP-8 (7.0 ft.) . . . . .	102
Figure 6-12. Background soil gas monitoring versus time at MP-9 . . . . .	103
Figure 6-13. Actively warmed Zone II soil gas monitoring versus time at (a) MP-3 and (b) MP-6 . . . . .	104
Figure 6-14. Zone I soil gas monitoring versus time at MP-13 . . . . .	106
Figure 6-15. No action control Zone III soil gas monitoring versus time at (a) MP-7 and (b) MP-10 . . . . .	107

Figure 6-16. (a) Total heterotrophic, (b) gasoline degrader, and (c) diesel fuel degrader populations at five borehole locations . . . . .	110
Figure 6-17. CO <sub>2</sub> production related to temperature and moisture at (a) Joe, (b) Shemp, (c ) Curly, (d) Larry, and (e) Moe sampling locations . . . . .	113
Figure 7-1. Present worth of expenditures versus expected return on property value for three bioventing treatment alternatives . . . . .	134
Figure I-1. The initial subsurface investigation . . . . .	185
Figure I-2. Bioventing system installations . . . . .	186
Figure I-3. Site monitoring and system maintenance . . . . .	186
Figure I-4. 2-inch diameter PVC bioventing well installed . . . . .	190

## List of Tables

Table 3-1. Summary of UAF Physical Plant LUST site contamination . . . . .	17
Table 3-2. Critical stress and displacement results from the ELSYM-5 analysis . . . . .	33
Table 3-3. Thermocouple installations at the UAF bioventing site . . . . .	41
Table 4-1. Approximate heat flux at a vent well versus heat tape output . . . . .	46
Table 4-2. Péclet Numbers and vent well convection influence . . . . .	47
Table 4-3. TDHC layer input data . . . . .	53
Table 4-4. Heat tape output and temperature data for the constant temperature environment experiment . . . . .	57
Table 4-5. Foamular 400 thermal conductivity data . . . . .	58
Table 4-6. Summary of thermal data for determination of insulation average thermal conductivity . . . . .	59
Table 4-7. Zone II surface boundary conditions . . . . .	64
Table 5-1. Functional soil gas monitoring points at the UAF bioventing site . . . . .	76
Table 5-2. July 1995 and June 1996 microbiological and geochemical sampling protocol . . . . .	80
Table 5-3. Bioventing system optimization test . . . . .	83
Table 6-1. Microbiological summary relating vadose zone conditions to treatment type . . . . .	109
Table 6-2. Summary of microbiological characterizations at the UAF Physical Plant LUST site . . . . .	117
Table 6-3. Groundwater geochemistry data for the UAF Physical Plant LUST site . . . . .	120
Table 7-1. Capital investment cost of a common heat tape . . . . .	123
Table 7-2. Capital investment cost of insulation . . . . .	125

Table 7-3. Capital investment costs of comparable thermal insulation systems . . . . .	126
Table 7-4. Estimated present day costs for three bioventing treatments . . . . .	130
Table A-1. D-1 sand-gravel specifications . . . . .	150
Table A-2. Summary of arctic and subarctic bioventing and soil warming case studies . . . . .	151
Table B-1. Typical value ranges for static stress-strain (elastic) modulus and Poisson's ration for selected soils . . . . .	156
Table H-1. Summary of soil analytical results . . . . .	180
Table I-1. Common soil and groundwater analytical testing methods for organics . . . . .	189
Table I-2. Bioventing TIS design configurations for active warming . . . . .	193

## Nomenclature

### *Acronyms & Abbreviations:*

ADEC	=	<b>Alaska Department of Environmental Conservation</b>
ADOT	=	<b>Alaska Department of Transportation</b>
AFB	=	<b>Air Force Base</b>
AFCESA	=	<b>U.S. Air Force Civil Engineering Support Agency</b>
AFI	=	<b>air freezing index</b>
AST	=	<b>above-ground storage tank</b>
ATI	=	<b>air thawing index</b>
BTEX	=	<b>benzene, toluene, ethylbenzene and xylene</b>
CPM	=	<b>counts per minute</b>
CRREL	=	<b>Cold Regions Research and Engineering Laboratory</b>
DNAPL	=	<b>dense non-aqueous phase liquid</b>
DPM	=	<b>decays per minute</b>
DRO	=	<b>diesel range organics</b>
EPA	=	<b>Environmental Protection Agency</b>
GRO	=	<b>gasoline range organics</b>
GWR	=	<b>gross weight rating</b>
LUST	=	<b>leaking underground storage tank</b>
MP	=	<b>monitoring point</b>
MPN	=	<b>most probable number</b>
NTL	=	<b>Northern Testing Laboratory</b>
ID	=	<b>one-dimensional</b>
PAH	=	<b>polycyclic aromatic hydrocarbons</b>
PCB	=	<b>polychlorinated biphenyl</b>
ppm	=	<b>parts per million</b>
ppb	=	<b>parts per billion</b>
POL	=	<b>petroleum, oil and lubricant</b>
PVC	=	<b>polyvinyl chloride</b>
cfm	=	<b>cubic feet per minute</b>
SFI	=	<b>surface freezing index</b>
STI	=	<b>surface thawing index</b>
SVE	=	<b>soil vapor extraction</b>
TC	=	<b>thermocouple</b>
TERC	=	<b>Total Environmental Restoration Contract</b>
TIS	=	<b>thermal insulation system</b>



TPH	=	total petroleum hydrocarbons
TRPH	=	total recoverable petroleum hydrocarbons
2D	=	two-dimensional
UAF-AFES	=	University of Alaska Fairbanks Agricultural Forestry Experiment Station
UAF-IAB	=	University of Alaska Fairbanks Institute of Arctic Biology
USCS	=	Unified Soil Classification System
USGS	=	United States Geological Survey
USGS-WRD	=	United States Geological Survey Water Resource Division
UST	=	underground storage tank
VW	=	vent well
WHC	=	water holding capacity

*Variables:*

$A$	=	[Vapor path] cross-sectional area
$A_o$	=	Amplitude of annual temperature variation
$A_{os}$	=	Soil surface temperature variation
$C$	=	Solute concentration or Volumetric specific heat
$C_m$	=	Solute molar concentration
$C_v, C_f$	=	Thawed, frozen volumetric specific heat
$d_{10}$	=	Effective grain size
$D$	=	Coefficient of diffusivity or hydrodynamic dispersion coefficient; domain
$D_d$	=	Diffusivity proportionality constant
$D_v$	=	Dispersive proportionality constant
$e$	=	Soil void ratio
$\dot{e}$	=	Vapor-filled portion of soil void ratio
$E_r$	=	Free energy (enthalpy)
$E_s$	=	Modulus of Elasticity
$F$	=	forcing function
$g$	=	Gravitational acceleration
$G$	=	Geothermal gradient
$G_s$	=	Specific gravity
$H$	=	Total pressure head; vent well screened interval length
$H$	=	Stratum thickness
$i$	=	time step
$I$	=	Hydraulic gradient; electrical current
$J_c$	=	Convective flux
$J_d$	=	Diffusive flux
$J_i$	=	Fluid flux in the $i$ direction
$J_s$	=	Total solute flux
$J_v$	=	Dispersive flux
$k$	=	Intrinsic or absolute permeability
$K$	=	Hydraulic conductivity
$K$	=	Thermal conductivity

$K_t, K_f$	= Thawed, frozen thermal conductivity
$L$	= Latent heat
$LHC$	= Latent heat contribution
$L_n$	= Latent heat for thaw front layer $n$
$m$	= Mass; vent well screened interval length
$n$	= Soil porosity
$n_t, n_f$	= Thawed, frozen Lunardini n-factors
$N$	= Blow count
$N_R$	= Reynolds number
$P$	= Power; vapor pressure; capillary pressure
$P_a$	= Ambient air water vapor pressure
$P_{atm}$	= Atmospheric pressure
$P_t$	= Gauge pressure at time $t_i$
$P_s$	= Saturated soil water vapor pressure
$P_w$	= Vent well gauge pressure
$P_{wabs}$	= Absolute vent well pressure
$P_\omega$	= Soil water vapor pressure (at moisture content $\omega$ )
$q$	= Darcy flux
$q_{(r-c)}$	= Radiative and convective heat flux
$Q$	= [Air-injection] flow rate
$Q_e$	= Evaporative heat contribution
$Q_{HT}$	= Heat tape energy contribution
$Q_L$	= Latent heat contribution
$r$	= Radial distance to vent well
$R$	= Universal gas constant; electrical resistance; radius of influence (vent well)
$R_n$	= Thermal resistance of layer $n$
$R_w$	= Vent well radius
$S$	= Degree of saturation
$Ste$	= Stefan Number
$t, t_i$	= Time
$t_1, t_2$	= Thaw season beginning and ending days
$T$	= approximate temperature solution
$T$	= Temperature
$T_f$	= Freezing temperature
$T_m$	= Mean annual air temperature
$T_{ms}$	= Mean annual soil surface temperature
$T_n$	= thaw front temperature for layer $n$
$T_s$	= Soil surface temperature
$u$	= Poisson's ratio
$U$	= Strain energy
$v$	= Darcy velocity
$v_{avg}$	= Average pore velocity
$V$	= Volume

$V$	= Voltage
$V_w$	= Volume of soil moisture (ice + liquid water)
$W$	= Work; Galerkin weighting function
$W$	= Watts
$x, y, z$	= Cartesian coordinates
$X_f$	= Depth of thaw
$Z$	= Gravitational potential
$z$	= Elevational difference
$\alpha$	= Thermal diffusivity
$\alpha_t, \alpha_f$	= Thawed, frozen thermal diffusivity
$\Delta$	= Change in quantity of associated variable
$\gamma$	= Soil or fluid unit weight
$\gamma_d$	= Soil dry unit weight
$\mu$	= Fluid dynamic viscosity
$\mu_a$	= Air dynamic viscosity
$\nu$	= Fluid kinematic viscosity
$\phi_s$	= Soil temperature phase lag
$\rho$	= Soil, fluid, or vapor density
$\theta$	= Volumetric soil moisture content
$\omega$	= Soil moisture content
$\phi$	= Total soil water potential
$\psi$	= Capillary potential; differential operator
$\epsilon$	= Strain
$\epsilon$	= error associated with approximate solution
$\delta$	= Dirac Delta function
$\lambda$	= Lambda coefficient
$\nabla$	= Gradient operator

*Trademark<sup>(TM)</sup> or Brand Name Equipment:*

Tedlar <sup>(TM)</sup>	= patented, inert, polymeric gas sampling bag, with thumb screw locks
Geoprobe <sup>(TM)</sup>	= patented, multi-functional, mobile drilling rig
GasTechtor <sup>(TM)</sup>	= Gastech, Inc. model 3252OX, potable O <sub>2</sub> and CO <sub>2</sub> gas analyzer
Trace-Techtor <sup>(TM)</sup>	= Gastech, Inc. hydrocarbon vapor tester
PetMate <sup>(TM)</sup>	= patented, pet porter
Gast	= patented, model R41 10-50 blower or model 4Z024 vacuum pump
Fuji	= patented blower
Wagner	= patented, model 0283016 power stripper
Radio Shack	= Micronta 3001 metal detector

## ACKNOWLEDGMENTS

It is with pleasure that I take this opportunity to thank Dr. Robert Carlson, a mentor, a friend, for his knowledge and guidance throughout this research endeavor. He, along with committee members Dr. Thomas Kinney, Dr. Joan Braddock, Dr. Stephen Sparrow, and Dr. John Zarling provided wisdom and support I needed to attain my Ph.D. Through them, cooperation between the departments of Civil & Environmental and Mechanical Engineering and with the Institute of Arctic Biology was made easy. Dr. Douglas Goering and Dr. Larry Bennett, thank you for your time and helpfulness. Special thanks go to Dr. Brenton Watkins, a true diplomat. My sincere appreciation to you all.

I wish to thank the Alaska Legislature and the Alaska Department of Environmental Conservation (ADEC) for appropriation of funds for this research project. Gratitude is also expressed to Messrs. George Burgess and Rolf Mey, for fund management and professional liaison between the project staff and the ADEC.

Thank you Peter, John, Lorren, Tom and the other troops for your desire to help.

## DEDICATION

To God:

You impart my gifts, bestow wisdom, and open doors.

To Mom & Dad:

Your constant LOVE sets the example.

and defines my humanity.

And to Dr. Jill:

I felt your prayers.

I love you all!

### Introduction

Since the early 1970's, the inception of federal and state regulatory mandates for aboveground and underground storage tanks (USTs) have perpetuated environmental cleanup efforts and the growth of the subsurface bioremediation industry. As of 1985, the Environmental Protection Agency (EPA) estimated as many as 100,000 leaking USTs within the United States (Thomas et al. 1995). These spills, along with other petroleum, oil and lubricant (POL) spills, have given rise to the expansion of remedial technologies.

The variety of successful soil and groundwater remedial technologies that have emerged include 1) *Physical Containment of Contaminants*: site capping, restrictive vertical barriers, surface and gradient controls, excavation and landfilling, excavation and asphalt incorporation, and groundwater pumping and containment techniques; 2) *In Situ Soil Treatments*: soil flushing, soil vapor extraction (SVE), solidification and stabilization, steam stripping, packed-bed bioreactors, bioaugmentation, bioventing, and enhanced bioremediation; 3) *Ex Situ Soil Treatments*: organic solvent extraction, soil washing with surfactants, SVE, slurry bioreactor and biocellular treatments, landfarming, composting and biomounding, solidification and stabilization, high temperature incineration, low temperature thermal stripping, and cold asphalt recycling; 4) *In Situ Groundwater Treatments*: air sparging, packed-bed bioreactors, vertical barrier-membrane processes, and bioaugmentation, and 5) *Ex Situ Groundwater Treatments*: bioslurping, air stripping, steam stripping, carbon adsorption, biological and biophysical treatments, membrane processes, and advanced oxidation treatments. Under unique conditions combinations of these technologies are sometimes used.

*In situ* bioremediation applications have emerged as low cost, nondestructive solutions for the degradation of petroleum contaminants in environmentally sensitive areas where time is not a constraint. Within arctic and subarctic regions extreme cold and frozen ground conditions either confine remedial efforts to the warmer summer season, or restrict their application all together. To date, proven successful bioremediation technologies in cold regions include landfarming, air sparging with SVE, bioventing, composting and enhanced biocellular treatments (Hinchee, 1994; Shannon & Wilson, 1992-95; AGRA Earth & Environmental, 1995). One consultant (Rockwell & Associates) is bioaugmenting with a Russian-engineered bacterium, which when introduced to piled, petroleum-contaminated soils, reportedly has resulted in rapid decline of diesel range organics during a 1996 summer application (Rockwell, 1996).

The occurrence of crude oil, fuel and POL spills, predominately related to the production of oil and natural gas in the U.S. and Canada or associated with military installations, has prompted the emergence of bioremediation efforts in North America. Some examples of spills that have occurred are:

- 1941-1958. Diesel and jet fuel spills at Alaska Aleutian Islands sites such as Eareckson Air Force Station, Adak Naval Air Station, Unalaska Island, Kodiak Island (U.S. Navy-currently U.S. Coast Guard Support Center), and PCB and fuel oil spills on Woody Island (abandoned U.S. Navy-Federal Aviation Authority radar and communication sites) (Janes, 1995).
- 1960s-1980s. Jet fuel spills at Elmendorf Air Force Base, Anchorage, Alaska (Janes, 1995).
- 1975-1976. Several incidents of refined oil spills associated with construction of the Trans-Alaska pipeline (Horowitz & Atlas, 1977).
- August 1976. An estimated 55,000 gallons of leaded MOGAS leaked from a buried pipeline at the Naval Arctic Research Laboratory, Barrow, Alaska (Horowitz & Atlas, 1977).
- July 1977. 80,000 gallons of crude oil spilled on tundra at Trans-Alaska pipeline valve station #7, near Franklin Bluffs, on Alaska's North Slope (Johnson, 1981).

- February 1978. Approximately 500,000 gallons of crude oil were spilled as an act of sabotage, at Steele Creek, near Fairbanks, Alaska (Johnson, 1981).
- 1988-1993. Various Anchorage, Alaska diesel and gasoline storage tank leak sites, including Municipal Light & Power, Garretts Tesoro, Mapco Store #5004, and Anchorage International Airport. Other Alaska sites include Soldotna Texaco, a former gasoline station in Nikiski, and the former diesel tank farm at Chignik (Shannon & Wilson, 1992-1995).
- Pre 1991. Multiple jet and diesel fuel spills at Fort Greeley, Eielson Air Force Base, and Fort Wainwright, in central Alaska (Janes, 1995).
- An unknown quantity of natural gas condensate polluted approximately 65,000 m<sup>2</sup> of developed land and muskeg surrounding a natural gas production plant in northwest Alberta, Canada (Moore et al., 1995).

Across Alaska, engineering firms such as AGRA Earth & Environmental (formerly RZA AGRA), Hart Crowser, and Shannon & Wilson have actively been remediating aboveground storage tanks (AST) and UST contaminated sites since 1987 (ADEC, 1996). As term contractors for the Alaska Department of Environmental Conservation (ADEC) and consultants for municipalities and the private sector, their efforts have primarily focused on the use of air-sparging with SVE and pump-and-treat methods for remediation of petroleum contaminants. One pilot study, using a time-release oxygenic powder to enhance a Fairbanks, Alaska air-sparging/SVE treatment site, is active (Queitzsch, 1996).

During the early 1990s, bioventing (soil venting to enhance bioactivity) appears to have emerged as a front-running bioremedial technology, with the preponderance of cold regions application occurring in Alaska. Table A-1 (Appendix A) presents a comprehensive summary of reported arctic and subarctic bioventing case studies. Some of these studies represent full-scale bioremediation efforts that have resulted in successful biodegradation of petroleum hydrocarbon contaminants in the vadose zone\*.

---

\* The vadose zone, is the area of the ground below the surface and above the water table



Other cold regions bioventing applications have occurred in the northern states of Washington, Montana, Wyoming, Minnesota, North Dakota, Michigan and in upstate New York (Browning & Associates, 1993). Outside the U.S. and Canada, only a few pilot studies or full-scale bioventing applications have been documented: in Antarctica (Kerry, 1993), the Netherlands (Urlings et al., 1990; van Eyk and Vreeken, 1989b) and in New Zealand (Hinchee and Ong, 1992).

A review of the bioventing case studies literature (Appendix A, Table A-2) suggests that temperature, after oxygenation, is the most important factor influencing biodegradation. The main focus of this research effort was to compare thermal enhancement techniques applied to bioventing of petroleum contaminated soils, with hopes of reducing remediation time and establishing guidelines for future use. The scope of this project includes (1) developing a suitable thermal insulation system to afford year-round bioventing, (2) modeling of the thermal regime below the three treatment areas, (3) relating monitored data (thermal, soil gas, microbiology and geochemistry) to thermally enhanced biodegradation, and (4) presenting the information in a way that is useful for future remediation efforts.

The concept of soil warming arctic and subarctic soils was considered in the mid-1960's to early 1980's by researchers experimenting with high-yield crop growth in Alaska. The University of Alaska Fairbanks Agricultural Experiment Station (UAF-AES) used clear polyethylene mulch and row covers to enhance the growing season and produce high-yield everbearing strawberries and sweet corn in Fairbanks and the Matanuska Valley (Dinkel et al., 1980; Dinkel, 1966). The polyethylene covers readily transmitted shortwave solar radiation to the fertilized soils, afforded increased soil temperatures and a longer summer growing season, and acted as moisture vapor collectors (retarding soil heat losses by absorbing longwave energy radiated from the soils).

Alaska researchers, in the 1970's, sought to enhance microbial growth to reestablish areas with damaged tundras (Mitchell, 1996). In 1972 the University of Alaska Fairbanks Agricultural and Forestry Experiment Station (UAF-AFES)-Palmer Research Station used plastic sheeting to cover and warm North Slope tundra plots. The experiment was deemed unsuccessful, as the plots were covered too long, producing moldy soils and vegetative decay.

### **2.1 Bioventing**

To the author's knowledge, the evolution of the term "bioventing" originated circa 1980 from a large-scale model experiment of forced aeration of the unsaturated zone to enhance recovery of spilled gasoline, conducted for the American Petroleum Institute (Texas Research Institute, 1980 and 1984). This experiment and a subsequent soil column study provided the first documented evidence that soil venting could enhance the biodegradation of petroleum contaminated soils (Texas Research Institute, 1980 and 1984). Bioventing

became to mean the process of supplying air or oxygen to the vadose zone, typically through a screened borehole injection technique, in order to enhance aerobic biodegradation of contaminants.

In 1983, the Netherlands company, Delft Geotechnics, under the direction of Jack van Eyk (then with Shell Oil), conducted bioventing field experiments for the remediation of gasoline contaminated soils (Staatsuitgeverij, 1986; van Eyk and Vreeken, 1989a and 1989b).

A 1988 case study in the Pollution Engineering journal, which described pulsed-air soil venting of a gasoline-contaminated excavated soil pile, alluded to the potential of soil warming as a means to enhance biodegradation rates (Conner, 1988). Also in the late 1980s, the Chevron Research Company performed soil venting field studies on gasoline, diesel oil and fuel oil contaminated sites in the United States, under the direction of Ely and Heffner (Leeson et al., 1995). An *in situ* soil venting process, by which hydrocarbons are volatilized and biodegraded, was patented. In their findings, Ely and Heffner suggested that nutrient and moisture enhancement may not be acceptable, because these additions could result in their flushing to the ground water table (Leeson et al., 1995).

In 1988, the U.S. Air Force Civil Engineering Support Agency (AFCEA) began its bioventing research and development program with a bioremediation project at Hill AFB, Utah. Other bioventing studies completed between 1988 and 1991 have documented biodegradation of petroleum hydrocarbons at military installations. Results from Tyndall AFB in Florida, Patuxent River NAS in Maryland, Fulton NAS in Nevada, and Tinker AFB in Oklahoma have been promising (Hinchee et al., 1992). Battelle Memorial Institute, headquartered in Columbus, Ohio, performed much of this research.

Between September and November of 1991, CH2M-Hill consultants performed a cold climate feasibility test on the composting of fuel-contaminated soil at Eielson AFB, near Fairbanks, Alaska (Simpkin et al., 1992). Excavated piles of the contaminated soils were nutrient-enriched and moisture controlled at both indoor and outdoor locations. Test results indicated that substantial heat was microbially generated and retained within the composted piles, even during the colder months of the test. As part of this same study, the impact of temperature on removing diesel, JP-4 jet fuel, and motor gasoline was discussed and modeled

using first order degradation kinetics (Simpkin et al., 1992).

Subsequent bioventing research by Battelle environmental scientists was conducted at Eielson AFB between 1991 and 1995 (Leeson et al., 1995). Review of the literature suggests that this *in situ* field study was the first to document the use of bioventing with soil warming, for the bioremediation of petroleum hydrocarbons. The results of this study were somewhat encouraging, despite active treatment design limitations. Here, groundwater was extracted, heated, and circulated through soaker hoses, housed inside five shallow (2.5 foot embedment depth), 50-foot long sewer pipes. Heat tape lined the inside of each pipe to keep the pipes from freezing. Active soil warming was induced before the conveyed water cooled and was discharged to the water table for recirculation. The perforated pipes were spaced 10 feet apart and the circulating water temperature was not regularly monitored. After two years, researchers attributed elevated biodegradation rates in shallow soils to increased temperatures induced by this active warming technique (Leeson et al. 1995). A comprehensive analysis of the heat and mass transfer aspects of this bioremedial effort was not published.

Currently, Komex International Limited is working with the Canadian oil and natural gas industry to perform bioventing feasibility studies for at least two additional sites in Alberta, Canada (Komex International, 1996). In the U.S., the federally funded Total Environmental Restoration Contract (TERC) was recently awarded to the national firm of Jacobs Engineering. This quarter-billion dollar contract will be used predominately for the bioremediation cleanup of military installations found throughout the country (ADEC, 1996).

### **2.1.1 Bioventing Applicability**

Bioventing is most successful in the remediation of contaminants that are readily biodegradable under aerobic conditions (Norris et al., 1994). To date, monoaromatic petroleum hydrocarbons (benzene, toluene, ethylbenzene, xylene, n-hexane) that result from automotive and jet fuels have been most readily bioremediated. Successful bioventing of polycyclic aromatic hydrocarbons (PAHs) and a mixture of acetone, toluene and naphthalene (Norris et al., 1994) have also been documented. PAHs and other polyaromatic hydrocarbons

are commonly found in heavier petroleum products such as asphalt, coal tars, refined waste sludge, and in chemicals used to treat wood. These compounds have strong soil adsorption properties, are less water-soluble, and consequently degrade much slower than monoaromatic hydrocarbons.

Two forms of bioventing are practiced to remediate hydrocarbon-contaminated soils. Soil vapor extraction draws ambient air through the contaminated vadose zone toward an extraction well. This bioventing configuration requires minimal air pumping and allows for direct monitoring of contaminant biodegradation at the well. The disadvantages of this type of treatment are the production of concentrated off-gas and reduced treatment of the smear zone. The smear zone is the soil region of groundwater fluctuation, in which contamination may be reintroduced into unsaturated soils. With vapor extraction, vapor flow paths (the least path of resistance) lie predominately above "wet" or saturated soils.

Air-injection bioventing relies on screened vent wells to oxygenate hydrocarbon-contaminated soils for successful aerobic biodegradation. Advantages include variable pumping flow rates and regulated volatilization and production of off-gases. This bioventing configuration is the cheapest method (doesn't require extraction wells) for oxygen enhanced biodegradation of hydrocarbons. This method requires that a number of soil gas monitoring points be installed throughout the areal extent of soil contamination, to measure local oxygen and carbon dioxide concentrations, as oxygen levels measured at the injection well are not representative of local conditions. Compared to soil venting by vapor extraction, air-injection bioventing affords increased biodegradation rates and some treatment of the smear zone (air sparging is associated with that portion of the screened interval that extends into the groundwater table).

With any bioventing application, biodegradability as a function of volatility must be considered. If a contaminant cannot be readily volatilized (its vapor pressure is too low), then bioventing may not enhance aerobic biodegradation. Figure 2-1 illustrates the bioventing treatability potential for common hydrocarbon compounds found in gasolines, diesel and jet fuels. In this figure the compound's physicochemical properties of vapor pressure and solubility are related to Henry's Law and to bioventing potential. Obeying Henry's Law,

gases become more soluble at higher pressures. That is, when an increased pressure is applied to the contaminant system, more gas is dissolved. Gasoline, jet and diesel compounds exhibiting vapor pressures between 1 and 0.001 atmospheres are capable of being successfully biovented.

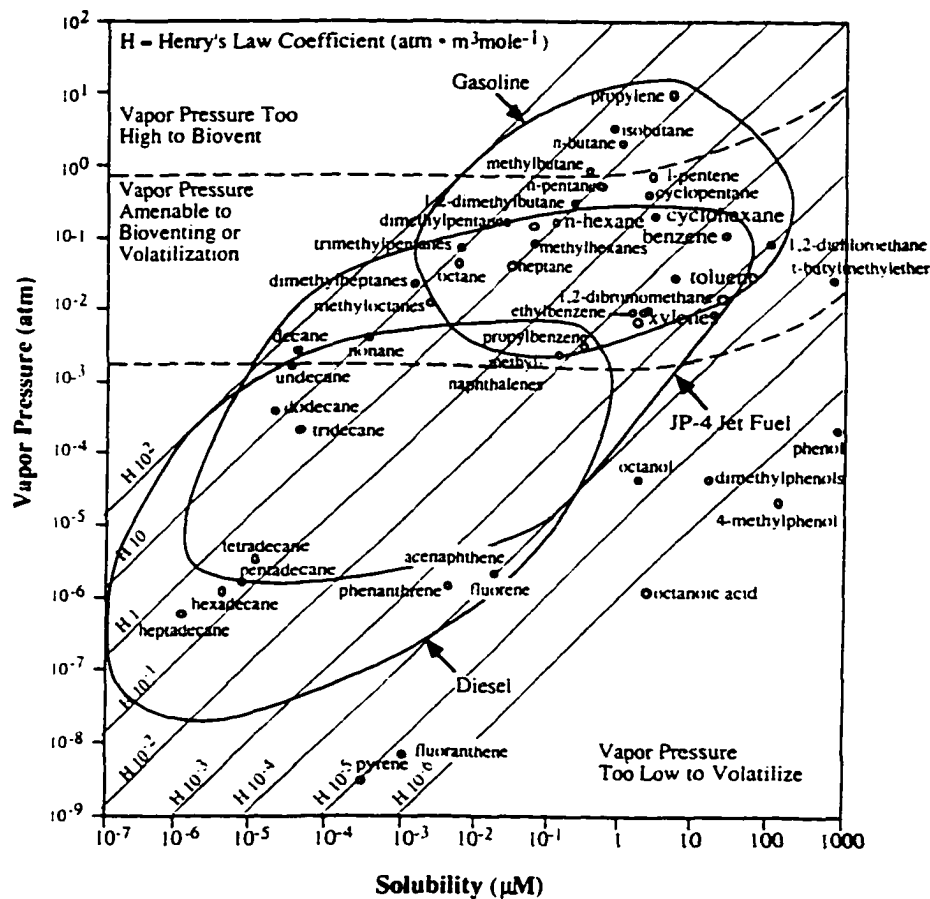


**Figure 2-1.** Physicochemical properties of common hydrocarbon compounds and their bioventing potential (reprinted from Hincbee et al., 1994; public domain).

### 2.1.2 Microbiology, Geochemistry and Environmental Considerations

The occurrence and proliferation of microorganisms in a subsurface environment are determined by various physicochemical factors. These factors include temperature, moisture content, soil porosity, redox potential, pH, and the concentrating and chemical forms of

organic and inorganic compounds. Liebig's Law of the Minimum states that total biomass of any microorganism is in direct proportion to the minimum concentration of an available nutrient meeting requirements of that microorganism. Shelford's Law of Tolerance stipulates that such abiotic parameters govern the abundance of microorganisms in any ecosystem, such that each of these factors must remain within the microorganism's tolerance range for that microorganism to succeed in a given environment (Atlas and Bartha, 1987).

Despite these considerations, environmental adaptation is paramount to effective bioremediation. Use of indigenous microflora reduces the time of microbial acclimation to the surrounding soil conditions and lowers the rejection rate. These benefits are more pronounced in soils where nontoxic contaminants have been in the environment for a long time (petroleum contamination at the UAF bioventing site had been present at least since 1984). Bioaugmentation with synthetic or genetically engineered microbes is costly, often ineffective, and much less controllable where an extreme climate can significantly alter physicochemical attributes. Additionally, it has been suggested that nonindigenous microflora generally have a greater potential to produce toxic derivatives through the biodegradation process (Alexander, 1994). The preponderance of bioventing evidence suggests that oxygen, temperature, and nutrient availability are the dominating physicochemical factors governing bioventing of BTEX (benzene, toluene, ethylbenzene and xylene) contamination in the vadose zone.

Temperature has been demonstrated to have a pronounced effect on biodegradation rates associated with bioventing of soils contaminated with fuels and other petroleum product compounds (Sayles et al., 1995; Moore et al., 1995). Alexander (1994) reports that below the 23°F to 32°F "activity threshold" most microorganisms become dormant or die. Increasing soil temperatures above freezing not only yields higher biodegradation rates but can afford year-round microbial activity.

Microorganisms are classified as *psychrophilic*, *mesophilic*, and *thermophilic* if their optimal growth temperatures are low (40-60°F), moderate (75-100°F), or high (100-140°F), respectively. In central Alaska, psychrophilic, and cold-tolerant mesophilic bacteria populations are common in soils. Cold-tolerant mesophiles have adapted the ability to sustain

protein synthesis to temperatures as low as 25°F and proliferate between 60°F and 75°F. This is supported by findings reported in cold regions bioventing literature, where biodegradation activity was measurable in contaminated soils even during the coldest months (Brar et al., 1993).

Additionally, the effects of temperature on microorganisms can be related to other environmental parameters such as moisture and pH. Moisture significantly influences the thermal death of microorganisms; moist heat is more effective than dry heat in killing microorganisms. Thermal killing is also influenced by pH. Microorganisms tend to be more resistant to high temperatures at neutral pH than at acid or alkaline pH values (Atlas and Bartha, 1987). At the UAF bioventing site, vadose zone soils typically exhibit low (6 to 14 percent) natural moisture contents\* and pH values between 6.2 and 6.4 (optimal for many microorganisms). Indigenous microbial populations may acclimate to relatively low moisture environments. However, bioventing at high injection rates can dry soils, perhaps having negative consequences on bioactivity within treatment areas.

Heterotrophic microorganism proliferation is largely governed by the amount of metabolizable organic matter present in soils, and the availability of essential inorganic nutrients. Inorganic compounds essential to successful bioventing include oxygen and hydrogen gases, ammonium and nitrate (unless organic nitrogen is plentiful), ferrous iron, calcium, magnesium, sodium, potassium, sulfate, and phosphate. The availability of oxygen and hydrogen affects the redox potential of the degradation realm. Heterotrophic

---

\* Moisture content alone does not necessarily translate to moisture "available" to soil microorganisms. A measure of water-filled pore space (degree of saturation) is more representative. The degree of soil saturation (S) can be expressed as  $S_e = \omega G_s$ , where  $e$  is the soil void ratio,  $\omega$  is moisture content, and  $G_s$  is the soil specific gravity. For the sandy-gravel [site] unsaturated soils,  $G_s = 2.65$  and  $e = 0.6$  are representative of Fairbanks glacio-alluvial deposits. Therefore, a 26 to 62 percent saturation range is associated with the natural moisture contents found across the UAF bioventing site.

Alternatively, soil biologists refer to available moisture in terms of a water potential ( $\phi$ ).  $\phi$  is the total soil water potential, equal to the sum of the capillary potential ( $\psi$ ), the gravitational potential (Z), and pressure, osmotic and electrochemical potentials (Fetter, 1993). Under the assumptions of soil homogeneity and that unsaturated soil pressures approximate atmospheric pressure within relatively shallow vadose zones (Hinchee, 1994), the later three potentials can be neglected. Consequently,  $\phi = -\psi(\theta) + Z$ . Here,  $\theta$  is the volumetric water content, equal to the ratio of moisture volume to the total volume of a unit of porous soil.



microorganisms use nitrogen and sulfur for protein formation and for biosynthesis (anabolism) of other molecular components. Phosphorus, as phosphate ( $\text{PO}_4$ ), is required for membrane and nucleic acid syntheses and for the generation of ATP (adenosine triphosphate, an energy source for metabolic activity) (Atlas, 1981).

Other environmental factors such as solar radiation, pressure (atmospheric, hydrostatic and osmotic), and salinity have minimal influence on effective bioventing of the vadose zone (Atlas and Bartha, 1987).

In general, normal changes in atmospheric pressure do not affect microorganisms. Without a groundwater table or saturation conditions, positive hydrostatic pressure is not a factor within the vadose zone. Similarly, most microorganisms have adaptive mechanisms enabling them to withstand subtle osmotic pressure differentiations that may occur across cell membranes. Geochemistry results for the UAF bioventing site typically exhibit salt concentrations less than 21 mg/L. Therefore, deleterious salt effects on microbial growth are not likely to occur.

### **2.1.3 Geotechnical Considerations**

Successful bioventing has been reported within gravels, gravely sands, fine sands, silty sands, glacio-alluvial silts and gravels, and silty soils (Table A-1, Appendix A). Site specific soil structure characteristics such as grain size and shape, porosity, permeability, and adsorption are significant parameters to consider in the design of a bioventing system and the timeliness of contaminant remediation. Clays and similarly cohesive soils with low air and water permeabilities, and high adsorption coefficients, are generally considered problematic with respect to effective bioventing. Standard bioventing is also considered less effective in arctic and subarctic regions where ice-rich soils trap contaminants and restrict oxygenation.

Sufficient oxygenation for successful bioventing of petroleum-contaminated soils depends on air-injection flow rate and soil porosity, permeability, diffusion, and adsorption characteristics. Effective bioventing occurs with low water infiltration and where soil particles have a high specific surface (i.e. a high surface area to mass ratio) to provide beneficial adsorption of contaminants at aggregate sites.

## 2.2 Enhanced Bioventing

Standard bioventing, as opposed to enhanced bioventing, solely involves supplying ambient air or pure oxygen to the unsaturated zone to enhance biodegradation rates. Other factors that affect the efficiency of a bioventing operation are available nutrients, temperature, moisture, soil structure, and microbial populations, specifically hydrocarbon degraders (INET, 1993).

Early bioventing research does not associate increased biodegradation rates with nutrient and moisture additions (Dupont et al., 1991; Miller et al., 1991). However, one later *ex situ* bioventing pilot study, performed by the Cold Regions Research and Engineering Laboratory (CRREL) at an Aleutian island military site, evidenced significantly reduced bioremediation time associated with fertilizer enhancement of diesel fuel contaminated soil piles. It may actually be disadvantageous to combine moisture addition with nutrient enhancement, in that elevated nitrate concentrations can be introduced into the groundwater table, furthering the propensity for environmental regulatory concern\*.

It has been demonstrated that microbial metabolic activity and hydrocarbon degrading efficiency can be thermally enhanced (Brar et al., 1993; Moore et al., 1995; Leeson et al., 1995) within subarctic and arctic soils, where indigenous microflora might otherwise exist in a dormant state throughout the long winter period.

---

\* High nitrite concentrations can occur, which can be toxic to many organisms. Furthermore, nitrate leachate into the groundwater below fertilized (nutrient-enriched) land can end up polluting natural water bodies (lakes, streams, ponds, etc.) by altering their natural ecosystems. The EPA now classifies some agricultural lands as National Pollution Discharge Environmental Sites (NPDES).

**Bioventing System and Thermal Insulation System (TIS) Designs**

**3.1 Site Description**

The University of Alaska Fairbanks (UAF) is west of the city of Fairbanks, in the interior region of Alaska. The research site was the UAF Physical Plant LUST (leaking underground storage tank) site, next to the Physical Plant building at the southeast corner of the main campus (Figure 3-1). Physical Plant operations primarily include maintenance and services to campus infrastructure and grounds.

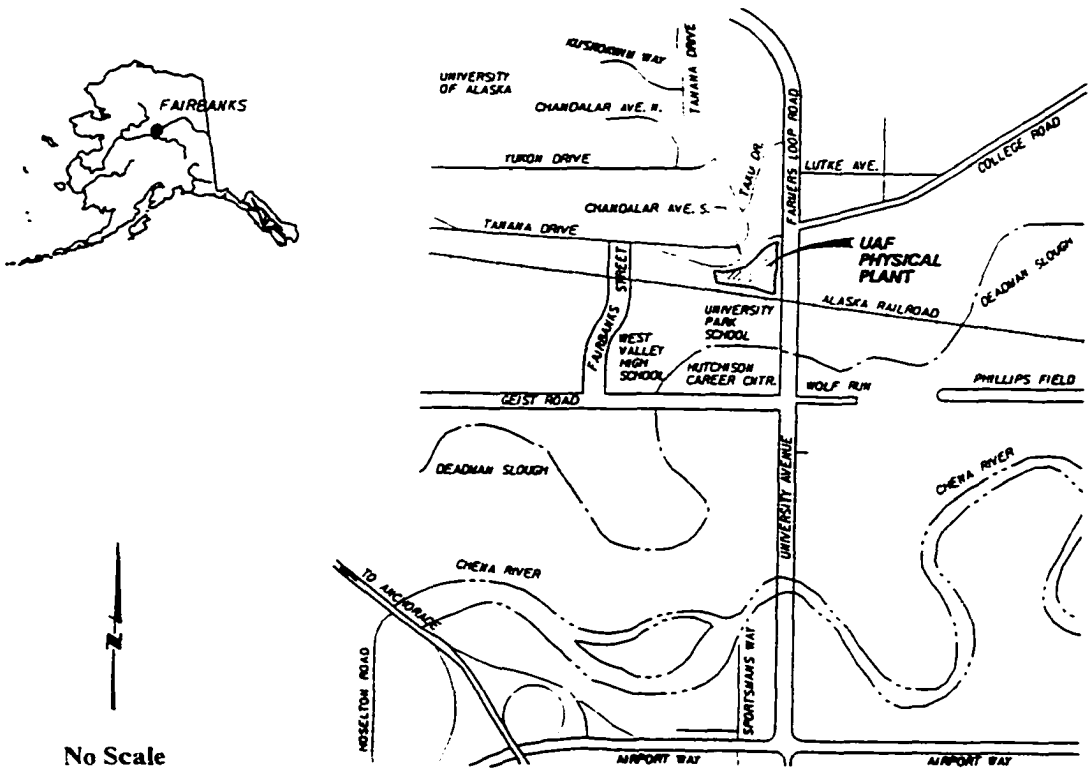


Figure 3-1. General site location map.

### **3.1.1 Climate**

The site is a subarctic location situated south of the White Mountains, at the north end of the Tanana Valley, within the continental climatic zone of Alaska. This climatic zone is characterized as having large daily and annual temperature variations, low humidity and precipitation, and generally light surface winds. Fairbanks lies within a region typically underlain by discontinuous permafrost, has a mean annual snowfall of about 70 inches, and a mean annual temperature of approximately 25°F. Air temperatures in the region can reach -60°F in winter, with summer highs occasionally exceeding 90°F (Hartman and Johnson, 1984).

### **3.1.2 History**

The UAF Physical Plant maintained several underground storage tanks and a fuel dispensing island for its fleet vehicles before August 1984. The tanks included a single 1,000 gallon diesel fuel tank, a single 1,000 gallon regular gasoline tank, and one 500-gallon tank (converted to unleaded gasoline use), all installed before 1968 and removed in August 1984 (Shannon & Wilson, 1990; Montgomery Watson, 1994). The tank farm and fuel island were located within the Physical Plant east parking lot, at the north end of a divider median.

During the tank removal process, pencil-sized holes were noted in the tanks, excavated soils were "grossly stained," hydrocarbon fumes were reportedly noxious, and a contaminant sheen was apparently visible at the groundwater table. Some contaminated soil was removed from the tank excavation pit and taken off-site; the pit was later backfilled with clean soil (Shannon & Wilson, 1990).

Discussion with Physical Plant personnel revealed that a 1,000 gallon aboveground waste oil storage tank was stored inside the vehicle maintenance shop, at the northeast corner of the building. Since the early 1980's, waste oils, degreasers, paint removers, and paint thinners, some containing methylene chlorides and trichloroethane, were routinely stored in this tank before its removal in 1989 (Shannon & Wilson, 1990). A certified waste handler regularly emptied this tank, for off-site disposal. No incidents of spills or leaks were reportedly associated with this tank. Before this tank was installed, a leach field, found

beyond the southern end of the Physical Plant building, was operated until 1984 for the floor-drain dispersal of these waste solvents (Montgomery Watson, 1994).

Although the general groundwater flow direction in the area was reported toward the west and southwest, a 1992 dewatering of a gravel pit less than one mile away reportedly lowered the area groundwater table and temporarily reversed groundwater flow directions; at one point all of the UAF LUST site monitoring wells were reported dry (Shannon & Wilson, 1990; Montgomery Watson, 1994; RZA AGRA, Inc., 1994). Additionally, seasonal groundwater table fluctuations can be associated with yearly spring breakup and increased water influx from the nearby Chena River. The normal flow gradient across the site was measured at approximately 2 feet per 1,000 feet (Montgomery Watson, 1994). To date, there has not been any link established between the leach field contamination (raw sewage and chlorinated solvents) and the site vadose zone UST contamination. The Physical Plant building drainage system was subsequently connected to the College Utilities System and the leach field abandoned.

For a more detailed description of the site history the reader may refer to early consulting reports (Shannon & Wilson, 1990; Montgomery Watson, 1992).

### **3.1.3 Contamination Assessment**

Four subsurface investigations were conducted at the site between 1987 and 1992 (Table 3-1). These investigations, including soil and groundwater analyses, soil gas probes, and an electromagnetic survey, were conducted to characterize subsurface conditions and delineate soil and groundwater contaminant plumes.

The results of the subsurface investigations showed that predominately gasoline-derived hydrocarbon contaminants were present in soils above the groundwater table, while these and some solvent derivatives, were found in the groundwater. Approximately 6,800 cubic yards of contaminated soils were delineated near the old UST tank farm.

**Table 3-1. Summary of UAF Physical Plant LUST site contamination.**

Investigator	Date	Scope of Work	Description
UAF	1984-1987	Sampled product wells UAF-9, 10 and 11.	PAHs and BTEX concentrations to 164 ppb detected in groundwater.
Shannon & Wilson	1987	Installed 2 groundwater monitoring wells.	Reported high level groundwater and moderate level soil contamination.
Shannon & Wilson	1990	Installed 2 soil borings to 21 ft., 7 monitoring wells to 25 ft., and 13 soil gas probes to 13 ft.	Reported <30 ppm TPH above 7 ft., <2,400 ppm TPH between 7-17 ft., and 300-500 ppm maximum total volatiles from soil gas probes. Also reported high TPH and low 1,1 and 1,2-dichloroethane, methylene chloride and trifluoromethane concentrations in groundwater south of the bioventing area. The groundwater table was delineated at between 13.5-15 ft.
JMM (Montgomery Watson)	1991-1992	Electromagnetic and soil gas surveys and 34 soil borings were performed, and 6 monitoring wells were installed.	Reported benzene <14 ppm, BTEX <729 ppm, and GROs <2,400 ppm in soils. Estimated 4,800 sf (1,800 cy.) of contaminated soil between 5-10 ft. and 25,000 sf. (5,000 cy) between 10-15 ft.
RZA AGRA	1994	Installed 6 vent wells to 17.5 ft.	Reported GROs <380 ppm and BTEX <630 ppm in soils.

GROs = gasoline range organics

PAHs = polycyclic aromatic hydrocarbons

BTEX = benzene, toluene, ethylbenzene, and xylenes

ppm = parts per million

ppb = parts per billion

### 3.2 Summary of Bioventing System Design

For an adequate bioventing system, geotechnical information, soil analytical and microbiological data, and engineering experience, all play key roles in the initial design phase. John Arambarri, a Master of Science graduate student with the University of Alaska

Fairbanks' Department of Civil Engineering in 1994, designed and installed the bioventing system for the Physical Plant LUST site (Arambarri, 1995). For the design, vadose zone soil classifications, grain-size distributions, permeabilities, and moisture contents were considered for strategic placement (Figure 3-2) of the six air-injection vent wells and pump sizing.

The typical vent well configuration consisted of 2-inch diameter CPVC pipe, vertically embedded to an average depth of seventeen feet. The bottom ten feet included 10-20 slot screening. End caps sealed the top and bottom of the well. Air was pumped through a ½-inch diameter rubber hose to a throat valve fitted through the side of the well top (approximately six inches down from the top). The Fuji blower was housed in a plastic, PetMate pet porter, fitted with a rubber flapper door cover. In the summer of 1994, this equipment and 14 soil gas monitoring points were installed. Monitoring points were placed throughout the area of soil contamination so that local O<sub>2</sub>, CO<sub>2</sub> and total petroleum hydrocarbon (TPH) concentrations could be measured throughout the vadose zone. TPH refers to the combined hydrocarbons emanating from the various petroleum contaminants (diesel and regular and unleaded gasoline) present.

Site *in situ* permeabilities were evaluated to estimate vent well radii of influence and to assess system design validity. During a permeability test, a single vent well was pumped at five cubic feet per minute (cfm) (Arambarri, 1995). Soil gas pressures were measured at various times during the 24-hour test period, at the vent well and at three separate monitoring points installed at various distances away from the vent well. In this way, pressures versus time data were obtained and used to calculate *in situ* permeabilities and infer vent well radii of influence. From the permeability test data, vent well radii of influence were typically calculated between 25 and 70 feet, adequate for sufficient oxygenation of the contaminated area with the initial design configuration. Vent wells were spaced approximately 25 to 50 feet apart, allowing for air-injection overlap. The sixth vent well was installed northeast of the main bioventing area, in an uncontaminated area, as a control.

The fourteen soil gas point borings were performed at the locations shown on Figure 3-2, in which one to three discrete soil gas monitoring points were installed at various depths in each. Each monitoring point consisted of a suction sieve sampling filter, attached to the

bottom of 1/4-inch diameter polyethylene tubing. The points were tied to rigid 1/2-inch diameter CPVC tubing. Each tube-monitoring point cluster was then vertically installed in the excavated boreholes before backfilling. Surface-mounted, metal risers (with lids) housed the capped sampling ends of the clustered monitoring points. Besides soil gas sampling, two respiration tests were conducted to evaluate winter and summer biodegradation rates.

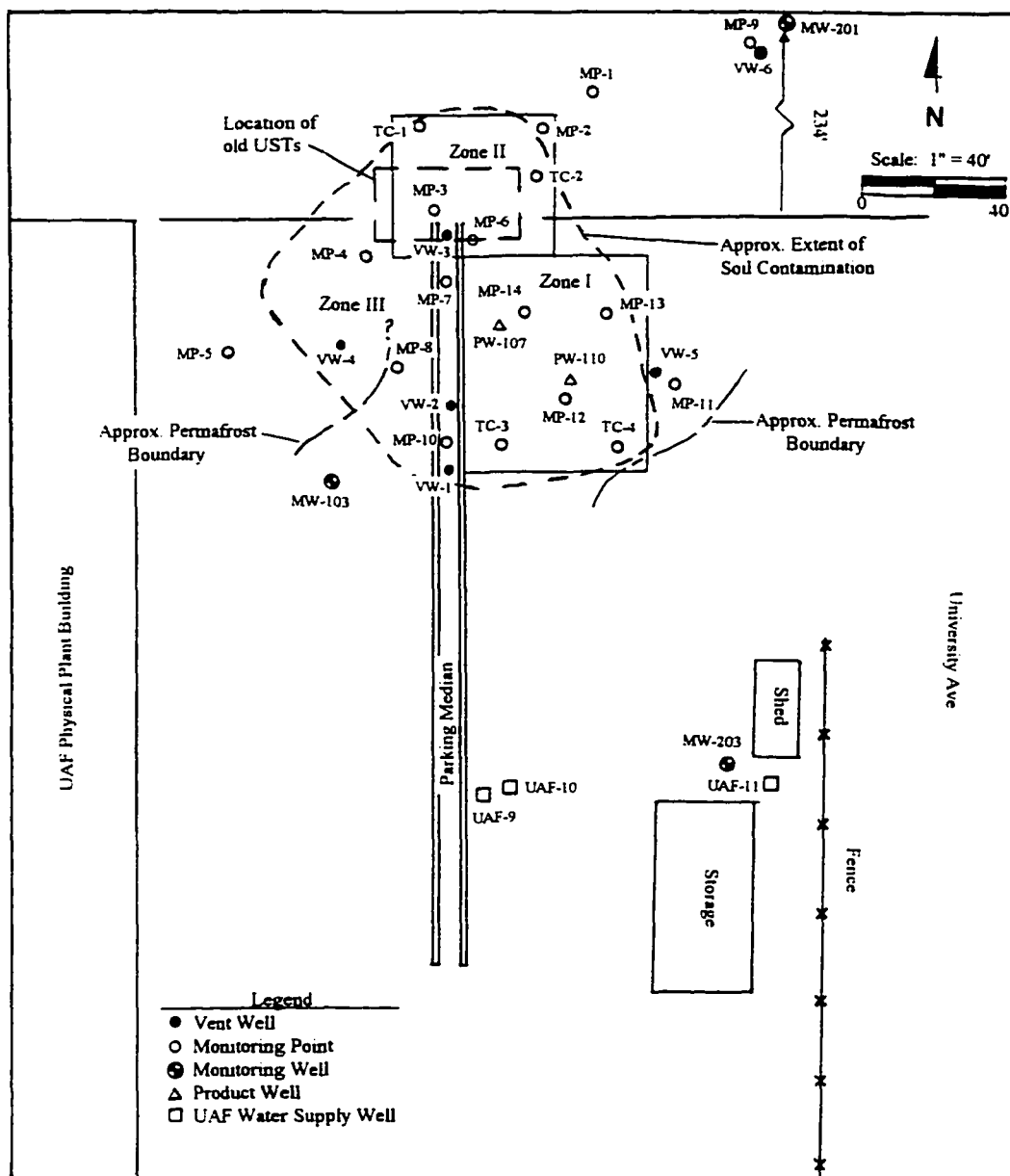


Figure 3-2. UAF Physical Plant bioventing system site plan.



Arambarri (1995) calculated a first year winter biodegradation rate of 0.54 ppm per day (mg/kg-day). A summer rate, eight times higher, reflected warmer soils and increased bioactivity with active soil warming treatment. Based on the initial biodegradation rates and minimum and maximum contaminant concentrations present, Arambarri estimated that it would take 1.9 to 12 years to successfully remediate this site. For a more comprehensive description of the UAF Physical Plant bioventing system, the reader is directed to the Arambarri (1995) report.

### **3.2.1 Soil Stratigraphy**

The general subsurface soil profile for the site is characterized by sand, silt and gravel fill from the ground surface to about 4 feet in depth. A layer of sandy to gravelly silt is encountered between 4 feet and 8 feet in depth, on average. Below that, and at least to 25 feet (maximum exploratory boring penetration depth), the soils are typically classified as well graded sandy gravel, representative of the area's characteristic glacio-alluvial deposits (Shannon & Wilson, 1990; Montgomery Watson, 1994). Fill soils may extend to about 10 feet in depth, the result of deposits used to fill in a Chena River slough that once traversed the site.

Poorly bonded to well bonded frozen soils are seasonally exhibited between 3 and 25 feet deep across portions of the site. Near monitoring point MP-8 and vent well VW-4 frozen ground was identified between 7 and 17 feet deep (Shannon & Wilson, 1990). Other borings drilled nearby and west of the divider median encountered thin layers of ice-rich soils at various depths between 5 and 10 feet. These segregated lenses were considered seasonally frozen soils. A partial permafrost boundary was also surmised during the early investigations, just east of the main bioventing treatment area and monitoring point MP-11 (Figure 3-2).

#### **3.2.1a Darcy Flow Theory and Site Specific Permeability**

As air permeability is a critical parameter in the design of an effective bioventing system, an understanding of vapor flow through the site unsaturated zone and validation of the soil air permeabilities as determined by Arambarri are necessary.

Soil permeability is a measure of the resistance to flow of a fluid through porous medium. The intrinsic or *absolute permeability* ( $k$ , in  $\text{ft}^2$ ) is dependent upon porous media characteristics such as grain-size distribution, porosity, roughness (shape) of soil particles, available moisture content, and fluid viscosity.

*Hydraulic conductivity* ( $K$ , in  $\text{ft/s}$ ), sometimes called the coefficient of permeability, relates to the ability of a porous medium to transport fluid. Unsaturated hydraulic conductivity is dependent on soil moisture content and thermal state. Constantz (1982) and others have shown that as moisture content and temperature are increased, the unsaturated hydraulic conductivity also increases. Soil intrinsic permeability is related to unsaturated hydraulic conductivity as

$$K = k \frac{\gamma}{\mu} \quad (\text{in ft/s}) \quad [3-1]$$

where the fluid unit weight  $\gamma = \rho g$  (in  $\text{lb}_m/\text{ft}^3$ ;  $g = 32.2 \text{ ft/s}^2$ ) and  $\mu$  is the fluid dynamic viscosity (in  $\text{lb}_f \cdot \text{s}/\text{ft}^2$ ).

The importance of measuring vadose zone air permeability for a bioventing project is paramount in the determination of the number of air injection vent wells and their associated radii of influence and spacing. However, because the vadose zone undergoes physical changes associated with water infiltration and variable moisture contents, the chemical quality of water (minerals and contaminants in solution), and extreme seasonal temperature variations, calculated intrinsic permeability values should be considered as order of magnitude approximations and, at best, as estimates for design.

Darcy's flow relates the volume quantity of fluid flow through a porous medium to soil permeability, and it can be applied to water and air propagation through the subsurface. However, Darcy flow was derived for viscous, incompressible, laminar fluids under steady-state conditions (Muskat, 1937). Turbulent flow in soils can occur when the flow through a porous medium varies due to flow path irregularities (increased moisture content and pressure effects on soil matrix structure). Consequently, non-Darcian velocity exists.

---

\* For a units check, the conversion  $1 \text{ lb}_f = 1 \text{ lb}_m \cdot \text{ft}/\text{s}^2$  is necessary

Darcy's Law and the continuity equation govern flow through a confined porous stratum. The respective governing equations are

$$\frac{Q}{A} = v = \frac{k}{\mu} (\nabla P + \gamma) \quad \text{and} \quad \frac{\partial(\epsilon \rho H)}{\partial t} = \nabla(v \rho H)$$

(after Johnson et al., 1990)

where

- $Q$  = flow rate (in cfm)
- $A$  = vapor path cross-sectional area (in ft<sup>2</sup>)
- $v$  = Darcy velocity (in ft/s)
- $\nabla$  = gradient operator (1/ft)
- $I$  = hydraulic gradient (dh/dl)
- $P$  = vapor pressure (in psf)
- $\epsilon$  = vapor-filled portion of soil voids
- $\rho$  = vapor density (in pcf)
- $H$  = stratum thickness (in ft)
- $t$  = time (in sec.)

Johnson et al. (1990) and Sellers et al. (1991) present the derivations of the following steady-state and transient air permeability relationships (equations [3-2] and [3-4]). Their derivations are based on earlier work by Bear (1972, 1979) and Todd (1980) and assume vapor flow is primarily horizontal, insignificant pressure changes throughout the stratum, and negligible changes in permeability caused by drying. These assumptions are applicable to the UAF site because 1) the TIS acts as a confining layer to upward vapor flow, 2) the vadose zone is relatively shallow, and 3) a low injection flow rate minimizes soil drying.

Johnson (1991), of Shell Development Company, developed the Modified Field Drawdown Method test for measuring steady-state *in situ* permeability. The method is applied to a bioventing system such that pressures are monitored at various distances (monitoring points) away from an air-injection vent well, and assumes the system is operating

under equilibrium conditions. The equation for intrinsic air permeability determination with this method is

$$k = \frac{Q \mu_a \ln\left(\frac{R_w}{R_1}\right)}{m \pi P_{atm} \left[1 - \left(\frac{P_{wabs}}{P_{atm}}\right)^2\right]} \quad (\text{in ft}^2) \quad [3-2]$$

where

- $Q$  = air-injection flow rate (in cfm)
- $\mu_a$  = dynamic viscosity of air (in lb/s-ft)
- $m$  = vent well effective screened interval length (in ft)
- $R_w$  = vent well radius (in ft)
- $R_1$  = radius of influence (in ft)
- $P_{atm}$  = atmospheric pressure (14.7 psi)
- $P_w$  = stabilized vent well gauge pressure (in psi)
- $P_{wabs}$  = absolute vent well pressure ( $P_{atm} + P_w$ )

The dynamic (transient) method of determining intrinsic air permeability requires differentiating changes in soil gas gage pressure, as true responses to the permeability test, from atmospheric pressure fluctuations. For a bioventing application, transient intrinsic air permeability determination can be adapted from the Cooper-Jacob Straight-Line method for evaluating hydraulic conductivity (Todd, 1980; Sellers et al., 1991; Hinchee et al., 1992). Using the Jacob Equation for hydraulic conductivity

$$K = \frac{2.3Q}{4\pi \Delta z m} \log\left(\frac{t_2}{t_1}\right) \quad [3-3]$$

---

\* The log term in this equation is a conversion from the natural log as  $2.303 \log_{10}(t_2/t_1) = \ln(t_2/t_1)$ . 2.303 is rounded off to 2.3

where  $\Delta z$  is the thickness of flow medium and  $t_1$  and  $t_2$  are test times at which corresponding gage pressures  $P_1$  and  $P_2$  are measured. Substituting this equation into equation [3-1], incorporating pressures via use of the hydrostatic law ( $\Delta P = \rho g \Delta z$ ), and rearranging yields

$$k = \frac{2.3Q \mu_a}{4\pi \Delta P m} \log\left(\frac{t_2}{t_1}\right) \quad [3-4]$$

Arambarri (1995) presented air permeability and radius of influence calculations for the UAF bioventing site. These permeabilities and a sample calculation for both the steady-state and transient conditions are presented in Appendix A.

Hinchee et al. (1992) suggest that the transient (Cooper-Jacob) method is more applicable to low permeability sites where the depth to [vent well] screened interval and screened interval length exceed 10 feet. For sites with sandy [and gravelly] soils, a shallow water table, and where vent well screening begins at depths greater than 10 feet, the transient method is less accurate. During the original permeability tests barometric pressures could not accurately be measured because of equipment limitations. Therefore, acceptance of the steady-state air permeabilities determined by Arambarri, for representation of the vadose zone at the UAF bioventing site, is necessary. Because Darcy's Law is applicable to most natural subsurface flow regimes (Todd, 1980), the assumption that it applies at the UAF research site is sound. The following analogy is made in support of the steady-state permeability values reported by Arambarri.

The stratigraphy beneath the UAF Physical Plant bioventing site can be generally classified with sand, silt and gravel fill comprising the upper 4 feet, and interbedded gray to brown sandy gravel alluvial deposits to 25 feet in depth. A local, undefined region of permafrost exists along the western edge of control Zone III (Figure 3-2). Composite soil samples from several monitoring well boreholes were analyzed for grain-size distribution by Montgomery Watson (1994). The results of the grain-size analysis showed that the sites silt fraction ranges between 16 and 26 percent, the sand fraction between 74 and 80 percent, with the remainder predominately gravels. According to the commonly used Unified Soil

Classification System (USCS) soil particles are considered silts if their grain-size diameters are less than 0.003 mm (Das, 1985). Knowing the sand fraction and using the 16-26 percent silt fraction range, the *effective size* ( $d_{10}$ ) -- the diameter corresponding to 10 percent finer than the #200 sieve on the grain-size distribution curves -- was estimated at between 0.0003 and 0.0009 inches.

The Reynolds number is used as the criterion to distinguish between laminar and turbulent flow through pipes and other large sections. It is the dimensionless ratio of inertial to viscous forces, and is usually defined for pipe flow as  $N_R = (\rho v D) / \mu$ . However, Darcy's Law can be applied to laminar flow in porous media with use of the effective particle size parameter  $d_{10}^*$  for the appropriate Reynolds number equation (Todd, 1980). Reynolds number for porous media flow can be expressed as

$$N_R = \frac{\rho v d_{10}}{\mu} \quad [3-5]$$

and is used to set the limit criteria for Darcy laminar flow. It is generally accepted that Darcy's Law is valid for  $N_R \leq 1$  (Ahmed and Sunada, 1969), for nonlinear (tortuous) flow through porous media.

Using the site specific intrinsic air permeabilities determined by Arambarri (Appendix A) the following argument is presented. Darcy velocity is

$$v = K I \quad [3-6]$$

where  $K = k \rho g / \mu_a$ . Therefore,

$$v = k \frac{\rho}{\mu_a} g I \quad [3-7]$$

---

\* The soil effective size ( $d_{10}$ ) parameter implies a measure of porosity, indirectly characterizing the fluid flow path through the porous medium.

Substituting this last expression for the Darcy velocity into equation [3-5] yields

$$N_R = k \frac{\rho^2}{\mu_a^2} g d_{10} I = \frac{k g d_{10}}{v_a^2} I \quad [3-8]$$

where  $v_a = \mu_a/\rho$  is the fluid kinematic viscosity (between 0°F and 80°F,  $v_a$  varies from  $1.2 \times 10^{-4}$  to  $1.7 \times 10^{-4}$  ft<sup>2</sup>/s),  $d_{10} = 0.009$  in.,  $k = 1.2 \times 10^{-9}$  ft<sup>2</sup> (the highest site air permeability value), and  $g = 32.2$  ft/s<sup>2</sup>. From the permeability test data reported by Arambarri (1995), discrete hydraulic gradients (with respect to an individual vent well) vary between 0.02 and 0.13 feet per foot. With these gradients, the calculated Reynolds numbers are less than 1 (see Appendix A for sample calculation and representative  $N_R$  values). Therefore, it suffices to say that Darcy flow and the steady-state permeability values reported by Arambarri represent flow through the porous media above the water table at the project site. The site specific permeability calculations and published representative permeability values for various soils are presented in Appendix A.

### 3.2.1b Variable Permeability and Velocity Profiling

For the previous permeability discussion it was assumed that vapors preferentially flow through larger soil pores, leaving both liquid hydrocarbons and moisture to occupy smaller pores. Therefore, removal of these “wetting fluids” (by either degradation or drying) was not expected to alter vapor flow paths significantly. This assumption was valid for the UAF bioventing site vadose zone (above the smear zone) since low moisture contents and low to moderate concentrations of petroleum contaminants prevailed. However, for sites where water and liquid hydrocarbons are found in soils at levels exceeding 20 percent by weight, drying induced by bioventing can significantly change soil vapor permeability (Johnson et al., 1990). Consequently, another method of determining site permeabilities for sound bioventing system design is required.

Velocity profiling (vertical and/or horizontal) can be incorporated into the bioventing system design, to more accurately reflect vapor velocity changes with time and to refine the

remediation time estimate as contaminant concentrations change.

Where vent well spacing does not afford radii of influence overlap, a tracer test can be easily and inexpensively performed to calculate the Darcy velocity. During the installation of a bioventing system a line of two or three evenly spaced soil gas monitoring points should be established between any two vent wells. Additional lineaments can be incorporated into the design when the unsaturated zone is more heterogeneous. At one vent well, a helium or argon tracer is injected into the vent stream. Initializing time with tracer injection, soil gas samples are subsequently collected in Tedlar<sup>(TM)</sup> bags, incrementally with time at the two (or three) monitoring points. The test duration is dependent upon soil profile characteristics. A portable gas analyzer can then be used to detect the tracer in the samples. Once the tracer has been detected at its lowest concentration, media velocity can be calculated from time and distance data\*. An average of the velocities determined along the line is the Darcy velocity for vapor travel. Where a number of discrete soil gas monitoring points are embedded throughout a multi-layered vadose zone, a velocity profile can be delineated. A similar test conducted from the other end of the line can be used for verification and further refinement of this average velocity. Substitution of this velocity into equation [3-7] can produce an accurate representation of the site [transient] permeability(s). The permanency of the lineaments allows one to redefine this velocity at any time and for variable air-injection flow rates.

This tracer test is less definitive where vent wells are closely spaced. Radii of influence overlap requires superposition of velocities and binary mixing of opposing flows. This being the case, linear and 3D velocity profiling can be determined with the use of a Geoprobe<sup>(TM)</sup> and a series of velocity points. The Geoprobe<sup>(TM)</sup> is used to drive and anchor the [velocity] monitoring points between two vent wells. Each monitoring point consists of a cluster of variable depth, 1/4-inch diameter poly-tubing, each tube perforated with 1/16-inch

---

\* Because gases have different molecular weights, they diffuse through soil at different rates. A correction factor, equal to the square root of the ratio of molecular weights for tracer gas and oxygen, should be applied to the field data to account for the different diffusion rates. Furthermore, the velocity measurements are approximate, as they do not completely account for areal and seasonal variability in gas dispersion rates.



diameter holes. After the tube clusters are installed, the remaining annular spaces are backfilled with coarse sand and capped with bentonite seals. A Bubble-Meter<sup>(TM)</sup> flow meter is surface-connected to measure flow at each tube within the points. In this way direct field measurements' account for velocity mixing from opposing flows.

### 3.2.2 Thermal Insulation System Design

Subarctic and arctic climates restrict bioventing to the short summer season where permafrost and/or frost-susceptible soils prevail. At the UAF site, primary consideration was given to the design of a thermal insulation system that would effectively warm the vadose zone year-round, thereby enhancing bioremediation. Two computer software packages were used in designing the thermal insulation systems (TISs). Thermal monitoring equipment was installed throughout the bioventing site. Subsequently, the *in situ* thermal data were then compiled and compared with an existing heat conduction model.

Three test plots were laid out at the UAF bioventing site for thermal treatment analysis. Two TISs were designed and installed, with monitoring results compared with that of the biovented control test plot. Based on early soil gas data, analytical data, and reported delineations of the contaminated soil plume, the bioventing site was partitioned into the three test plots as shown in Figure 3-2.

#### 3.2.2a ELSYM-5 Stress-Strain Analysis on TISs

For this study, the bioventing treatment area was designed to accommodate smooth operation of Physical Plant services; driving lanes circumnavigate the site and the parking median. Therefore, design considerations for the Zone I and II TISs required stress-strain analyses of the materials under traffic loading conditions. SRA Technologies, Incorporated, under contract to the Federal Highway Administration, developed the ELSYM-5 computer program. The Alaska Department of Transportation and Public Facilities (ADOT&PF) routinely uses this software as a standard for the design of roads and highways in Alaska. ELSYM-5 requires site specific soil layer characteristics (Poisson ratios, moduli of elasticity, and layer thicknesses) and typical loading applications as input parameters. ELSYM-5 then

applies conventional principles of elasticity to determine the three-dimensional stresses and strains and point displacements under load.

The RZA AGRA (1994) drilling logs for vent wells VW-1 through VW-5 provided the representative soil classifications and blow counts (a measure of soil densities) for layer elastic moduli determinations. Bowles (1988) presents a series of empirical equations for determining field moduli of elasticity (Young's Modulus). Incorporating the drilling log blow count numbers (N) into the appropriate equation for each layer of the vadose zone, I established a representative soil elasticity profile for ELSYM-5 (Figure 3-3). The appropriate elastic moduli equations, in units of psi, are

$$\begin{aligned}
 E_{s1} &= 723 (N+15) \quad \text{for sand} & E_{s3} &= 1736 (N+6) & \text{for gravelly sand and gravel} \\
 E_{s2} &= 434 (N+6) \quad \text{for silty sand} & E_{s4} &= 868 (N+6) & \text{for gravelly sand and gravel: } N \le 15 \\
 & & E_{s5} &= 868 (N+6) + 2894 & \text{for gravelly sand and gravel: } N > 15
 \end{aligned}$$

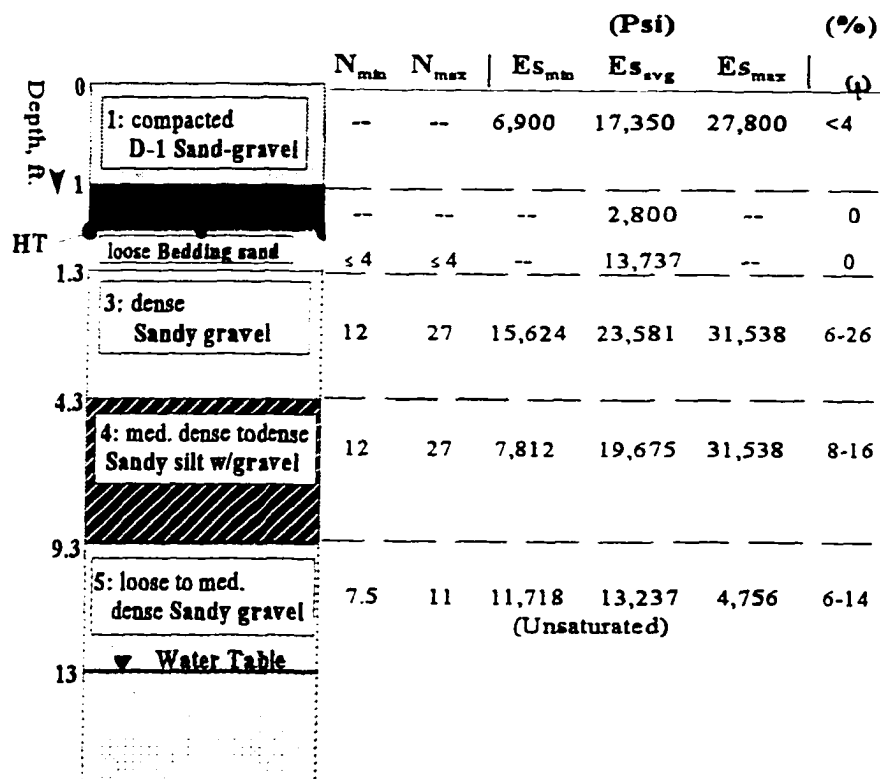


Figure 3-3. Example soil profile and input parameters for ELSYM-5 analysis.

Average elastic moduli for the soil profile layers were checked for reliability against published values for the loose to dense soils. A Poisson's Ratio ( $\mu$ ) of 0.35 was chosen for the profile soils (Bowles, 1988). This value is commonly used for silts, sands, and gravelly sands. The calculations for the average elastic moduli and published values can be found in Appendix B.

Field moduli of elasticity depend on soil type, density, and thermal state. The modulus of elasticity tends to increase as soil freezes. Poisson's ratio for granular soils tends to decrease as soils freeze (Andersland and Ladanyi, 1994). Therefore, use of the summertime drilling log data for the static ELSYM-5 analysis sufficed for the design of the worst case scenario. Figure 3-3 illustrates a general example subsurface soil profile for the computer analysis. Maximum and minimum field blow count numbers and moduli of elasticity reflect density and moisture content variability across the bioventing site.

An inventory of the Physical Plant vehicles, including their gross weight ratings (GWR), wheel patterns, and a traffic volume summary were also necessary for the ELSYM-5 analysis. Fleet vehicles and heavy maintenance equipment ranged from 3,000 to 5,200 pound passenger cars to 20 to 28 ton GWR capacity Caterpillar scrapers and eight cubic yard dumptrucks. Considering lane widths and typical daily traffic patterns, maximum static loadings on the Zone I and Zone II TIS pads were modeled with the side-by-side parking of the two largest vehicles (a fully loaded eight cubic yard dump truck and a fully loaded garbage truck or Caterpillar scraper). Therefore, the TIS materials would have to withstand a maximum long-term application of approximately 100,000 pounds, applied at the pad corner (critical location) by a series of combination single-axle and tandem-axle, single and dual wheel loadings.

Several surface applied and embedded designs were considered for the thermal enhancement of the UAF bioventing site. Design configurations included 1) sawdust, 2) sawdust over polyethylene with plywood, 3) sand and gravel over polystyrene, and 4) an embedded hot water circulation system, among others. Material considerations included strength, durability, cost, and availability. Designs were scrutinized for applicability, durability, and cost of installation and maintenance. The thermal analysis idea was to compare

two TIS treated test plots to that of an untreated, biovented plot. Since excavation and embedment costs would be high, and after ruling out inappropriate or otherwise deemed ineffective materials, the final TIS designs were considered for surface application only.

The final designs incorporated combinations of soft bedding sand, extruded polystyrene insulation, D-1 sand and gravel, and an electrical heat tape network (Zone II only). D-1 construction soils are classified according to Alaska Test Method T7. The aggregate specifications are shown in Appendix B (Table B-1).

By manipulating the general TIS/soil profile (Figure 3-3), that is, varying individual TIS material thicknesses, cost and quantity of the chosen materials are considered in the optimization of the thermal designs. Primary consideration was given to the polystyrene layer, because heat loss and heat tape protection were critical concerns. The D-1 surface layer was incorporated primarily to protect underlying TIS materials and provide a smooth driving surface. Some additional winter insulating benefit would also be realized. Because the ELSYM-5 analysis is limited to a five-layer system, the thin 2-inch bedding sand layer was incorporated into the underlying dense sandy gravel. A depth weighted average modulus of elasticity was calculated and attributed to this combined third layer.

ELSYM-5 analyses determined that the static loading of the TIS pads, with the side-by-side parking of the two largest Physical Plant vehicles, would not exceed the 40 pounds per square inch compressive strength rating of the polystyrene insulation. Figure 3-4 illustrates the loading scheme for the worst case scenario, a large scraper next to a fully loaded eight cubic yard dumptruck. Critical stress-strain analysis points were midpoints between 2 and 4-wheel groupings and between the 2 vehicle tandem-axle groupings (Figure 3-4 rectangles). The critical depths for analysis were the top and bottom of the polystyrene layer. The vehicles were loaded to maximum capacity and analyzed individually by ELSYM-5. Normal, shear, principal and principal shear stresses and strains were determined for these critical points, at the two depths (12.01 and 14 inches below the TIS surfaces).

After the vehicles were individually analyzed, superposition of stresses and strains was applied at critical junction points; i.e., where wheel (load) groupings of the two vehicles were close to each other. In theory, the maximum stresses realized in the insulation under loading

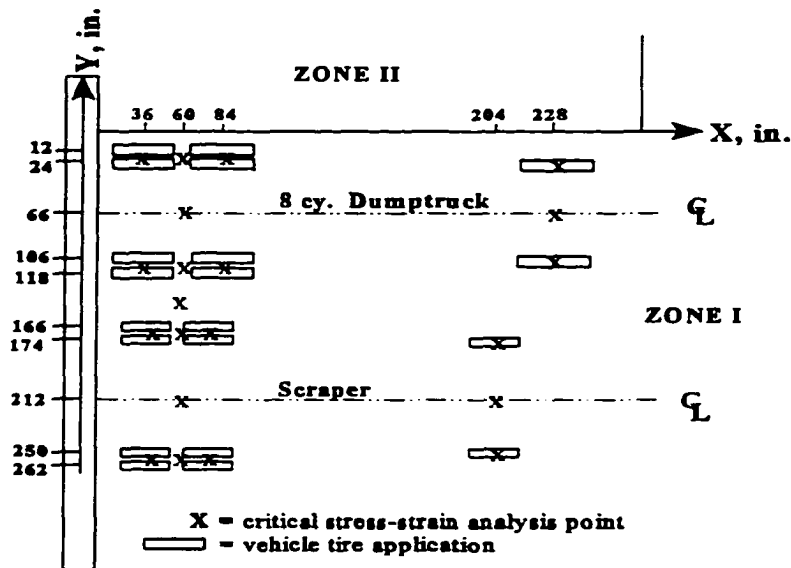


Figure 3-4. Critical load points for ELSYM-5 stress-strain analysis.

will not exceed 14.8 psi, providing a design factor of safety of 2.75. Associated displacements of less than 0.034 inches compression would be realized in the polystyrene. Maximum strains realized did not exceed 0.003 in/in (Appendix C). Under uniaxial load this translates to maximum strain energy densities\* of less than 0.01 and 0.1 psi in the insulation and D-1 overburden, respectively. Table 3-2 summarizes the ELSYM-5 computer results. The comprehensive computer results for the final TIS designs are included as Appendix C

A passive TIS was installed over the ground surface as the Zone I test plot. This passive system consisted of a 2-inch thick layer of soft fine bedding sand, below 2 inches of extruded polystyrene insulation, and with a 12-inch surface layer of clean D-1 sand-gravel material. This TIS pad was leveled, compacted, and graded with 1:5 border slopes. This test plot spanned an area of approximately 54 x 60 square feet, abutting the east side of the parking median that runs through the bioventing site.

\* Strain energy is a measure of the work done when an elastic material deforms (undergoes displacement) under load, and can be related to the likelihood of material failure. This strain energy, under uniaxial load, is calculated from

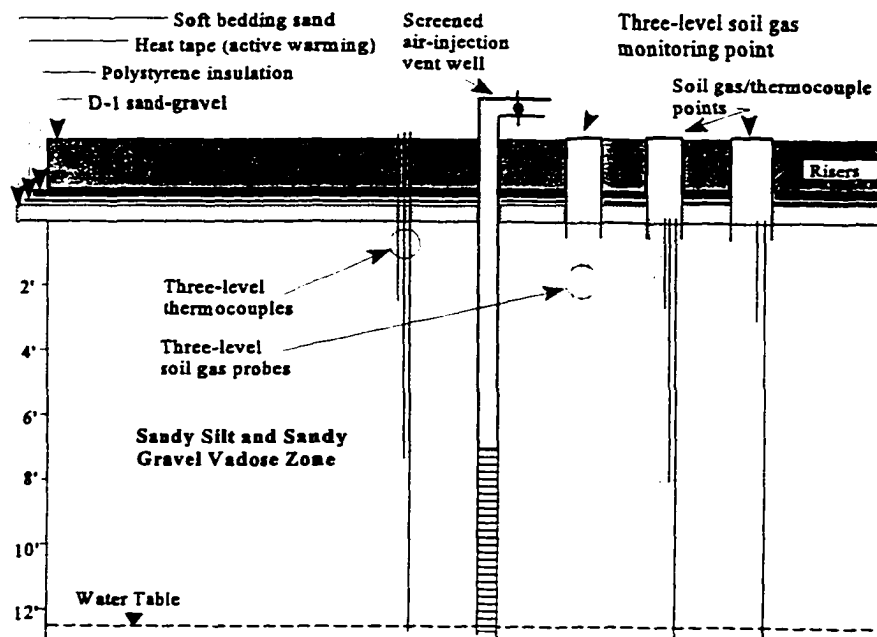
$$U = \frac{E_{\max} \epsilon^2}{2}$$

where  $\epsilon$  is strain.

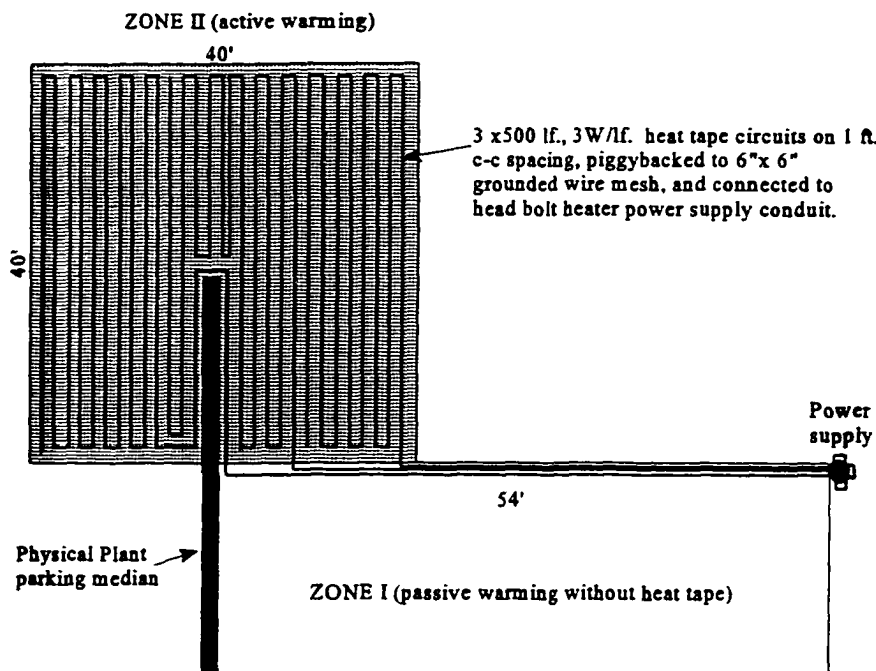
**Table 3-2.** Critical stress and displacement results from the ELSYM-5 analysis.

<b>Vehicle and Stress Descriptions</b>	<b>Stresses (psi) @</b> <b>(top of) (bottom of)</b> <b>polystyrene</b>		<b>Polystyrene Compression</b> <b>(in.)</b>	<b>Critical Point X, Y Coordinates</b> <b>(refer to Fig. 3-4)</b>
<b>Dumptruck</b>			0.023	60,18 and 60,112
normal stresses	1.43	1.74		60,18 and 60,112
shear stresses	0.19	0.19		60,66
principal stresses	2.03	1.74		60,18 and 60,112
princ. shear stresses	0.60	0.39		60,18 and 60,112
<b>Scraper</b>			0.034	48,170
normal stresses	12.7	12.65		48,170
	12.6	10.9		204,174 and 204,250
	12.65	11.4		48,170
shear stresses	1.09	1.2		48,256
principal stresses	12.8	12.8		48,142
	12.6	10.9		48,170
		11.4		204,174 and 204,250
princ. shear stresses	4.38			48,256
	4.37			204,174 and 204,250
		2.7		204,174 and 204,250
		2.95		48,170
		2.6		48,256

The Zone II TIS, covering approximately 40 x 40 square feet of contaminated soil and the old UST tank locations, was designed similarly. However, active soil warming was introduced with the incorporation of 1,500 lineal feet of electrical heat tape, tied to a wire mesh (6-inch x 6-inch grid) that was embedded between the soft bedding sand and the polystyrene insulation. The three watt per linear foot heat tape was aligned in north-south lineations, at one foot center-to-center spacing, forming three 500 foot circuits. Each circuit was electrically fed from a common service head bolt outlet located at the northeast corner of the Zone I TIS treatment pad. A ½-inch diameter, 5-foot long copper rod was fastened to the wire mesh anchor grid and driven into the ground to act as an electrical ground. Schematic diagrams of the Zone I (without heat tape) and Zone II thermally enhanced plots are shown in Figure 3-5.



(a)



(b)

Figure 3-5. (a) Cross-sectional view of Zone I and Zone II thermally enhanced bioventing treatment design, and (b) plan view of Zone II electrical heat tape installations.

Concern for damage to the electrical heat tape and polystyrene insulation materials under loading warranted a load test. Specifically, heat tape was turned on edge when rounding bends along the circuit lineations. Therefore, a concern was that the heat tape might crimp around the wire mesh below or the insulation might deform under load.

Before installation, Rolf Mey, of UAF Planning & Project Services, performed a dynamic load test on a model simulation of the Zone II TIS. A short strip of heat tape was fixed both flat and on edge between wire mesh and polystyrene insulation materials. The model was then placed between rigid metal top and bottom plates on a hydraulic press machine. Loading was applied to the top plate, increasing steadily until the 40 psi insulation rating was realized or component failure (insulation or heat tape) occurred. The results of the test showed that the TIS materials retained their design integrity to at least 40 psi. Beyond the 40 psi loading the heat tape embedded itself into the underside of the insulation rather than crimping or deforming over the wire mesh.

Because of the potential high cost of repairs to damaged heat tape and polystyrene insulation, the TIS's were maintained for long-term use under restricted vehicular traffic operation. Traffic was limited to vehicles weighing less than 10,000 pounds GVW, effectively increasing the polystyrene design factor of safety.

### **3.2.2b BERG-2 Freeze-Thaw Analysis**

Besides the strength concerns for the TIS materials, it was necessary to examine the insulation layer thickness related to depths of freeze. BERG-2 computer software (Conner and Braley, 1988) was used for the preliminary thermal analysis of the TISs.

BERG-2 solves the *modified Berggren equation* (a modification of the *Neumann* one-dimensional heat diffusion solution) to determine approximate maximum depths of thaw or freeze in multilayered soil systems. The program essentially calculates the portion of the surface thawing (or freezing) index required to move the thaw (or freeze) front down through the successive layers (Braley, 1984). The total depth of thaw or freeze is the sum of these layers. For example, a depth of thaw is calculated as



$$X_f = \frac{STI \lambda^2}{L_n \left( \frac{R_n}{2} + \sum R_{n-1} \right)} \quad [3-9]$$

- where
- $STI = n_i(ATI)$ , the surface thawing index (in °F-days)
  - $n_i$  = surface thaw n-factor (further discussed in section 4.5.4a)
  - $ATI$  = air thawing index, in °F-days (see Appendix E for typical calculation)
  - $L_n = \gamma_d (\omega/100)144$ , the latent heat for thaw front layer  $n$  (in BTU/ft<sup>3</sup>)
  - $\omega$  = soil moisture content (in %)
  - $R_n \dots R_{n-1}$  = individual layer thermal resistances, equal to layer thicknesses divided by their respective average thermal conductivities (in hr-ft<sup>2</sup>-F°/BTU)
  - $\lambda$  = dimensionless Lambda Coefficient (accounts for soil sensible heat)

The Lambda Coefficient ( $\lambda$ ) is determined from published graphs with knowledge of the fusion parameter ( $\mu$ ), or Stefan Number ( $Ste$ ), and a thermal ratio ( $\alpha$ ) of absolute values of initial surface temperature-to-freezing temperature and freezing temperature-to-mean soil layer temperature ( $T_{mst}$ ) differentials. If the phase change isotherm ( $T_f$ ) is moving through the  $n$ th layer of a multilayered strata,  $\lambda_n$  is found after using depth weighted average specific and latent heat properties to calculate the Stefan Number as  $Ste_n = C_{avg} (T_{mst} - T_f)/L_{avg}$ . A depth of freeze calculation ( $X_f$ ) is performed with appropriate substitution of the surface freezing index ( $SFI$ ) for  $STI$ . The  $SFI$  is the product of the air freezing index ( $AFI$ ) and surface freeze n-factor ( $n_f$ )

The computer program specifies a latent heat value of 0.001 BTU/ft<sup>3</sup> for rigid, plastic, foam insulation (Zone I and II applications) so that equation [3-9] is not divided by zero. This also allows the model to determine if the thaw (or freeze) front is contained within this layer (Braley, 1984). BERG-2 also estimates thaw consolidation of the multilayered system.

Specific heat capacities, conductivities, and latent heats were determined by BERG-2. In specifying the geographic location, Fairbanks, Alaska, average air temperature

climatological data are incorporated within the computer code. The site general soil profile (Figure 3-3), was again used for the BERG-2 analysis. This time, however, the thin bedding sand layer was individually identified as part of the multilayered profile.

LAYER NUMBER 1 OF 7	
1: GRAVEL 2: SAND 3: SILT 4: ASPHALT 5: CONCRETE 6: INSULATION	
MATERIAL NUMBER .....	1
THICKNESS OF LAYER (FT) .....	1
<b>THAW CYCLE</b>	
FROZEN % MOISTURE .....	4
FROZEN DENSITY OF LAYER (LB/FT <sup>3</sup> ) .....	130
FROZEN HEAT CAPACITY (BTU/FT <sup>3</sup> -°F) .....	24.7
FROZEN CONDUCTIVITY (BTU/FT-HR-°F) .....	1.15
LATENT HEAT (BTU/ FT <sup>3</sup> ) .....	749
THAWED % MOISTURE .....	4
THAWED DENSITY OF LAYER (LB/FT <sup>3</sup> ) .....	130
THAWED HEAT CAPACITY (BTU/FT <sup>3</sup> -°F) .....	27.3
THAWED CONDUCTIVITY (BTU/FT-HR-°F) .....	1.37
<b>FREEZE CYCLE</b>	
LATENT HEAT OF FUSION (BTU/ FT <sup>3</sup> ) .....	749
FROZEN DENSITY (LB/FT <sup>3</sup> ) .....	130
FROZEN HEAT CAPACITY (BTU/FT <sup>3</sup> -°F) .....	24.7
FROZEN CONDUCTIVITY (BTU/FT-HR-°F) .....	1.15

**Figure 3-6.** Typical individual layer geotechnical parameters for BERG-2 analysis.

Computer simulations were generated from specific geotechnical data from boring logs of vent wells VW-1 through VW-5. Figure 3-6 illustrates the typical individual layer parameters BERG-2 incorporated in the overall freeze-thaw analysis. For the snow covered D-1 case (Figure 3-7a), and without snow cover (Figure 3-7b), the depth of thaw and freeze estimates are illustrated for the VW-3 (active warming) location. If the depth of estimated thaw is greater than that of potential freeze (Figure 3-7a), then frozen ground conditions

should not predominate the subsurface. However, for a surface condition without snow cover in winter, BERG-2 estimated a greater depth of freeze (Figure 3-7b). With continuous active warming (heat tape), no freeze cycling was anticipated for the Zone II test plot.

The BERG-2 simulations for soils in the vicinity of vent wells VW-1 through VW-3 indicated that estimated thaw depths would be significantly greater than potential freeze depths. The TIS designs should, in theory, limit any potential freeze front to soils above the contamination level (7 foot depth) within the Zone I and II treatment areas. Additionally, the advantages of active soil warming would further reduce, if not eliminate, a potential freeze front within the Zone II vadose zone.

Location		Thaw N	Frez N	MAAT	Thaw °F-day	Frez °F-day	Thaw Days	Frez Days
Fairbanks		1.70	0.50	26	2967	5303	161	204
T C H Y A C W L E	Frozen % Moisture	4.0	0.0	6.0	7.0	10.0	12.0	14.0
	Frozen Density	130.0	1.80	110.0	125.0	128.0	122.5	117.4
	Latent Heat	749	.001	950	1260	1844	2117	2367
	Frozen Heat Capacity	24.70	3.00	22.00	25.63	28.17	28.17	28.18
	Frozen Conductivity	1.15	0.02	0.82	1.51	2.27	2.21	2.15
	Thawed % Moisture	4.0	0.0	6.0	7.0	10.0	12.0	14.0
	Thawed Density	130.0	1.80	110.0	125.0	130.0	124.9	120.0
	Thawed Heat Capacity	27.30	3.00	25.30	30.00	35.10	36.22	37.20
	Thawed Conductivity	1.37	0.02	0.99	1.47	1.83	1.71	1.59
	Initial Thickness	1.00	0.17	0.17	3.00	5.00	3.70	10.00
	Amount Thawed	1.00	0.17	0.17	3.00	0.84	0.00	0.00
	Consolidation	----	----	----	----	0.02	0.00	0.00
	Final Thickness	1.00	0.17	0.17	3.00	4.98	3.70	10.00
	F C R Y E C E L Z E E	Latent Heat	749	0	950	1260	1872	2158
	Frozen Density	130.0	1.83	110.0	125.0	128.0	122.5	117.4
	Frozen Heat Capacity	24.70	3.00	22.00	25.63	28.17	28.17	28.18
	Frozen Conductivity	1.15	0.02	0.82	1.51	2.27	2.21	2.15
	Initial Thickness	1.00	0.17	0.17	3.00	4.98	3.70	10.00
	Amount Frozen	1.00	0.17	0.17	2.02	0.00	0.00	0.00
<b>Estimated Thaw = 5.18 ft.</b>		<b>Consolidation = 0.02 ft.</b>				<b>Freeze = 3.36 ft.</b>		

(a) VW-3 (with snow cover)

Figure 3-7. BERG-2 freeze-thaw analyses at VW-3 for (a) snow cover and (b) without snow cover surface conditions.

Location		Thaw N	Frez N	MAAT	Thaw °F-day	Frez °F-day	Thaw Days	Frez Days
Fairbanks		1.70	1.00	26	4000	6900	165	200
		<b>1</b>	<b>2</b>	<b>3</b>	<b>4</b>	<b>5</b>	<b>6</b>	<b>7</b>
T C H Y A C W L E	Frozen % Moisture	4.0	0.0	6.0	7.0	10.0	12.0	14.0
	Frozen Density	130.0	1.80	110.0	125.0	128.0	122.5	117.4
	Latent Heat	749	001	950	1260	1844	2117	2367
	Frozen Heat Capacity	24.70	3.00	22.00	25.63	28.17	28.17	28.18
	Frozen Conductivity	1.15	0.02	0.82	1.51	2.27	2.21	2.15
	Thawed % Moisture	4.0	0.0	6.0	7.0	10.0	12.0	14.0
	Thawed Density	130.0	1.80	110.0	125.0	130.0	124.9	120.0
	Thawed Heat Capacity	27.30	3.00	25.30	30.00	35.10	36.22	37.20
	Thawed Conductivity	1.37	0.02	0.99	1.47	1.83	1.71	1.59
	Initial Thickness	1.00	0.17	0.17	3.00	5.00	3.70	10.00
	Amount Thawed	1.00	0.17	0.17	3.00	0.84	0.00	0.00
	Consolidation	----	----	----	----	0.02	0.00	0.00
	Final Thickness	1.00	0.17	0.17	3.00	4.98	3.70	10.00
F C R Y E C E L Z E E	Latent Heat	749	0.00	950	1260	1872	2158	2419
	Frozen Density	130.0	1	110.0	125.0	128.0	122.5	117.4
	Frozen Heat Capacity	24.70	1.80	22.00	25.63	28.17	28.17	28.18
	Frozen Conductivity	1.15	3.00	0.82	1.51	2.27	2.21	2.15
	Initial Thickness	1.00	0.02	0.17	3.00	4.94	3.70	10.00
	Amount Frozen	1.00	0.17	0.17	3.00	3.10	0.00	0.00
<b>Estimated Thaw = 7.33 ft.</b>		<b>Consolidation = 0.06 ft.</b>			<b>Freeze = 7.44 ft.</b>			

(b) VW-3 (without snow cover)

**Figure 3-7 continued.**

It is interesting to note that although vent wells VW-4 and VW-5 are located within and adjacent to reported permafrost boundaries, their BERG-2 depths of freeze calculations (for the snow cover case) were less than those for the other three vent well locations. The VW-4 and VW-5 depth of freeze calculations cannot be relied upon for design since field temperature data revealed frozen ground at greater depths in winter. The assumption that mean annual surface temperatures above freezing does not apply at these locations. Additionally, because of soil heterogeneities, VW-4 and VW-5 boring log information was not necessarily applicable for BERG-2 analyses of the whole of Zone I and Zone III treatment plots.

### 3.2.2c Thermocouple Installations

Type T thermocouples were used for the thermal monitoring of the three treatment plots. T-type thermocouples are constructed with copper and constantan male spades for easy insertion into an Omega microprocessing thermometer. Two or three thermocouples were typically tied to a ½-inch diameter CPVC conduit, each fastened separately at a different position (length) along the conduit. The CPVC-thermocouple assemblies were then placed into the excavated boreholes, which were then backfilled. Thermocouples were consequently installed at various depths between 1.5 and 16.0 feet throughout the bioventing site vadose zone. Table 3-3 identifies the fourteen thermal monitoring points (Figure 3-2) with their respective discrete thermocouple embedment depths.

Efforts were made to install thermocouples at similar depths throughout the vadose zone. However, collapse of loosened sandy-gravel soils at depth in the borings, during auger [drilling] extraction, prevented installations to the groundwater table at some monitoring points. Notwithstanding, a minimum of four thermal monitoring points were strategically implanted within each of the three treatment areas. Sufficient thermocouples were imbedded so that subsurface temperatures could be extrapolated or inferred to the groundwater table from compiled data. The thermocouple installations took place during June, July and early October 1994. The Zone I and II TIS materials were also installed in early October 1994. Active soil warming began on November 7, 1994 and was continuously operated throughout the bioremediation effort.

**Table 3-3.** Thermocouple installations at the UAF bioventing site  
(refer to Figure 3-2 for monitoring point locations).

<b>Treatment Area</b>	<b>Thermal Monitoring Point</b>	<b>Embedment Depth (ft.)*</b>
Background	MP-9	7.8, 12 and 14.8
Zone I (passive warming)	MP-12	5.3, 9.5 and 12.4
	MP-13	2.5, 8 and 10
	MP-14	1, 4.5 and 9.5
	TC-3	1.2 and 4.2
	TC-4	4, 7 and 10
Zone II (active warming)	MP-3	7.7
	MP-6	8.3
	TC-1	4.7 and 6.7
	TC-2	1.5, 6.8 and 9.2
Zone III (no action control)	MP-7	7, 10 and 12.5
	MP-8	3 and 7
	MP-10	4.8, 9 and 16.9
	MP-11	7.1, 11.3 and 14.2

\* Depth below natural ground surface.

---

## Heat Transfer Theory and Biovented Soils

Primary consideration is given here to heat transfer analysis of the three test plots. This chapter defines and compares the site specific heat transfer problem for each of the treatment zones. The appropriate conductive heat transfer equation and boundary conditions for each are presented for modeling. Convective heat transfer, associated with venting at the injection wells, is shown to have minimal contribution to overall soil warming.

### 4.1 General Equations of Transfer

Luikov (1966) and Bear (1972) derive the comprehensive system of fluid momentum, energy, and mass transfer equations that pertain to porous media. Their analyses incorporate a variety of transfer coefficients into the differential equations to account for variability in moisture contents, soil structure, velocity distributions, temperature and other parameters. A summary of the general equations of momentum and mass transfer are presented in Appendix E. The reader is directed to initial work by Luikov (1966) and Bear (1972), and later treatises by Johnson et al. (1990) and Fetter (1993), for quantitative analyses of contaminant fate and transport phenomenon in unsaturated soils.

The Zone II (actively warmed) test plot is used for the following qualitative heat transfer discussion.

## 4.2 The Heat Transfer Problem

Heat transfer within the unsaturated zone of surface-insulated treatment areas is assumed to be governed by conduction. This is because 1) convection, associated with injection well venting, is negligibly small, 2) moderate soil permeabilities, 3) the polystyrene insulation layer is effectively impervious to surface-water infiltration, and 4) the TIS materials collectively diminish surface convection (due to variable winds and air density) influence on the subsurface.

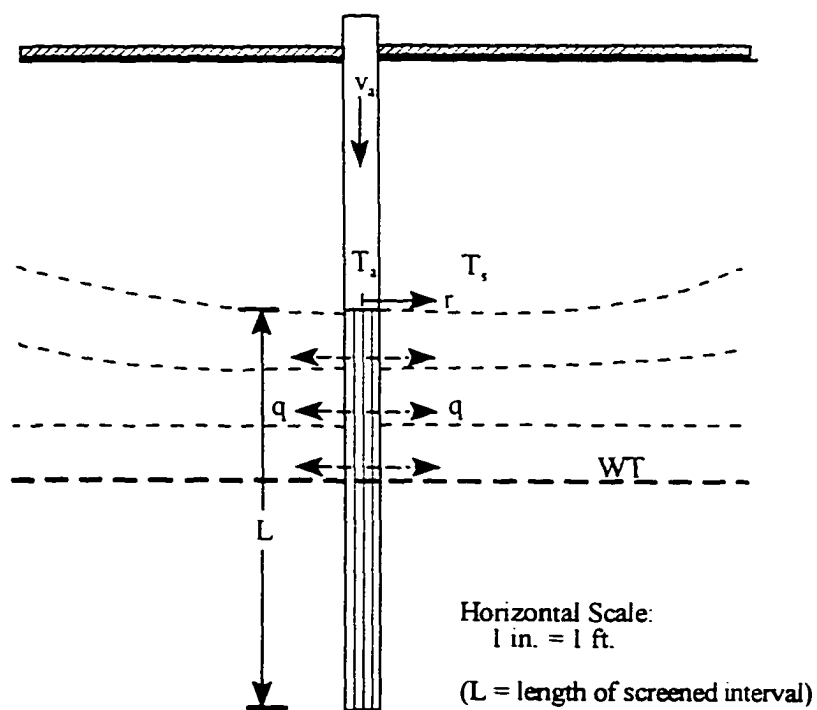
However, some measure of surface heat transfer occurs through convection, long wave (infrared) and solar radiation, and evaporation. These transfers are most influential to the untreated (Zone III) test plot. Delineating surface boundary conditions with appropriately chosen *n-factors* accounts for their effects (section 4.6.4a). Additionally, incidental convective heat losses were locally realized within the test plots, where monitoring point casings and riser extensions acted as vertical transfer conduits. Winter ice-crystal formations on the undersides of riser lids and steamy summertime conditions within riser head spaces evidenced this convection. To negate local convective heat losses, plugs of 2-inch thick polystyrene insulation, mounted to 2-inch thick plywood bases, were installed in all monitoring point risers.

## 4.3 Convection and Soil Venting

Convective heat transfer also occurs at the vent wells. Convective warming occurs seasonally, when the injected air temperature is greater than the temperature of the soils surrounding the vent wells. In winter, when the injected air temperature is colder than the soil temperature(s), no warming occurs with vent well convection. The following discussion will show that this convective heat contribution to soil warming is localized and negligible when compared to the heat conduction occurring.

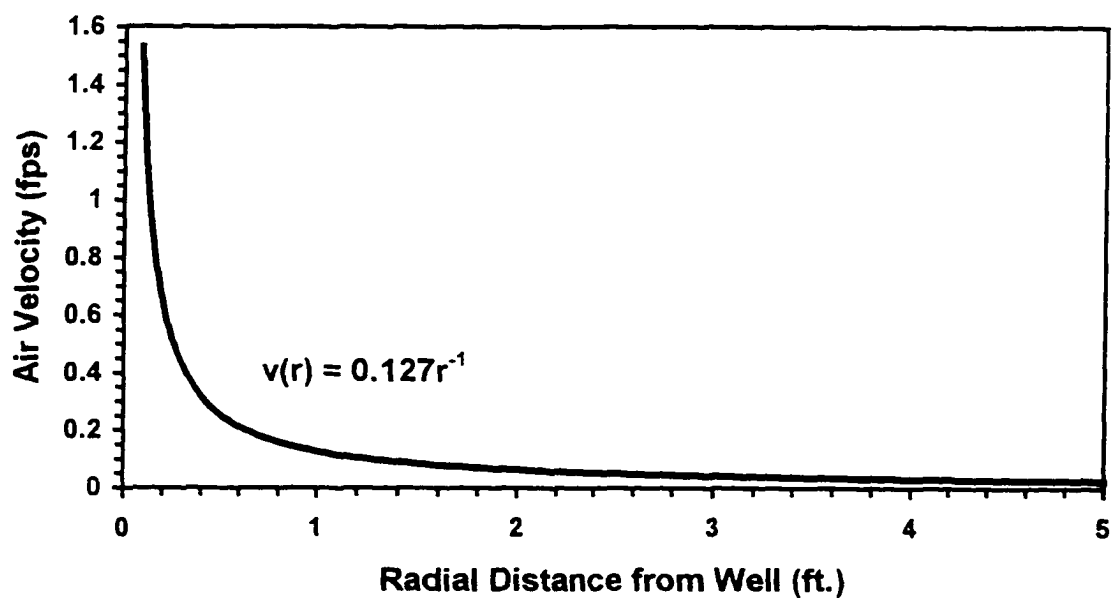
A type T thermocouple was installed through the top of vent well VW-5, allowing the air-injection temperature to be measured during thermal monitoring events. The temperature difference between atmospheric and injected air attests to warming induced by the vent well blowers. This temperature differential typically measured between 15°F and 22°F.





(a)

### Velocity Profile at a Vent Well



(b)

**Figure 4-1.** (a) Convective heat transfer and (b) conceptual velocity distribution at a vent well.

For the Zone II [and Zone I] test plots, heat flux from the vent well screens essentially follows flow paths that are confined by the groundwater table and surface TIS materials (Figure 4-1a). A measure of vent well heating effect, based on the mass flow rate of air, can be approximated by

$$q = \dot{m}_a C_{pa} (T_a - T_s) \quad [4-1]$$

where  $q$  = heat flux (in BTU/hr)  
 $\dot{m}_a$  = air mass flow rate (in lb<sub>m</sub>/hr), equal to  $\rho_a Q$  ( $Q = 2$  cfm, the injection rate)  
 $\rho_a$  = average air density, equal to 0.08 lb<sub>m</sub>/ft<sup>3</sup>\*  
 $C_{pa}$  = average air specific heat at constant pressure, equal to 0.24 BTU/lb<sub>m</sub>-°F\*  
 $T_a$  = injection well air temperature (in °F)  
 $T_s$  = average soil temperature (in °F)

Assuming a negligible pressure differential through a vent well, and according to the measured injection air and subsurface soil temperatures (Table 4-1), convective heat flux was calculated between 0 and 100 BTU/hr over the effective season (mid-March through September). The 1500 feet of heat tape produced between 8415 and 14100 BTU/hr over its operating temperature range (Table 4-1). Therefore, the heat contribution from one vent well (VW-3) represented less than 1.3 percent that of the electrical heat tape. The effects of this negligibly small contribution are further diminished during winter, when the vadose zone soils were warmer than the injected air.

The comparative magnitude between these two heat contributions was further realized with use of the Péclet Number ( $P_e$ ). The Péclet Number, the product of the Reynolds and Prandtl numbers and a ratio of convective to conductive heat transfer, can be approximated for uniform horizontal flow through porous medium as

$$P_e = N_R P_r = (v d_{10} / \nu_a)(\nu_a / \alpha) = v d_{10} / \alpha \quad [4-2]$$

(after Nield and Bejan, 1992)

---

\*Although the density and specific heat of air vary with temperature, their variability is very small over a large temperature range ( $\rho_a$  is 0.09 to 0.07 pcf between -20 °F and 100 °F;  $C_{pa}$  is 0.239 to 0.241 BTU/lb<sub>m</sub>-°F between 0 °F and 200 °F) (Wark, 1983).

where  $\nu_a$  = air kinematic viscosity (in ft<sup>2</sup>/s)  
 $v$  = uniform Darcy velocity (in ft/s)  
 $\alpha$  = soil thermal diffusivity (in ft<sup>2</sup>/s); the ratio of soil thermal conductivity (K) to volumetric specific heat (C)  
 $d_{10}$  = effective [grain] size (in ft) (When known, the average soil particle diameter should be used.)

**Table 4-1.** Approximate heat flux at a vent well versus heat tape output.

Date	T <sub>s</sub> <sup>*</sup> (°F)	T <sub>s</sub> <sup>^</sup> (°F)	q (BTU/hr)	Heat Tape Operating Temp. (°F)	q <sub>HT</sub> <sup>*</sup> (BTU/hr)
June 5, 1995	83.4	43	100		
July 28, 1995	90.6	50	93.5	80	8415
Sept. 8, 1995	64.8	48	38.7		
Oct. 20, 1995	37.3	46	nc		
Nov. 25, 1995	1.3	45	nc		
Jan. 19, 1996	-7.0	43	nc	30	14100
Mar. 22, 1996	53.6	44	22.1		
April 22, 1996	84.2	45.5	89.2		

\*Measured at VW-5. <sup>^</sup> Average soil temperature from the top of the vent well screened interval to the groundwater table. \*Hourly rate based on equation [4-11] (sec. 4.6.2), multiplied by 1500 linear feet of tape. nc = no convective heat contribution (typically between Oct. and mid-March).

Maintaining flow continuity (2 cfm) between the vent well and its radius of influence, the air velocity through the vadose zone can be expressed as a function of the radial distance (r) out from the well as  $v(r) = 0.127r^{-1}$ . The air velocity decreases rapidly within a short

\* From

$$v_r = \frac{v_w A_w}{A_r} = \frac{v_w (2\pi r_w L)}{2\pi r L} = \frac{v_w r_w}{r} = \frac{Q_w r_w}{A_w r} = \frac{\left(\frac{2\text{ft}^3}{\text{min}} \cdot \frac{1\text{min}}{60\text{s}}\right) \cdot \left(\frac{1}{12}\text{ft}\right)}{\pi \left(\frac{1}{12}\text{ft}\right)^2} \cdot \frac{1}{r} = 0.127r^{-1}$$

where subscripts w and r on velocity (v), area (A), radius (r), and flow rate (Q) terms are with respect to injection well and radial geometries (Figure 4-1a), respectively.

[radial] distance from the well (Figure 4-1b). Substituting this expression as the uniform Darcy velocity in the Reynolds number, equation [4-2] becomes

$$P_e = v(r) \cdot d_{10} / \alpha \quad [4-3]$$

As the radial distance ( $r$ ) away from the well is increased, the air velocity through the soil decreases and the Péclet Number becomes smaller. For the range of frozen and thawed thermal diffusivities associated with soil layers 5 and 6 (sec. 4.6.1, Table 4-3) Péclet Numbers declined to 1 or less for soils within five feet from the vent well (Table 4-2). In other words, convective warming, associated with an injection well, is a small contribution to the overall heat transfer through the subsurface. Only soils in the immediate vicinity of a well were influenced by injected air temperatures that were typically less than 20°F above ambient on any given day of bioventing.

**Table 4-2.** Péclet Numbers and vent well convection influence.

Radius, $r$ (ft.)	$\alpha_t^*$ (ft <sup>2</sup> /s)	$P_e$	$\alpha_r^{\wedge}$ (ft <sup>2</sup> /s)	$P_e$
0.1	0.0000067	57	0.0000133	29
0.2	0.0000067	28	0.0000133	14
0.5	0.0000067	11	0.0000133	5.7
1.0	0.0000067	5.7	0.0000133	2.9
2.0	0.0000067	2.9	0.0000133	1.4
3.0	0.0000067	1.9	0.0000133	0.9
5.0	0.0000067	1	0.0000133	0.5

\*Based on Layer 5, thawed soil properties (sec. 4.6.1, Table 4-3)

<sup>^</sup>Based on Layer 6, frozen soil properties (sec. 4.6.1, Table 4-3)

#### 4.4 Heat Diffusion Analysis

Derivation of the transient heat conduction equation(s) requires consideration of the overall soil warming aspect of the bioventing process. Below the Zone II treatment pad, a state of relative thermal equilibrium was established throughout the vadose zone after some time of continuous heat tape operation. It took approximately two months to create a "thermal bulb" of influence. Subsequently, temperature gradients became smaller over time and were realized primarily in the vertical ( $z$ ) direction and laterally ( $x$  and  $y$  directions) at the test plot boundaries.

When analyzing an element of unsaturated soil (a unit thickness of 1 in the  $y$  direction), the heat conduction problem can be treated two-dimensionally without sacrificing accuracy (except at the treatment area boundaries).

Consider a unit volume of the biovented vadose zone under the initial assumptions of constant thermal conductivities (constant  $K_x$  and  $K_z$ , but  $K_x \neq K_z$ ) and otherwise isotropic conditions. Figure 4-2 illustrates the conservation of heat energy through this soil volume as energy in equals energy out plus the change in internal energy with respect to time, or

$$Q_{in} = Q_{out} + \Delta Q \quad [4-4]$$

where, using Fourier's law,

$$Q_{in} = Q|_z + Q|_x = - \left[ K_z A_z \frac{dT}{dz} \right]_z - \left[ K_x A_x \frac{dT}{dx} \right]_x$$

$$Q_{out} = Q|_{z+\Delta z} + Q|_{x+\Delta x} = - \left[ K_z A_z \frac{dT}{dz} \right]_{z+\Delta z} - \left[ K_x A_x \frac{dT}{dx} \right]_{x+\Delta x}$$

(areas  $A_z = 1 \Delta x$  and  $A_x = 1 \Delta z$ )

and

$$\Delta Q = Q_c - Q_L - Q_e - Q_{HT}$$

$$Q_c = V C \frac{dT}{dt} \quad (\text{volume } V = \Delta y \Delta z \Delta x = 1 \Delta z \Delta x)$$

In these relationships  $Q_c$ ,  $Q_L$ ,  $Q_e$  and  $Q_{HT}$  represent the *soil sensible heat*, latent heat, *heat of [evaporative] dissociation*, and heat tape contributions (in BTU/hr) to the overall change in heat energy occurring within the element. Here also,  $C$  is *volumetric specific heat*, latent heat is associated with phase changes (freeze-thaw cycles), and  $\Delta$  indicates an incremental change with distance.

Substitution of the various heat contributions into equation [4-4] and rearranging terms yields

$$- \left[ K_z \Delta x \frac{dT}{dz} \right]_z + \left[ K_z \Delta x \frac{dT}{dz} \right]_{z+\Delta z} - \left[ K_x \Delta z \frac{dT}{dx} \right]_x + \left[ K_x \Delta z \frac{dT}{dx} \right]_{x+\Delta x} = \Delta z \Delta x C \frac{dT}{dt} + Q_L + Q_e - Q_{HT} \quad [4-5]$$

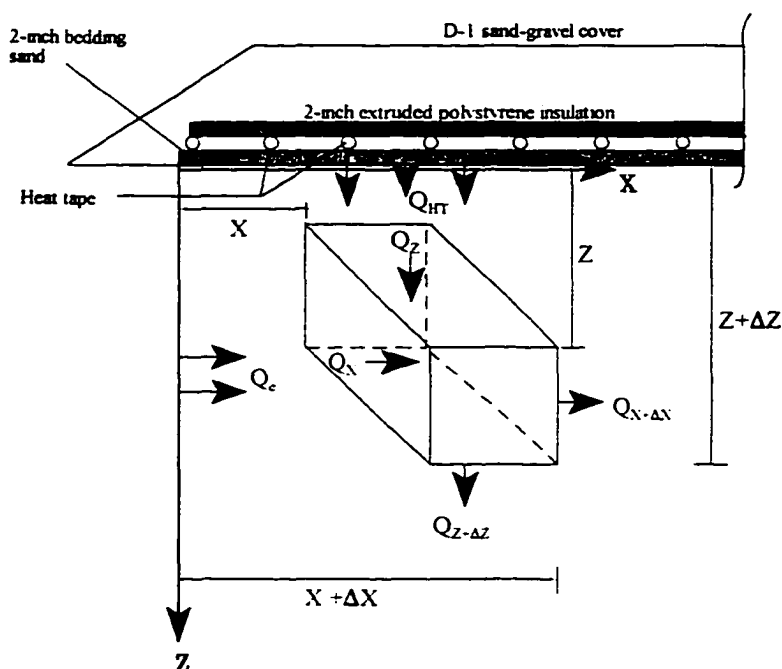


**Figure 4-2.** Heat transfer through a volumetric unit of Zone II unsaturated soil.

Dividing equation [4-5] by  $\text{area} \Delta z \Delta x$  and taking the limit as  $\Delta z \Delta x$  approaches 0 results in the non-steady state 2D heat flux equation

$$\frac{\partial}{\partial z} \left( K_z \frac{\partial T}{\partial z} \right) + \frac{\partial}{\partial x} \left( K_x \frac{\partial T}{\partial x} \right) = C \frac{\partial T}{\partial t} + q_L + q_e - q_{HT} \quad [4-6]$$

where  $q_L$ ,  $q_e$ , and  $q_{HT}$ , are heat generation terms per unit volume.

With respect to the Zone II treatment plot, latent heat effects can be neglected since no freeze-thaw cycling occurred within the vadose zone throughout the year. Additionally, heat loss through moisture evaporation, induced by soil venting, is negligible even compared to convection at the vent wells. This later assertion is supported by the microbiological testing results (sec. 6.4.2), in that the low injection flow rate used (2cfm) throughout bioventing caused little appreciable soil drying. The impervious nature of the surface TIS cover also likely aided in reducing moisture content losses. Therefore, equation [4-6] can be reduced to the governing 2D heat diffusion equation for Zone II thermal analysis

$$\frac{\partial}{\partial z} \left( K_z \frac{\partial T}{\partial z} \right) + \frac{\partial}{\partial x} \left( K_x \frac{\partial T}{\partial x} \right) = C \frac{\partial T}{\partial t} - q_{HT} \quad [4-7]$$

For homogeneous and isotropic media, soil thermal conductivities and specific heats are assumed constant throughout each individual layer. Consequently, the Zone II heat diffusion equation can be further reduced to

$$\frac{\partial^2 T}{\partial z^2} + \frac{\partial^2 T}{\partial x^2} = \left( \frac{C}{K} \right) \frac{\partial T}{\partial t} - \frac{q_{HT}}{K} \quad [4-8]$$

where the relationship  $K/C$  is the thermal diffusivity ( $\alpha$ ).

This partial differential equation is first order in time and second order in space, requiring an initial temperature(s) condition and at least four boundary conditions to solve. These initial and boundary conditions are defined in section 4.6.5.

#### 4.5 About TDHC

Extreme surface temperature changes associated with cold regions can produce a high degree of variability in vadose zone physicochemical and physicommechanical characteristics. Additionally, some measure of variability in geotechnical parameters and geochemical transformations cannot be accounted for with practical computer modeling. Nevertheless, the UAF treatment zone geometries and site specific boundary conditions do allow a finite element numerical analysis, with approximate solution to the heat diffusion problem.

Zarling and Goering (1985) developed the two-dimensional heat conduction (TDHC) finite element code capable of varying soil thermal properties at incremental time steps. The 2D, unsteady state heat conduction equation (4-6) is solved by applying a technique formulated using the Galerkin weighted residual process to discretize the time and space domains of a soil regime (Goering, 1984). The process solution requires:

- 1) dividing the treatment area (Zone II in this case) into smaller subregions (soil columns), and then discretizing the representative subregion into a finite element grid.

- 2) applying the Galerkin weighted residual process to the discretized (divided) time and space domains,
- 3) thereby producing a set of simultaneous equations for each incremental time step, and
- 4) approximating a temperature field for each time step by solving the corresponding set of equations.

Step 1 is arbitrarily accomplished by the user and requires an input data file (sec.4.6.1, Table 4-3) be supplied. The user then defines the program run time, output data interval, and the problem initial boundary conditions (section 4.6.5). Steps 2 and 3 are accomplished by TDHC, provided the governing equation (4-8) can be written in the form

$$\psi[T] - F = \varepsilon \quad (\text{after Goering, 1984}) \quad [4-9]$$

where

- $\psi$  = differential operator
- $T$  = approximate temperature solution
- $F$  = forcing function (right hand side of equation [4-8])
- $\varepsilon$  = error, associated with approximate solution

The error is minimized by the multiplication of a weighting function, integrating this product over the problem domain, with the resultant set equal to zero (Goering, 1984). In equation form, the integration looks like

$$\int_D W_i \varepsilon dD = \int_D W_i (\psi [T] - F) dD = 0 \quad [4-10]$$

where

- $W_i$  = Galerkin weighting function for time step  $i$
- $D$  = problem domain

The Galerkin weighting function is chosen such that the differential operator ( $\psi$ ) is rendered statistically independent of as many linearly independent functions (domain variables) as possible (Keener, 1988). Essentially, the Galerkin weighted residual process minimizes the effects of variability in the independent soil and physicochemical properties.



For a comprehensive understanding of the TDHC model the reader should consult the original work by Goering (1984).

Kane et al. (1991) demonstrated that TDHC could be used with confidence to model the soil thermal regime. For geotechnical application, TDHC affords qualitative computer modeling as long as small incremental time steps are applied. The TDHC model is used, with slight modification, to account for the Zone II self-regulating heat tape variable output.

#### **4.6 The Zone II Heat Conduction Problem Defined**

Soil warming within the Zone II confines is a spatial differential heat transfer problem, and can be modeled one-dimensionally during the first two years of bioventing operation. The two-inch polystyrene insulation layer minimizes heat loss to the [surface] overlying D-1 soils. Heat is generally conducted downward through the vadose zone from the heat tape grid, with some lateral escape at the boundaries. Once a state of relative thermal equilibrium is reached within soils to the water table, heat transfer becomes more two-dimensional at the treatment area boundaries. Comparisons between the month-to-month field temperature data for the twenty months of bioventing, indicated a thermal state that had not yet achieved relative equilibrium within the treated unsaturated soils. The cooler soils at the groundwater table continued to conduct heat in the vertical ( $z$ ) direction. Therefore, a thin, rectangular, columnar soil element (Figure 4-5) suffices for the TDHC one-dimensional analysis of the interior region of the active warming test plot.

Beyond two years, as dominant heat losses occur at the boundaries, the heat transfer problem evolves into a 2D analysis. A cross-sectional cut through the boundary of one side of the test plot, defined in cartesian coordinates, would suffice for TDHC modeling (see section 4.8).

A number of input parameters need to be defined before an accurate assessment of heat transfer can be performed by TDHC. First, for the site general profile (Figure 3-3), soil dry unit weights ( $\gamma_d$ ), average moisture contents, latent and specific heats, and thermal conductivities need to be quantified. Second, the heat tape energy contribution in equation [4-7] needs to be defined. The representative thermal conductivity of the polystyrene

insulation layer must be defined for the “operational” temperature range associated with the bioventing effort. Lastly, boundary conditions must be delineated with respect to treatment zone geometry and the groundwater table.

#### 4.6.1 Site Specific Geotechnical Parameters

Including the thin bedding sand layer for the thermal analysis, and differentiating between saturated and unsaturated soils in the deepest strata, the Figure 3-3 soil profile is redefined with 6 layers according to Table 4-3. Table 4-3 summarizes the geotechnical parameters necessary for TDHC input. Layer thicknesses, soil dry unit weights, and moisture contents are average values based on historically reported laboratory data.

**Table 4-3.** TDHC layer input data.

Sub-region	Material	Geotechnical Parameters							
		D (ft.)	$\gamma_d$ (pcf)	$\omega$ (%)	L ( $\frac{\text{BTU}}{\text{ft}^2}$ )	$K_r$ ( $\frac{\text{BTU}}{\text{hr-ft-}^\circ\text{F}}$ )	$K_r$ ( $\frac{\text{BTU}}{\text{hr-ft-}^\circ\text{F}}$ )	$C_i$ ( $\frac{\text{BTU}}{\text{ft}^2-^\circ\text{F}}$ )	$C_r$ ( $\frac{\text{BTU}}{\text{ft}^2-^\circ\text{F}}$ )
1	Compacted D-1 sand-gravel	1	130	4	749	1.37	1.15	27.3	24.7
2	Polystyrene insulation	0.167	1.8	0	0	0.0165 <sup>Δ</sup>		0.54*	
3	Soft bedding sand	0.167	85	4	490	0.49	0.25	17.8	16.1
4	Dense sandy-gravel	3	125	7	1260	1.47	1.51	30.0	25.6
5	Med.dense-dense sandy silt w/gravel	5	110	8	1267	0.67	0.65	27.5	23.1
6	Loose-med.dense sandy gravel	3.7	120	6	1037	1.24	1.16	27.6	24.0

Δ Based on a weighted average of thermal conductivities over the operational temperature range of the insulation during the bioventing process (see section 4.6.3).

\*  $C_r = C_i = \gamma_t (0.3 \text{ BTU/lb-}^\circ\text{F})$ , assuming no moisture is absorbed by the insulation.

Volumetric specific heats and latent heats were then calculated from the data using

$$C_f = \gamma_d (0.17 + 0.5\omega/100) \quad (\text{frozen soils})$$

$$C_t = \gamma_d (0.17 + 1.0\omega/100) \quad (\text{thawed soils})$$

$$L = \gamma_d (\omega/100)144$$

where subscripts f and t denote frozen and thawed soil conditions. Average thermal conductivities, based on the site specific  $\omega$  and  $\gamma_d$  values, were extrapolated from published frozen and unfrozen thermal conductivity charts (Andersland and Ladanyi, 1994).

#### 4.6.2 Heat Tape Energy Contribution

The manufacturer's specification for the Zone II Chromalux SRL3-2 heat tape thermal output rating is nominal 3 watts per linear foot, operating at 50°F and with 240 volts of power supplied. This rating is based on a laboratory pipe application test, where a first-order linear relationship for heat output ( $q_{HT}$ ) as a function of temperature was approximated as  $q_{HT} = -0.09T + 14.68$  (BTU/ hr-ft). For this test, the heat tape's external environment was air.

The self-regulating, rapid-trace heating cable is designed with twin copper buss wires, sheathed with a semiconductive polymer (Polyolefin) core, whose electrical resistance varies with temperature. Therefore, as the process temperature drops in the rate equation, the core's heat output increases. Conversely, heat output decreases as the heat tape temperature rises. However, for geotechnical application and operation at 208 volts, a new output rating model is required.

The manufacturer's specification indicates that for the alternate 208 volt operation, the average heat tape energy output is 80 percent that of the 240 volt specification. This corresponds to a rate equation of  $q_{HT(80\%)} = -0.072T + 11.74$  (BTU/ hr-ft). However, a direct power comparison using Kirchoff's Law suggests a 75 percent alternate energy output as

$$P_1 = \frac{I_1^2}{R} \quad \text{and} \quad P_2 = \frac{I_2^2}{R}$$

$$\frac{P_2}{P_1} = \frac{V_2^2}{V_1^2} = \frac{(208V)^2}{(240V)^2} = 0.75$$

$$P_2 = 0.75 P_1$$

where  $P$  is power,  $V$  is voltage and  $R$  is resistance. At a 25 percent reduction, the corresponding heat tape rate equation is  $q_{HT(75\%)} = -0.0675T + 11.01$  (BTU/ hr-ft). The discrepancy can be clarified with an understanding of the operational characteristics of a heating circuit and experimental analysis.

The long heat tape “open” circuits can be considered current dividers, with an infinite number of resistors connected in parallel across the element wires (the semi-conductive Polyolefin core). As some energy is lost by heating the copper wires, the amount of the loss across each resistor is proportional to the square of its current; the  $I^2R$  loss. Voltage dissipation results as current is continuously divided at successive resistors along the circuit length. In other words, the overall circuit resistance causes a voltage loss over the length of the circuit. The nature of the semi-conductive core is to minimize current division, reduce overall circuit resistance, and essentially “close” the loop. For a full length circuit (595 ft. for the SRL3-2 heat tape), the manufacturer indicates a maximum 10 percent voltage drop (at a 50 F operating temperature) by circuit’s end. As the operating temperature is increased, the energy loss is less. The converse is true with lower operating temperatures. Thicker copper circuit wires would conduct electricity more efficiently. However, the added cost for more protective sheathing material(s) may not justify this circuit benefit.

A series of experiments were performed on an eight-foot section of the Chromalox SRL3-2 heat tape, in a cold room maintained by the UAF School of Engineering. The heat tape, wired through its power connector box, was hard-wired to an interior, wall-mounted junction box. The junction box face plate was removed so that input current and voltage could be monitored with a clamp-on ammeter and digital voltmeter, respectively. This test circuit was rated for variable temperature operation under three conditions: 1) suspended in air, 2) embedded in [site] sandy gravel soils, and 3) laid between sandy gravel soils and Zone

II TIS materials. For the two soil experiments, a thin-walled, wooden, 8' x 9" x 7" box was constructed to hold the test circuit and TIS materials. Three T type thermocouples were taped to the heat tape, near the beginning, middle and end of the circuit. As the cold room temperature was varied between 72 F (ambient) and -15 F during each experiment, both the heat tape output and operating temperature were monitored over time.

The results of these experiments indicated that the heat tape output ratings were very similar for the three experiments. However, temperature variability across the circuit length indicated that the heat tape was temperature sensitive. The temperature differentiations are likely attributed to heat tape intrinsic properties and to surrounding soil moisture content and density variability. The two thermocouples mounted near the circuit ends also may have been influenced by boundary conditions.

A fourth experiment was conducted, in which the test circuit was enclosed inside 2-inch diameter (1-inch inside diameter) polyethylene pipe insulation. Two thermocouples were taped to the heat tape and extruded through razor cuts in the tubing. The insertion cuts and tube ends were sealed with weatherproof tape and insulation plugs, respectively, to form a completely sealed, constant temperature chamber. The cold room was heated up to 88 F and then gradually cooled to -10 F over 8 hours. The thermocouples and heat tape output energy were measured throughout the first half of the test at 5, 10, 15, 20, 30, and 45 minute intervals, as the cold room temperature dropped to -2 F. A final reading was taken 240 minutes later, to end the experiment.

Temperature variability between the thermocouples was reduced to less than 2 F (Table 4-4). The average thermocouple temperature was then calculated and used to plot the heat output versus temperature as Figure 4-3. The experimental heat tape rate equation is

$$q_{HT} = -0.0757T + 11.67 \text{ (BTU/ hr-ft)} \quad [4-11]$$

which is very close to that of the manufacturer's 208 volt specification. Equation [4-11] was used for the Zone II TDHC analysis.

**Table 4-4.** Heat tape output and temperature data for the constant temperature environment experiment.

TC1(°F)	TC2(°F)	TC <sub>avg</sub> (°F)	Q (BTU/hr-ft)
--	--	160.0	0
108.6	109.6	109.1	3.51
107.0	107.0	107.0	3.51
102.1	103.9	103.0	3.69
99.6	101.1	100.4	3.69
96.5	97.8	97.2	3.69
93.7	95.7	94.7	4.61
90.2	92.0	91.1	4.61
87.8	89.6	88.7	4.61
83.6	85.1	84.4	5.46
81.5	82.6	82.1	5.46
78.3	80.0	79.2	5.46
75.1	76.8	76.0	6.45
72.5	74.1	73.3	6.45
67.2	68.9	68.1	6.82
58.2	57.8	58.0	7.37

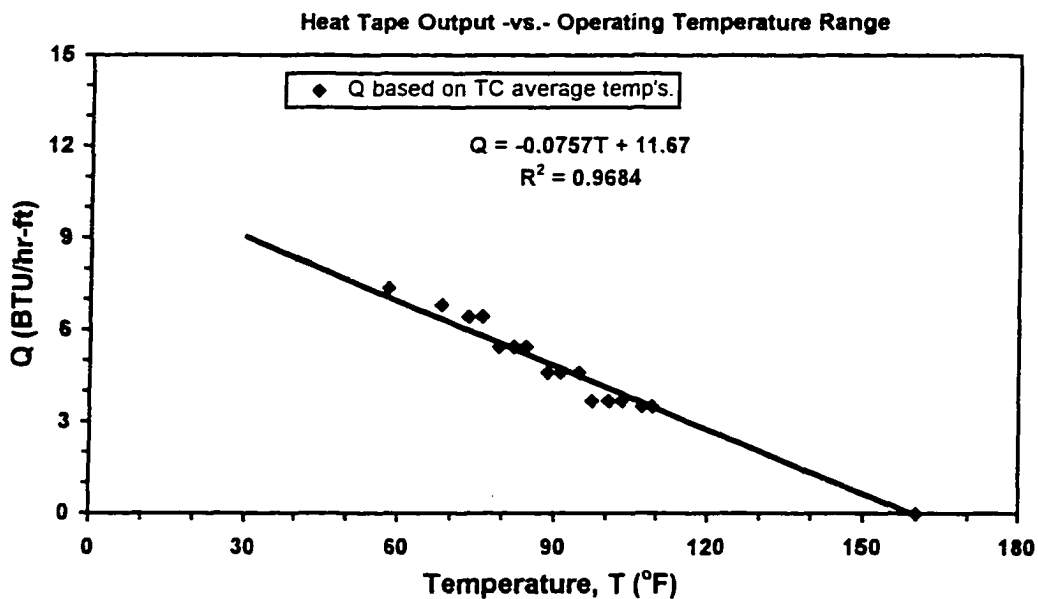


**Figure 4-3.** Experimental heat tape output versus operating temperature range.

### 4.6.3 Polystyrene Insulation Thermal Conductivity

Table 4-5 represents the Foamular 400 thermal conductivity information as supplied by Dow Chemical. This data was used to plot the variable temperature rating curve for this extruded polystyrene insulation (Figure 4-4).  $T_{mean}$  is the mean temperature of the temperature differential across one inch of insulation.

Table 4-5. Foamular 400 thermal conductivity data.

$T_{mean}$ (°F)	R value	$K^*$ (BTU-in/hr-ft <sup>2</sup> -°F)	$K^*$ (BTU/hr-ft <sup>2</sup> -°F)
-60	6.4	0.156	0.013
0	5.9	0.1695	0.0141
10	5.71	0.175	0.0146
25	5.6	0.1786	0.0149
40	5.4	0.185	0.0154
50	5.3	0.1887	0.0157
75	5.0	0.2	0.0167

$K^* = 1/R$  (per inch of insulation).  $K^{\circ} = K^*/12$  (conversion from inches to feet; from manufacturer's specification to standard thermal conductivity units).

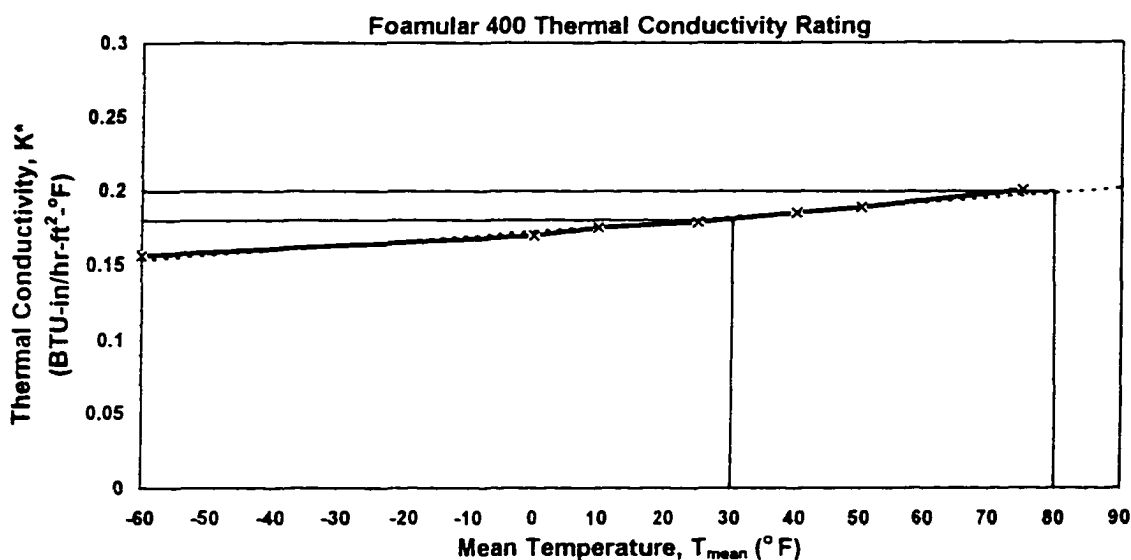


Figure 4-4. Foamular 400 thermal conductivity rating curve.

TC-2-1.5 was the shallowest thermocouple under the Zone II TIS pad and was embedded at the bottom of an iron pipe riser, 1.5 feet below the heat tape. During the heat tape installation, the circuit heating cable was routed around and in contact with the TC-2 riser. Since metal acts as an excellent heat conductor, it was surmised that the monthly TC-2-1.5 field temperature data closely approximated the operating temperatures at the heat tape. Using this thermal data for the bottom of the insulation and the sinusoidal surface temperature variations (equations [4-15] and [4-16]) to estimate corresponding temperatures at the insulation top, it was concluded that the polystyrene operated within the 30°F to 80°F mean temperature range throughout bioventing (Figure 4-4). The corresponding thermal conductivity range per inch of insulation was between 0.18 and 0.2 BTU-in/hr-ft<sup>2</sup>-°F, with a weighted average value of 0.0165 BTU/hr-ft<sup>2</sup>-°F. Table 4-6 summarizes the thermal data used to define the insulation thermal conductivity operating range.

**Table 4-6.** Summary of thermal data for determination of insulation average thermal conductivity.

Date	Insulation Temperatures (°F)			
	Bottom*	Bottom Avg.	Top <sup>a</sup>	T <sub>mean</sub>
Dec-94	48.6-57.0	52.8	8.7	30.8
Jan-95	57.2-58.5	57.9	-12.9	35.4
Feb-95	58.4-60.8	59.6	-4.5	32.0
Mar-95	61.4-63.1	62.3	13.2	37.8
Apr-95	71.1-73.8	72.5	35.6	54.0
May-95	75.5-79.3	77.4	56.9	67.2
Jun-95	82.1-85.8	84.0	71.5	77.8
Jul-95	88.2-86.3	87.3	75.7	81.5
Aug-95	86.6-86.8	86.7	68.3	77.5
Sep-95	83.1-84.3	83.7	51.2	67.5
Oct-95	79.2-73.4	76.3	29.0	52.7
Nov-95	72.1-63.1	67.6	18.8	43.2
Dec-95	61-55.7	58.4	8.7	33.6
Jan-96	61.6-55.7	58.7	6.4	33.0
Feb-96	55-64.6	59.8	12.5	36.1
Mar-96	67.7-69.6	68.6	25.4	47.0
Apr-96	77.4	77.4	41.8	59.6
May-96	76-78.8	77.4	56.9	67.1

\*Based on thermocouple TC-2-1.5 *in situ* temperatures. <sup>a</sup>**Bold** temperatures calculated using equation [4-16]; otherwise calculated using equation [4-15].



#### 4.6.4 Boundary Conditions

The surface energy balance generally establishes the thermal regime throughout the vadose zone. Energy exchange at the UAF bioventing site ground surface includes short wave [solar] radiation, long wave [infrared] radiation, convection, conduction, and evaporation (condensation). Evapotranspiration and energy transferred by rain and snow are considered negligible since there is no plant cover and because the magnitude of precipitative energy is generally considered small in comparison to the other energy exchanges (Zarling and Braley, 1988).

Total solar radiation received at the ground surface is the sum of direct (beam) and diffuse (atmospheric scattering by clouds, dust, and pollutants) radiation. Some short wave radiation is reflected or adsorbed by the impeding atmosphere. Weather services routinely measure incoming solar radiation (insolation) throughout the United States. Additionally, different surfaces discharge or absorb light energy depending upon their emissive or absorptive properties. The amount of solar radiation retained by the ground can be approximated as the product of incoming radiation and the surface absorptivity (Andersland and Ladanyi, 1994). Short wave absorptivities (1-surface albedo) and albedos (the ratio of light reflected by a surface to that received by it) for various surface conditions can be found in numerous cold regions publications.

Net long wave radiation between earth and sky is difficult to measure because of lack of reliable data on atmospheric variability of temperature and sky emissivity (Zarling and Braley, 1988). On a clear day, the magnitude of net long wave energy radiated from the earth is greater than on a cloudy day, when some radiation is reflected back.

Surface convective heat transfer is a function of relative air and surface temperatures, wind speed, and surface roughness. Over a twenty-four hour day, convection can be difficult to measure accurately because of thermal state variability and turbulence at the surface-air interface. Two conditions give rise to surface convection. First, when the ground is warmer than the air above it, the air closest to the ground is warmer and less dense than higher air and tends to rise. For a large temperature difference, this air density profile can be quite unstable, giving rise to conductive and convective heat transfer (Andersland and Ladanyi, 1994).

Convection is also associated with air movement (turbulence) relative to the ground surface, and varies with wind velocity and surface irregularities.

Evaporation (and sublimation) can account for a large portion of the total energy lost to the atmosphere. At the UAF site, evaporation primarily accounts for latent heat energy flux at the TIS surfaces. Some sublimation (the conversion of frozen moisture to vapor without liquefaction) may be associated with active warming treatment and heat losses through the insulation layer in winter. Because of data acquisition impracticality and required assumptions relating to surface homogeneity and stability at the surface-air interface, it is difficult to assess this portion of the overall surface energy transfer. Andersland and Ladanyi (1994) discuss the "equivalent air temperature" method of arbitrarily assigning a daily heat quantity to evaporation, based on soil moisture content and other surface parameters.

With surface applied insulation and active warming underneath, the surface energy balance for the Zone II test plot is essentially reduced to a heat conduction problem and a description of the ground surface temperature. Because average annual air temperature curves generally exhibit sinusoidal temperature variations, it is logical to assume a sinusoidal ground surface temperature variation. Two methods for determining the surface temperature boundary condition are generally accepted: 1) an exact method (using actual field temperature data) and 2) the *n-factor* approximation. The first method requires *in situ* data logging throughout the annual surface temperature cycle. This exact method accounts for variability in snow accumulations and melting, solar insolation, wind, and air temperature.

The *n-factor* approach, in conjunction with a sinusoidal air temperature variation, is used to derive the surface boundary condition in the absence of actual soil surface temperature data. Surface freezing and thawing *n-factors* are defined as the ratios of the surface freezing index (*SFI*) to air freezing index (*AFI*) and surface thawing index (*STI*) to air thawing index (*ATI*), respectively. Air temperatures and *AFI* and *ATI* are generally available for most Alaska locations in the Environmental Atlas of Alaska (Hartman and Johnson, 1984). In the absence of actual soil surface temperature data, carefully chosen surface *n-factors* can be used from published values. Lunardini (1978) presents *n-factors* from a number of Fairbanks sites, for various surface conditions. However, because *n-factors*

are [surface] temperature dependant, and therefore, a function of the total surface energy balance, they are both site specific and time varying. Lunardini (1978) suggests that use of applicable published n-factors can incur  $\pm 20$  percent deviation from accurate representation of a site's surface temperature relationship. However, for active warming, heat tape energy input dominates the subsurface thermal regime. The overlying insulation layer further minimizes surface temperature effects on the vadose zone. Some latitude in choosing appropriate n-factors is afforded.

A columnar element of the Figure 3-3 soil profile is used to generate the discrete mesh for 1D finite element analysis. Due to symmetry between heat tape lineations, the chosen

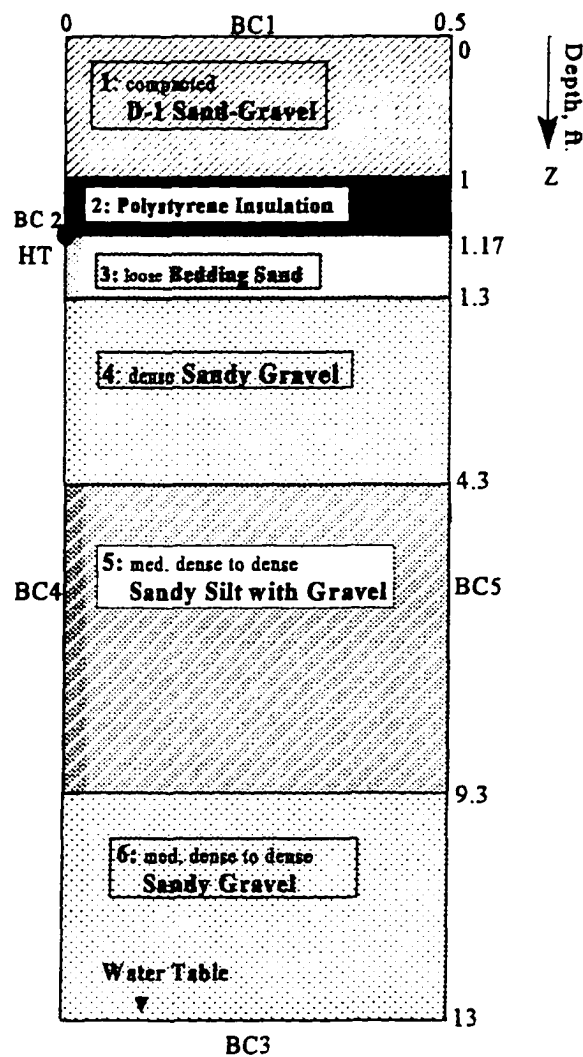


Figure 4-5. Soil column for TDHC analysis.

element was 0.5 feet wide and 13 feet deep (the average water table depth) as shown in Figure 4-5. Boundary conditions BC1 through BC5 denote the surface, heat tape, water table, and vertical sides, respectively.

#### 4.6.4a Surface Boundary Condition

Zarling and Braley (1988) presented sinusoidal equations that describe harmonic air and ground temperature variations. The sinusoidal soil surface temperature variation is

$$T_s(t) = T_{ms} - A_{os} \cos \left[ \frac{2\pi(t - \phi_s)}{365} \right]_{rad} \quad [4-12]$$

where the mean annual soil surface temperature is approximated as

$$T_{ms} = \frac{n_t(ATI) - n_f(AFI)}{365} + T_f \quad [4-13]$$

and the amplitude of the soil surface temperature variation can be determined as

$$A_{os} = \frac{n_t ATI - (T_{ms} - T_f)(t_{2s} - t_{1s})}{\frac{365}{\pi} \sin \left[ \frac{2\pi(t_{1s} - \phi_s)}{365} \right]_{rad}} \quad [4-14]$$

In these equations  $T_f$  is the freezing temperature,  $\phi_s$  is the soil surface temperature phase lag (from January 1), and  $t_{1s}$  and  $t_{2s}$  are the beginning and ending days of the surface thawing season, respectively calculated as

$$t_{1s} = \frac{365}{2\pi} \arccos \left( \frac{T_m - T_f}{A_{os}} \right)_{rad} + \phi_s \quad \text{and} \quad t_{2s} = \frac{365}{2\pi} \left[ 2\pi - \arccos \left( \frac{T_{ms} - T_f}{A_{os}} \right)_{rad} \right] - \phi_s$$

$A_{os}$  is calculated iteratively, using appropriate air temperature data\* to first approximate  $t_{1s}$  and  $t_{2s}$ . From the Environmental Atlas of Alaska, for Fairbanks, a mean annual air temperature ( $T_m$ ) of 25.6°F, an amplitude of annual variation ( $A_o$ ) of 35°F, and a phase lag of 8 days can be used to initially estimate the length of the thawing season. Then, thawing and freezing indices  $ATI$  and  $AFI$  can be calculated. For a specific surface condition, appropriate n-factors are then used in conjunction with these indices to estimate  $T_{ms}$ . Next, the first approximation for  $A_{os}$  is determined using these initial  $t_{1s}$ ,  $t_{2s}$ , and  $T_{ms}$  values. Improved values for  $t_{1s}$  and  $t_{2s}$  are then recalculated using this first  $A_{os}$  approximation. Solving again for a new  $A_{os}$  improves its value, which in turn is used to calculate a more precise  $T_s$ . It should be noted that a measure of TIS system performance is directly related to the surface boundary condition. Therefore, appropriate n-factors must be carefully chosen to accurately reflect the active annual soil surface temperature variation  $T_s$ .

Two general surface conditions prevail on the Zone II treatment pad. The D-1 sand-gravel pad is either snow covered or without snow cover. Table 4-7 and equations [4-15] and [4-16] summarize the n-factor method parameters and the harmonic soil surface temperature variations. The actual calculations for these equations are included in Appendix F.

**Table 4-7. Zone II surface boundary conditions.**

Case	Surface Condition	$n_t$	$n_f$	$T_{ms}$ (°F)	$A_{os}$ (°F)	$\phi_s$ (days)
1	D-1 sand-gravel with snow	1.7	0.5	38.6	32.4	8
2	D-1 sand-gravel without snow	1.7	1.0	31.3	44.5	8

Soil surface temperature variations (in °F):

$$\text{case 1} \quad T_s(t) = 38.6 - 32.4 \cos[0.0172 (t - 8)]_{\text{rad}} \quad [4-15]$$

$$\text{case 2} \quad T_s(t) = 31.3 - 44.5 \cos[0.0172 (t - 8)]_{\text{rad}} \quad [4-16]$$

---

\* For preliminary design, local air temperature data for the most recent year should be used. For modeling after one year of bioventing, recorded, site specific, daily air temperatures should be used to compute the air temperature variation and first approximations for  $t_{1s}$  and  $t_{2s}$ . The Environmental Atlas of Alaska average air temperature data can also be used, if no other climatological data is available.

The case 1 surface temperature variation was used for the TDHC second year thermal analysis (November to May) as snow cover was the prevailing surface condition during this period. Equation 4-16 is more applicable during long periods without snow cover.

#### 4.6.4b Other Boundary Conditions

The heat tape boundary condition (BC2 in Figure 4-5) is modeled as a node with fixed heat flux and can be defined as a function of temperature according to equation [4-11]. However, since half of the heat tape output is transferred to adjacent soils outside the Figure 4-5 element of analysis, equation [4-11] should be divided in half for the TDHC rate equation:  $q_{HT} = -0.0378T + 5.83$  (BTU/ hr-ft). The heat tape boundary condition can be modeled initially as a node with fixed heat flux. This initial fixed heat flux value was actually 4.71 BTU/hr-ft, calculated from the aforementioned half-rate equation for the measured [November 7, 1994] start-up, natural ground surface temperature. The half-rate equation is then incorporated into the TDHC code and used for subsequent modeling.

The water table boundary condition (BC3) is modeled as a horizontal boundary with harmonic temperature variation. Groundwater temperatures were measured at the time of quarterly water sampling efforts. The groundwater temperature appeared to remain between 33°F and 40°F throughout the year. With a mean annual temperature of 36.5°F, and an amplitude of variation of 3.5°F, a sinusoidal temperature variation was determined from

$$T_{gw}(t) = T_{m(gw)} - A_{\alpha(gw)} \cos\left(\frac{2\pi(t - \phi)}{365}\right)_{rad}$$

as 
$$T_{gw}(t) = 36.5 - 3.5 \cos [0.0172(t - 8)]_{rad} \quad [4-17]$$

Alternatively, since the groundwater temperature variability was relatively small over the course of a year, a constant temperature boundary approximation could be used with little sacrifice to model accuracy.

The side boundaries shown in Figure 4-5 are specified as zero heat flux boundaries since they represent lines of symmetry with respect to the whole of the Zone II soil thermal regime. Therefore, boundary conditions BC4 and BC5 are modeled as

$$\frac{\partial T}{\partial x} = 0 \quad \text{at } x = 0 \text{ and } x = 0.5 \text{ ft.} \quad [4-18]$$

#### 4.6.4c Initial Temperature Conditions

Initial subsurface temperatures for the Zone II soil column (Figure 4-5) were estimated based on November 7, 1994 thermal data collected from monitoring points MP-3, MP-6, TC-1 and TC-2. These temperatures are needed for the TDHC input file and are identified in the next section.

#### 4.6.5 The Zone II Heat Conduction Problem Summarized

The general heat transfer problem through the Zone II unsaturated soils can be modeled after equation [4-7], with the aforementioned applicable boundary conditions. Although equation [4-7] is a 2D partial differential equation, the second term on the left side of the equation has negligible influence on the TDHC analysis of a thin, elemental soil column (Figure 4-5). In other words, because heat tape spacing is small and the element of analysis is consequently thin in the  $x$ -direction but deep in the  $z$ -direction, TDHC essentially performs a 1D heat transfer analysis with the 2D equation. The problem is summarized here for clarity and TDHC analysis.

Governing heat conduction equation:

$$\frac{\partial}{\partial z} \left( K_z \frac{\partial T}{\partial z} \right) + \frac{\partial}{\partial x} \left( K_x \frac{\partial T}{\partial x} \right) = C \frac{\partial T}{\partial t} - q_{HT}$$

Initial subsurface temperatures (Figure 4-5):

Layer 1 (28°F)	Layer 3 (29.5°F)	Layer 5 (33°F)
Layer 2 (29°F)	Layer 4 (31°F)	Layer 6 (34°F)

$$\begin{aligned}
\text{BC1: (case 1)} \quad T_s(t) &= 38.6 - 32.4 \cos[0.0172 (t - 8)]_{\text{rad}} \\
\text{(case 2)} \quad T_s(t) &= 31.3 - 44.5 \cos[0.0172 (t - 8)]_{\text{rad}} \quad (\text{in } ^\circ\text{F}) \\
\text{BC2:} \quad q_{HT} &= -0.0378T + 5.83 \quad (\text{BTU/hr-ft}) \\
\text{BC3:} \quad T_{gw}(t) &= 36.5 - 3.5 \cos [0.0172(t - 8)]_{\text{rad}} \\
\text{BC4 and BC5:} \quad \frac{\partial T}{\partial x} &= 0
\end{aligned}$$

#### 4.7 The Zone I and Zone III Heat Transfer Problems

The passive (Zone I) and control (Zone III) test plots were modeled after equation [4-6] as

$$\frac{\partial}{\partial z} \left( K_z \frac{\partial T}{\partial z} \right) + \frac{\partial}{\partial x} \left( K_x \frac{\partial T}{\partial x} \right) = C \frac{\partial T}{\partial t} + L \delta(T - T_f) \quad [4-19]$$

where

$L$  = latent heat (in BTU/ft<sup>3</sup>)

$T_f$  = freeze-thaw temperature (in °F)

$\delta$  = Dirac delta function

The right hand side of equation [4-19] is an expression for the enthalpy change across any finite temperature range. Figure 4-6 (dashed curve) graphically represents the realistic enthalpy “spike” associated with a phase change at the freezing temperature ( $T_f$ ) for a coarse-grained, moist soil. Enthalpy change across any finite temperature range  $T_2 - T_1$  may be expressed as

$$\frac{dH}{dT} = C = c_s + L \delta(T - T_f) \quad [4-20]$$



where  $c_s$  is soil sensible heat capacity. As the freeze-thaw front moves through the soil, the latent heat in equation [4-20] is incrementally “stepped” up or down as a function of temperature (Figure 4-6, solid “step” curve). This latent heat of fusion can be represented with a finite integral in which temperature is interpolated smoothly through the phase change isotherm with incorporation of a Dirac Delta function ( $\delta$ ).

The Dirac Delta formalism is an “improper” mathematical function (tool) in that it is essentially zero everywhere within its defined range except at a singularity location (Salam and Wigner, 1972). Since phase change occurs at a discrete temperature,  $\delta$  is useful because an integral of the product of  $\delta$  and latent heat as a function of temperature is simply equal to the latent heat of fusion evaluated at the discrete [freezing] temperature ( $T_f$ ):

$$L(T_f) = \int_{T_1}^{T_2} L \delta(T - T_f) dT \quad [4-21]$$

One can apply this rationale at the freeze-thaw isotherm within a soil finite element of analysis (Figure 4-7) as well. Similar to the Galerkin weighted residual process previously applied to temperature and the space domain (sec. 4.5, equation [4-10]), the latent heat contribution is discretized over the finite element problem domain. Essentially, the product of the latent heat term and one or two shape functions (related to physical and temperature gradient characteristics associated with the elemental freeze-thaw isotherm (Figure 4-7)) is integrated with respect to temperature as

$$LHC = L \int_a^b \delta(T - T_f) [N]^T \frac{dz'}{dT} dT = \frac{L}{|\nabla T|} \int_a^b [N]^T dT \quad [4-22a]$$

for 1D analysis, and

$$LHC = L \int_a^b \delta(T - T_f) [N]^T [N] \frac{dz'}{dT} dT dx' = \frac{L}{|\nabla T|} \int_a^b [N]^T [N] dx' \quad [4-22b]$$

(after Goering, 1984)

for 2D analysis. Here, the problem domain is a typical triangular finite element in the TDHC analysis (Figure 4-7), line a-b represents the freeze-thaw front through the element, and

$LHC$  = latent heat contribution (in BTU/ft<sup>3</sup>)

$[N]^T$  = linear temperature shape function for the  $z'$  direction

$[N]$  = linear shape function representative of the  $a$ - $b$  isotherm (the  $x'$  direction)

$\nabla T$  = constant temperature gradient (throughout the finite element)

$$dz'/dT = 1/|\nabla T|$$

Again the reader is directed to the original work by Goering (1984) for further understanding of the finite element method as applied to the TDHC model.

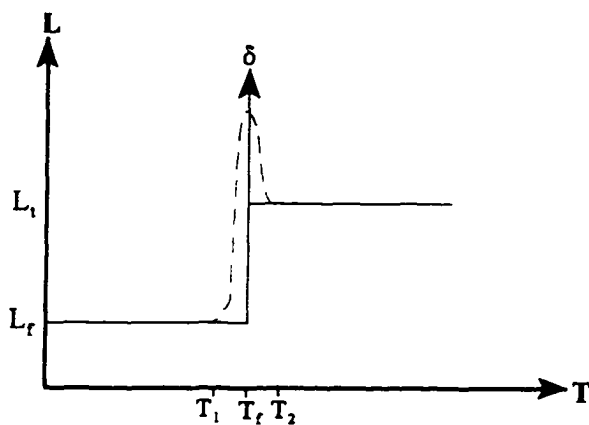


**Figure 4-6.** Dirac delta function applied to soil latent heat (after O'Neill, 1983).

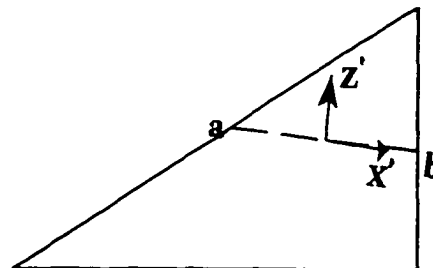


**Figure 4-7.** Freeze-thaw isotherm within a soil finite element (after Goering, 1984).

#### 4.7.1 Boundary Conditions

The same surface, side and groundwater table boundary conditions defined for the previous Zone II model were applicable to Zones I and III. However, the elemental soil columns were redefined (Figures 4-8a and 4-8b) for these treatment areas. Furthermore,

representative [layer] initial temperatures were required that reflected the November 7, 1994 field temperature data collected from these plots. Appropriate Table 4-3 data is again used for the TDHC analyses of these test plots.

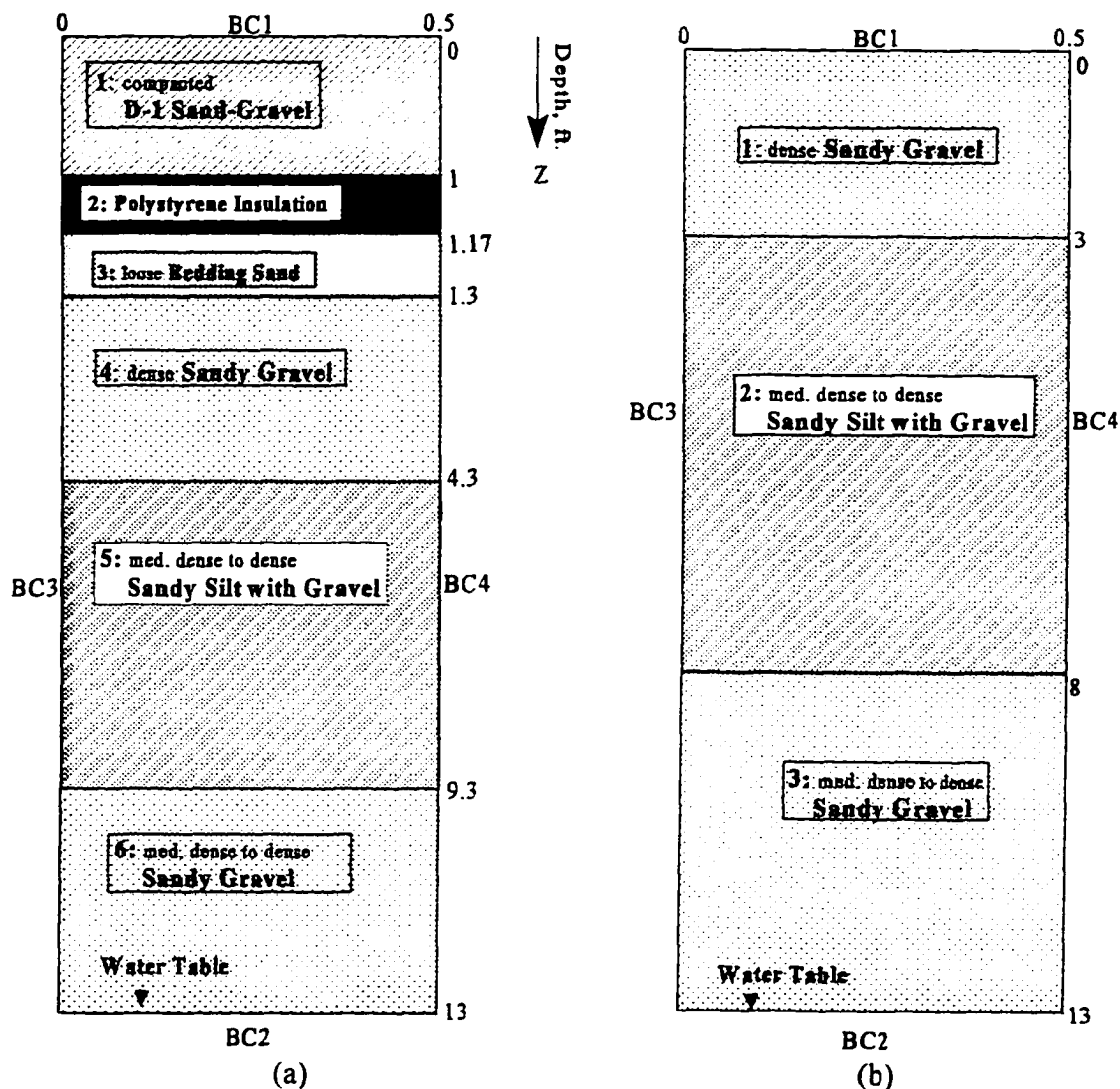


Figure 4-8. Soil columns for (a) Zone I and (b) Zone III TDHC analyses.

#### 4.7.2 The Zone I Heat Conduction Problem Summarized

The general heat transfer problem through the Zone I unsaturated soils can be modeled using equation [4-19], with the following initial and boundary conditions:

Governing heat conduction equation:

$$\frac{\partial}{\partial z} \left( K_z \frac{\partial T}{\partial z} \right) + \frac{\partial}{\partial x} \left( K_x \frac{\partial T}{\partial x} \right) = C \frac{\partial T}{\partial t} + L\delta(T - T_f)$$

Initial subsurface temperatures (Figure 4-8a):

Layer 1 (28°F)    Layer 3 (29.5°F)    Layer 5 (33.5°F)  
 Layer 2 (29°F)    Layer 4 (30°F)    Layer 6 (35°F)

BC1: (case 1)     $T_s(t) = 38.6 - 32.4 \cos[0.0172(t - 8)]_{\text{rad}}$  (in °F)  
 (case 2)     $T_s(t) = 31.3 - 44.5 \cos[0.0172(t - 8)]_{\text{rad}}$

BC2:     $T_{\text{gw}}(t) = 36.5 - 3.5 \cos [0.0172(t - 8)]_{\text{rad}}$

BC3 and BC4:     $\frac{\partial T}{\partial x} = 0$

#### 4.7.3 The Zone III Heat Conduction Problem Summarized

The general heat transfer problem through the Zone III unsaturated soils can also be modeled after equation [4-19], with the following initial and boundary conditions:

Governing heat conduction equation:

$$\frac{\partial}{\partial z} \left( K_z \frac{\partial T}{\partial z} \right) + \frac{\partial}{\partial x} \left( K_x \frac{\partial T}{\partial x} \right) = C \frac{\partial T}{\partial t} + L\delta(T - T_f)$$

Initial subsurface temperatures (Figure 4-8b):

Layer 1 (28°F)    Layer 2 (32°F)    Layer 3 (32.8°F)

BC1: (case 1)     $T_s(t) = 38.6 - 32.4 \cos[0.0172(t - 8)]_{\text{rad}}$  (in °F)  
 (case 2)     $T_s(t) = 31.3 - 44.5 \cos[0.0172(t - 8)]_{\text{rad}}$

BC2:     $T_{\text{gw}}(t) = 36.5 - 3.5 \cos [0.0172(t - 8)]_{\text{rad}}$

BC3 and BC4:     $\frac{\partial T}{\partial x} = 0$

#### 4.8 Zone II Boundary Analysis

At the edges of the active warming test plot, heat is lost to adjacent soils that are much cooler in winter. A 2D analysis was performed on a section of vadose zone encompassing one side of the treatment pad (Figure 4-9). The section was divided into fourteen subregions with the soil types noted and the same as in Figure 4-5.

Boundary conditions used for this model were of four types. Along the surfaces of the section, the n-factor approach was again used to arrive at sinusoidal surface temperature variations. Table 4-7 data and equations [4-15] and [4-16] were representative of the seasonal surface boundary conditions. Equation [4-17] sufficed for the bottom groundwater table boundary condition. Vertical borders were specified as zero heat flux boundaries. Because of symmetry with respect to the test plot centerline, this assumption along the centerline forces the opposing side of the test plot to have identical temperatures. At 55 feet from the centerline, the vertical boundary beyond the TIS toe was defined far enough from the toe so that heat flow was again one-dimensional. The heat tape boundary condition was defined as a function of temperature according to equation [4-11]. This boundary condition was modeled initially as a series of nodes with fixed heat flux. The initial heat flux value was 9.44 BTU /hr-ft, calculated for a temperature of 29.5°F (the approximate subsurface temperature at the heat tape level on November 7, 1994). These boundary conditions and initial approximate subsurface temperatures are summarily expressed below.

Subregion initial subsurface temperatures (Figure 4-9):

1 (28°F)	2 (28°F)	3 (28°F)	4 (29°F)	5 (29.5°F)
6 (31°F)	7 (29°F)	8 (28°F)	9 (33°F)	10 (33°F)
11 (33°F)	12 (34°F)	13 (34°F)	14 (34°F)	

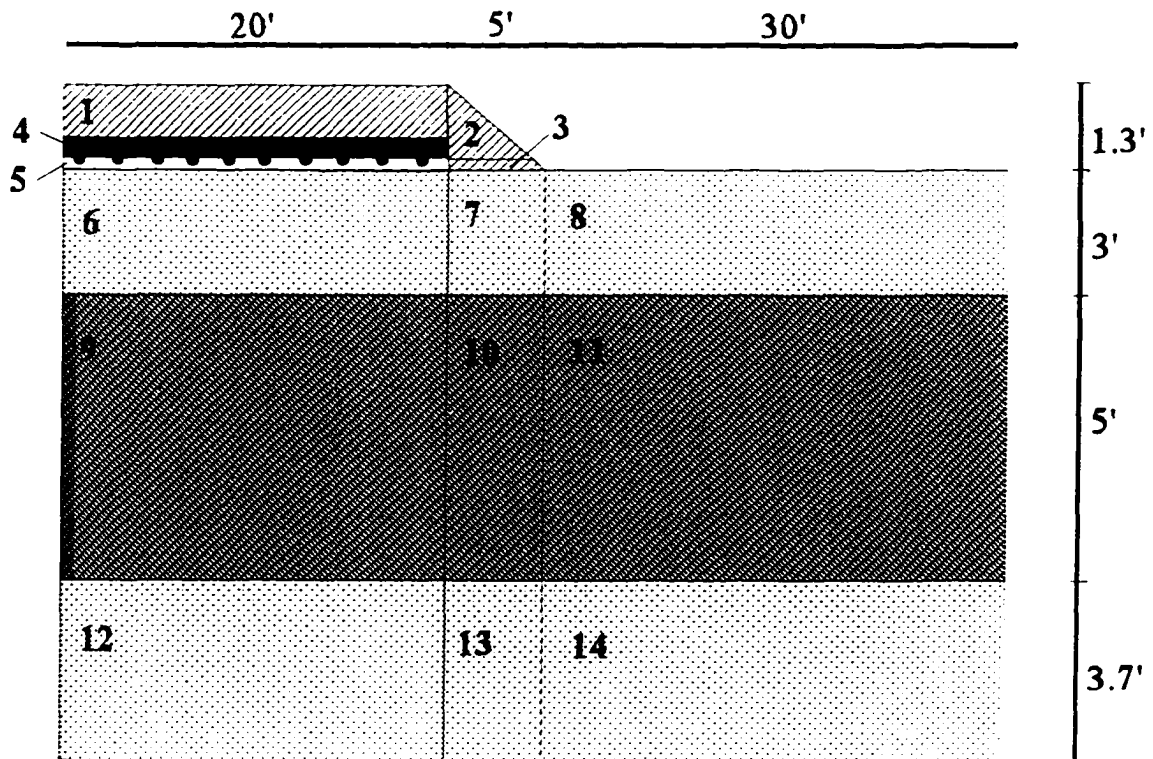
Surface boundary condition:

$$\begin{aligned}
 \text{(case 1)} \quad T_s(t) &= 38.6 - 32.4 \cos[0.0172 (t - 8)]_{\text{rad}} \\
 \text{(case 2)} \quad T_s(t) &= 31.3 - 44.5 \cos[0.0172 (t - 8)]_{\text{rad}}
 \end{aligned}
 \quad (\text{in } ^\circ\text{F})$$

Bottom groundwater boundary condition:  $T_{gw}(t) = 36.5 - 3.5 \cos [0.0172(t - 8)]_{\text{rad}}$

Vertical boundary condition (at  $x = 0$  and  $x = 55$  ft.):  $\frac{\partial T}{\partial x} = 0$

Heat tape boundary condition:  $q_{HT} = -0.0757T + 11.67$  (BTU/hr-ft)



**Subregion Legend**

1,2,3	D-1 Sand-Gravel
4	Insulation
5	Bedding Sand
6,7,8,12,13,14	Sandy Gravel
9,10,11	Sandy Silt with Gravel

Figure 4-9. Zone II finite element region for TDHC boundary analysis.

---

## Monitoring and Testing Methods

### 5.1 Thermal Monitoring

Thermocouple monitoring at the UAF bioventing site began on November 3, 1994, as vadose zone background temperatures were measured at all fourteen thermal monitoring points (Figure 3-2). The Zone II heat tape was turned on by November 7, after which daily monitoring occurred through January 2, 1995. As temperature variability within the vadose zone abated, monitoring frequency was decreased to four and five day intervals through February 17, 1995. Subsequent monitoring then occurred on a weekly basis until the end of March 1995, and biweekly thereafter. More frequent monitoring occurred during spring breakup and summer-to-fall transition periods.

An Omega model HH21 microprocessor thermometer was used to record temperature measurements. During a monitoring event, power was shut off to the heat tape, to minimize potential for electrical eddy current\* interference on temperature measurements. In this way, temperatures from the site surface to the water table were monitored over time.

Occasionally, localized convection at the monitoring points allowed moisture to accumulate in riser head spaces. In winter, ice buildup on the underside of the insulation

---

\* The heat tape circuit is designed as a highly conductive, low resistance, heating element. Operating under 60 Hz alternating current, the heat tape generates a local and variable electromagnetic field and can induce [conductive] *superficial eddy currents*. These eddy currents are temporary (short duration) and feeble if the circuit is low resistance (Loeb, 1902). Because of the heat tape's protective and insulating layers, and unless there are great and sudden changes in electromagnetic field fluctuations, these induced eddy currents will have negligible heating effect on surrounding media. Granular soils, unlike a solid metal body in the neighborhood of a conductor generating substantial eddy currents, will experience negligible heating associated with superficial eddy currents. This hypothesis was verified by recording same temperature measurements from Zone II thermocouples with the heat tape turned on and off.

plugs and moisture in the wood bases would freeze the plugs to the riser casings. When this happened, a portable Wagner<sup>(TM)</sup> power stripper (a blow dryer) was used to thaw the bond so that the type T thermocouples could be read.

## 5.2 Soil Gas Monitoring

The fourteen soil gas monitoring points (Figure 3-2, MP-1 through MP-14) were sampled monthly for oxygen, carbon dioxide and total petroleum hydrocarbon (TPH) concentrations. A Gast<sup>(TM)</sup> 1/2-horsepower vacuum pump was used to draw soil gas to the surface through 1/4-inch diameter polyethylene tubing. Discrete monitoring points were typically purged for one minute before soil gas sampling. Soil gas samples were stored in 2 ml Tedlar<sup>(TM)</sup> bags. A Trace-Teclor<sup>(TM)</sup> hydrocarbon vapor tester and GasTeclor<sup>(TM)</sup> meters were then used to measure TPH concentrations and percent oxygen and carbon dioxide, respectively. Instrument recalibration was performed after every third sampling event using measured hexane, O<sub>2</sub>, and CO<sub>2</sub> in nitrogen specialty gases.

Periodically, a few discrete monitoring points were rendered inoperative due to freezing soils and ice buildup inside the sample tubing. Additionally, there were periods where the deepest monitoring points were permeated by rising groundwater and/or were clogged with fines. Table 5-1 identifies functional soil gas monitoring points at the bioventing site.

### 5.2.1 Background Levels and Operating Injection Flow Rate

Bioventing soil gas baseline data was established in July and August 1994. Ambient levels of the three soil gases (O<sub>2</sub>, CO<sub>2</sub> and TPH) were recorded at each monitoring point before the vent wells were started. The vent wells were then brought on-line during a 72-hour system start-up period over the last three days of August 1994.

Between November 3 and December 15, 1994, immediately after the TIS materials were installed and the heat tape was turned on, an air-injection flow rate test was performed. During this test, vent wells VW-1, VW-2, VW-3, and VW-5 were independently shut down one at a time, while varying injection flow rates at the other three wells. Each time a vent



well was shut down, soil gas measurements were recorded. Sequentially, each well would then be turned back on while another was shut off, and so on. In this way a suitable system-wide air-injection flow rate was established so that artificial volatilization and hydrocarbon stripping were reduced (see section 5.5 for a discussion on determining suitable air-injection flow rates). This was done so that thermal enhancement effects could be directly attributed to "true" biodegradation. A winter bioventing respiration test was (sec. 5.3) then performed during the first week of January 1995. Consequently, vent well blowers were adjusted and maintained at 2 cfm for the first full year of thermally enhanced bioventing. This 2-cfm injection flow rate was considered the equilibrium operating condition for the blowers.

**Table 5-1.** Functional soil gas monitoring points at the UAF bioventing site.

<b>Treatment Area</b>	<b>Soil Gas Monitoring Point</b>	<b>Discrete Soil Gas Sampler Embedment Depths (ft.)*</b>
Background	MP-9	8.5
Zone I (passive treatment)	MP-12	5.5 and 12.5
	MP-13	8 and 10
	MP-14	7.5
Zone II (active treatment)	MP-1	6 and 8
	MP-2	8.5 and 14
	MP-3	6.7 and 14
	MP-4	9 and 11.5
	MP-6	8.3
Zone III (no action control)	MP-7	7, 10 and 12.5
	MP-8	7
	MP-10	5, 9.5 and 12
	MP-11	7.3, 8 and 14.3
Next to the Physical Plant building	MP-5	8.4 and 12

\* Depth below natural ground surface.

### 5.3 Biodegradation Rates

Arambarri (1995) describes the *in situ* respiration test incorporated to provide the first estimate of biodegradation rates at the UAF bioventing site. The December 1994 test, developed by Hinchee and associates at Battelle (Hinchee and Ong, 1992), used a helium gas tracer to evaluate diffusion of oxygen into neighboring oxygen-poor soils. During a 24-hour period, air mixed with 1 percent helium was injected into a single vent well. After shutting all blowers off, soil gas samples from twelve monitoring points were collected and analyzed for oxygen, carbon dioxide and helium gas concentrations. Graphs of the gas concentrations versus time were then used to estimate utilization rates. Comparison of the oxygen and helium diffusion curves was made to assess biodegradation.

A subsequent respiration test was performed in June 1995. Since the bioventing system had then been fully operational for nearly eight months, and a background [uncontaminated] oxygen utilization rate was previously established during the earlier winter test, a tracer test was not required. By shutting down the blowers and monitoring soil gases ( $O_2$  and  $CO_2$ ) at all the monitoring points over a 72-hour period, a general site summertime biodegradation rate was determined for the 2-cfm venting rate.

### 5.4 Microbiology and Geochemistry

Microbiological and geochemical data can be used to evaluate biodegradability potential of a soil regime; geochemistry analysis over time can present evidence that contaminant reduction has occurred. Engineers traditionally estimate biodegradation rates over time to assess treatment efficacy.

During this full-scale field study, microbiological and geochemical sampling was performed on a limited basis, to provide secondary information in support of thermally enhanced bioventing.

On July 5, 1995 five, hollow-stem auger, standard penetration test (SPT) borings were drilled at the bioventing site. The borings, identified as Curly, Larry, Moe, Shemp, and Joe, were performed at the locations shown in Figure 5-1. Sampling location Joe was the control for this first round event; Moe was the uncontaminated and biovented control

sampling location. The other three sampling locations were placed within the main bioventing area. The scope of this drilling event was to collect 3-inch diameter, split-spoon, undisturbed soil samples (three from each borehole) from various depths to the groundwater table.

The fifteen soil samples were taken to the UAF Institute of Arctic Biology (UAF-IAB) for microbiological analyses. A duplicate series of soil samples was taken to the state registered Northern Testing Laboratory (NTL) for EPA methods 160.3, 8015 and 8020 organic analyses. Additionally, groundwater samples were collected from three monitoring wells and were airfreighted to the United States Geological Survey Water Resource Division (USGS-WRD) national laboratory in Arvada, Colorado. Full-range organic and inorganic geochemistry analyses were performed on the samples according to USGS Schedules 1307, 1904 and 101.

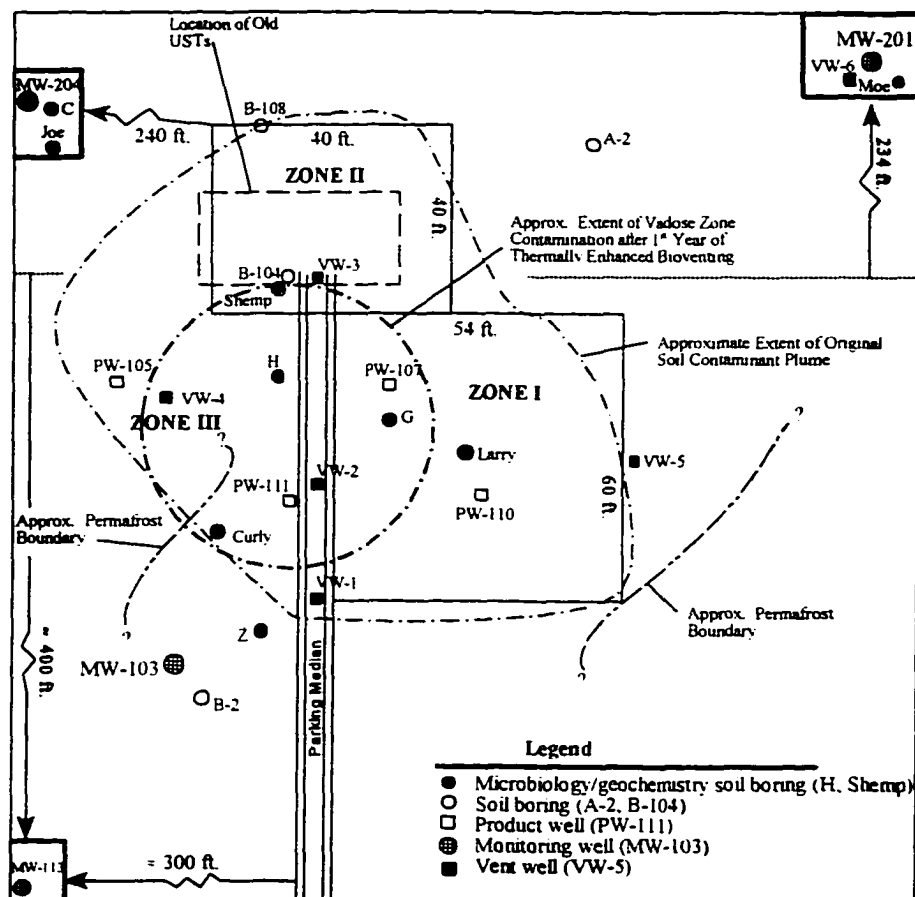


Figure 5-1. July 1995 and June 1996 soil sampling locations.

A similar second-round soil sampling event was conducted on June 24, 1996. The four 15-foot borings, identified as C, H, G and Z (Figure 5-1), were performed for soil sampling and testing similar to the July 1995 event. Soils were again analyzed at NTL, with microbiological and geochemical analyses to be performed at the UAF-IAB. Groundwater samples were again collected and shipped to the USGS for analyses. At the time of this writing, the UAF-IAB analytical results were not completed. The USGS analytical data and partial UAF-IAB results are included for this discussion.

The sampling schedules for these two events are shown in Table 5-2, with soil sample numbers 1, 2 and 3 typically representative of the unsaturated, smear (capillary fringe), and saturated zones, respectively. Groundwater samples from monitoring wells MW-210, MW-103, and MW-113 were collected at the groundwater table during both sampling events. The summer groundwater table was typically encountered between twelve and thirteen feet below the ground surface.

Sampling requirements for accurate microbiological assessments are more stringent than the SPT protocol outlined in the American Society of Testing and Materials engineering standard. Driving the split-spoon sampling tube down through soils during SPT standard drilling affords microbiological cross-contamination potential along the core sample-spoon interface. To obtain the most representative microbiological sample from a specific depth, thin outer layers of the retrieved sample core were stripped away with a decontaminated cutting edge. Sterile, individually sealed, sampling scoops were used to take soils from the split-spoons. Rubber gloves were also used in the sample transfers from split-spoon to air-tight glass sample jars. A new sampling scoop was used for each soil specimen collected. All other sampling equipment and auger sections were decontaminated with methanol or trisodium phosphate detergent, then washed with distilled water before reuse.

Enumeration assays and total activity measurements were performed in the UAF-IAB laboratory on the fifteen 1995 soil samples. These tests yield information about microbial populations present and bioactivity.

**Table 5-2.** July 1995 and June 1996 microbiological and geochemical sampling schedules.

<b>Boring</b>	<b>Treatment/Description</b>	<b>Sample #</b>	<b>Depth (ft.)</b>
<b>(July 1995)</b> Curly	Bioventing Control for Thermal Treatment	Curly #1	5-7.5
		Curly #2	10-12.5
		Curly #3	12.5-14.5
Moe	Bioventing Background; No Soil Contamination	Moe #1	7-8.5
		Moe #2	10-12
		Moe #3	12-14
Joe	Background for Microbiology; No Bioventing, No Vadose Soil Contamination	Joe #1	7-9
		Joe #2	9- 11
		Joe #3	11-13
Shemp	Bioventing with Active Warming	Shemp #1	8-10
		Shemp #2	11-13.5
		Shemp #3	13.5-15.5
Larry	Bioventing with Passive Treatment	Larry #1	8-9.5
		Larry #2	9.5-11.5
		Larry #3	11.5-13.5
<b>(June 1996)</b> C	No Bioventing, No Soil Contamination	C1	7-8.5
		C2	11.5-13.5
G	Bioventing; Zone of Remaining Soil Contamination	G1	6.5-8
		G2	12.5-14
H	Bioventing; Zone of Remaining Soil Contamination	H1	4.5-6
		H2	6.5-8
		H3	13-15
Z	Downgradient of Zone of Remaining Soil Contamination	Z1	4.5-6
		Z2	6.5-8
		Z3	13-15
<b>(July 1995 and June 1996)</b>			
MW-201		-	GW
MW-103		-	GW
MW-113		-	GW

GW denotes groundwater samples collected at the groundwater table.

#### 5.4.1 Enumeration Assays

Enumeration assays were needed to estimate numbers of heterotrophic microorganisms and gasoline and diesel fuel degrading microorganisms. The testing protocols

used for these assays were a standard heterotrophic most-probable-number (MPN) enumeration method and a tetrazolium violet MPN technique, developed by Peter Catterall and Dr. Joan Braddock at the UAF Institute of Arctic Biology.

The tetrazoleum violet enumeration assay essentially consisted of a 96-well microtiter plate, in which serial dilutions (1:10) of soil slurry ( $10^{-1}$  to  $10^{-9}$ ) were mixed with equal volumes of Bushnell-Haas broth (Atlas, 1993) containing 0.0025 percent tetrazoleum violet. Before incubation, a sole source of carbon was stirred into each well to provide an oxidizable substrate for microbial growth. The selected carbon substrate is generally the contaminant that the investigator is interested in biodegrading. In this case, either diesel fuel or gasoline was added and the microtiter wells were incubated at room temperature for two to three weeks. When growth is present, the tetrazoleum redox dye is converted from its original colorless soluble state to a colored insoluble formazan that collects at the bottom of the microtiter wells. This insoluble tetrazoleum formation absorbs light at 590 nanometers; increasing absorbancies can then be determined by a 96-well plate reader. Discrete population counts (enumerations) were read at the end of three weeks.

#### 5.4.2 Activity Measurements

Activity of the microbial population was also measured to identify differences associated with various treatment regimes. Treatment regimes consisted of laboratory microcosms constructed with 75 grams of soil sample, placed in one-half pint mason jars fitted with septa gas sampling ports, and incubated under variable moisture and temperature conditions. Microcosms were incubated for five weeks at 39°F, 50°F, 59°F and 77°F, with moisture contents adjusted to 60 percent of the sample's water holding capacities (WHC). Two additional microcosms were incubated at 50°F; one sample was incubated at the *in situ* moisture content while the other was saturated. In this way CO<sub>2</sub> produced over time could be measured and compared with *in situ* soil gas measurements. Carbon dioxide was quantified using a Shimadzu GC14-A gas chromatograph equipped with a thermal conductivity detector.

### 5.4.3 Groundwater Sampling

In the summers of 1995 and 1996 two groundwater sampling events were performed for organic and inorganic geochemistry analyses. Groundwater was sampled at monitoring wells MW-201, MW-113, and MW-103 (Figure 5-1). These samples represented groundwater upgradient, downgradient, and at the bioventing site. The purpose of these sampling and testing events was to further understanding of the microbiological processes occurring with the bioremediation effort.

Sampling kits were prepared and supplied by both the USGS and NTL. Each kit included three 50 ml and two 500 ml glass jars, bubble bags (for the 50 ml samples), a chain of custody log, and insulated coolers. Each well was sampled with a 36-inch, single check valve, Teflon™ disposable bailer. Before bailing, approximately fifteen gallons of water were purged from each well using an ESCO™ Well Purger, peristaltic pump. Groundwater conductivity measurements typically stabilized after purging of between twelve and fifteen gallons of water. Rubber gloves were used to prevent sample contamination by the sampler. Immediately after collection, all samples were sealed, logged and packed in ice inside the coolers. The NTL samples were delivered on the same day as sample collection. The USGS samples were airfreighted overnight to their Arvada, Colorado laboratory.

### 5.4.4 Statistics

Statistical analyses were not performed on the microbiological data for several reasons: 1) early subsurface investigations never clearly differentiated contamination levels across the UAF bioventing site, 2) subsurface heterogeneities, and 3) site specific statistical inferences require a number of microbiological sampling and testing events (at considerable additional cost). Furthermore, to the author's knowledge, only one other thermally enhanced bioventing project is documented for possible statistical comparison. However, no microbiological data or qualitative thermal analyses were reported in the findings for that project.

### 5.5 Bioventing Optimization Test

After first-round microbiology and geochemistry sampling and testing was performed in July 1995, *evolutionary operation* (Box and Draper, 1969) was considered for further bioventing optimization. This "tuning process" essentially increases air-injection flow rates incrementally, with follow-up air quality and soil gas monitoring, until optimal biodegradation is achieved without risk to human health. The optimal system-wide flow rate was to become the basic mode of future system operation.

**Table 5-3.** Bioventing system optimization test (Evolutionary Operation).

Sampling Event	GW Depth		Air Injection Flow Rate Q (cfm)	Soil Gas TPH (ppm)				
	MW-201	MW-202		MP-6	MP 7-7	MP 7-10	MP 7-12.5	MP-8-7
1	-	-	2.0	35	12,000	9,800	20,000+	2,900
2	14.86	15.89	2.0	30	16,500	20,000+	20,000+	2,500
3	15.23	16.10	2.75	38	20,000+	20,000+	20,000+	2,300
4	15.05	15.87	3.2	72	20,000+	20,000+	20,000+	4,000
5	-	-	2.0	48	16,000	16,000	20,000+	3,200

Soil Gas TPH (ppm)								Sampling Event
MP 12-5.5	MP 12-12.5	MP 10-5	MP 10-9.5	MP 10-12	MP 13-8	MP 13-10	MP 14-7.5	
51	40	195	165	210	86	52	76	1
66	210	180	190	220	78	82	210	2
140	500	170	160	370	110	62	410	3
112	158	260	250	250	1,000	850	2,200	4
80	160	155	140	185	130	110	290	5

During the evolutionary process, vent well air-injection flow rates were increased to as high as 3.2 cfm, with soil gas measurements performed no sooner than 48 hours after each flow rate increase. The area of highest contamination (Zone III vicinity of MP-7, MP-8 and



MP-10) and adjacent monitoring wells MP-12, MP-13 and MP-14 were monitored during this pilot study. Monitoring point MP-6 was also measured as a relative control, where BTEX contamination had been remediated and TPH concentrations were reduced to baseline levels. Groundwater levels were also measured upgradient (at MW-201) and downgradient (at MW-202) of this test area when soil gas samples were collected.

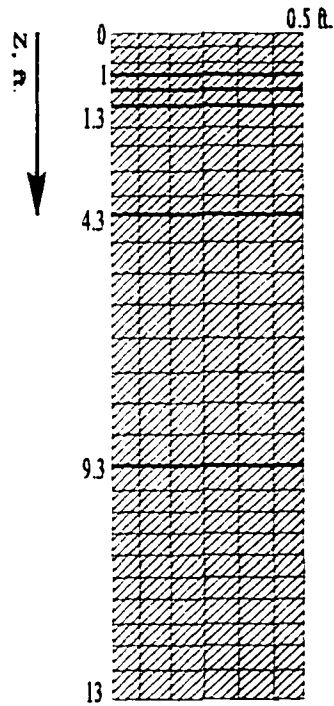
Baseline soil gas concentrations were first recorded as sampling event #1, for the 2-cfm operating mode injection rate. As air-injection flow rates were increased, soil gas TPH concentrations generally increased throughout the test area (Table 5-3). A small increase in the air-injection flow rates was apparently associated with measureable increases in soil gas TPH concentrations at some monitoring points. This phenomenon suggests that volatilization (hydrocarbon stripping) could be enhanced even with slight increases in system-wide bioventing flow rates. Therefore, to minimize stripping and to preserve thermally enhanced bioventing efficacy, the 2-cfm operating mode was maintained as the optimal rate.

## 5.6 TDHC Heat Transfer Modeling

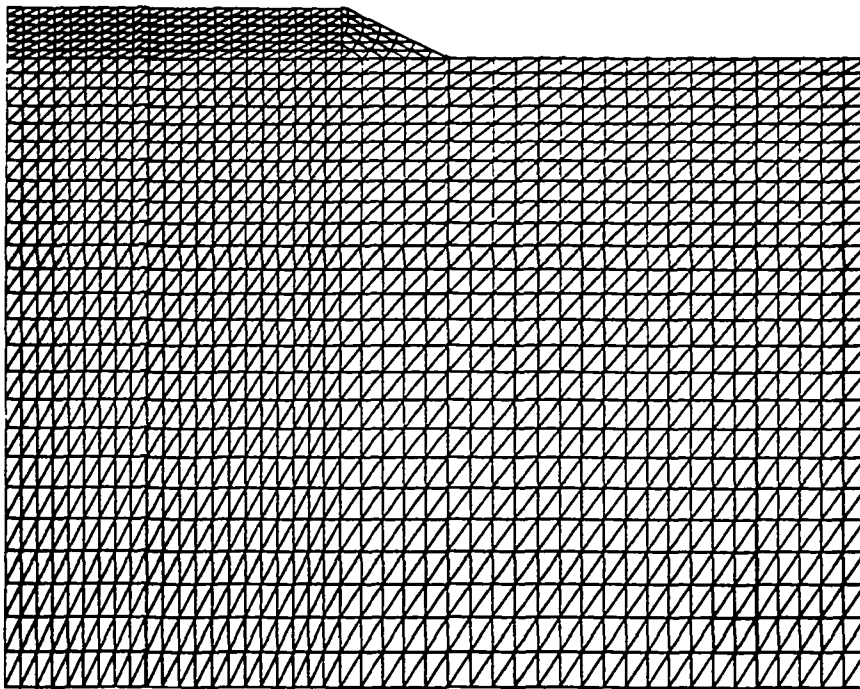
The finite element mesh (Figure 5-2) generated for the Zone I and II TDHC analyses is based on the Figure 4-5 columnar soil profile. Seven columns and three to thirty-five rows of nodes define the triangular elements comprising the six soil layers. A similar three layer grid (based on Figure 4-8b), made up of seven columns and seven to thirty-five rows of nodes, was used for the Zone III analysis.

Figure 5-3 is the finite element mesh generated for the Figure 4-9 boundary analysis problem. Five to eleven rows, and five to twenty-one columns define the triangular elements comprising the multilayered system.

TDHC was run for both 2-year and 4-year simulations, applying both case 1 and case 2 (sec. 4.6.4a) surface boundary conditions. For the analyses, it was important to accurately define the initial [average] temperatures for each layer. With accurate temperatures TDHC can be run for the actual project duration time with confidence in the results. However, carelessly chosen initial value temperatures requires that TDHC be run beyond "real time".



**Figure 5-2.** Typical TDHC finite element mesh for 1D analysis.



**Figure 5-3.** Boundary problem finite element mesh.

to filter out the effects of these inaccuracies on the simulated temperatures. The initial temperatures identified in the Chapter 4 problem summaries for each treatment zone were based on actual field temperatures measured at the start of active warming (November 7, 1994). The thermal data and problem definition portion of the grid input files required for the TDHC analyses are included in Appendix G.

---

**Analyses and Results**

Bioventing data collected between November 1994 and July 1996 have been compiled and analyzed for inclusion here as supporting evidence that thermally enhanced bioventing can increase biodegradation rates and reduce overall remediation time of hydrocarbon contaminants. At sites where nutrients and organic contaminants are sufficiently available to afford biodegradation, temperature may be the second most significant parameter affecting bioventing, after oxygenation. Therefore, primary emphasis is given here to the thermal aspects of soil gas, microbiology and geochemistry data, and heat transfer as they relate to bioventing effectiveness.

**6.1 Thermal Comparisons**

Nineteen months of thermocouple data collected from the three test plots were compared in the forms of whiplash curves and specific depth temperature profiles over time. Quarterly subsurface whiplash curves reflect the dynamic thermal regimes and influences by the TISs and climate changes. Year to year monthly comparisons are also presented to illustrate variability in snow cover and meteorological conditions for the same time periods. Comparisons of TDHC model output and measured subsurface temperatures are then made for the last six months (November 1995 to May 1996) of thermal monitoring.

**6.1.1 Whiplash Curves**

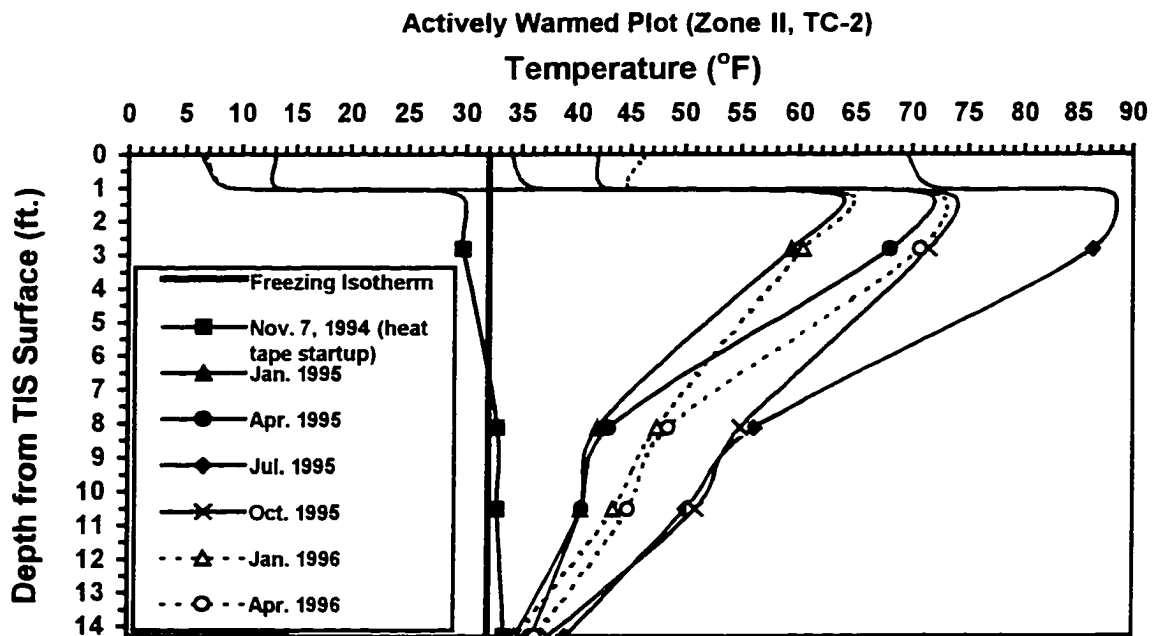
Quarterly whiplash curves were generated from the field thermal data for the three treatment zones (Figures 6-1a, b and c). The January and July curves represent peak winter and summer subsurface temperatures, respectively. The April and October curves best reflect

thermal conditions during spring breakup and fall snowfall transition periods. Hash-line curves depict second year (1996) January and April subsurface thermal conditions.

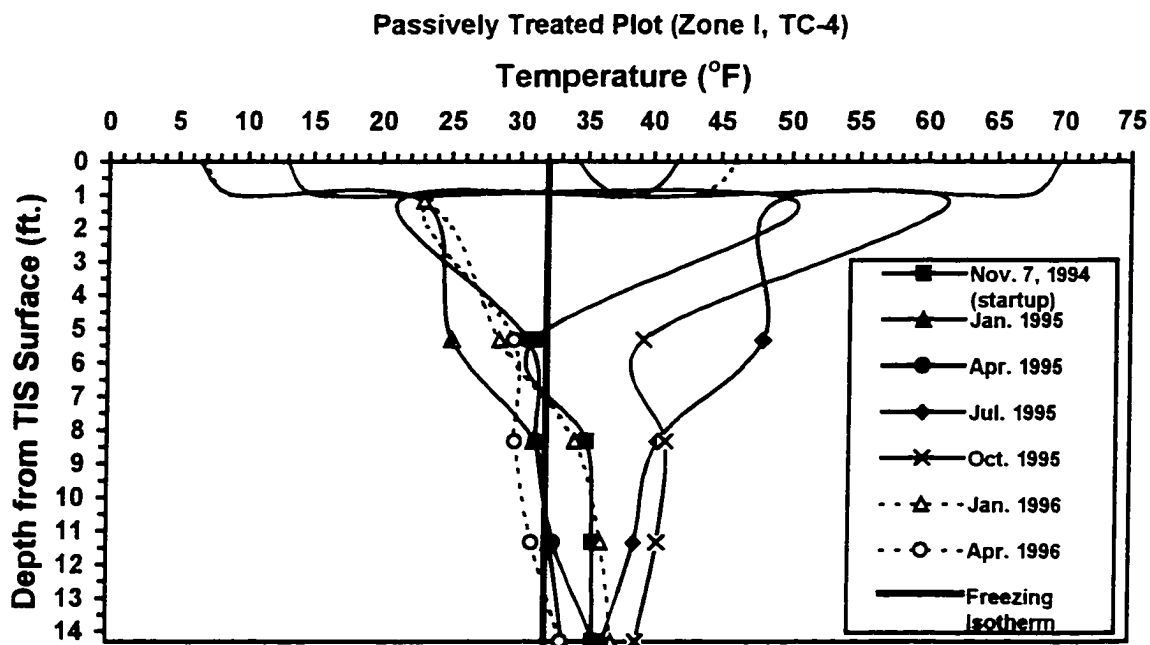
Whiplash curves are typically used to display temperatures as a traveling wave that moves into the ground with time. The influence of surface temperature changes on the soil thermal regime arrive at successive depths at progressively later times. Ideally, whiplash curves would exhibit smooth "trumpet" curves through the subsurface, shifting from left to right between peak winter to peak summer months. However, as Figures 6-1(a), (b) and 6-2 illustrate for the UAF bioventing site, true whiplash curves can be significantly modified by variability in surface conditions and soil warming. Installation of TIS materials, seasonal snow cover and climatic variability, and soil heterogeneities all influence the shape of whiplash curves.

With respect to Figures 6-1 and 6-2, the plotted surface temperatures are based on calculations using the sinusoidal surface temperature variations defined in section 4.6.4a. Here the referenced surface is synonymous with the top of the D-1 sand-gravel layer. The deepest temperatures plotted (at the water table) are based on quarterly groundwater temperature measurements taken during sampling efforts. Otherwise, the plotted temperatures through the TIS materials reflect theoretical calculations based on heat flux conservation across the upper layers (see Appendix H for sample calculations). Monitoring points TC-2 (Zone II, actively warmed), TC-4 (Zone I, passive treatment) and MP-10 (Zone I, control) were chosen as representative of the three test plots. The thermal gradients across the Zone II TIS materials (Figures 6-1a and 6-2) are modeled with site atmospheric, heat tape operating, and TDHC temperatures (immediately below the insulation layer).

A comparison of the three test plot whiplash curves evidences pronounced effects of active warming on the Zone II unsaturated soils (Figure 6-1a). Year-round thermal profiles plot consistently to the right of (above) the freezing isotherm. Similarities between the Zone I (Figure 6-1b) and control (Figure 6-1c) whiplash curves suggests only slight thermal enhancement from passive treatment. In fact, specific comparison of the July and October 1995 curves on these two figures suggests that passive TIS materials were disadvantageous to soil warming in summer.

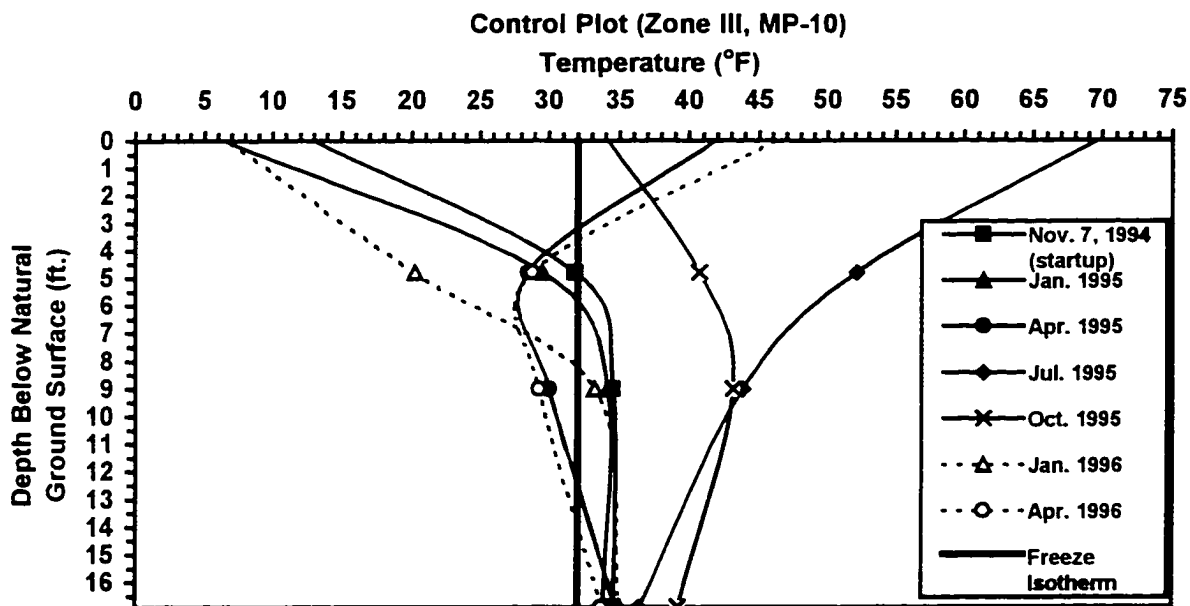


(a)



(b)

Figure 6-1. (a) TC-2, (b) TC-4 and (c) MP-10 vadose zone whiplash curves.



(c)

Figure 6-1 continued. (c) MP-10 vadose zone whiplash curves.

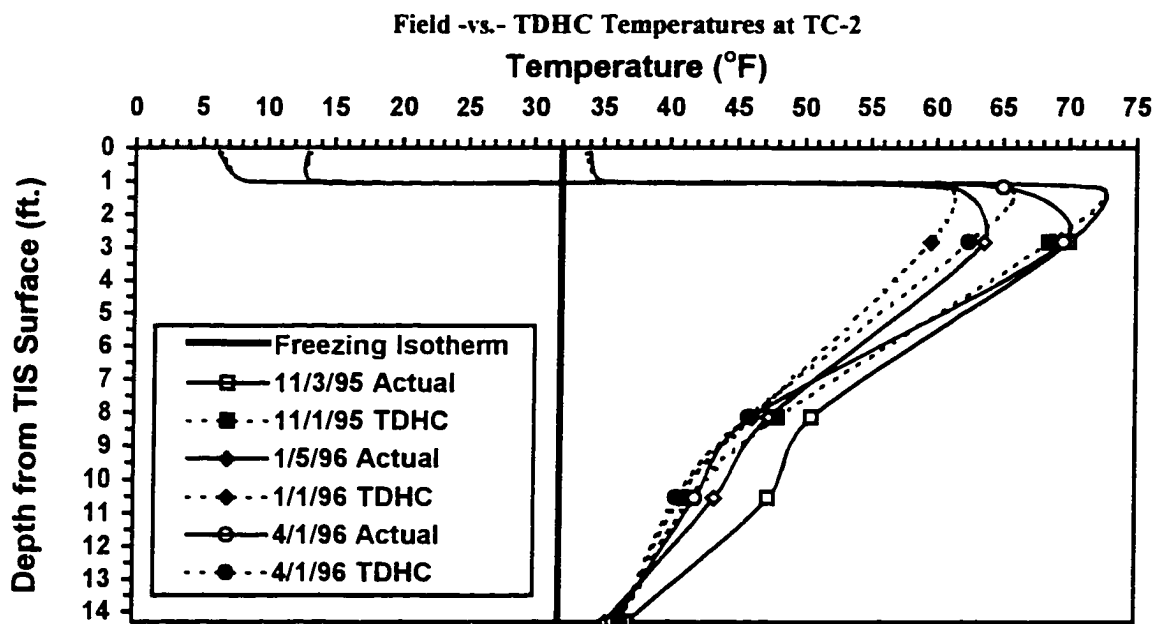


Figure 6-2. Comparison of actual and TDHC based subsurface temperatures at TC-2.

Surface condition variability and the effects of insulation can be seen when comparing the two January whiplash curves for each of the three test plots. During the winter of 1994-95, early, moderate snow accumulations dominated the surface cover. Snow removal was conducted by the UAF Physical Plant in mid-December. New snows again covered the bioventing site after late January. Late and light snow cover provided little additional insulation from harsher air temperatures during the second winter. This surface condition variability appears to be reflected in the upper 9 feet of the January 1995 and January 1996 control plot whiplash curves (Figure 6-1c). The opposite is true for the two January whiplash curves in Figure 6-1(b). Surface conditions apparently had less effect on subsurface soils beneficially protected by surface insulation. Surface cover variability had even lesser effect on actively warmed soils below insulation, where the artificial heat source (heat tape) governs thermal influence. The successively warmer Zone II January-to-January and April-to-April thermal profiles (Figure 6-1a) suggests progressive active warming.

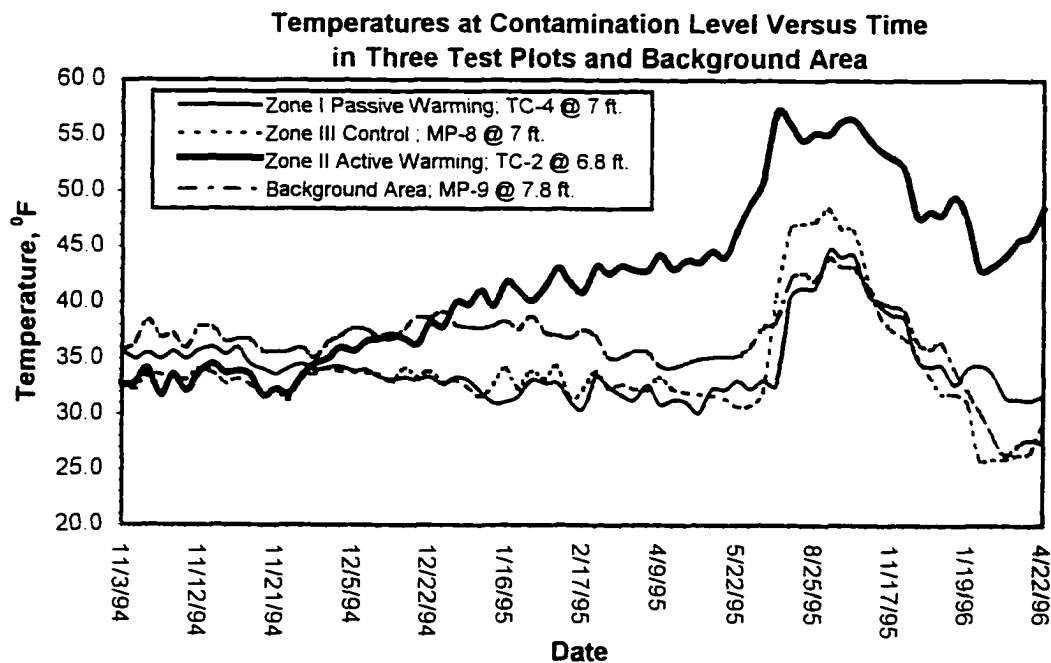
Figure 6-2 presents instantaneous whiplash curves based on actual field temperatures collected on specific dates during the second winter of thermally-enhanced bioventing. Whiplash curves plotting TDHC simulated temperatures for these [approximate] dates are included for comparison. Further discussion about the TDHC results is left to section 6.1.3.

### **6.1.2 Time Variance Temperature Profiles**

Figures 6-3 through 6-6 represent year-round thermal data collected from specific vadose zone depths across the bioventing site. Figure 6-3 compares subsurface temperatures at the "contamination level" (the 7-foot depth was synonymous with the bottom of the now-removed USTs) for the three test plots and background area. Figure 6-4 compares temperatures at the 10-foot intermediate depth. Figure 6-5 charts soil temperatures near the groundwater table. Figure 6-6 compares subsurface temperatures for the area of highest soil contamination to those at the background area.

As previously illustrated in the whiplash curves, the time variance graphs clearly show that the Zone II vadose soils were actively warmed between 8°F and 16°F above background and other test plot soils. It is also apparent from these graphs that the untreated Zone III





**Figures 6-3.** Subsurface temperatures at the contamination level versus time at three test plots and background area.

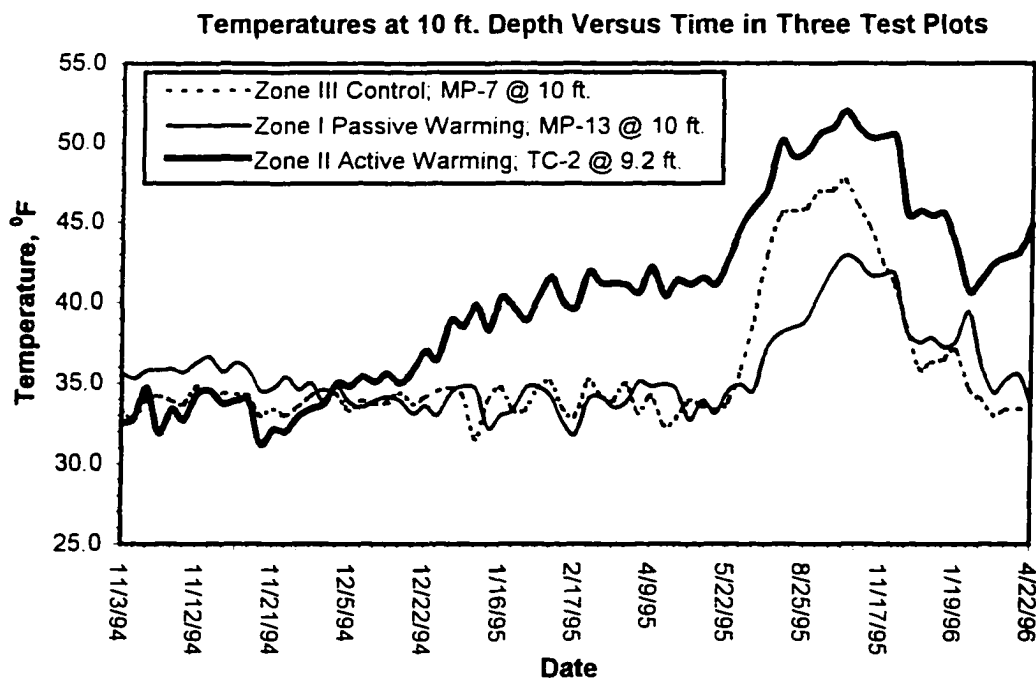


**Figure 6-4.** Subsurface temperatures at the 10-foot depth versus time at three test plots.

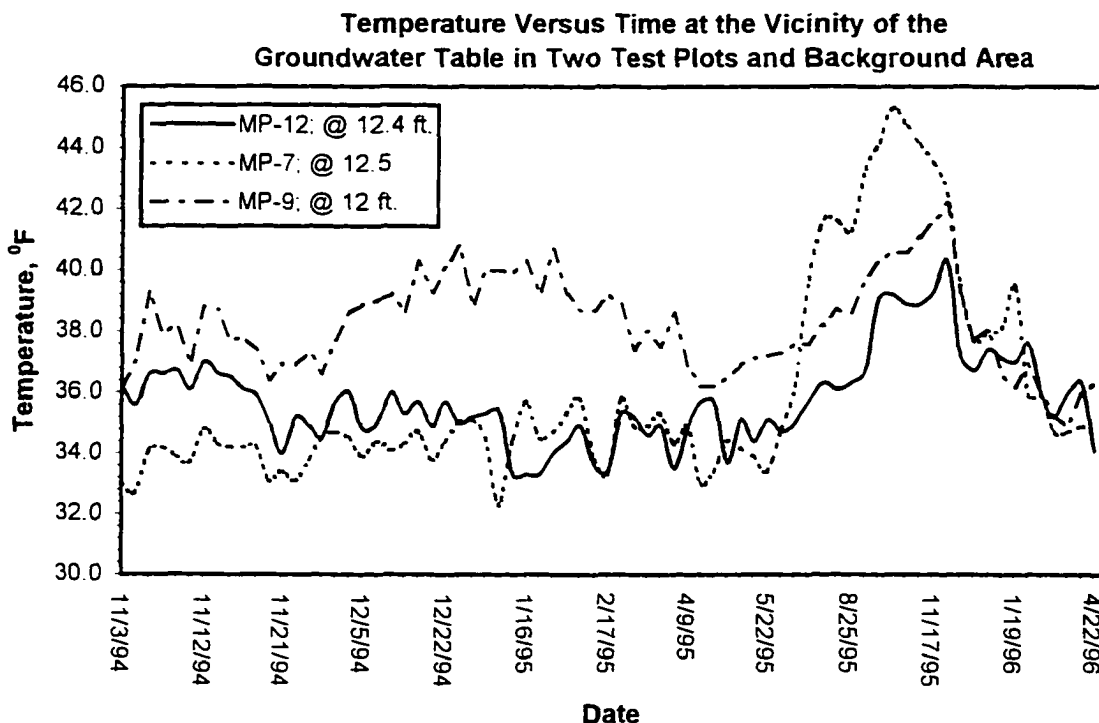


**Figure 6-5.** Subsurface temperatures versus time near the groundwater table in two test plots and background area.

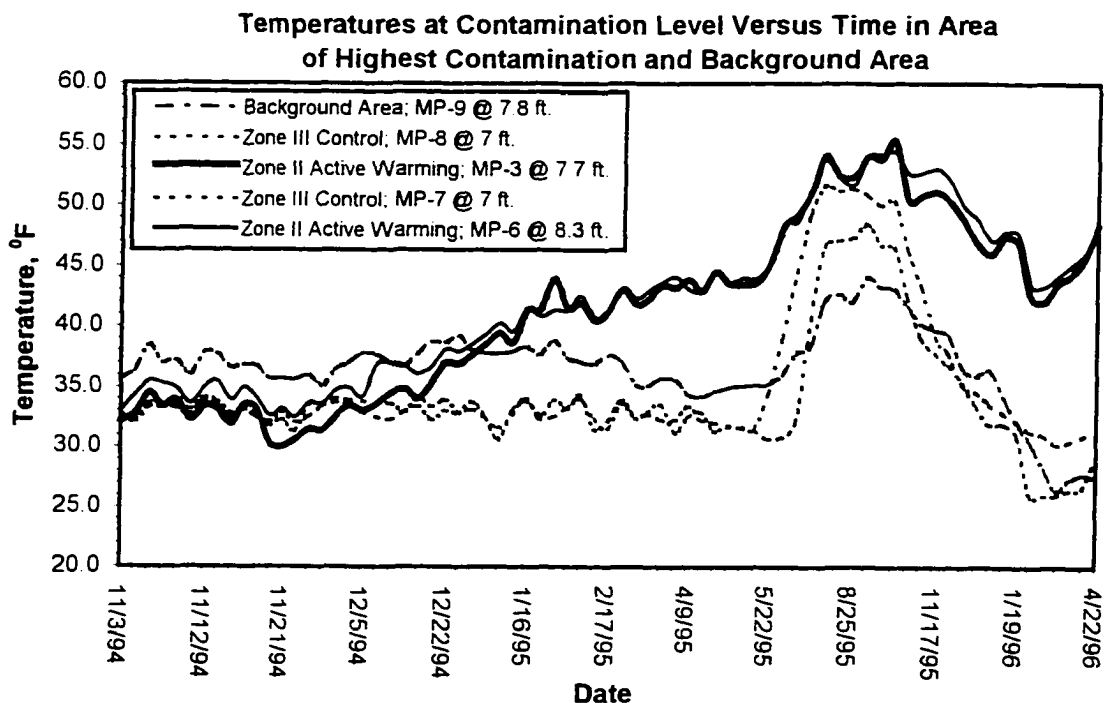


**Figure 6-6.** Subsurface temperatures at the contamination level versus time in the area of highest contamination and background area.

unsaturated soils were more effectively warmed by solar radiation during the summer months than were passively treated soils. Zone I TIS surface materials apparently became thermally limiting in summer, and perhaps somewhat disadvantageous to biodegradation efficacy.

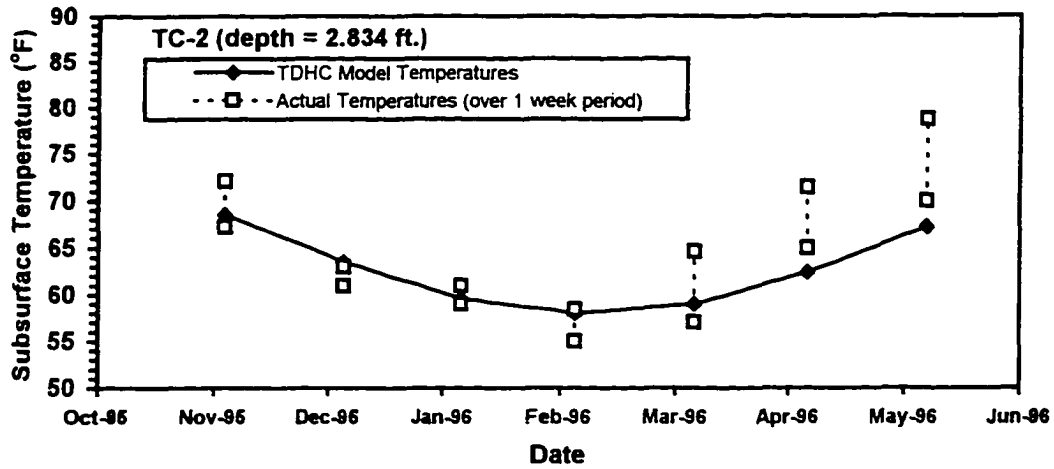
Most interesting is the summertime thermal data collected from the area of highest contamination (Figure 6-6). Soil chemistry and soil gas data consistently measured highest contaminant levels at MP-7 and MP-8, respectively. Solar radiation influence between May and October 1995 increased control plot soil temperatures to near those recorded for the actively warmed treatment area (Figures 6-4 and 6-6).

### **6.1.3 Model and Field Temperature Comparisons**

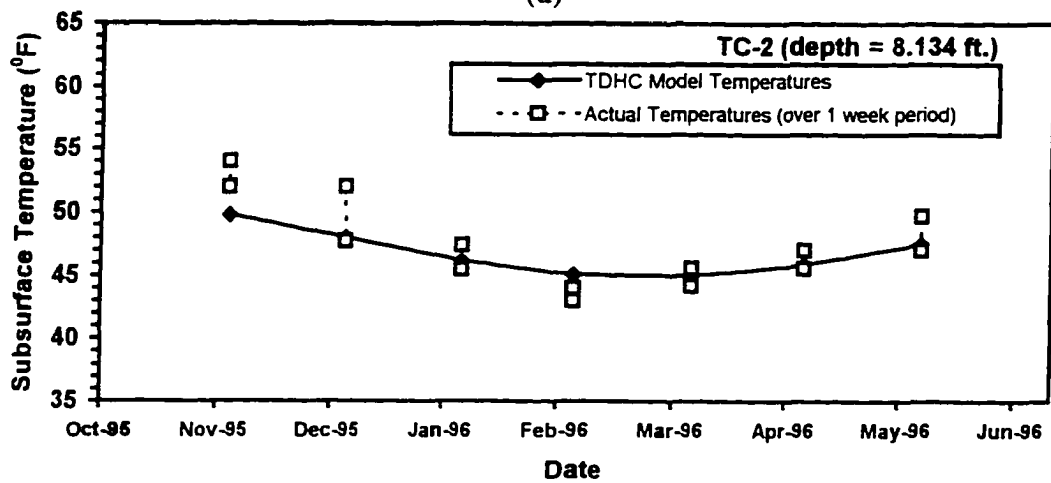
TDHC generated temperatures were compared with the measured subsurface temperatures at discrete thermal monitoring points within the three test plots, for the 1D analyses. The last six months of thermal data was chosen for comparisons. This afforded one full year of program runs to minimize errors associated with initial value layer temperatures, and to “realize” a state of relative thermal equilibrium for active warming (Zone II). The model curves are the theoretical temperatures for the end of each month (or first of each month for the 2D Zone II boundary analysis) of the second year period between November 1995 and May 1996. The actual field data, depicted as temperature ranges (1D analyses), represents thermocouple readings taken at different times during the week spanning the end of each month. The discrete thermocouple depths indicated are with respect to the TIS surfaces or the actual ground surface (control Zone III). Selected comparative profiles for each treatment zone are included here for analysis (Figures 6-7 through 6-10). Additional comparison plots are included in Appendix G.

#### **6.1.3a Zone II**

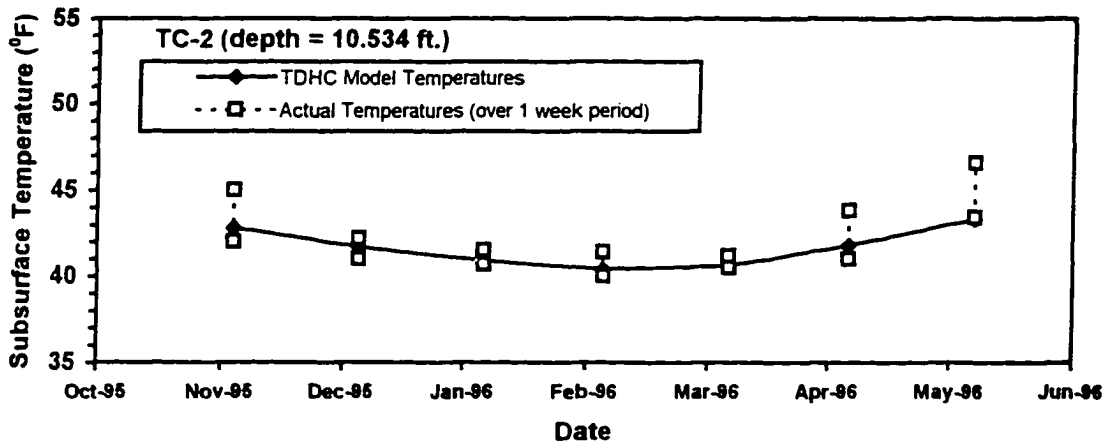
The TC-2 monitoring point was chosen to best represent the Zone II test plot for 1D analysis because of its interior location and because it maintained three operating thermocouples at various depths. From the shallowest (Figure 6-7a) to the deepest (Figure 6-7c) thermocouple depths, model and actual temperatures generally correlated to within a



(a)



(b)



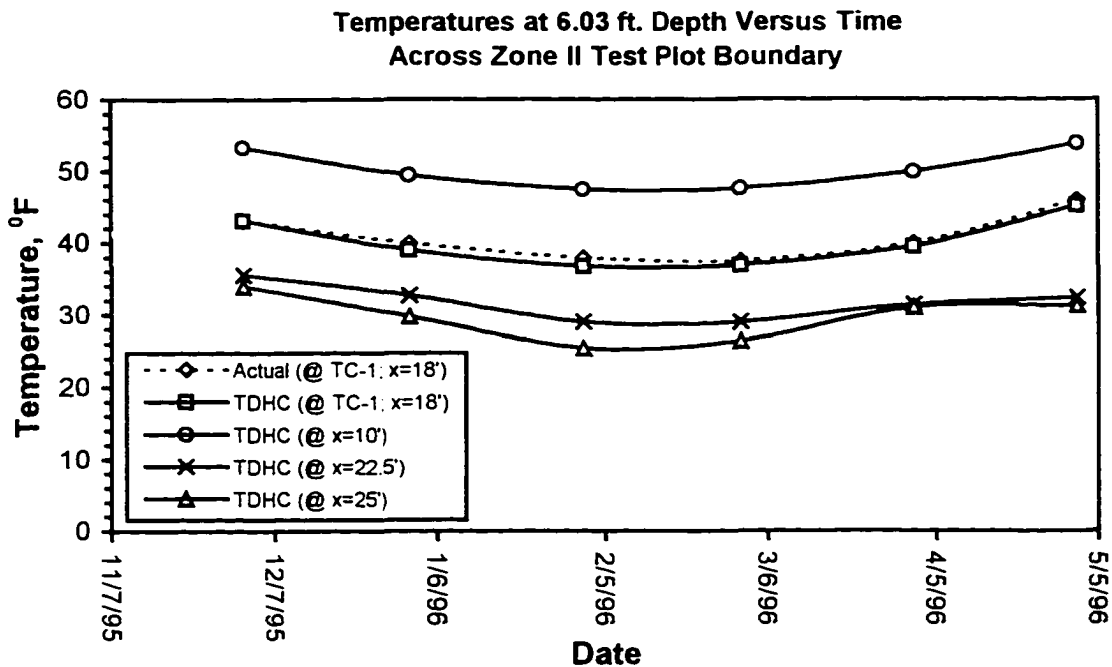
(c)

Figure 6-7. Comparison of TDHC model output and measured Zone II temperatures at (a) TC-2 (2.834 ft.), (b) TC-2 (8.134 ft.), and (c) TC-2 (10.534 ft.).

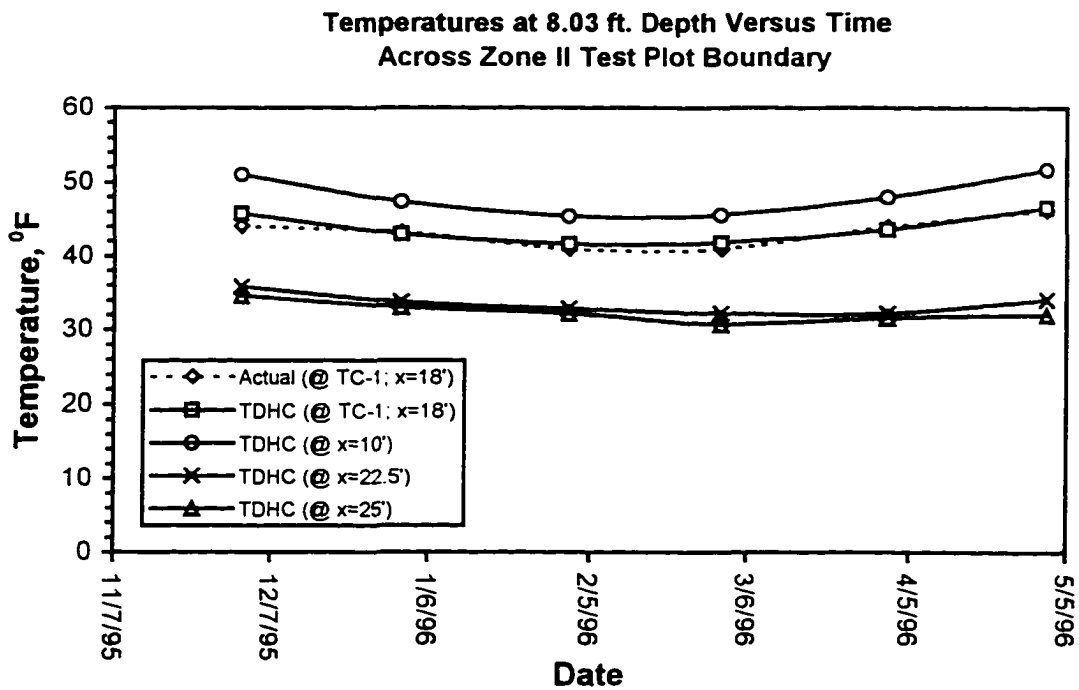
couple of degrees Fahrenheit. However, an increase in the measured weekly temperature ranges for April and May 1996, and the [warmer] departure of the actual from the modeled temperatures at shallow depth (at 2.834 feet in depth), is attributed to changes in the surface boundary condition. Recall that the approximated surface boundary condition (case 1, equation [4-15]) was based on reasonable [published] n-factors and atmospheric temperature data. Because shallow depth soils are more likely to be influenced by the surface boundary condition, it would have been better to use actual soil surface temperature data to define site specific n-factors. At the deeper TC-2 thermocouple depths, the effects of surface temperature variations are not realized this far below insulating materials and a continuous surficial heat source. Consequently, a greater degree of model versus field temperature correlation is apparent.

Thermal monitoring point TC-1 was chosen to verify model accuracy for the Zone II test plot, 2D, boundary analysis. TC-1 was installed at the northwest quadrant of the Zone II TIS pad (Figure 3-2), approximately two feet from the pad's sloped perimeter. With respect to Figure 4-9, this location is eighteen feet from the left edge (TIS pad centerline). Using the two discrete TC-1 thermocouple depths (6.03 and 8.03 feet) for this analysis, subsurface temperatures were modeled and compared at various distances from the test plot centerline (Figures 6-8a and b). Again, with reference to the Figure 4-9 centerline (at  $x = 0$ ), horizontal distances 10 feet, 18 feet, 22.5 feet, and 25 feet, represent locations midway to the pad perimeter, two feet from the top of the side-slope, midway through the side-slope, and at the base of the slope, respectively. For the case 1 condition (equation [4-15]), the TC-1 [actual] field temperatures were modeled to within one 1°F for the last six months of bioventing (Figures 6-8a and b). With sufficient accuracy determined for the 2D analysis, the other plotted TDHC thermal curves are reliable.

Several thermal observations are noted in the Figure 6-8 thermal comparisons. First, shallow soils nearer the TIS perimeters experience greater heat loss to the surrounding cooler environment than do deeper soils at the same location. Secondly, significant lateral heat loss occurs from under the outermost five feet of TIS pad and peripheral sloped regions. Lastly, the depth of freeze can be expected to reach the contaminant level (7 foot depth vicinity) at



(a)



(b)

**Figure 6-8.** Comparison of subsurface temperatures across a Zone II perimeter boundary at (a) 6.03 feet, and (b) 8.03 feet in depth.

the toe of the sloped perimeter region during the two coldest months of the year. Together, these analogies suggest that a moderate increase in the size of TIS coverage is necessary to afford acceptable thermal treatment of the soil contaminant plume periphery.

### 6.1.3b Zone I

Monitoring points MP-13 and MP-14 were chosen to best represent the Zone I test plot because of their thermal profile similarities. From the shallowest (Figures 6-9a and 6-10a) to the deepest (Figure 6-9c and 6-10c) thermocouple depths, model and actual temperatures agreed to within one to two degrees Fahrenheit.

When comparing the model and actual temperatures for these monitoring points, two trends are realized at the shallowest and deepest thermocouple levels. At shallow depths, the TDHC thermal profiles reflect slightly warmer simulated temperatures than the actual measured soil temperatures. Again, especially without heat tape, shallow soils were more likely to be influenced by surface temperature variations. At depth (Figures 6-9c and 6-10c), the model profiles appear as near straight-line curves with time. For TDHC analysis, the groundwater table was modeled as a constant temperature boundary when the problem was defined (section 4.7.2). Consequently, as TDHC simulated the thermal regime approaching the water table, the year-round temperature profile was expected to be constant at 36.5°F

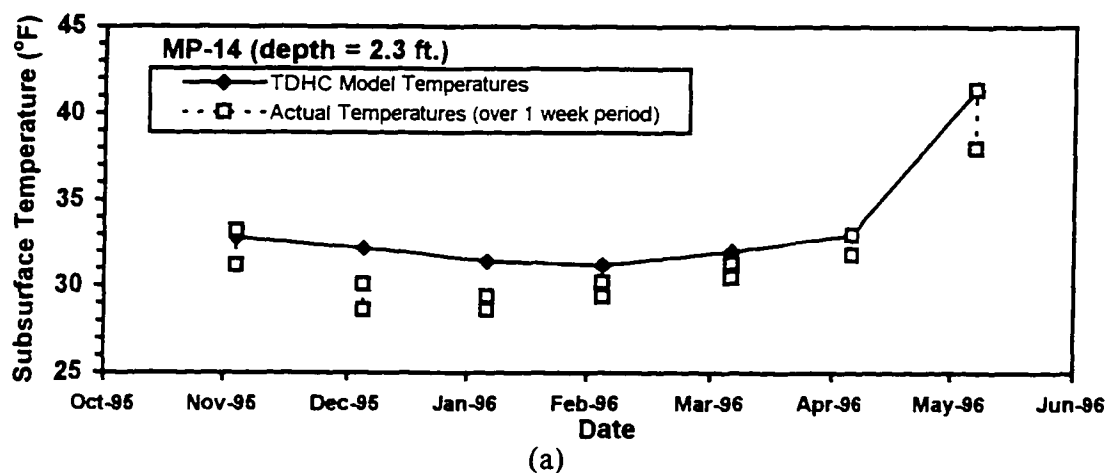
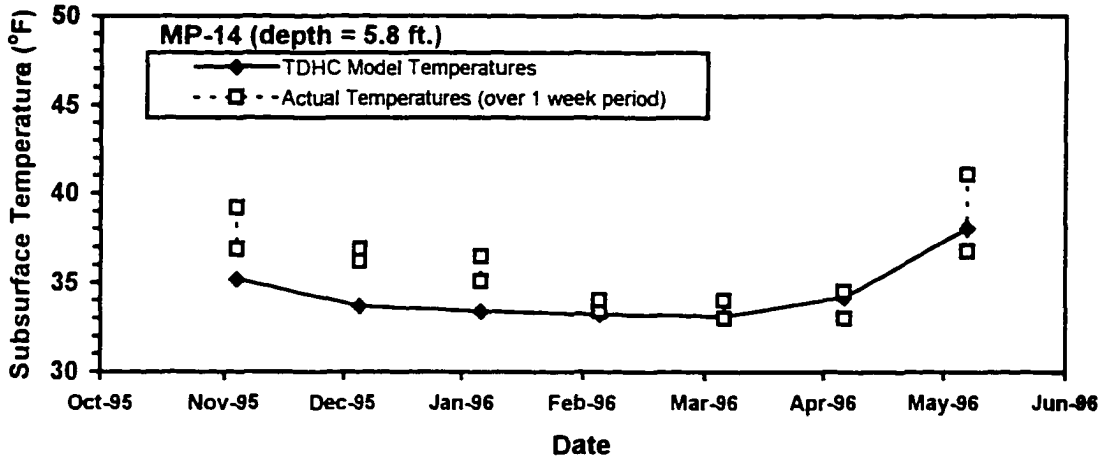
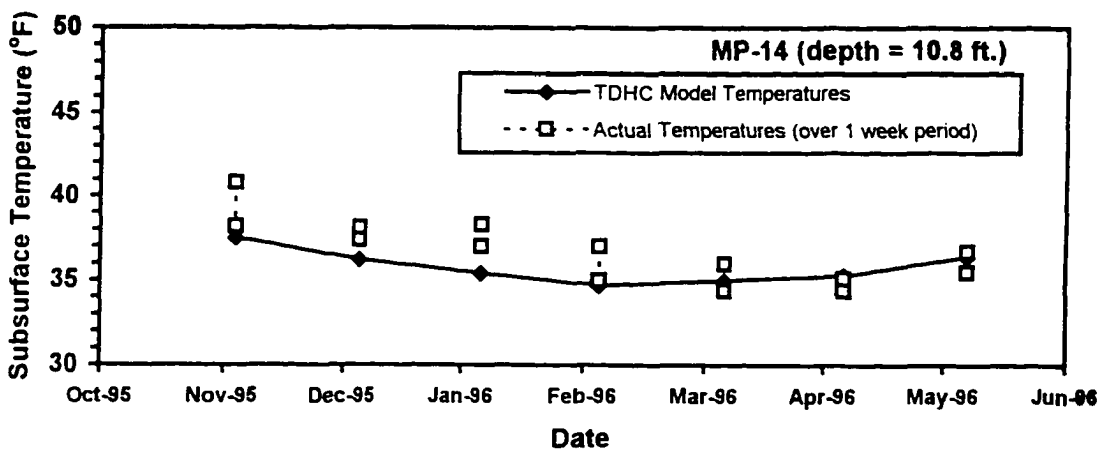


Figure 6-9. Comparison of TDHC model output and measured Zone I temperatures at (a) MP-14 (2.3 ft.), (b) MP-14 (5.8 ft.) and (c) MP-14 (10.8 ft.).



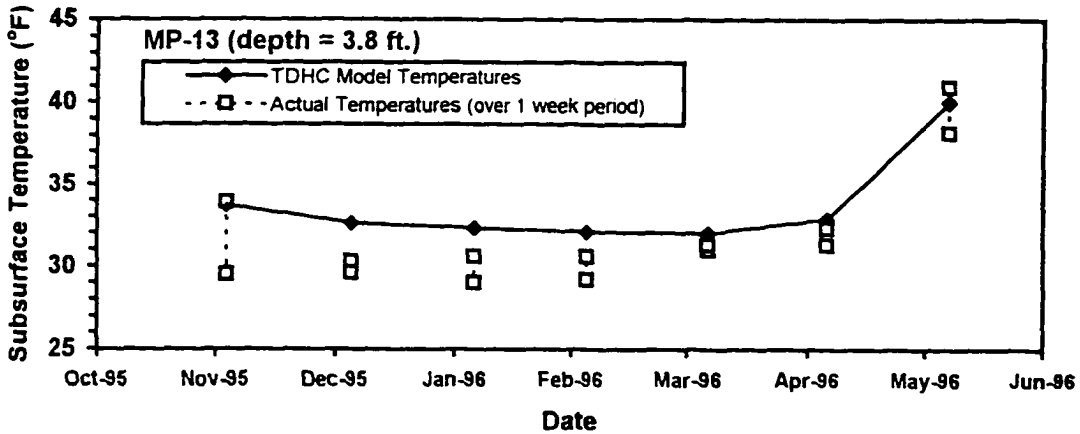
(b)



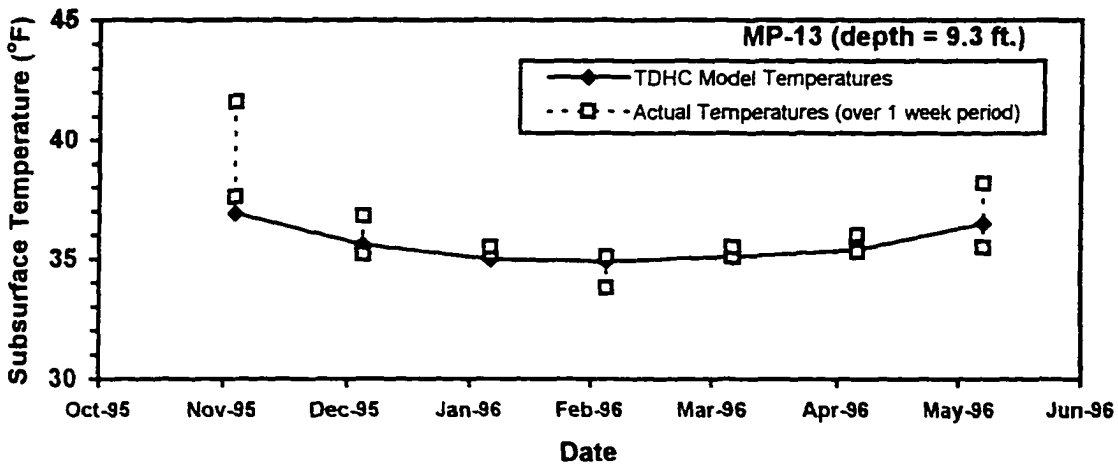
(c)

Figure 6-9 continued.

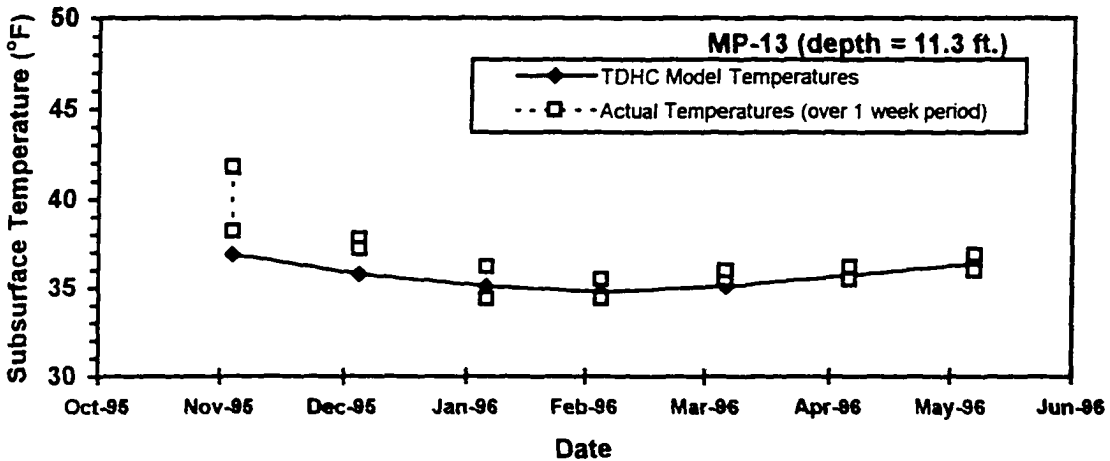




(a)



(b)



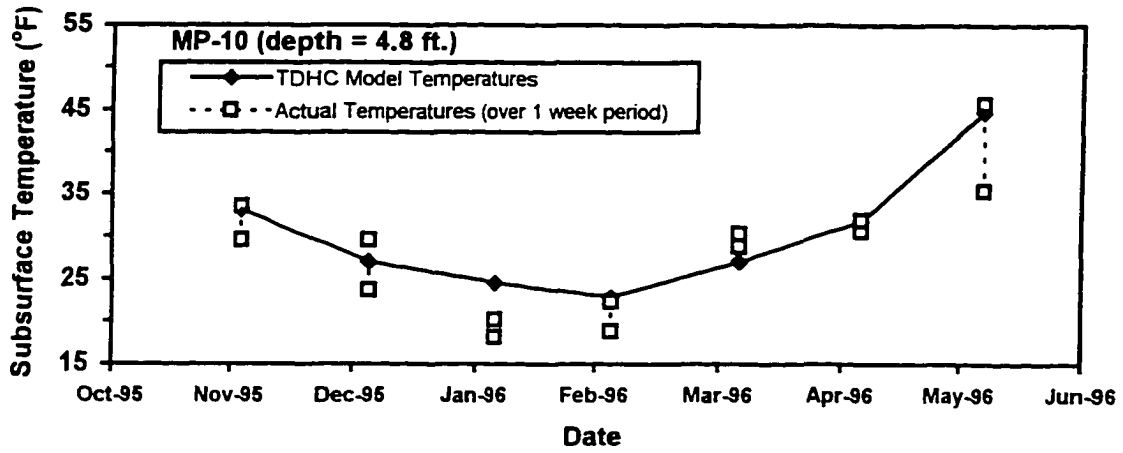
(c)

Figure 6-10. Comparison of TDHC model output and measured Zone I temperatures at (a) MP-13 (3.8 ft.), (b) MP-13 (9.3 ft.) and (c) MP-13 (11.3 ft.).

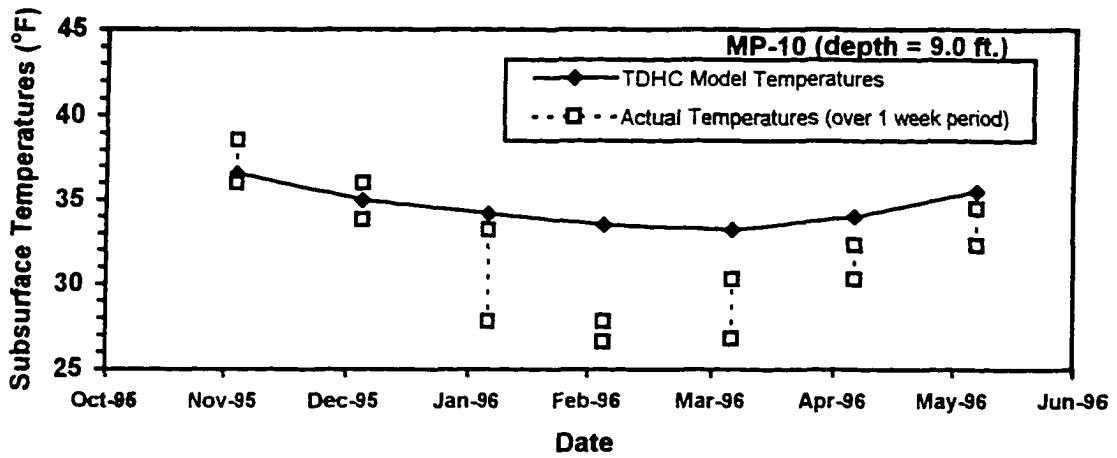
### 6.1.3c Zone III

Surficial soils within the control plot exhibited more sinuous temperature variations (Figure 6-11a) than did thermally enhanced soils. This was expected since the absence of TIS materials did not limit atmospheric influence on the subsurface thermal regime. Figure 6-11a is typical of the control test plot, in that model and measured soil temperatures generally agreed to within a degree for the upper five to six feet of vadose zone. However, frost-susceptible soils, and intermittent permafrost were identified below seven feet in depth between MP-8 and MP-10 (Shannon & Wilson, 1990; Montgomery Watson, 1992). The measured field temperatures below this depth at these two monitoring points (Figures 6-11b and 6-11c) reflect the anomalous condition(s). Soil temperatures dropped below freezing after December at MP-8 (Figure 6-11c). TDHC closely modeled the thermal regime at this depth. However, the TDHC temperatures began to plot consistently above the field data below this depth (Figure 6-11b) in this area. This is because the geotechnical input parameters (Table 4-3) were generically defined for the TDHC analyses and did not account for localized frozen ground conditions. Subfreezing soil temperatures in this vicinity were previously exhibited in the Figure 6-1c whiplash curve for MP-10.

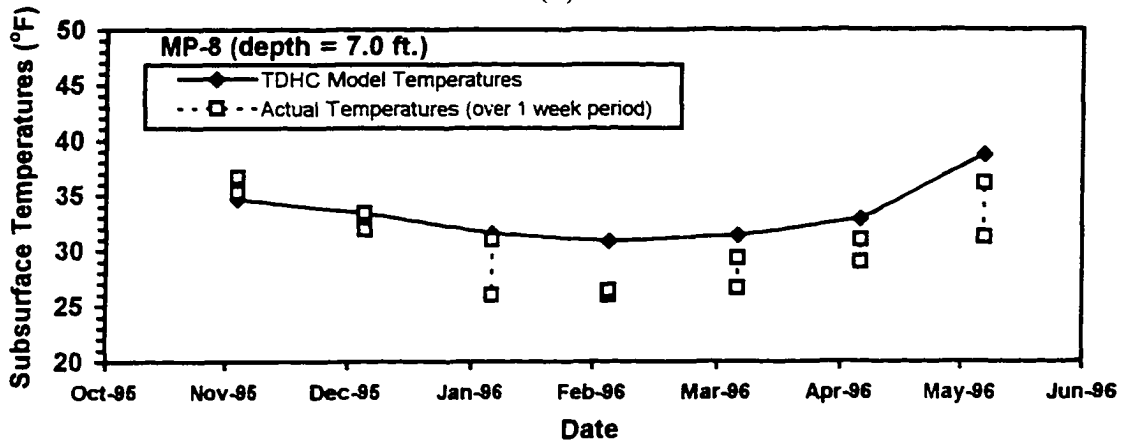
Cross-comparison of the represented thermal profiles (Figures 6-7a, 6-9a, 6-10a, and 6-11a) clearly demonstrates the beneficial effects of active warming over passive treatment and conventional bioventing without thermal enhancement.



(a)



(b)



(c)

Figure 6-11. Comparison of TDHC model output and measured Zone III temperatures at (a) MP-10 (4.8 ft.), (b) MP-10 (9.0 ft.) and (c) MP-8 (7.0 ft.).

## 6.2 Soil Gas Comparisons

Soil gas data are presented in support of thermally enhanced biodegradation with time. The data are by no means quantitative, but can be used to indicate fluctuations in bioactivity and to reflect changes in contaminant levels.

Figures 6-12 through 6-15 are representative soil gas plots versus time for the background area, and the three treatment plots. Soil gas monitoring point MP-9 (Figure 6-12) was established as a bioventing control location where no history of vadose zone contamination had occurred. Average nominal TPH concentrations of less than 50 ppm were typically recorded at this location. Baseline  $O_2$  and  $CO_2$  levels were measured at 20.5 and 0.4 percent, respectively (Arambarri, 1995).

Soil gas monitoring points MP-3 and MP-6 were located near vent well VW-3, within actively warmed Zone II. The MP-3 and MP-6 graphs (Figure 6-13) represent local soil gases measured over time within clean backfilled soils (after the UST tank removals) and adjacent BTEX contaminated soils, respectively. The MP-3 TPH concentrations and  $O_2$  and  $CO_2$  levels were comparable to uncontaminated background (Figure 6-12) conditions. In slight contrast, low level contamination associated with periodic mild fluctuations in  $O_2$  and  $CO_2$  levels occurred before June 1995 at MP-6. Biodegradation activity and a decline in TPH concentrations to nominal values were since recorded at MP-6.

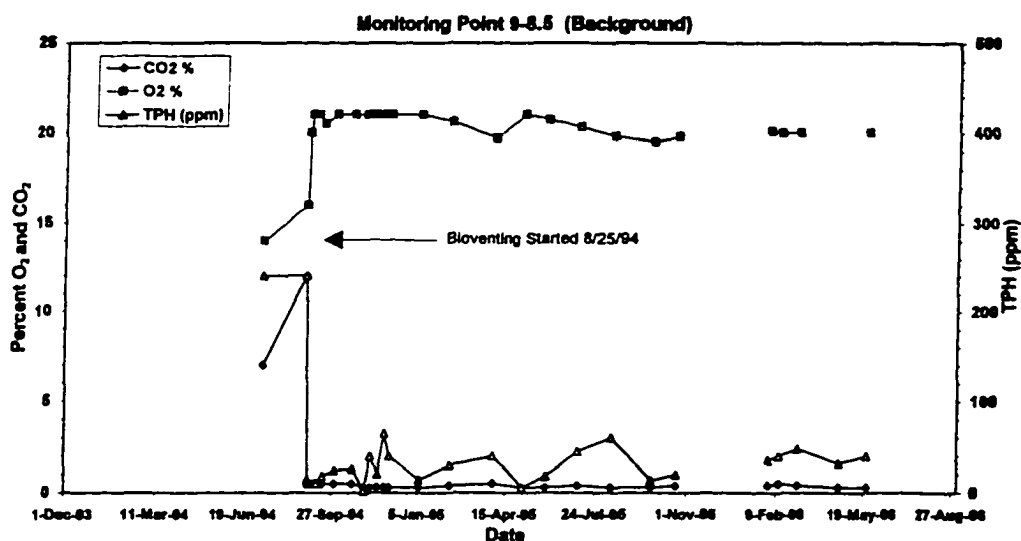
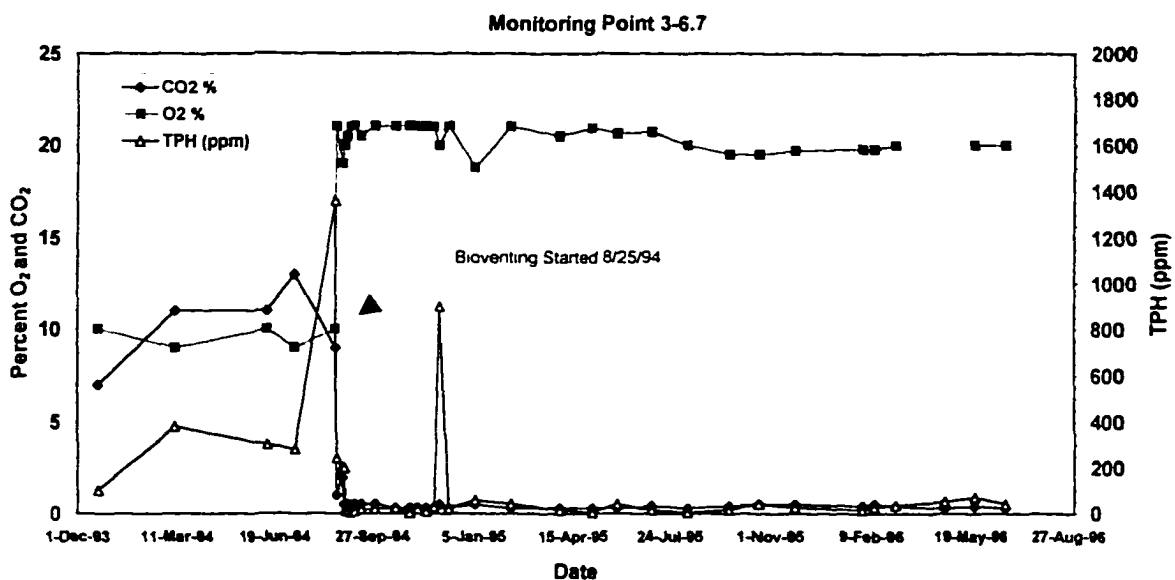
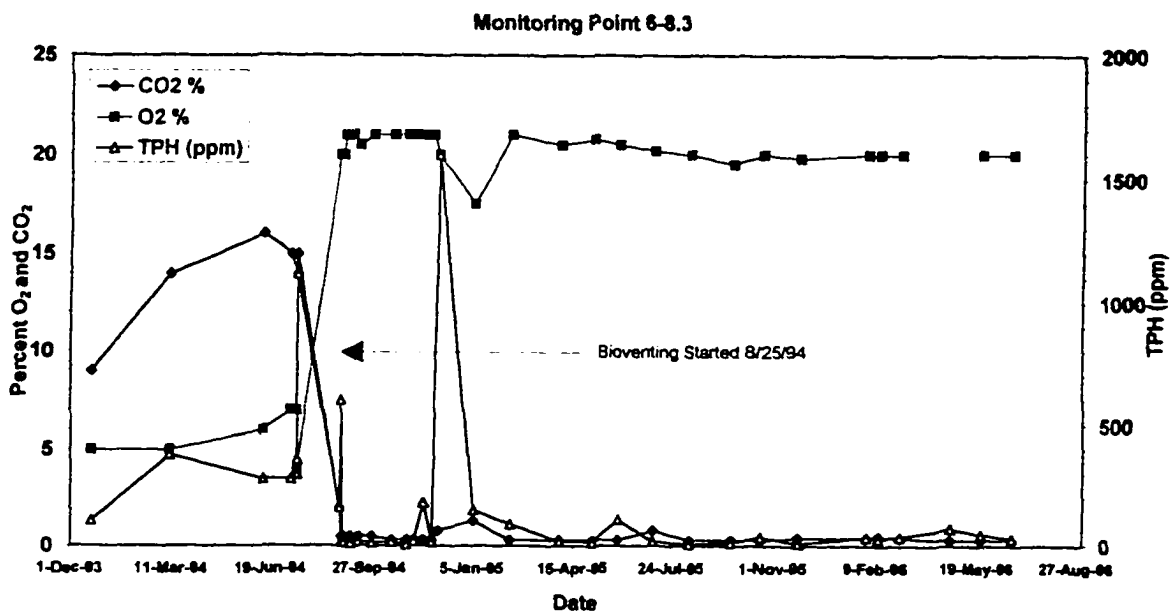


Figure 6-12. Background soil gas monitoring versus time at MP-9.



(a)



(b)

**Figure 6-13.** Actively warmed Zone II soil gas monitoring versus time at (a) MP-3 and (b) MP-6.

Soil gas monitoring points MP-12, MP-13 and MP-14 are located within the Zone I interior (Figure 3-2). Moderate TPH concentrations between 500 and 3,000 ppm (typically less than 1,000 ppm) were measured from contaminated soils to the groundwater table before midsummer 1995. Since August 1995 O<sub>2</sub> and CO<sub>2</sub> levels most often reflected baseline conditions. However, anomalous TPH spikes at depth were associated with the winter to spring seasonal transition periods (Figure 6-14; MP-13 representative). TPH spikes to 900 ppm, measured at depth between early April to mid-May 1995 and 1996, apparently were associated with groundwater fluctuations.

An explanation for this phenomenon can be surmised after looking at site groundwater level data and water characteristics associated with the 1995 spring breakup period. First, the continuously ascending TPH data trend between January and May 1995 (Figure 6-14) is misleading. The soil gas charts presented plot trendlines over time, of data collected approximately once a month. The trends do not accurately reflect subsurface soil gas concentrations between monitoring events. With that in mind, the TPH spikes in question were associated with the shorter time period centered around breakup. Secondly, soil analytical data (presented in Appendix H) indicated that remaining contamination in the vicinity of MP-13 was at the smear zone-groundwater table interface. Lastly, MP-103 groundwater depth data collected on March 15, 1997, April 2, 1995, and May 31, 1995 measured the water table at 13.81, 14.42, and 12.83 feet below the natural ground surface, respectively, in the main bioventing area.

As the groundwater table dropped between mid-March and early April, BTEX contamination was reintroduced into the expanding vadose zone (adsorbed to soils). With venting, oxygenation induced volatilization and enhanced bioactivity. O<sub>2</sub> and CO<sub>2</sub> fluctuations associated with the TPH spikes support this hypothesis. With breakup, an infusion of snowmelt waters from the surface contributed to the rising water table in early April. By the end of May the groundwater table had once again risen to shrink the vadose zone. Figure 6-14 clearly depicts the descent in TPH and O<sub>2</sub> and CO<sub>2</sub> levels synonymous with reduced bioactivity, as the spike event ended.

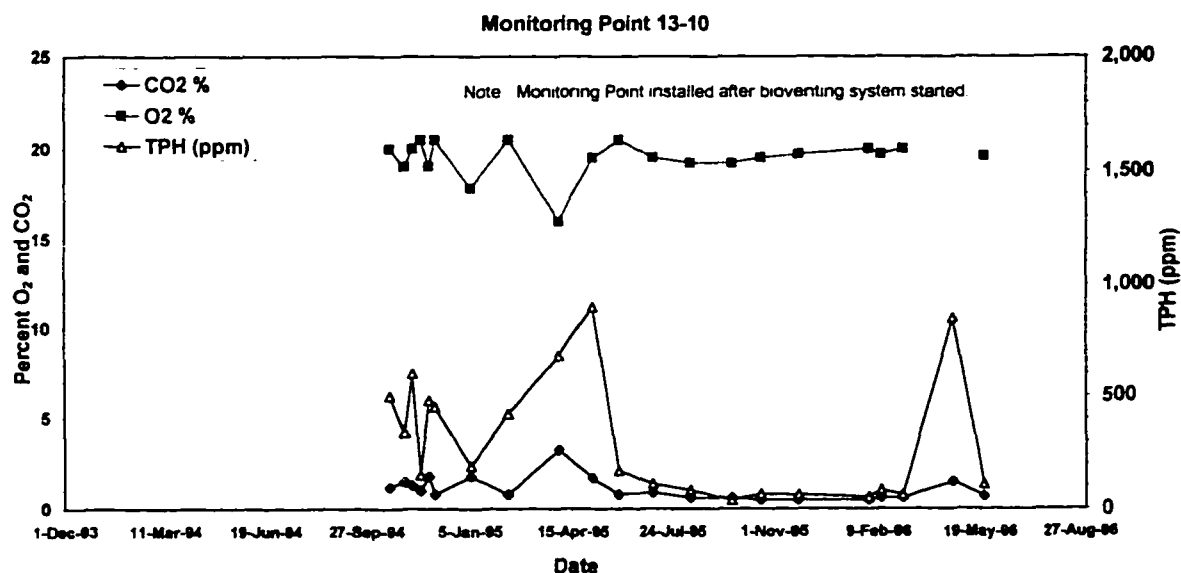
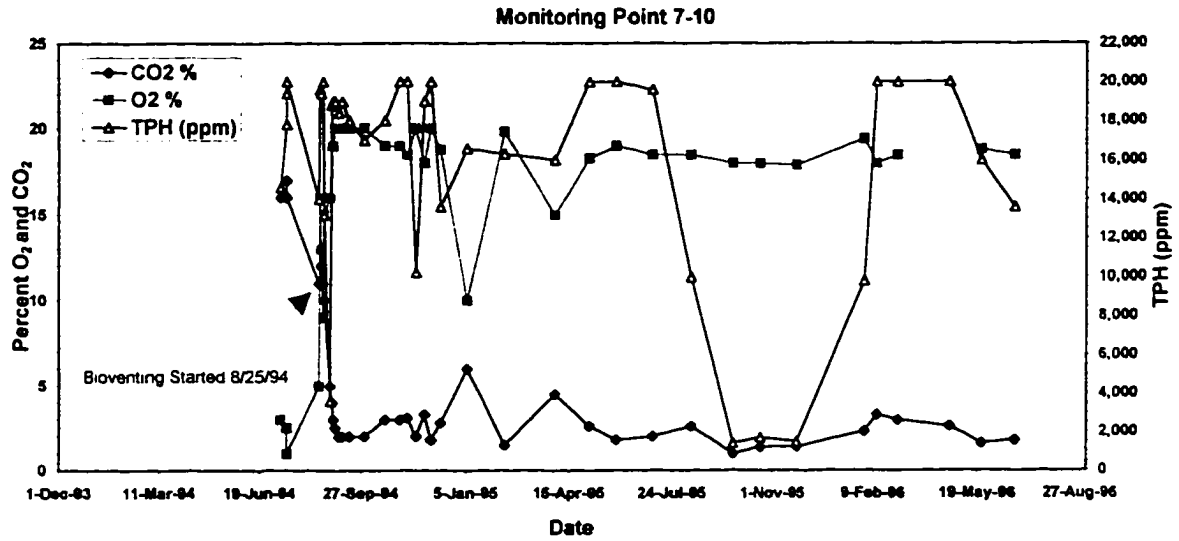
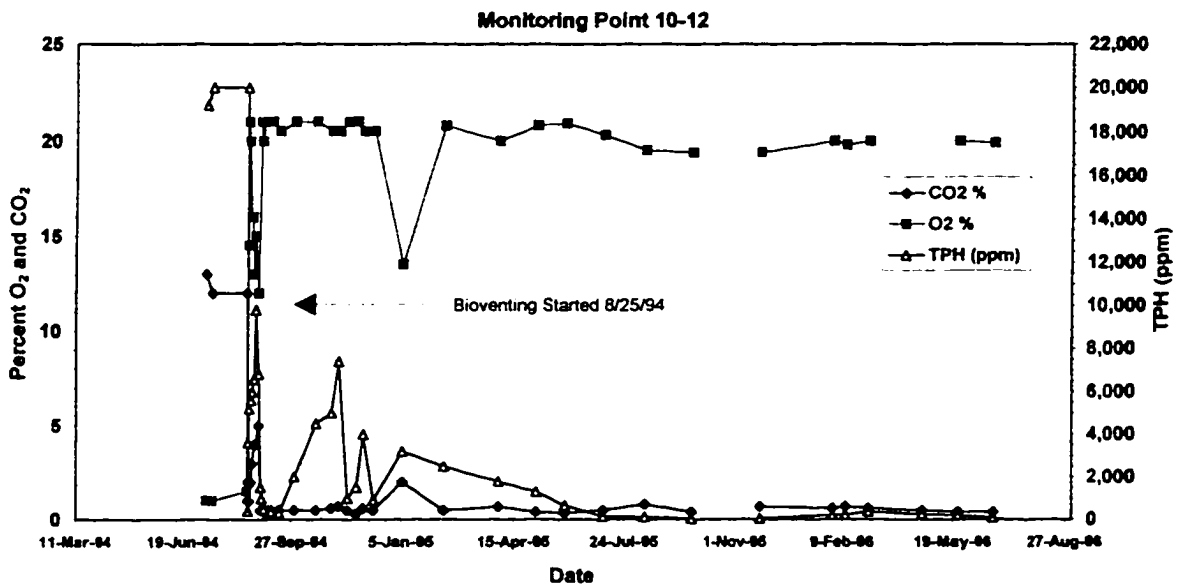


**Figure 6-14.** Zone I soil gas monitoring versus time at MP-13.

Prior to mid-April 1995, wintertime biodegradation was evidenced by reductions in O<sub>2</sub> and increases in CO<sub>2</sub> soil gas concentrations associated with high levels of TPH at MP-7 (Figure 6-15a) and MP-10 (Figure 6-15b). Much of this bioactivity was likely associated with the lower part of the vadose zone, where soils were generally more contaminated and less susceptible to freeze. During breakup, April melt water infiltrations and groundwater fluctuations were associated with declines in carbon dioxide production and resurging TPH concentrations (Figures 6-14 and 6-15a). Periods where the vadose zone experienced significant wetting and rise in the groundwater table, suggested episodes deleterious to bioactivity. Significant wetting events within the vadose zone can trigger microbial death and a rapid decline in biomass (Alexander, 1994). After restabilization of soil moisture levels, increases in biodegradation rates were evident throughout the summer.



(a)



(b)

Figure 6-15. No action control Zone III soil gas monitoring versus time at (a) MP-7 and (b) MP-10.



A sharp September 1995 reduction in TPH concentrations at MP-7 and MP-8 (Figure 6-15a), while O<sub>2</sub> and CO<sub>2</sub> levels remained stable at about 18 and 1.4 percent, respectively, and then another ascending TPH spike in February was perplexing. As TPH exceeded 20,000 ppm at all three MP-7 monitoring depths during this event, MP-8 at the 7-foot contamination level measured TPH at less than 3,000 ppm. Frost-susceptible soils or intermittent permafrost near MP-8 did not seem restrictive to biodegradation rates, as associated O<sub>2</sub> levels fell while CO<sub>2</sub> levels increased. These soil gas anomalies were also exhibited at MP-7, but more so at the deeper 10 and 12.5 foot monitoring depths. An influx of groundwater or rise in capillary action within the smear zone may have occurred, with a surge in volatilization predominately responsible for the elevated TPH concentrations. A similar anomalous event was observed at MP-7 and MP-8, associated with artificially induced volatilizations during the system optimization test (Table 5-3, sec. 5.5).

### 6.3 Biodegradation Rates

Bioventing literature reports typical degradation rates between 1 and 20 mg/kg/day for BTEX and jet fuel contaminated soils. The corresponding air-injection flow rates were often in excess of 8 to 10 cfm. However, these degradation rates generally do not distinguish between hydrocarbon contamination that is truly biodegraded versus that which is artificially volatilized (stripped) by excessive soil venting. Off-gas generation and potential hazards to human health are sometimes ignored or simply not considered at remote or restricted sites. Hydrocarbon stripping will likely occur with bioventing of porous soils at such high venting rates. At the UAF site, qualitative thermal analyses and air quality standards required that hydrocarbon stripping be minimized. Through the system optimization test process, venting at 2 cfm was determined suitable to minimize stripping.

During the first year of bioventing, an average winter biodegradation rate of 0.54 mg/kg/day was determined by Arambarri (1995). In June 1995, I performed a respiration test to compare biodegradation rates for the three treatment plots. Biodegradation rates of 4.5 mg/kg/day, 1.8 mg/kg/day, and 1.9 mg/kg/day were determined for the active warming, passive treatment, and control test plots, respectively, at the constant 2-cfm venting flow rate.

These rates correspond to a site average summertime rate of 2.7 mg/kg/day. However, these discrete biodegradation rates (for the individual test plots) were not considered reliable for two reasons. First, contaminant dispersion and remediation requirements did not afford isolation of the test plots. Second, the levels of soil contamination were not the same for each treatment zone and across boundaries. This was evident when comparing the Zone III (highest soil contamination) rate to that of Zone I (passive treatment). It would be impractical to differentiate between biodegradation attributed to thermal enhancement with that attributed to contaminant level variability.

#### 6.4 Microbiology and Geochemistry Analyses

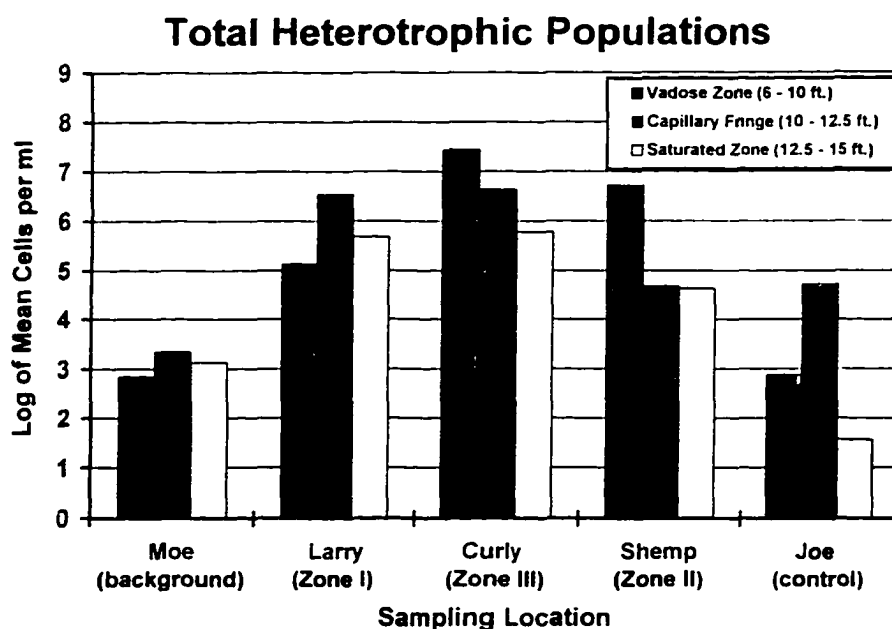
The microbiological results herein are predominately from one [1995] sampling event, with single data replications of enumeration assays and activity measurements. Mr. Peter Catterall, of UAF-IAB, performed the laboratory analyses. Levels of contamination are also reported for the June 1996 event. Microbial population measurements are inherently variable with time and location. As such, single replication did not allow for estimating that variability or making statistical comparisons.

**Table 6-1.** Microbiological summary relating vadose zone conditions to treatment type.

Sampling Location	Active Warming	Passive Insulation	Contamination Level Above Smear Zone (ppm)	Date	Moisture Content (%)
Joe	No	No	0.051 (total BTEX) 0.04 (total BTEX)	June 1991 July 1995	13
Moe	No	No	0.18 (total BTEX) ND	June 1991 July 1995	4
Shemp	Yes	Yes	300 (GRPH) ND	June 1990 July 1995	6
Curly	No	No	104 (GRPH) 27 (GRPH)	June 1990 July 1995	6
Larry	No	Yes	20 (GRPH) ND	July 1990 July 1995	2.5
C	No	No	0.16 (total BTEX)	June 1996	-
G	No	Yes	0.44 (total BTEX)	June 1996	-
H	No	No	0.03 (total BTEX)	June 1996	-
Z	No	No	0.06 (total BTEX)	June 1996	-

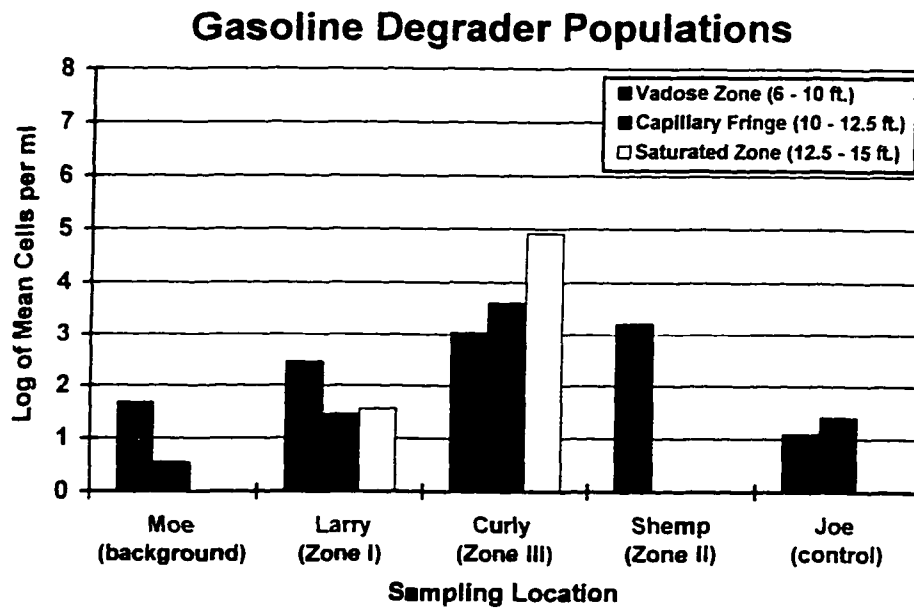
### 6.4.1 Microbial Populations

The total heterotrophic population appears to be related to the level of hydrocarbon contamination present (Figure 6-16a). For example, the greatest number of total heterotrophs ( $\approx 4.8 \times 10^7$  cells/ml) apparently occupied vadose zone soils from sampling borehole Curly. Curly was located near and downgradient from the old leaking USTs. With respect to the thermal treatment zones, the lowest heterotrophic populations ( $< 3,500$  cells/ml) were encountered at sampling borehole Moe, located in the uncontaminated [soil] background vicinity of MP-9 and vent well VW-6. Additionally, elevated heterotrophic numbers appeared associated with vadose zone contamination at Shemp, but more so with smear zone and groundwater level contamination at Larry (Zone I). For purpose of microbiological discussion, the terms "smear zone" and "capillary fringe" are considered synonymous. Sampling location Shemp was at the clean backfill and low-level contamination interface of the old USTs excavation pit.

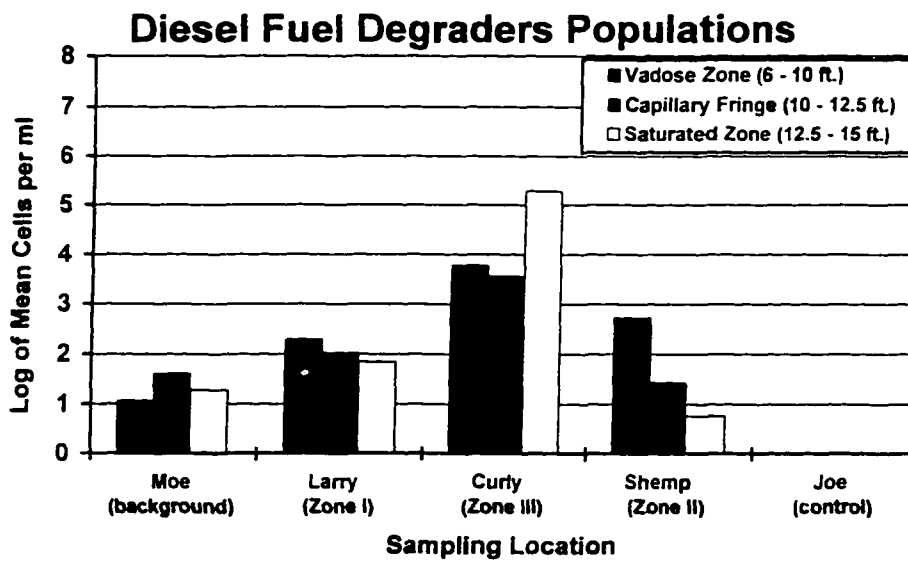


(a)

**Figure 6-16.** (a) Total heterotrophic, (b) gasoline degrader, and (c) diesel fuel degrader populations at five borehole locations.



(b)



(c)

Figure 6-16 continued.

Sampling location Joe, the uncontaminated, non-biovented control for microbiology analysis, was located between the northwest corner of the Physical Plant building and monitoring well MW-204 (Figure 5-1). Upper vadose and saturated zone heterotrophic numbers at Joe approached background (Moe) levels (Figure 6-16a). However, an elevated microorganism population was encountered at the capillary fringe depths. This anomaly may be explained from boring log and geochemical data, which revealed a perched water table at 9 feet, with 22 to 30 percent soil organic matter. High moisture contents and natural organic substrate(s) are most likely responsible for this increase in biomass.

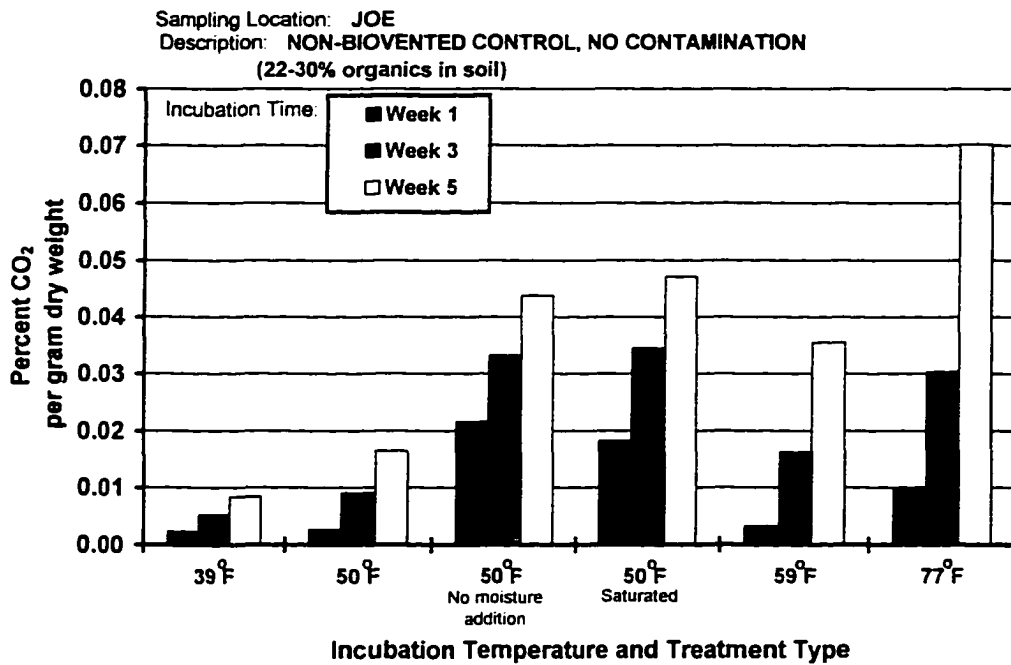
Furthermore, nearly identical CO<sub>2</sub> production levels were measured for both *in situ* and saturated composite soil samples from Joe (Figure 6-17a, sec. 6.4.2). The elevated CO<sub>2</sub> production at the 50°F incubation temperature suggests psychrophilic metabolism of the available organics. Psychrophiles generally metabolize optimally at less than 60°F. The perched water table simulates conditions at the groundwater table, but at shallower depth. Therefore, the two treatment types represent similar subsurface regimes.

The largest numbers of gasoline and diesel fuel degraders were found at Curly and Shemp (Figures 6-16b and c). At Shemp, the high populations of gasoline degraders were found in vadose zone soils. In contrast, downgradient at Curly, the highest populations of gasoline and diesel fuel degraders were encountered at the groundwater table. The Curly findings, in agreement with soil gas and NTL geochemistry data, suggest that remaining BTEX contamination can be found at the smear zone-groundwater table interface near Curly, MP-7 and MP-8.

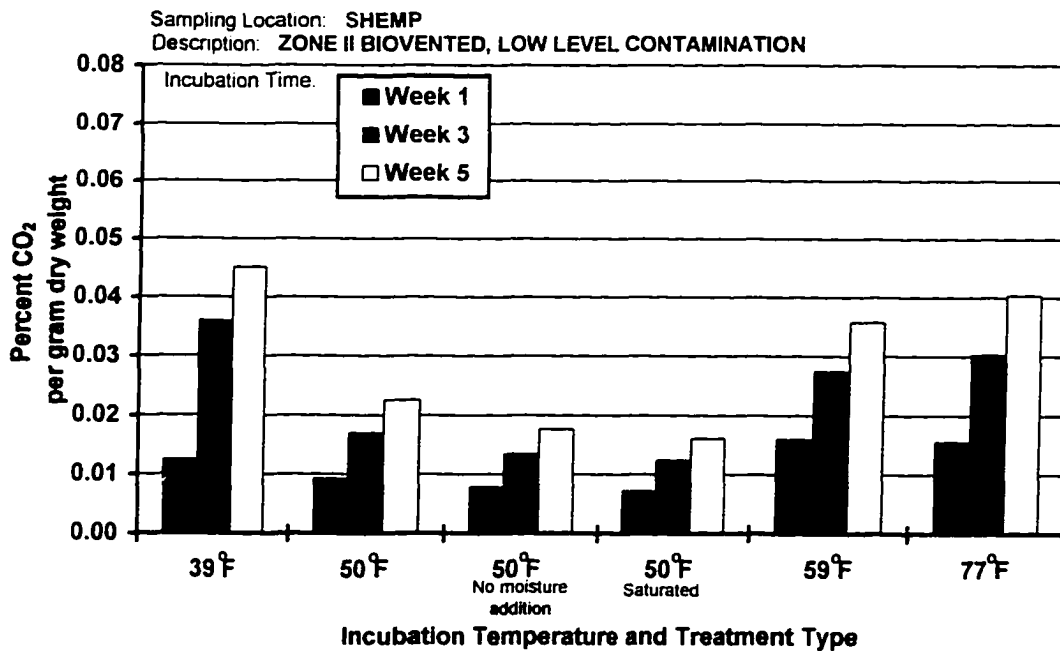
#### **6.4.2 Temperature, Moisture and Bioactivity**

Composite samples from depths generally between 7 and 12.5 feet (the contaminant level) were incubated at various temperatures, with variable moisture contents, in an attempt to relate these soil parameters to CO<sub>2</sub> respiration. These activity measurements are by no means qualitative, but some inferences can be made with respect to biodegradation potential.

For the contaminated vadose zone soils (Figures 6-17b, c and d), increased temperatures were generally associated with elevated CO<sub>2</sub> respirations. However, since

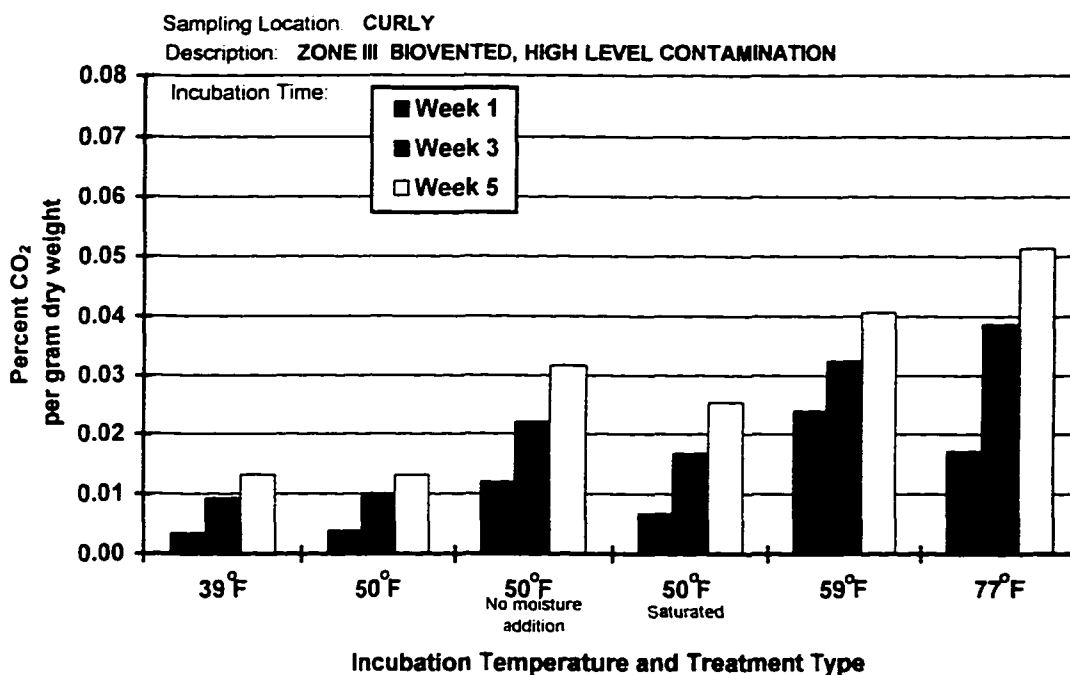


(a)

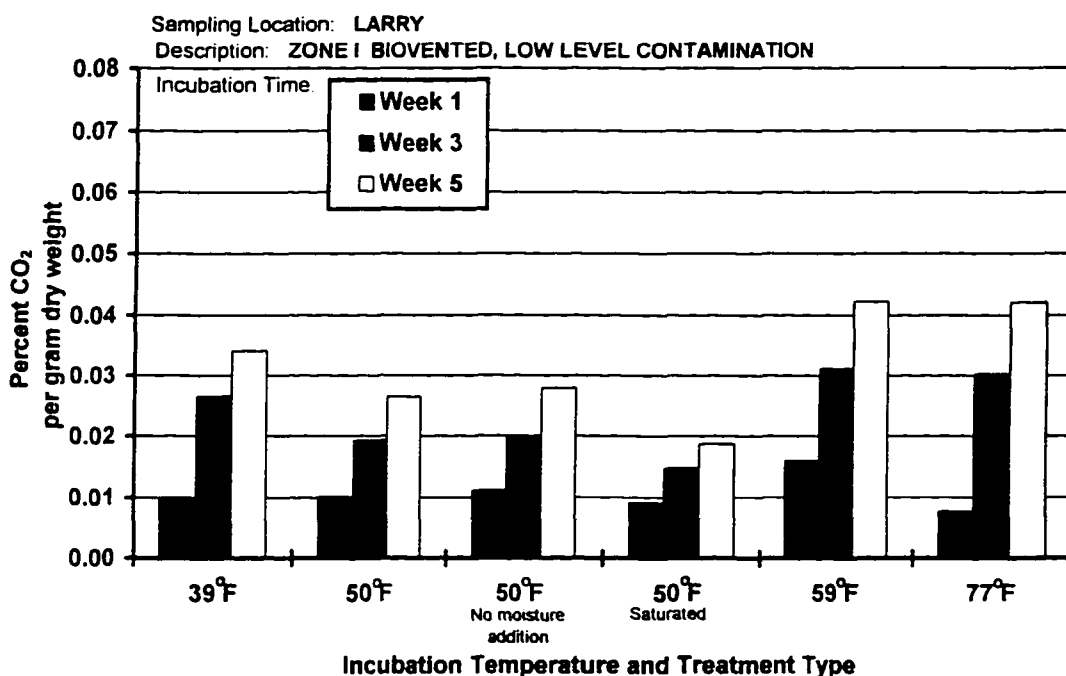


(b)

Figure 6-17. CO<sub>2</sub> production related to temperature and moisture at (a) Joe, (b) Shemp, (c) Curly, (d) Larry, and (e) Moe sampling locations.

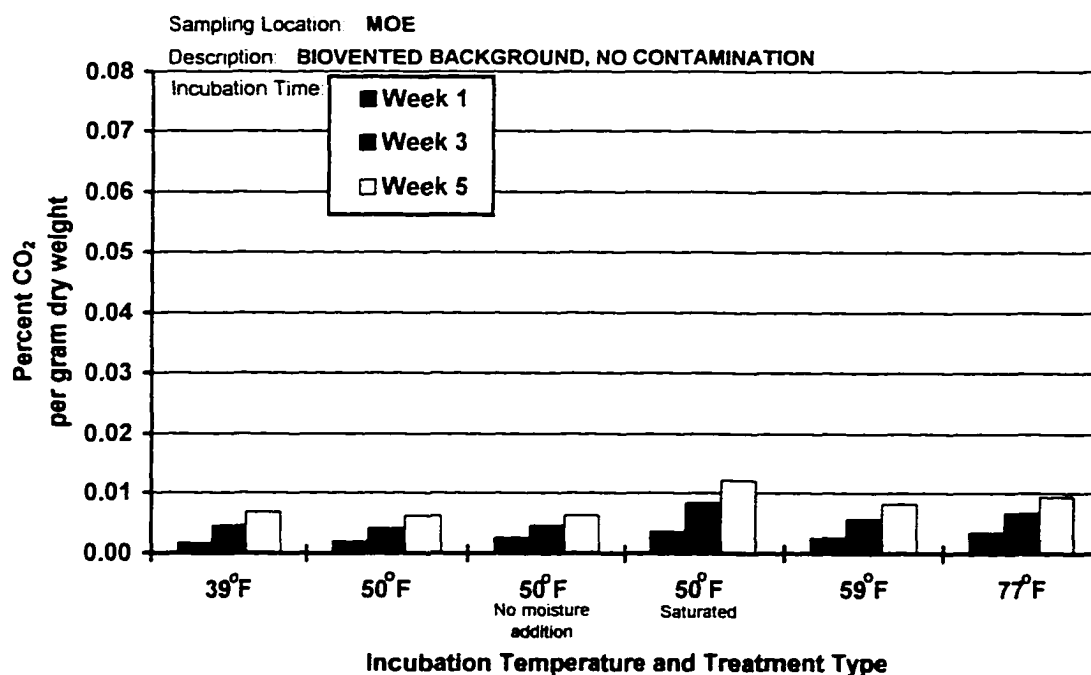


(c)



(d)

Figure 6-17 continued.



(e)

Figure 6-17 continued.

subfreezing temperatures dominated the vadose zone at Curly (Zone III) between November and May, mesophilic microorganisms may have accounted for bioactivity in the frozen soils. At Shemp (Figure 6-17b), increased respiration at both cooler and warmer temperatures may indicate coexistence between cold tolerant mesophilic and psychrophilic microorganisms. Between 39°F and 50°F, accumulated CO<sub>2</sub> concentrations of 0.035 and 0.045 percent per gram dry weight of soil (%/gdw) were comparable to the highest respiration rates (between 0.042 to 0.052 %/gdw) found at Curly.

Because the Shemp soil samples were taken from the actively warmed (Zone II) treatment area, the effects of temperature are not clear. Perhaps mesophilic populations take over at warmer temperatures, after a relatively short acclimation period.



Little effect of temperature on respiration was noted for the Moe soil samples (Figure 6-17e). These results would be expected where organic substrates (natural or contaminant) are in limited supply. However, at Joe, notable CO<sub>2</sub> productions between the 50°F and 77°F incubation temperatures suggests that higher temperature was conducive to increased bioactivity.

At Larry (Figure 6-17d), low-level variability in respiration was exhibited over the range of incubation temperatures. This was likely a result of testing a composite sample of relatively cleaned soils, from a location where remaining organic contaminants lie at or very near the groundwater table.

Moisture content variability did not appear to be a significant factor affecting biodegradation rates at the background (Moe) and main bioventing area sampling locations (Shemp and Larry). However, at Curly (Figure 6-17c), where the natural moisture content was measured less than three percent, bioactivity seemed to diminish with increased moisture at 50°F.

For all four incubation temperature treatments on the Joe control samples, the soils were dried down to the 60 percent WHC from a saturated state (consequence of a perched water table). This effectively lowered microbial populations, which resulted in lower respiration rates as compared to the 50°F "no moisture addition" and "saturated" bar graphs (Figure 6-17a).

Increased air-injection flow rates could have caused further drying of the vadose zone. It was surmised that any reduction in the already low natural moisture contents would likely reduce biodegradation efficiency. Due to the limited number of microbiological sampling locations and the apparent anomalous subsurface conditions at Joe (a perched water table and high natural organic content), a relationship between moisture content and natural organic biodegradations versus contaminant driven biodegradations cannot be postulated.

A summary of the microbiological and geochemical characterizations, with respect to temperature and moisture is presented (Table 6-2).

**Table 6-2.** Summary of microbiological characterizations at the UAF Physical Plant LUST site (after the first year of thermally enhanced bioventing).

<b>Parameter</b>	<b>Joe</b> Background for Microbiology; No Bioventing, No Contamination	<b>Moe</b> Bioventing Background; No Contamination	<b>Curly</b> (Zone III) Bioventing Control for Thermal Treatment	<b>Shemp</b> (Zone II) Bioventing with Active Warming (heat tape)	<b>Larry</b> (Zone I) Bioventing with Passive Warming (insulation)
<b>Highest Microbial Populations (cells/ml of sample):</b>					
Heterotrophs	Capillary fringe ( $\approx 75,000$ c/ml)	Capillary fringe ( $\approx 3,500$ c/ml)	Vadose zone & capillary fringe ( $\approx 48 \times 10^6$ c/ml)	Vadose zone ( $\approx 7.5 \times 10^6$ c/ml)	Capillary fringe & saturated zone ( $\approx 5.5 \times 10^6$ c/ml)
Gasoline Degradars	Capillary fringe ( $\approx 50$ c/ml)	$\approx 70$ c/ml	Saturated zone ( $\approx 95,000$ c/ml)	Vadose zone ( $\approx 2,500$ c/ml)	$\approx 450$ c/ml
Diesel Degradars	none	$\approx 60$ c/ml	Saturated zone ( $\approx 230,000$ c/ml)	Vadose zone ( $\approx 750$ c/ml)	$\approx 250$ c/ml

**Table 6-2 continued.**

<b>Parameter</b>	<b>Joe</b> Background for Microbiology; No Bioventing, No Contamination	<b>Moe</b> Bioventing Background; No Contamination	<b>Curly</b> (Zone III) Bioventing Control for Thermal Treatment	<b>Shemp</b> (Zone II) Bioventing with Active Warming (heat tape)	<b>Larry</b> (Zone I) Bioventing with Passive Warming (insulation)
<b>Temp.</b>	Microbial activity acclimated to 50°F. Increased bioactivity also associated with higher temperatures.	Microbial activity low at all depths and incubation temperatures.	Mesophilic microbial acclimation likely above 50°F. Temperature doubling more than doubles bioactivity.	Microbial activity greatest at 39°F and above 50°F; cold tolerant mesophiles and psychrophiles may coexist.	Microbial activity acclimated to temperatures above 59°F. Possible indication of mesophilic and psychrophilic coexistence.
<b>Moisture</b>	Microbial activity acclimated to high moisture content.	Drying (bioventing) had little effect on bioactivity. However, O <sub>2</sub> and high moisture limiting to carbon availability in the absence of contamination.	Microbial activity acclimated to low moisture content. Increased moisture associated with some reduction in bioactivity.	Bioactivity not moisture sensitive.	Bioactivity delimiting at saturated condition.

\* c/ml = cells per milliliter

### 6.4.3 July 1995 and 1996 Geochemical Results

Geochemistry analyses were performed on groundwater samples, rather than soil, for three reasons. First, the majority of remaining contamination was in the groundwater and within the smear zone by the summer of 1995 (Figure 5-1). Second, it was less expensive to run organic and inorganic testing on groundwater. Lastly, nutrients in solution are often more readily available to microbial populations. The groundwater geochemistry data were generated from two sampling events performed one year apart, and is by no means comprehensive. The following discussions are axiomatically presented to foster a better understanding of the biochemical processes associated with this bioventing site.

Inorganics and BTEX concentrations (Table 6-3) were measured from groundwater samples collected from monitoring wells MW-201, MW-103 and MW-113. These wells form a northeast-to-southwest lineation (the groundwater flow direction) that spans the UAF site (Figure 3-2). MW-201 was developed approximately 250 feet northeast of the main bioventing area. MW-103 was immediately downgradient of the main bioventing treatment area. MW-113 was further downgradient, approximately 200 feet southwest of the Physical Plant building.

For this discussion, MW-201 can be considered a groundwater entry point into the bioventing site and MW-113 an exit point. By the summer of 1995 BTEX concentrations were below the state's proposed cleanup levels at MW-201 and at MW-113 (Table 6-3). At MW-103, representative of the highest contaminant levels, concentrations were measured at 300  $\mu\text{g/L}$ , 610  $\mu\text{g/L}$ , and 670  $\mu\text{g/L}$ , for benzene, ethylbenzene, and xylene compounds, respectively. By July 1996, these BTEX constituents were further reduced. Only benzene remained above the minimum acceptable levels at MW-103.

Some evidence of ammonification (nitrogen mineralization) was noted in the geochemistry data at MW-103 and MW-113. Some nitrification of ammonia [to nitrate] was evident at MW-201. Since nitrification is an autotrophic process, and since no soil contamination exists at MW-201, this could be considered background level bioactivity. Downgradient at MW-113, nitrate and nitrite were virtually gone, a likely consequence of low residual contaminant concentrations present. Historically, the groundwater BTEX

concentrations at MW-113 were very low. At MW-103, in the presence of petroleum contamination, nitrification was not indicated by the data. Hypothetically, the contaminant was being metabolized as carbon (from hydrocarbons) was mineralized to CO<sub>2</sub>.

**Table 6-3.** Groundwater geochemistry data for the UAF Physical Plant LUST site (concentrations in mg/L or ppm) (also see Appendix H).

Constituent	MW-201		MW-103		MW-113	
	(1995)	(1996)	(1995)	(1996)	(1995)	(1996)
Nitrogen:						
as Ammonia (NH <sub>3</sub> )	0.11	0.16	0.78	1.7	1.6	2.27
as Nitrate (NO <sub>3</sub> <sup>-</sup> )	0.18	1.0	0.04	ND	0.04	0.2
as Nitrite (NO <sub>2</sub> <sup>-</sup> )	0.01	0.005	0.01	ND	0.01	ND
Phosphate (PO <sub>4</sub> )	0.01	0.01	0.02	0.63	0.01	ND
Sulfate (SO <sub>4</sub> )	51	51	30	19	53	75
Calcium	100		94		100	
Magnesium	16		19		24	
Sodium	9.3		14		21	
Potassium	6.4		4.5		4.5	
Iron, soluble	0.1	0.03	14	16.3	16.0	18.53
Chloride	7.5	9.7	17	33.2	25	35.6
Fluoride	0.1		0.1		0.2	
pH	6.4	6.9	6.4	6.8	6.2	6.7
Alkalinity (as CaCO <sub>3</sub> )	266		273		323	
Dissolved Oxygen	--	1.09	--	0.16	--	0.18
Benzene (0.02)*	0.0004	0.0003	0.3	0.26	0.0013	0.0007
Toluene (5)*	0.2	ND	0.004	0.019	0.2	ND
Ethylbenzene (5)*	0.2	ND	0.61	0.34	0.2	ND
Xylene (74)*	0.2	ND	0.67	0.53	0.2	ND

ND = not detected in concentrations > 0.02 mg/L

\* Based on EPA Region III Risk-Based Concentrations (transfers from soil to groundwater), established (subject to approval) March 1995 by the ADEC.

As another potential indicator of increased biological mineralization at the groundwater level, oxygen (through bioventing) was the predominate terminal electron acceptor available at MW-103. As free oxygen was consumed, the redox potential likely decreased, and iron became more soluble. This analogy could explain the 14 mg/L and 16.3 mg/L soluble iron concentrations measured at MW-103, as compared with the extremely low iron concentrations (0.1 mg/L and 0.03 mg/L) encountered at MW-201. The similarly high soluble iron concentrations encountered at MW-113 are most likely a function of iron leachate from a huge gravel pile overlying this well location and groundwater migration from the MW-103 source area of petroleum contamination.

BTEX concentrations decreased between the 1995 and 1996 groundwater data at MW-103. This is an indication that my treatments also resulted in some degradation of these compounds in groundwater. Upward groundwater fluctuations likely introduced "new" BTEX contamination into the smear zone. This new contamination was subjected to bioventing and the thermal treatments. Additionally, some portion of each vent wells' screened interval was always below the water table; air sparging (oxygenation and volatilization) of the upper saturated zone was also occurring.

## **6.5 Historical Soil Analytical Results**

A summary of the laboratory analytical results for soil samples collected at the UAF Physical Plant LUST site, since the summer of 1990, is presented in Appendix H. This information is included to illustrate the overall reductions in vadose zone contamination through the summer of 1996. These and other results were submitted to UAF Project & Planning Services in June and August of 1996, to initiate site closure proceedings with the Alaska Department of Environmental Conservation.

---

**Economic Analyses**

An economic analysis was performed for cost evaluation and comparison between a conventional bioventing system and two thermally enhanced systems. The analysis provides generic installation and operating and maintenance (O&M) costs for the thermal systems studied at the UAF site. Various heat tape and polystyrene insulation configurations were considered, with a practical TIS design incorporated into the total project cost evaluation. This cost evaluation is based on current (1997) heat tape and insulation prices, standard engineering costs (Browning & Associates, 1993 and 1996), and actual UAF bioventing project costs where applicable. The evaluation does not reflect total project expenditures because of the extensive monitoring, testing and modeling required for innovative research.

Operating costs for the thermally enhanced bioventing systems were estimated based on a site with 6,000 cubic yards (cy) of petroleum contaminated soils at a maximum TPH contaminant level of 2,400 ppm (mg/kg). This volume represents a 10,800 square foot area, with a fifteen foot vadose zone (including the smear zone). The chosen site for evaluation resembles the UAF site and is consistent with a typical commercial storage tank facility. Necessary power supply is assumed accessible. Various insulation materials are considered. Active warming schemes reflect heat tape operating at 110-120 volts. A typical bioventing system includes the installation of five air injection wells to seventeen feet.

Three bioventing test plots were evaluated at the UAF site. A control plot was monitored to evaluate conventional bioventing at ambient conditions (without thermal

enhancement). An active warming test plot incorporated surface heating with electrical heat trace and polystyrene insulation. A third test plot was passively treated with surface applied polystyrene insulation. These three scenarios are compared, for the 6,000 cy model site, in the final "present day costs" and present worth evaluations.

### 7.1 Electrical Heat Tape

A Chromalox corrosion resistant (CR) and basic (Std.) heat tape were compared on a cost per foot and cost per square foot basis, for various spacing scenarios (Table 7-1). The corrosion resistant model is recommended for geotechnical application and is considered in the overall economic analyses. It is clear from the Table 7-1 data that if spacing can be increased, the total capital expenditure for heat tape will be less. Increased spacing associated with a higher output heat tape generally requires use of a thicker insulation layer.

**Table 7-1. Capital investment cost of a common heat tape.**

Heat Tape Model	Spacing (ft.)	(110-120 Volt Use) Heat Tape Cost				(208-240 Volt Use) Heat Tape Cost			
		(\$/ft)		(\$/sf)*		(\$/ft)		(\$/sf)*	
		CR <sup>o</sup>	Std.	CR <sup>o</sup>	Std.	CR <sup>o</sup>	Std.	CR <sup>o</sup>	Std.
3W/lf.	2	5	5	2.50	2.50	6	5	3.00	2.50
	5	5	5	1.00	1.00	6	5	1.20	1.00
	10	5	5	0.50	0.50	6	5	0.60	0.50
5W/lf.	5	7	6	1.40	1.20	8	7	1.60	1.40
	10	7	6	0.70	0.60	8	7	0.80	0.70
8W/lf.	8	8	7	1.00	0.875	9	8	1.125	1.00
	10	8	7	0.80	0.70	9	8	0.90	0.80
10W/lf.	10	8	8	0.80	0.80	10	9	1.00	0.90
	12	8	8	0.67	0.67	10	9	0.83	0.75

CR = corrosion resistant heat tape; Std. = standard or basic heat tape model.

<sup>o</sup> Protected, deluxe (braided, jacketed and self-regulating) models.

\* (\$/ft) cost divided by spacing. For reels exceeding 1000 feet in length, a 30% discount is realized in Fairbanks, Alaska.



## 7.2 Insulation

Various insulating materials available in Alaska were compared on a cost per board foot and cost per square foot basis (Table 7-2). Expanded (molded) and extruded polystyrene materials are high strength, closed cell structures that can be used for bioventing sites that must remain open (operational). At first glance, expanded polystyrene appears cheaper to use than extruded polystyrene insulation. Irrespective of similar thermal resistances (R-values), compressive strengths, maximum continuous operating temperatures, and design factor of safeties, expanded foam boards can absorb more moisture and experience thermal deficiency by 15% (McFadden and Bennett, 1991). Therefore, a thicker [expanded polystyrene] insulation may be required to afford similar thermal resistance provided by a thinner extruded polystyrene layer.

Polyurethane foam, polyisocyanurate, and sawdust insulations can be used for remote or closed sites if maintained free of significant dead and live loads, and no protective overburden (D-1 sand-gravel) is required. Because all three materials have high moisture absorption potential, geotechnical application warrants that they be sealed with protective plastic sheeting to preserve thermal resistance. The cost of poly-sheeting is generally low and worth the investment because of added thermal resistance (0.8 to 1.0 R-value per sheet). A disadvantage of using polyurethane or polyisocyanurate is that some ultraviolet degradation can occur with exposure. Furthermore, polyurethane foam has a maximum operating temperature that is 30°F below that of common heat tape. Consequently, this insulation could undergo melting if used in conjunction with heat tape.

Sawdust experiences a significant reduction in thermal efficacy when moistened. Enclosed, yet exposed to moisture and solar radiation, sawdust can undergo decay during the warm season. Polyisocyanurate can be used at operational sites as an alternative to extruded and expanded polystyrenes. This material has a higher thermal resistance and a cost per square foot between those of the two polystyrenes. However, its lower compressive strength will limit the size of surface loadings.

Table 7-3 evaluates the [1997] cost to install comparable TISs for an open bioventing site. Heat tape (HT), insulation (IN), D-1 sand-gravel (D1), and installation (LE, labor and

equipment) costs are summarized. The evaluation compares expanded polystyrene and the cheapest extruded polystyrene. Once again, similar R-value systems favor using expanded polystyrene to reduce capital investment costs. However, diminished thermal resistance during wetting may increase power costs enough to justify using extruded polystyrene.

**Table 7-2. Capital investment cost of insulation.**

Insulation	Avg. R Value ( $\frac{\text{ft}^2\text{-hr-}^\circ\text{F}}{\text{BTU-in}}$ )	Insul. Thickness (in)	Insulation Cost		Insulation Properties <sup>o</sup>			
			(\$/BF)*	(\$/sf) <sup>Δ</sup>	Comp. Strength (Psi)	MA <sub>max</sub> (Vol.%)	T <sub>max</sub> (°F)	FS
<b>Extruded Polystyrene</b>								
-Foamular 400 <sup>(TM)</sup>	5	2	0.40	0.80	25-50	<2	180	3-5
		3	0.40	1.20				
		4	0.40	1.60				
-Styrofoam <sup>(TM)</sup>	5	2	0.34	0.68	25-60	<2	165	3-5
		3	0.34	1.02				
		4	0.34	1.36				
<b>Expanded Polystyrene</b>								
-Insulfoam <sup>(TM)</sup>	4.8	2	0.25	0.50	25-40	3-4	165	3-5
		3	0.25	0.75				
		4	0.25	1.00				
<b>Polyurethane Foam</b> (formed on-site)	5.7	2	0.40	0.80	<10	<30	150	>5
		3	0.40	1.20				
		4	0.40	1.60				
<b>Polyiso-cyanurate</b> (rigid board)	7	2	0.31	0.62	10-25	15-20	165	3-5
		3	0.31	0.93				
<b>Sawdust</b>	2	6	0.05*	0.30	<5	>30	150	>5
		8	0.05*	0.40				
		10	0.05*	0.50				

\* BF = board foot, a volume based unit for building material, expressed as 1 ft x 1 ft x 1 in.  
<sup>Δ</sup> (\$/BF) multiplied by insulation thickness. •Cost reflects a \$15/cy loading charge; the sawdust itself is often free. ° Insulation properties include compressive strength, maximum moisture absorption (MA<sub>max</sub>), maximum continuous operating temperature (T<sub>max</sub>), and the factor of safety (FS) recommended to retain compressive strength (range is for dead loads and live loads). Retail costs per board foot and insulation properties obtained from Dow Chemical, Western Insulfoam (in Alaska), and McFadden and Bennett (1991).

**Table 7-3. Capital Investment Costs of Comparable Thermal Insulation Systems (in \$).**

Insulation Type and Thickness	Corrosion Resistant Heat Tape (110-120 voltage)									
	(3W/lf) Spacing		(5W/lf) Spacing			(8W/lf) Spacing		(10W/lf) Spacing		
	2 ft	5 ft	5 ft	7.5 ft	10 ft	8 ft	10 ft	10 ft	12 ft	
<b>Expanded Polystyrene -Insulfoam<sup>(TM)</sup></b>	2 inches (R9.5)		27000 HT	10800 HT	15000 HT	10000 HT	7500 HT	10800 HT	8640 HT	8640 HT
			5400 IN	5400 IN	5400 IN	5400 IN	5400 IN	5400 IN	5400 IN	5400 IN
			5200 DI	5200 DI	5200 DI	5200 DI	5200 DI	5200 DI	5200 DI	5200 DI
			<u>5000 LE</u>	<u>4500 LE</u>	<u>4500 LE</u>	<u>4400 LE</u>	<u>4300 LE</u>	<u>4400 LE</u>	<u>4300 LE</u>	<u>4300 LE</u>
			42600	25900	30100	25000	22400	25800	23500	23500
	3 inches (R14)		10800 HT		10000 HT	7500 HT	10800 HT	8640 HT	8640 HT	
			8100 IN		8100 IN	8100 IN	8100 IN	8100 IN	8100 IN	8100 IN
			5200 DI		5200 DI	5200 DI	5200 DI	5200 DI	5200 DI	5200 DI
			<u>5000 LE</u>		<u>4500 LE</u>	<u>4400 LE</u>	<u>4500 LE</u>	<u>4400 LE</u>	<u>4400 LE</u>	<u>4400 LE</u>
			29100		27800	25200	28600	26350	26350	
	4 inches (R19)					7500 HT	10800 HT	8640 HT	8640 HT	7240 HT
						10800 IN	10800 IN	10800 IN	10800 IN	10800 IN
					5200 DI	5200 DI	5200 DI	5200 DI	5200 DI	
					<u>4800 LE</u>	<u>5000 LE</u>	<u>4800 LE</u>	<u>4800 LE</u>	<u>4760 LE</u>	
					28100	31800	29450	29450	27950	

Table 7-3 continued.

Insulation Type and Thickness	Corrosion Resistant Heat Tape (110-120 voltage)									
	(3W/lf) Spacing		(5W/lf) Spacing			(8W/lf) Spacing		(10W/lf) Spacing		
	2 ft	5 ft	5 ft	7.5 ft	10 ft	8 ft	10 ft	10 ft	12 ft	
Extruded Poly. -Styrofoam <sup>(TM)</sup>	2 inches (R10)	27000 HT	10800 HT	15000 HT	10000 HT	7500 HT	10800 HT	8640 HT	8640 HT	
		7340 IN	7340 IN	7340 IN	7340 IN	7340 IN	7340 IN	7340 IN	7340 IN	
		5200 D1	5200 D1	5200 D1	5200 D1	5200 D1	5200 D1	5200 D1	5200 D1	
		<u>5000 LE</u>	<u>4500 LE</u>	<u>4500 LE</u>	<u>4400 LE</u>	<u>4300 LE</u>	<u>4400 LE</u>	<u>4300 LE</u>	<u>4300 LE</u>	
		44500	27800	32000	26900	24300	27700	25500	25500	
	3 inches (R15)		10800 HT		10000 HT	7500 HT	10800 HT	8640 HT	8640 HT	
			11000 IN		11000 IN	11000 IN	11000 IN	11000 IN	11000 IN	
			5200 D1		5200 D1	5200 D1	5200 D1	5200 D1	5200 D1	
			<u>5000 LE</u>		<u>4500 LE</u>	<u>4400 LE</u>	<u>4500 LE</u>	<u>4400 LE</u>	<u>4400 LE</u>	
			32000		30700	28100	31500	29200	29200	
4 inches (R20)					7500 HT	10800 HT	8640 HT	8640 HT	7240 HT	
					14700 IN	14700 IN	14700 IN	14700 IN	14700 IN	
					5200 D1	5200 D1	5200 D1	5200 D1	5200 D1	
					<u>4800 LE</u>	<u>5000 LE</u>	<u>4800 LE</u>	<u>4800 LE</u>	<u>4700 LE</u>	
					32200	35700	33300	33300	31800	

HT = heat tape cost; IN = insulation cost; D1 = D-1 sand-gravel top layer cost (based on 1 ft thickness); LE = labor and equipment cost associated with the TIS installation.

### 7.3 Heat Loss and Power Considerations

The rate of conductive heat loss through the insulation decreases as the insulation thickness increases. For example, the heat loss through the insulation can be calculated from

$$q = \frac{A(T_{as} - T_{HT})}{xR} \quad [7-1]$$

where

- $q$  = heat loss (in BTU/hr)
- $A$  = 10,800 square feet of insulated treatment area
- $T_{as}$  = atmospheric or overlying soil temperature ( $0^{\circ}\text{F}$ )
- $T_{HT}$  = heat tape operating temperature ( $70^{\circ}\text{F}$ )
- $x$  = insulation thickness (in inches)
- $R$  = insulation thermal resistance ( $5 \text{ ft}^2\text{-hr-}^{\circ}\text{F}/\text{BTU-in}$ )

For this example we need to compare only the differences associated with varied insulation thickness ( $x$ ) over the treatment area. All other terms remain the same. Therefore, for a 2-inch thick layer of insulation, with a temperature differential ( $T_{as}-T_{HT}$ ) of  $70^{\circ}\text{F}$ , approximately 75,600 BTU/hr is lost through the insulation. For a 3-inch layer, the heat loss is 50,400 BTU/hr. The heat loss through four inches of insulation is 37,800 BTU/hr over the same area. A 33% reduction in heat loss is realized when the insulation layer is increased by one inch. Doubling the insulation thickness reduces heat losses by approximately 59%.

By increasing the insulation thickness of a TIS pad, it is possible to sufficiently warm the vadose zone with a higher rated heat tape at increased spacing, while reducing capital investment and operating costs. Consider a TIS constructed of a 2-inch layer of styrofoam, over 3W/lf heat tape with five-foot spacing. From Table 7-3, the capital costs for this insulation and heat tape are \$7,340 and \$10,800, respectively. The power cost over a two year period, at a rate of \$0.11/kW-hr, can be calculated as

$$P(\$) = \frac{3W}{lf} \cdot 2165ft(of\ heat\ tape) \cdot \frac{24hr}{1\ day} \cdot 730days \cdot \frac{1kW}{1000W} \cdot \frac{\$0.11}{kW-hr} = \$10,300$$

The sum of these capital and power costs equals \$28,440. The capital costs for a 5W/lf heat tape at ten-foot spacing, three inches of insulation (Table 7-3), and two years of power consumption, are \$10,800, \$11,000, and \$8,712, respectively. The sum of these three expenditures is \$30,512. A \$2,072 differential is realized. When one considers that 33% more heat is transferred to the vadose zone when using a 3-inch insulation layer, the potential remedial time savings will likely justify the additional \$2,072 capital investment.

#### **7.4 Bioventing Treatment Cost Comparisons**

In the treatment cost evaluation (Table 7-4), installation costs for the three bioventing systems are based on optimum site logistics and assume 110-120 volt available power supply. For 208-240 volt consideration, one additional dollar (less 30% discount for some applications) per foot of heat tape can be expected when using the 5W and 8W trace. Major costs include labor, material, equipment and O&M. Salvage costs are also included in the comparisons, since they can be realized with shorter remedial projects. The evaluation assumes the site must be maintained for continuous use (open) and that recompaction of surface D-1 materials will not be necessary. Present day (1997) costs for implementation of each bioventing scheme are presented for comparison (Table 7-4).

Remediation time is significantly reduced and varies according to the soil warming method used. For example, based on average biodegradation rates derived from the early assessments by Arambarri (1995), contaminant levels, and experience, conventional bioventing alone at the UAF site would require approximately 7 years to remediate. With active warming, the remediation time was 1.7 years. Therefore, conventional bioventing will require additional monitoring and incur higher O&M costs. Lower O&M costs and salvage savings associated with active warming systems may, in some cases, offset initial higher capital costs.

A few additional comments should be made about the bioventing cost evaluation (Table 7-4). Capital costs do not include any expenditures associated with a pilot test. A qualitative feasibility study, with knowledge of site specific geotechnical and contaminant parameters, can yield a sufficient recommendation for design of an adequate bioventing

**Table 7-4.** Estimated present day costs (in \$) for three bioventing treatments.

<b>Task</b>	<b>Conventional Bioventing</b>	<b>Active Warming (with heat tape)</b>	<b>Passive Treatment (insulation only)</b>
<b>Capital Costs:</b>			
Initial Site Visit	4,500	4,500	4,500
Work Plan/Preparation	7,000	7,000	7,000
In-house Design	7,000	7,000	7,000
Regulatory Approval	3,000	3,000	3,000
<b>Bioventing Construction:</b>			
Drilling & sampling	18,000	18,000	18,000
Opt'l. (microbiological sampling & testing) Installations	(7,500)	(7,500)	(7,500)
- 5 injection wells	5,000	5,000	5,000
- 8 soil gas MP's	1,200	1,200	1,200
- 8 thermocouple strings		1,200	1,200
- TIS materials		25,200	17,000
	<b>45,700</b>	<b>72,100</b>	<b>63,900</b>
<b>O&amp;M Costs:</b>			
Monitoring	24,500	7,500	14,000
Blower Maintenance	2,000	500	1,200
Power	9,550	10,850	5,500
Final Sampling Event	14,000	14,000	14,000
	<b>50,050</b>	<b>32,850</b>	<b>34,700</b>
<b>Salvage Costs<sup>a</sup>:</b>			
Salvage		-6,100	-1,500 <sup>b</sup>
<b>Total Costs</b>	<b>95,700</b>	<b>98,850</b>	<b>97,100</b>
<b>Remediation Time</b>	7 yrs.	1.7 yrs.	4 yrs.
<b>Cost per Cubic Yard<sup>c</sup></b>	<b>\$16.00</b>	<b>\$16.48</b>	<b>\$16.18</b>

<sup>a</sup> Estimates provided by Ghemm Company (general contractors, Fairbanks); based on percentage devaluation of blowers and heat tape and 100 % D-1 recovery without labor and equipment charges.

<sup>b</sup> D-1 recovery alone, at 60% of original expense.

<sup>c</sup> Estimated based on required remediation of a 6,000 cy site, with a 2,400 ppm maximum contaminant level, low venting flow rates (2-4 cfm), and average biodegradation rates.

system without a pilot study. However, sites where permafrost, highly frost-susceptible soils, or other anomalous subsurface conditions might exist probably will require a pilot study.

An optional \$7,500 first cost for a microbiological study was not included in the total costs, costs per square foot, or cost per cubic yard values reported. This optional “bare minimum” expenditure can be performed at the time of initial subsurface exploration work to minimize drilling costs. There is value in performing a microbiological analysis early on, in that system optimization can result in further reduction of the project remediation time. If this occurs, additional time savings and reduced monitoring costs may likely offset this capital cost. Furthermore, the microbiological results might suggest other enhancements (moisture and nutrient additions) for more efficient bioremediation.

#### 7.4.1 Present Worth Analysis

Section 7.3 established bioventing treatment alternatives. These capital investment alternatives are now evaluated based on the time value of money. The primary benefit of early remediation is that property is made available for sale, reuse, or redevelopment without owner liability. With this in mind, the owners evaluation criteria for treatment choice may be reduced to the answer to a simple question: “Does my expected future return on my property transaction (sale, reuse, or redevelopment) justify the costs associated with my choice of treatment?”

Considering capital expenditures, O&M costs, and salvage, all other things being considered equal, a present worth analysis can be performed using Table 7-4 and a *minimum attractive rate of return* (MARR). The MARR should be higher than the cost of securing money and recognize inflation (Bennett, 1995). This analysis assumes a prime interest rate of 7% and annual inflation of 3%; the expected rate of return is at least 10%. Cost flow diagrams for each treatment scheme are presented and present worth equations are formulated for comparison. The present worth equations represent returns as negative (-) and expenditures as positive (+) cash flows.

The general equation for present worth (PW) of treatments can be expressed as



$$PW = CI + A(P/A,i,n) - S(P/F,i,n) - X(P/F,i,n) \quad [7-1]$$

where

- $CI$  = single payment capital investment cost (in \$)
- $A$  = O&M uniform series of [annual] payments (in \$)
- $S$  = single payment salvage recovery (in \$)
- $X$  = expected future property value (in \$)
- $i$  = minimum attractive rate of return (10%)
- $n$  = number of years of treatment
- $(P/A,i,n)$  = present worth factor on a uniform series of payments
- $(P/F,i,n)$  = present worth factor on a single payment

Present worth factors used were obtained from standard Compound Interest Factor Tables (Bennett, 1995) commonly appended to economics texts. For the three bioventing schemes (Table 7-4), the cost flow diagrams and present worth equations are summarized below. O&M costs are considered annuities as indicated. Capital investments and salvage recoveries are identified at the left (downward arrows) and right sides (bottom upward arrows) of the cost flow diagrams. The 1.7 year active warming remediation time was rounded up to 2 years so that published present worth factors could be used in the analysis.

Conventional bioventing:

$$PW_c = 45,700 + 7150(P/A,10,7) - X(P/F,10,7)$$

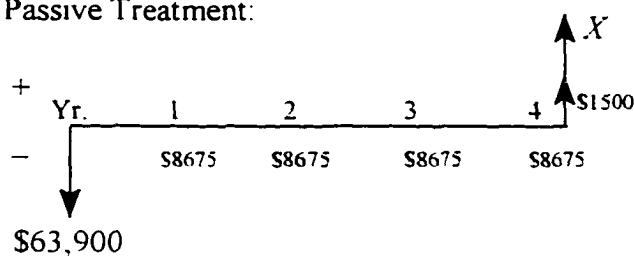
$$= 80,500 - 0.5132 X \quad [7-2]$$

Active warming:

$$PW_a = 72,100 + 16,425(P/A,10,2) - 6100(P/F,10,2) - X(P/F,10,2)$$

$$= 95,550 - 0.8264 X \quad [7-3]$$

Passive Treatment:



$$\begin{aligned} PW_P &= 63,900 + 8,675(P A, 10, 4) - 1,500(P F, 10, 4) \\ &\quad - X(P F, 10, 4) \\ &= 90,400 - 0.683 X \end{aligned}$$

[7-4]

Subscripts c, a, and p in equations [7-2] through [7-4] denote conventional, active warming, and passive treatment bioventing. The present worth of bioventing costs (PW) versus expected return on property value ( $X$ ) after treatment were then plotted for a range of returns for each alternative (Figure 7-1). Again, property value return can be associated with the sale, reuse, or redevelopment of the land. Each of the three curves intersect at a minimum expected return on property value (vertical dashed lines). For example, when comparing conventional bioventing and active warming alternatives, the minimum expected return is \$48,050. That is, active warming treatment should be the method of choice if one can realistically expect a return on investment greater than \$48,050 after two years of treatment. A similar comparison with passive treatment requires a larger expected return (\$58,300) to warrant its use. When comparing the active warming to passive treatment alternatives, a significantly lower expected return is required to warrant active thermal enhancement.

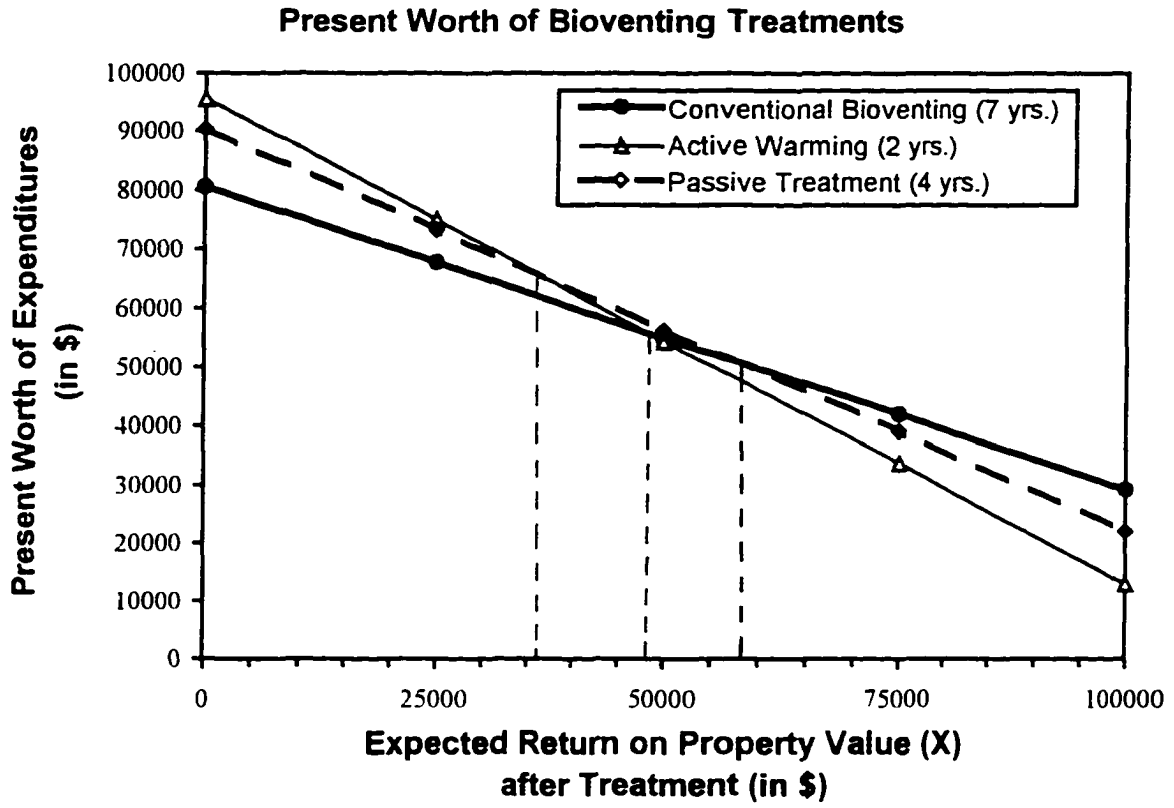


Figure 7-1. Present worth of expenditures versus expected return on property value for three bioventing treatment alternatives.

---

## Conclusion and Recommendations

Comparisons of the three tested thermal regimes showed that bioventing with active warming increased vadose zone temperatures by as much as 15°F above those of passively treated and control test plot soils. From the water table to the ground surface, soils warmed with heat tape experienced wintertime temperatures between 40-62°F and between 45-88°F in summer. At these temperatures, psychrophiles and cold-tolerant mesophiles proliferate and degrade organic materials more efficiently. Actively warmed soils were kept above freezing year-round, providing a thermal environment for effective bioremediation.

Passive treatment warmed subsurface soils no more than a few degrees above normal (as compared to control test plot soils) in winter. Freeze-thaw cycling did occur within the passively treated vadose zone, but to a lesser extent in duration than within the biovented control plot. In summer, passive TIS surface materials adversely reduced the effects of solar warming on the subsurface and contributed to lingering cooler temperatures.

The control test plot comprised the area of highest smear zone contamination and low-level upper soil contamination. Frost-susceptible soils and a permafrost boundary were identified (from historic boring logs) within portions of the vadose zone here. Biodegradation was seasonally diminished as wintertime subsurface temperatures were recorded as low as 18°F.

Soil analytical results comparing Shemp (Figure 5-1) data to historical data (Table 6-1 and Table H-1) suggest that bioventing with active warming remediated much of the Zone II soil contamination within one year. Comparing the Shemp soil analytical results to those of Larry and G (1995 and 1996 sampling events) suggests slower biodegradation of

contaminants with passive treatment.

Because surface-applied insulation diminishes the thermal effects of the sun on the subsurface in summer, conventional bioventing will usually be more beneficial to bioremediation than passive treatment during this time of year. However, the converse is true during winter, when TIS materials insulate the subsurface from subfreezing air temperatures.

For open bioventing sites, more concern for the TIS design must be given. Before installation, the UAF TIS designs were scrutinized for load applicability and thermal efficacy. ELSYM-5 and BERG-2 software were the tools of choice. These computer programs are proven and are routinely applied to engineering practice in Alaska. Other similar software packages are likely available for purchase.

ELSYM-5 analysis and a compression test on a scale model of the TIS indicated that the insulation and heat tape materials would retain design strength and shape under loading, provided a reasonable factor of safety was incorporated. BERG-2 analyses provided depth of freeze calculations below insulation that generally indicated that soils at the contaminant level (deeper than seven feet) should not freeze. With active warming it was shown that vadose zone soil freezing was prevented altogether. Results from BERG-2 were less reliable for areas where heterogeneous and frost-susceptible soils prevail (Figure 6-1c).

The three test plot thermal regimes were modeled using a two-dimensional heat conduction program (TDHC) developed at UAF. Zone II analysis required modification of the program code to account for artificial [heat tape] heating. Solar radiation and water infiltration effects were reduced by the insulating TIS materials. Convective losses at the monitoring points could be neglected since the risers were insulated. Convective heat transfer, induced by the low flow rate(s) at the injection wells, was also shown to be negligible. Consequently, TDHC effectively modeled the conduction problems, typically defining the subsurface thermal regimes to within a couple of degrees of measured field data. Qualitative modeling required accurate assessment of initial soil layer temperatures and demonstrated the effects of boundary conditions.

Soil gas concentrations ( $\text{CO}_2$  and TPH) in the vadose zone are predominately a function of contaminant levels, bioactivity, and volatilization. With active warming,  $\text{O}_2$  and

CO<sub>2</sub> concentrations approached baseline levels, and background TPH concentrations were realized within the first year of thermally enhanced bioventing. The July 1995 soil analytical data confirmed that remaining BTEX contamination was predominately in the groundwater under Zone II. Within the passively treated and control test plots, significant spikes in soil gas measurements appeared associated with groundwater movements and/or seasonal transition periods.

It is the opinion of this researcher that an understanding of site specific soil microbiology should be an integral part of any bioventing project. Funding was available for limited microbiology and geochemistry testing. The scant results appeared to indicate a relationship between temperature and biodegradation. Enumeration assays and activity measurements on soil samples collected from this site related moisture and temperature effects to bioactivity. Laboratory test results suggested that, irrespective of soil moisture content, CO<sub>2</sub> respiration (biodegradation) increased at higher temperatures (between 50°F and 80°F). As expected, elevated heterotrophic populations were generally found in association with higher contaminant levels. Combined results of the microbiological analyses prompted an attempt to optimize bioventing efficiency.

At the UAF bioventing site, the venting flow rate was kept low in order to disassociate artificial hydrocarbon stripping from true biodegradation. However, for future bioventing operations, the venting rate will likely be higher and determined based on off-gas productions and air quality requirements.

As with any remediation project, a cost-benefit analysis will be an inherent factor when determining treatment methodology. It has been demonstrated here that the benefit of time savings warrants the use of thermally enhanced bioventing if an acceptable return on investment is realized through the sale, redevelopment, or reuse of property. If a contaminated site can remain closed for some time, less expensive conventional or passive treatment may be acceptable alternatives. However, if a property is to remain open, and has considerable commercial value, bioventing with active warming can remediate petroleum contamination faster and cheaper.

When thermally enhanced bioventing is used, the cost of TIS materials and power may be the determining factors for design. Expanded polystyrene is less expensive to use than extruded insulations, provided its thermal resistance is maintained with moisture [and solar] protection. Less quantity of a higher rated (output) heat tape, in combination with thicker overlying insulation, can be practical while reducing overall project costs in the long run (section 7-3).

Depending upon vadose zone thickness and plume peripheral contaminant concentrations, the area of TIS coverage may have to be enlarged to account for boundary heat losses and possible reduction in biodegradation efficiency. For the 2D boundary analysis problem discussed in section 6.1.3a, approximately five additional feet of TIS coverage on all sides would sufficiently reduce heat losses for acceptable treatment of a fifteen foot thick, uniformly contaminated vadose zone. With respect to the 10,800 square foot example treatment area presented in Chapter 7, this translates to a twenty-percent increase in coverage area. However, a typical soil contaminant plume can be expected to have highest contaminant concentrations at the point of impact and lesser concentrations at the plume periphery. A determination regarding total area of thermal enhancement must be based on site specific subsurface characterizations and contamination assessments.

A guideline for thermally enhanced bioventing in cold regions is presented in Appendix I. Considerations for applicability, cost, and treatment variations were incorporated into the design guide, for practical application by engineers, biologists and environmental scientists.

### **Recommendations**

Optimization of a bioventing operation can be achieved over time by trial and error methods or by assessing biodegradation rates. Perhaps an investigative microbiological study would establish more efficient bioventing earlier on. During the initial contamination assessment phase, microbiological sampling and testing should be performed simultaneously with standard geotechnical assessments. Information about microbial populations and the effects of temperature, moisture, and the contaminants (treatability study) on them can be

incorporated into the system design phase. With an optimal design before installation, monitoring requirements and project duration can be expected to be reduced.

Active thermal enhancement with surface applied TIS materials is likely to always be cheaper than embedded systems. A TIS comprising deluxe (protected) and self-regulating heat tape, polystyrene insulation, and a secure overburden layer, has been proven to effectively enhance bioventing of petroleum contaminated soils. Future investigators are encouraged to consider alternative combinations of TIS materials identified herein and report findings.

The level of contamination will not likely determine the applicable TIS design; climate, soil structure, and depth of contamination will. Contamination at deeper depths may require a higher rated heat tape and thicker insulation for effective enhancement.



---

## References

- Alaska Dept. of Environmental Conservation. 1996. Personal review of historical files and records.
- AGRA Earth & Environmental. 1995. Corrective Action Plan: Former UST System Physical Plant Site University of Alaska Fairbanks, a report prepared for UAF Planning & Project Services.
- Ahmed, N., and D. K. Sunada. 1969. Nonlinear Flow in Porous Media. *Journal of Hydraulics Division, American Society of Civil Engineers*, v. 95, no. HY6, pp. 1847-1857.
- Alexander, Martin. 1994. Biodegradation and Bioremediation. Academic Press, Inc., San Diego, CA., pp. 16-36, 196-217, 241-245.
- Andersland, Orlando B., and Branko Ladanyi. 1994. An Introduction to Frozen Ground Engineering. Chapman & Hall, London, England, pp. 146-148.
- Arambarri, John W. 1995. Installation and Monitoring of a Bioventing System to Remediate Petroleum Contaminated Soils; M.S. Project Report to Department of Civil Engineering, University of Alaska Fairbanks.
- Atlas, R. M. 1981. Microbial Degradation of Petroleum Hydrocarbon's: An Environmental Perspective. *Microbiology Review*, 45: pp. 180-209.
- Atlas, Ronald M., and Richard Bartha. 1987. Microbial Ecology Fundamentals and Applications. 2nd Ed. Benjamin/Cummings Publishing Company, Inc., Menlo Park, CA., pp. 233-259.
- Atlas, Ronald M. 1993. Handbook of Microbiological Media. Ed.: Lawrence C. Parks. CRC Press, Inc., p. 757.
- Bear, Jacob. 1972. Dynamics of Fluids in Porous Media. American Elsevier Publishing Company, Inc., New York.

- Bear, Jacob. 1979. *Hydraulics of Groundwater*. McGraw-Hill, Inc.
- Bennett, F. Lawrence. 1995. *Engineering Economics: A Primer*. Date-Line Copies, Inc., Fairbanks, Alaska, pp. 11-21, 173.
- Bowles, Joseph E. 1988. *Foundation Analysis and Design*. McGraw-Hill, Inc., 4th Ed., pp. 99-106, 266.
- Box, E. P. George and Norman R. Draper. 1969. *Evolutionary Operation*. John Wiley & Sons, Inc., New York, New York, pp. 3-20, 152-175.
- Braley, W. Alan. 1984. A Personal Computer Solution to the Modified Berggren Equation. Institute of Water Resources/Engineering Experiment Station-UAF, Report No. AK-RD-85-19, pp. 1-5.
- Brar, Gurdarshan S., Paul M. Currier, Charles M. Reynolds, and Joseph B. Millhouse. 1993. Remediation of Petroleum Contaminated Soils Through Bioventing in Cold Regions. *Proceedings of Superfund XIV Conference and Exhibition*, Nov. 30-Dec. 1, 1993.
- Brown, Edward J. And Joan F. Braddock. 1990. "Sheen-Screen, a Miniturized Most-Probable-Number Method for Enumeration of Oil-Degrading Microorganisms." In: *Applied and Environmental Microbiology*, Dec. 1990, pp. 3895-3896.
- Brown, Edward J., Sol M. Resnick, Carl Rebstock, Huan V. Luong and Jon Lindstrom. 1991. "UAF Radiorespirometry Protocol for Assessing Hydrocarbon Mineralization Potential in Environmental Samples." In: *Biodegradation*, Kluwer Academic Publishers, Netherlands, v. 2, pp. 121-127.
- Browning & Associates. 1993. Unpublished Summary of Bioremediation Case Studies. Kansas City, Kansas.
- Canadian Association of Petroleum Producers (CAPP). 1994. Soil Vapor Extraction and Bioventing Program Summary Report: 1993 to Spring 1994. Unpublished report prepared by Komex International Limited, June 1994.
- Conner, J. S. 1988. Case Study of Soil Venting. *Pollution Engineering*, 7, pp. 74-78.
- Das, Braja M. 1985. *Principles of Geotechnical Engineering*. PWS Publishers, Boston, Massachusetts, pp. 7-32, 66-72, 81-103.
- Dinkel, Donald H., Patricia J. Wagner, and Grant E. M. Matheke. 1980. Growing Everbearing Strawberries as Annuals in Alaska, UAF Cooperative Extension Service, Circular 35.

- Dinkel, Donald H. 1966. Growing Sweetcorn in Alaska's Cool Environments. UAF-AES. Bulletin 39.
- Dupont, R., W. Doucette, and R. E. Hinchee. 1991. "Assessment of In Situ Bioremediation Potential and the Application of Bioventing at a Fuel-Contaminated Site." In: R.E. Hinchee and R.F. Olfenbuttel (Eds.), *In Situ Bioreclamation*, Butterworth-Heinemann, Stoneham, Massachusetts, pp. 262-282.
- Fetter, C. W. 1993. Contaminant Hydrogeology. Macmillan Publishing Company, New York, pp. 35-114, 43-45, 181-186.
- Goering, D. J. 1984. Unsteady-state Heat Conduction by the Finite Element Method, M. S. Thesis, University of Alaska Fairbanks.
- Hartman, C. W., and P. R. Johnson. 1984. Environmental Atlas of Alaska. University of Alaska Fairbanks.
- Hinchee, R. 1994. "Bioventing of Petroleum Hydrocarbons." In Norris, Robert D. Et al. (Ed.), *Handbook of Bioremediation*. Robert S. Kerr Environmental Research Laboratory. Lewis Publishers, Boca Raton, Florida, pp. 39-59.
- Hinchee, R. E., S. K. Ong, R. N. Miller, D. C. Downey, and R. Frandt. 1992. Test Plan and Technical Protocol for a Field Treatability Test for Bioventing. U. S. Air Force Center for Environmental Excellence.
- Hinchee, Robert E., and Say Kee Ong. 1992. A Rapid In Situ Respiration Test for Measuring Aerobic Biodegradation Rates of Hydrocarbons in Soil. *Journal of Air & Waste Management Association*, v. 42, no.10, ISBN 1047-3289, pp. 1305-1312.
- Horowitz, A. And R. M. Atlas. 1977. Response of Microorganisms to and Accidental Gasoline Spillage in an Arctic Freshwater Ecosystem. *Applied Environmental Microbiology*, v. 33, no. 6, pp. 1252-1258.
- International Network for Environmental Training, Inc. (INET). 1993. Bioventing: Principles, Applications, and Case Studies, an INET training program.
- Janes, E. 1995. Personal communication. Fort Wainwright Army Base, Fairbanks, Alaska.
- Johnson, L. A. 1981. Revegetation and Selected Terrain Disturbances Along the Trans-Alaska Pipeline, 1975-1978. CRREL Report 81-12, p. 115.
- Johnson, P.C. 1991. HyperVentilate Users Manual. Shell Development, Houston, Texas. p. 3.

- Johnson, P. C., M. W. Kemblowski, and J. D. Colthart. 1990. Quantitative Analysis for the Cleanup of Hydrocarbon Contaminated Soils by In-Situ Soil Venting. *Groundwater*, 28(3), pp. 413-429.
- Kane, Douglas L., Larry D. Hinzman and John P. Zarling. 1991. "Thermal Response of the Active Layer to Climatic Warming in a Permafrost Environment." In: *Cold Regions Science and Technology*, Elsevier Science Publishers. B.V., Amsterdam, 19(1991), pp. 111-122.
- Keener, James P. 1988. Principles of Applied Mathematics (Transformation and Approximation). Addison-Wesley Publishing Co., Redwood City, CA., pp. 91, 202, 344.
- Kerry, Elizabeth. 1993. Bioremediation of Experimental Petroleum Spills on Mineral Soils in the Vestfold Hills, Antarctica. *Polar Biology*, 13(3), pp. 163-170.
- Komex International. 1996. Personal Communication. Calgary, Alberta, Canada.
- Leeson, Andrea, Robert E. Hinchee, Jeffrey A. Kittel, and Eric A. Foote. 1995. Environics TOC Task 3 Bioventing Feasibility Study, Eielson AFB Site; Final Report to Environmental Quality Directorate of the Armstrong Laboratory, Tyndall AFB, FL.
- Loeb, Leonard B. 1902. Fundamentals of Electricity and Magnetism. Hohn Wiley & Sons, Inc., New York, pp. 127, 243, 314.
- Luikov, A. V. 1966. Heat and Mass Transfer in Capillary Porous Bodies (English translation of original Russian book published by Academy of Sciences U.S.S.R., Minsk, 1961). Pergamon Press, New York.
- Lunardini, V. J. 1978. Theory of n-Factors and Correlation of Data. In: *Proceedings of 3rd International Conference on Permafrost, Edmonton, Alberta, Canada*. Ottawa: National Research Council of Canada, Vol. 1, pp. 41-46.
- McFadden, Terry T., and F. Lawrence Bennett. 1991. Construction in Cold Regions: *A Guide for Planners, Engineers, Contractors, and Managers*. John Wiley & Sons, Inc., New York, pp. 244-245.
- Miller, R. N., C. Vogel, and R. E. Hinchee. 1991. "A Field-Scale Investigation of Petroleum Hydrocarbon Biodegradation in the Vadose Zone Enhanced by Soil Venting at Tyndall AFB, Florida." In: R.E. Hinchee and R.F. Olfenbuttel (Eds.), *In Situ and On-Site Bioreclamation*, v. 1, Butterworth-Heinemann, Stoneham, Massachusetts, pp. 283-302.

- Mitchell, Bill. 1996. Personal communication. Retired, UAF-AFES Palmer Research Station.
- Montgomery, James M. 1992. Site Characterization and Presentation of Remedial Alternatives for the University of Alaska Fairbanks Physical Plant. Draft report.
- Montgomery Watson. 1994. Site Characterization and Presentation of Remedial Alternatives for the University of Alaska Fairbanks Physical Plant. Final Report.
- Moore, Brent J., James E. Armstrong, Jim Barker, and Paul E. Hardisty. 1995. "Effects of Flowrate and Temperature During Bioventing in Cold Climates." In: Hincee, Robert E. et al (Ed.), *In Situ Aeration: Air Sparging, Bioventing, and Related Remediation Processes*. Bioremediation Series, Book 3(2), Third International In Situ and On-Site Bioreclamation Symposium. Battelle Press, Columbus, Ohio. pp. 307-314.
- Morris, D. A., and A. I. Johnson. 1967. Summary of Hydrologic and Physical Properties of Rock and Soil Materials, as Analyzed by the Hydrologic Laboratory of the U. S. Geological Survey 1948-60. In U. S. G. S. Water-Supply Paper 1839-D, 42.
- Muskat, Morris. 1937. *The Flow of Homogeneous Fluids Through Porous Media*. McGraw-Hill Book Company, Inc., pp. 55-100.
- Nield, D. A., and A. Bejan. 1992. *Convection in Porous Media*. Springer-Verlag, Inc., New York, pp. 25, 47-50, 69, 262-270.
- Norris, Robert D., Hincee, Brown, McCarty, Samprini, Wilson, Kampbell, Reinhard, Bouwer, Borden, Vogel, Thomas, and Ward. 1994. *Handbook of Bioremediation*. Robert S. Kerr Environmental Research Lab, Lewis Publishers/CRC Press, Inc.
- O'Neill, K. 1983. "Fixed Mesh Finite Element Solution for Cartesian Two Dimensional Phase Change." *Journal of Energy Resources Technology*, No. 105, pp. 436-441.
- Queitzsch, William. 1996. Personal Communication. Gilfilian Engineering & Environmental Testing, Inc., Anchorage, Alaska.
- Rockwell, Mark. 1996. Personal Communication. Rockwell Environmental Services, Fairbanks, Alaska.
- RZA AGRA, Inc. 1994. University of Alaska Fairbanks Air-Injection Wells: Project Number: 94096 LPP1, a report prepared for UAF Planning and Project Services.

- Sayles, Gregory D., Andrea Laeson, Robert E. Hincsee, Catherine M. Vogel, Richard C. Brenner, and Ross N. Miller. 1995. "Cold climate Bioventing with Soil warming in Alaska." In: Hincsee, Robert E. et al. (Eds.), *In Situ Aeration: Air sparging, Bioventing, and Related Remediation Processes*. Bioremediation Series, Book 3(2), Third International In Situ and On-Site Bioreclamation Symposium. Battelle Press, Columbus, Ohio, pp. 297-306.
- Schwartz, L. 1972. "La 'fonction'  $\delta$  et les noyaux." In: Salam, Abdus, and E. P. Wigner (Eds.) *Aspects of Quantum Theory*. Cambridge University Press, Great Britain, pp. 179-182.
- Sellers, K. L., T. A. Pedersen, and C. Y. Fan. 1991. Soil-Air Permeability Method Evaluation. *HMC-Northeast '91 Conference Proceedings*. Boston, Massachusetts. Hazardous Materials Control Research Institute.
- Shannon & Wilson. 1990. Contamination Assessment, UAF Physical Plant Tank Site. Final Report.
- Shannon & Wilson. 1992-1995. Unpublished project report summaries of case studies (Fred Brown, Anchorage, Alaska).
- Simpkin, Thomas J., Davis Walter, and James Doesburg. 1992. Treatment of Fuel Product Contaminated Soil in a Cold Climate Using Composting Technology. *Air & Waste Management Association 85th Annual Meeting & Exhibition*. Kansas City, Missouri, June 1992.
- Slone, Herbert. 1996. Personal communication. Owens Corning, U.S.A
- Staatsuitgeverij. 1986. Proceedings of a Workshop , 20-21 March, 1986. *Bodembeschermingsreeks* No.9; *Biotechnologische Bodemsanering*, pp. 31-33. Reportnr. 851105002, ISBN 90-12-054133, Ordernr. 250-154-59; Staatsuitgeverij Den Haag: The Netherlands.
- Texas Research Institute. 1980. Laboratory Scale Gasoline Spill and Venting Experiment. American Petroleum Institute, Interim Report No. 7743-5:JST.
- Texas Research Institute. 1984. Forced Venting to Remove Gasoline Vapor from a Large-Scale Model Aquifer. American Petroleum Institute, Final Report No. 82101-F:TAV.
- Thomas, Howard, David Jensen, and Brad Authier. 1995. Remediation of Crude-Oil-Contaminated Soils Beneath a Containment Liner. *Proceedings of Geophysical Environmental 2000, American Society of Civil Engineers*, New Orleans, February 1995.

- Todd, Davis K. 1980. *Groundwater Hydrology*, 2nd Edition. John Wiley & Sons, Inc., New York, pp. 64-77, 91-106, 129-136
- Urlings, L.G.C.M., H.B.R.J. van Vree, and W. van der Galien. 1990. Application of Biotechnology in Soil Remediation. *Envirotech Vienna*, Westarp Wiss., Essen, pp. 238-251.
- van Eyk, J., and C. Vreeken. 1989a. "Model of Petroleum Mineralization Response to Soil Aeration to Aid in Site-Specific, In Situ Biological Remediation." In: *Groundwater Contamination: Use of Models in Decision-Making; Proceedings of an International Conference on Groundwater Contamination*. Jousma et al. (Eds.), Kluwer, Boston/London, pp. 365-371.
- van Eyk, J., and C. Vreeken. 1989b. Venting-Mediated Removal of Diesel Oil from Subsurface Soil Strata as a Result of Stimulated Evaporation and Enhanced Biodegradation. *Hazardous Waste and Contaminated Sites, Envirotech Vienna*, v 2(3), ISBN 389432-009-5, Westarp Wiss., Essen, pp. 475-485.
- Zarling, J. P. and D. J. Goering. 1985. Geotechnical Thermal Analysis with a Microcomputer. *Civil Engineering in the Arctic Offshore*, ASCE, New York, N.Y., pp. 604-616.
- Zarling, John P. and W. Alan Braley. 1988. "Geotechnical Thermal Analysis." In: *Embankment Design and Construction in Cold Regions; Technical Council on Cold Regions Engineering Monograph*. Johnson et al. (Eds.), The American Society of Civil Engineers, pp. 35-44.

---

**Sample Permeability and Reynolds Number Calculations, D-1 Specifications, and Bioventing Case Studies**

**Sample Intrinsic Permeability Calculations** for UAF Physical Plant LUST bioventing site vadose zone (after Arambarri, 1995):

Vent well: VW-5

Monitoring point: MP-10-9.5

Date: August 24, 1994

Air injection flow rate:  $Q = 5$  scfm

Vent well radius:  $R_w = 1$  in

Vent well gauge pressure:  $P_w = 0.7$  in. water

Vent well effective screened interval:  $H(\text{or } m) = 8.5$  ft

Conversions:

1 m = 39.37 in

1 ft<sup>2</sup> = 929.03 cm<sup>2</sup>

1 in. water =  $3.61 \times 10^{-2}$  psi

1 N = 0.2247 lb

1 darcy =  $1 \times 10^{-8}$  cm<sup>2</sup>

Steady-state permeability test:

$$Q = 5 \text{ ft}^3/\text{min} \times 1 \text{ min}/60 \text{ s} = 0.0833 \text{ ft}^3/\text{s}$$

$$@ 18^\circ \text{C}, \mu_a = 1.805 \times 10^{-5} \text{ N}\cdot\text{s}/\text{m}^2 \times 0.2247 \text{ lb}/1 \text{ N} \times 1 \text{ m}^2/(39.37)^2 \text{ in}^2 = 2.617 \times 10^{-9} \text{ lb}\cdot\text{s}/\text{in}^2$$

$$R_w = 1 \text{ in} \times 1 \text{ ft}/12 \text{ in} = 0.0833 \text{ ft}$$

$$P_w = 0.7 \text{ in. H}_2\text{O} \times 3.61 \times 10^{-2} \text{ psi}/\text{in. H}_2\text{O} = 0.0253 \text{ psi}$$

$$P_{\text{atm}} = 14.7 \text{ psi}$$



$$P_{wabs} = P_{atm} + P_w = 14.7 \text{ psi} + 0.0253 \text{ psi} = 14.725 \text{ psi}$$

$$k = \frac{Q \cdot \mu_a \cdot \ln\left(\frac{R_w}{R_1}\right)}{H \cdot \pi \cdot P_{atm} \left[1 - \left(\frac{P_{wabs}}{P_{atm}}\right)^2\right]} = \frac{0.0833 \text{ ft}^3/\text{s} (2.617 \times 10^{-9} \text{ lb-s/in}^2) \ln(0.0833 \text{ ft}/63 \text{ ft})}{8.5 \text{ ft} (\pi) (14.7 \text{ lb/in}^2) [1 - (14.725 \text{ psi}/14.7 \text{ psi})^2]}$$

$$k = 1.2 \times 10^{-9} \text{ ft}^2 \quad (1.15 \times 10^{-6} \text{ cm}^2)$$

Transient permeability test:

$$t_1 = 1 \text{ min.} \quad P_1 = 0.06 \text{ in. water}$$

$$t_2 = 12 \text{ min.} \quad P_2 = 0.09 \text{ in. water}$$

$$k = \frac{\mu_a \cdot K}{\rho g} \quad \text{where} \quad K = \frac{2.3Q}{4\pi \cdot m \cdot \Delta z} \cdot \log\left(\frac{t_2}{t_1}\right) \quad [\text{Jacob Equation}]$$

$$\text{and} \quad \Delta P = \rho g \Delta z = P_2 - P_1 = 0.03 \text{ inches } H_2O \times \left(\frac{3.61 \times 10^{-2} \text{ lb/inch}^2}{1 \text{ inch } H_2O}\right) = 0.00108 \text{ lb/inch}$$

$$k = \frac{2.3Q \cdot \mu_a}{4\pi \cdot m \cdot \Delta P} \cdot \log\left(\frac{t_2}{t_1}\right) = \frac{2.3 (0.0833 \text{ ft}^3/\text{s}) (2.617 \times 10^{-9} \text{ lb-s/in}^2)}{4\pi (8.5 \text{ ft}) (0.00108 \text{ lb/in}^2)} \times \log(12/1)$$

$$k = 4.67 \times 10^{-9} \text{ ft}^2 \quad (4.34 \times 10^{-6} \text{ cm}^2)$$

#### Summary of Permeabilities for UAF Bioventing Site:

Vent Well	Monitor Point	Depth (ft.)	Steady-state Perm. (cm <sup>2</sup> )	Steady-state Perm. (ft <sup>2</sup> )
1	MP-6	8	1.4 × 10 <sup>-7</sup>	1.5 × 10 <sup>-10</sup>
2	MP-10	9.5	1.7 × 10 <sup>-7</sup>	1.9 × 10 <sup>-10</sup>
3	MP-2	8.5	4.4 × 10 <sup>-7</sup>	4.7 × 10 <sup>-10</sup>
5	MP-10	9.5	1.15 × 10 <sup>-6</sup>	1.2 × 10 <sup>-9</sup>

**Typical Air Permeabilities for Various Soils:**

Soil Material	Permeability (cm <sup>2</sup> )	Permeability (ft <sup>2</sup> )
Coarse gravel	10 <sup>-5</sup> to 10 <sup>-4</sup>	10 <sup>-8</sup> to 10 <sup>-7</sup>
Medium gravel	10 <sup>-5</sup>	10 <sup>-8</sup>
Fine gravel	10 <sup>-6</sup> to 10 <sup>-5</sup>	10 <sup>-9</sup> to 10 <sup>-8</sup>
Coarse sand	10 <sup>-6</sup> to 10 <sup>-5</sup>	10 <sup>-9</sup> to 10 <sup>-8</sup>
Medium sand	10 <sup>-8</sup> to 10 <sup>-6</sup>	10 <sup>-11</sup> to 10 <sup>-9</sup>
Fine sand	10 <sup>-9</sup> to 10 <sup>-7</sup>	10 <sup>-12</sup> to 10 <sup>-10</sup>
Silts and clays	< 10 <sup>-9</sup>	< 10 <sup>-12</sup>

**Sample Reynolds Number Calculation** for flow through UAF Physical Plant LUST bioventing site vadose zone:

Vent well: VW-5

Radius of influence (R<sub>i</sub>): 63 ft.Kinematic viscosity of air at 0°F (ν<sub>a</sub>): 1.2 x 10<sup>-4</sup> ft<sup>2</sup>/sSteady-state permeability (k): 1.2 x 10<sup>-9</sup> ft<sup>2</sup>

$$v = \frac{Q}{\pi R_i^2} = \frac{0.083 \text{ cfs}}{\pi (0.63 \text{ ft})^2} = 6.657 \times 10^{-6} \text{ fps}$$

Using equation [3-7] and since  $v_a = \mu_a/\rho$ 

$$I = \frac{v v_a}{g k} = \frac{6.657 \times 10^{-6} \text{ ft/s} (1.2 \times 10^{-4} \text{ ft}^2/\text{s})}{32.2 \text{ ft/s}^2 (1.2 \times 10^{-9} \text{ ft}^2)} = 0.02 \text{ ft/ft}$$

$$N_R = \frac{k g d_{10}}{v_a^2} I = \frac{1.2 \times 10^{-9} \text{ ft}^2 (32.2 \text{ ft/s}^2) (0.009/12 \text{ ft}) \times (0.02 \text{ ft/ft})}{(1.2 \times 10^{-4} \text{ ft}^2/\text{s})^2} = 0.0004$$

Summary:

Vent Well	Discrete Hydraulic Gradient, <i>I</i> (ft/ft)	Reynolds Number, <i>N<sub>R</sub></i>
VW-5 (highest site permeability)	0.02	0.0004
VW-1 (lowest site permeability)	0.13	0.00033

**D-1 Sand-gravel Specifications:****Table A-1. D-1 sand-gravel specifications.**

<b>ATM (Alaska Test Method) T7*</b>	
<b>Aggregate Diameter (in.) or Sieve #</b>	<b>% Passing (by weight)</b>
1.5	--
1	100
3/4	70 - 100
3/8	50 - 80
#4	35 - 65
#8	20 - 50
#40	8 - 30
#200	0 - 6

\* Gravel aggregate from crushed stone of cobbles, of uniform quality, and without impurities. Fracture rating is 70% minimum.

**Table A-2.** Summary of arctic and subarctic bioventing and soil warming case studies.

<b>Location &amp; Time</b>	<b>Contamination Description</b>	<b>Hydrocarbon Contamination Levels (mg/kg or ppm)</b>	<b>Treatment and Analyses</b>	<b>Reference</b>
Eielson AFB, near Fairbanks, Alaska. Sept. 1991- fall 1995.	Soil and ground-water contamination with JP-4 jet fuel.	0.2- 5,000 (TPH)	Bioventing with soil warming of 2-7 ft. of sandy silt over sandy gravel vadose zone. Analysis of biodegradation rates vs. temperature. Results reflect increased biodegradation rates with increased soil temperature.	Leeson et al, 1995
Kenai, Alaska	Soil contaminated with crude oil.		Bioventing respiration test in shallow, silty sand vadose zone.	Hinchee and Ong., 1992
U.S. Coast Guard UST sites, Kodiak, Alaska. 1992.	UST gravel/rock packing contaminated with fuel.		Bioventing feasibility study. Project discontinued after excessive rainfall infiltration washed away contamination.	Komex International Limited
Former diesel tank farm site, Chignik, Alaska. 1993.	Soil and ground-water contaminated with diesel fuel.	Gross contamination.	Ex situ biocellular treatment of 3,450 cy of diesel contaminated soil using nutrient-enhanced, lateral air-injection bioventing and passive vapor extraction of off-gas. Results indicate successful remediation of hydrocarbons.	Shannon & Wilson, 1992-1995

**Table A-2 continued**

<p>Oil production gravel pad, North Slope of Alaska. Summers of 1993-1994; year-round monitoring.</p>	<p>Fuel (primarily diesel)contaminated gravel pad and surface waters above arctic tundra and permafrost.</p>	<p>1,000-12,000 (TPH)</p>	<p>Bioventing demonstration system with vapor and water extraction within 1.5m thick gravel pad. Analyses of biodegradation rates vs. temperature. Results reflect increased biodegradation rates with warmer soil temperatures. Report of biodegradation activity in winter. Soil warming recommended to reduce remediation time.</p>	<p>Simpkin et al, 1994</p>
<p>Eareckson AFS, Shemya Island, Alaska. Jan. 1993-1994.</p>	<p>Soil contaminated with &gt; 67,000 gallons of diesel fuel.</p>	<p>&lt; 1,304 (TPH)</p>	<p>Ex situ bioventing pilot study on encapsulated, gravel-sand soil piles; fertilized vs. unfertilized. Results reflect temperature increases and reduced bioremediation time (115 days vs. 15 months) of fertilized soils.</p>	<p>Brar et al (CRREL), 1993</p>
<p>F.E. Warren site, near Cheyenne, Wyoming. Jan. 1993-present.</p>	<p>Soil contaminated with petroleum fuels.</p>		<p>Bioventing with pure oxygen versus ambient air injection. Passive warming experiment with plastic surface covering. Results indicate no significant biodegradation enhancement from pure oxygen injection, some passive warming of shallow surficial soils, and soil moisture retention.</p>	<p>Battelle Memorial Institute</p>

Table A-2 continued.

<p>Gulf Strachan Gas Plant, 200km NW of Calgary. Alberta, Canada. Summers 1993-present</p>	<p>Soil and ground-water contaminated with a free-phase, natural gas condensate plume</p>	<p>2,000-5,000</p>	<p>Bioventing with SVE of 7-8m thick, clayey silt fill over glacial-fluvial sand and gravel vadose zone. Variable flow rate and extraction rate biodegradation optimization tests. Analysis of biodegradation rates vs. temperature. Results indicate increased biodegradation with warmer soil temperatures. Biodegradation observed in winter also.</p>	<p>Moore et al, 1994, CAPP, 1994</p>
<p>Alyeska Valdez Marine Terminal, Valdez, Alaska. Three spill sites. June 1993-present.</p>	<p>Tank containment soils contaminated with oily draw-off waters above bedrock.</p>	<p>200-7,800 (DRO)</p>	<p>Bioventing of 10-20 foot thick, sand and gravel containment soils, above CBA/flexible liners. Analysis of biodegradation rates vs. temperature. Results indicate increased biodegradation in warmer soils. No appreciable decrease in biodegradation rates during winter for this maritime climate site.</p>	<p>Thomas et al, 1995</p>
<p>Eielson AFB, near Fairbanks, Alaska. Two spill sites. Summer 1995-present.</p>	<p>Soil and ground-water contaminated with JP-8 jet fuel.</p>	<p>28-11,000 (DRO-soil); ND-57(DRO-groundwater)</p>	<p>Bioventing of 5-8 foot gravelly sand and silty sand vadose zone with removal of free-phase product at the water table. Feasibility study for SVE potential.</p>	<p>AGRA Earth &amp; Environmental, Inc.</p>
<p>Greeley burn pits, Delta Junction, Alaska. Two sites. Summer 1995-present.</p>	<p>Soil contaminated with diesel fuel and some pesticides</p>	<p>200-5,000 (DRO); · 0.5 ppb (DDT)</p>	<p>In-situ landfarming (upper 4-5 feet of vadose zone) with nutrient enhanced bioventing, to 30 ft. depth of coarse, glacio-alluvial, gravel-sand fill. Low cost, solar power feasibility study.</p>	<p>AGRA Earth &amp; Environmental, Inc.</p>

Table A-2 continued.

Fort Wainwright, Fairbanks, Alaska. May 1995-present.	POL contaminated stockpiled soil.	5-750 (GRO) 1,200 (DRO) 23,600 (TRPH)	Biocellular remediation with fertilizer, moisture, and oxygen enhancement. Passive soil warming with geotextile cover, to restrict injected air and moisture losses.	Army Corp of Engineers, Fort Wainwright
Old U.S. Navy Radar Station site, Hofn, Iceland. Aug. 1995-present.	Soil contaminated with JP-5 jet fuel.	10,000 (TPH)	Bioslurping operation: free-phase product recovery with bioventing of 2-5 ft. thick, volcanic sand vadose zone, above bedrock. Initial results to be reported in 1996.	Battelle Memorial Institute.
Elmendorf AFB, Anchorage, Alaska. Several sites. Summer 1995- present.	Soils contaminated with UST fuels and other petroleum products.		Bioventing with heated air injection. Active soil warming experiments to treat silty sands and gravels, silts and clays, and glacial outwash deposits of sands, gravels, and silts. Systems specially designed for frost-susceptible soils.	USAF
Several prospective petroleum industry sites, Alberta, Canada. 1996- future.	POL spills.	Unknown	Bioventing is being considered at several petroleum industry related spill sites for future remediation.	Komex International Limited

TPH= total petroleum hydrocarbons

TRPH=total recoverable petroleum hydrocarbons

DRO= diesel range organics

GRO= gasoline range organics

---

**Moduli of Elasticity Calculations and Typical Values for Soil Elastic Modulus and Poisson's Ratio**

**Moduli of Elasticity Calculations for ELSYM-5 Analysis:**

Layer 1:  $E_{smin} = 6,900 \text{ psi}^*$  \*From Table 2-7. p. 99 (Bowles 1988)

$$E_{smax} = 27,800 \text{ psi}^*$$

$$E_{svrg} = (6,900 + 27,800)/2 = 17,350 \text{ psi}$$

Layer 2:  $E_s = 2,800 \text{ psi}$  From manufacturer's specifications

Layer 3: For  $N = 4$

$$E_{s1} = 723 (N+15) = 13,737 \text{ psi}$$

Layer 4: For  $N = 12$

$$E_{s4} = 868 (N+6) = 15,624 \text{ psi}$$

For  $N = 27$

$$E_{s5} = 868 (N+6) + 2894 = 31,538 \text{ psi}$$

$$E_{svrg} = (15,624 + 31,538)/2 = 23,581 \text{ psi}$$

Layer 5: For  $N = 12$

$$E_{s2} = 434 (N+6) = 7,812 \text{ psi}$$

For  $N = 27$

$$E_{s5} = 31,538 \text{ psi}$$

$$E_{svrg} = (7,812 + 31,538)/2 = 19,675 \text{ psi}$$

Layer 6: For  $N = 7.5$

$$E_{s4} = 868 (N+6) = 11,718 \text{ psi}$$

For  $N = 11$

$$E_{s4} = 868 (11+6) = 14,756 \text{ psi}$$

$$E_{svrg} = (11,718 + 14,756)/2 = 13,237 \text{ psi}$$

General soil profile Poisson's Ratio:  $u = 0.35$



**Table B-1. Typical Value Ranges for Static Stress-Strain (Elastic) Modulus and Poisson's Ratio for Selected Soils\***

Soil	E <sub>s</sub>		u
	(psi)	(ksf)	
Sand (commonly used)			-0.1 to 1.0 (0.3 - 0.4)
silty	1040 - 3150	150 - 450	
loose	1350 - 3500	200 - 500	
dense	6900 - 11800	1000 - 1700	
Sand, Gravelly Sand (commonly used)			-0.1 to 1.0 0.3 - 0.4
loose	6900 - 20800	1000 - 3000	
dense	13900 - 27800	2000 - 4000	
Silt	280 - 2800	40 - 400	0.3 - 0.35

\*After Bowles, 1988

ELSYM-5 Stress-Strain Analysis

8 cy. dumptruck loading:

LAYER	ELASTIC MODULUS	POISSONS RATIO	THICKNESS
1	17350.	.350	12.000 IN
2	2800.	.350	2.000 IN
3	23063.	.350	38.000 IN
4	19675.	.350	60.000 IN
5	13237.	.350	SEMI-INFINITE

TEN LOAD(S), EACH LOAD AS FOLLOWS

TOTAL LOAD..... 6170.00 LBS  
 LOAD STRESS.... 110.00 PSI  
 LOAD RADIUS.... 4.23 IN

LOAD	LOCATED AT	
	X	Y
1	36.000	12.000
2	36.000	24.000
3	36.000	106.000
4	36.000	118.000
5	84.000	12.000
6	84.000	24.000
7	84.000	106.000
8	84.000	118.000
9	228.000	24.000
10	228.000	106.000

RESULTS REQUESTED FOR SYSTEM LOCATION(S)

DEPTH(S):  
 Z= 12.01 14.00  
 X-Y POINT(S):  
 X Y  
 60.00 18.00  
 60.00 65.00  
 60.00 112.00  
 228.00 65.00  
 60.00 166.00

Z= 12.01 LAYER NO. 2

X Y  
 60.00 18.00  
 60.00 65.00  
 60.00 112.00  
 228.00 65.00  
 60.00 166.00

NORMAL STRESSES  
 SXX -.2025E+01 -.1082E+00 -.2025E+01 -.8605E-02 -.6048E-01  
 SYY -.8213E+00 -.1942E+00 -.8213E+00 -.1509E+00 -.7378E-01  
 SZZ -.1431E+01 .2527E-01 -.1431E+01 .3152E-02 -.2128E-01

## SHEAR STRESSES

SXY	.1938E-02	-.6519E-09	-.1938E-02	-.3109E-09	-.3603E-02
SXZ	.2422E-02	.2758E-02	.2422E-02	-.1209E-01	.1466E-02
SYZ	.4374E-01	-.1496E-08	-.4374E-01	.0000E+00	-.1871E+00

## PRINCIPAL STRESSES

PS 1	-.8182E+00	.2532E-01	-.8182E+00	.1072E-01	.1415E+00
PS 2	-.1434E+01	-.1082E+00	-.1434E+01	-.1617E-01	-.6052E-01
PS 3	-.2025E+01	-.1942E+00	-.2025E+01	-.1509E+00	-.2365E+00

## PRINCIPAL SHEAR STRESSES

PSS 1	.6036E+00	.1098E+00	.6036E+00	.8079E-01	.1890E+00
PSS 2	.3081E+00	.6678E-01	.3081E+00	.1344E-01	.1010E+00
PSS 3	.2955E+00	.4298E-01	.2955E+00	.6735E-01	.8799E-01

## DISPLACEMENTS

UX	.2434E-03	.2555E-03	.2434E-03	-.1003E-02	.2065E-03
UY	.6403E-03	.2586E-11	-.6403E-03	.0000E+00	-.9312E-03
UZ	.2298E-01	.1825E-01	.2298E-01	.1121E-01	.1251E-01

## NORMAL STRAINS

EXX	-.4417E-03	-.1752E-04	-.4417E-03	.1539E-04	-.9715E-05
EYY	.1387E-03	-.5899E-04	.1387E-03	-.5320E-04	-.1613E-04
EZZ	-.1553E-03	.4682E-04	-.1553E-03	.2106E-04	.9181E-05

## SHEAR STRAINS

EXY	.1869E-05	-.6286E-12	-.1869E-05	-.2998E-12	-.3474E-05
EXZ	.2335E-05	.2660E-05	.2335E-05	-.1166E-04	.1414E-05
EYZ	.4218E-04	-.1443E-11	-.4218E-04	.0000E+00	-.1804E-03

## PRINCIPAL STRAINS

PE 1	.1403E-03	.4685E-04	.1403E-03	.2471E-04	.8765E-04
PE 2	-.1568E-03	-.1754E-04	-.1568E-03	.1174E-04	-.9736E-05
PE 3	-.4418E-03	-.5899E-04	-.4418E-03	-.5320E-04	-.9458E-04

## PRINCIPAL SHEAR STRAINS

PSE 1	.5820E-03	.1058E-03	.5820E-03	.7791E-04	.1822E-03
PSE 2	.2971E-03	.6439E-04	.2971E-03	.1296E-04	.9738E-04
PSE 3	.2849E-03	.4144E-04	.2849E-03	.6495E-04	.8484E-04

Z= 14.00 LAYER NO, 2

X	Y
60.00	18.00
60.00	65.00
60.00	112.00
228.00	65.00
60.00	166.00

## NORMAL STRESSES

SXX	-.1228E+01	-.9518E-01	-.1228E+01	-.2912E-01	-.6003E-01
SYY	-.9612E+00	-.1183E+00	-.9612E+00	-.7829E-01	-.5501E-01
SZZ	-.1736E+01	-.1428E-01	-.1736E+01	-.1838E-01	-.2642E-01

## SHEAR STRESSES

SXY	.1071E-02	-.1988E-09	-.1071E-02	-.1276E-09	-.1825E-02
SXZ	.2472E-02	.2823E-02	.2473E-02	-.1238E-01	.1477E-02
SYZ	.4559E-01	.1977E-09	-.4559E-01	.0000E+00	-.1902E+00

## PRINCIPAL STRESSES

PS 1	-.9586E+00	-.1418E-01	-.9586E+00	-.1025E-01	.1500E+00
PS 2	-.1228E+01	-.9528E-01	-.1228E+01	-.3724E-01	-.6006E-01
PS 3	-.1739E+01	-.1183E+00	-.1739E+01	-.7829E-01	-.2314E+00

## PRINCIPAL SHEAR STRESSES

PSS 1	.3900E+00	.5207E-01	.3900E+00	.3402E-01	.1907E+00
PSS 2	.1345E+00	.4055E-01	.1345E+00	.1349E-01	.1050E+00
PSS 3	.2555E+00	.1153E-01	.2555E+00	.2052E-01	.8569E-01

## DISPLACEMENTS

UX	.2331E-03	.2446E-03	.2331E-03	-.9609E-03	.1977E-03
UY	.6365E-03	.3163E-11	-.6365E-03	-.1819E-11	-.1062E-02
UZ	.2250E-01	.1832E-01	.2250E-01	.1123E-01	.1252E-01

## NORMAL STRAINS

EXX	-.1013E-03	-.1742E-04	-.1013E-03	.1685E-05	-.1126E-04
EYY	.2712E-04	-.2858E-04	.2712E-04	-.2202E-04	-.8838E-05
EZZ	-.3463E-03	.2159E-04	-.3463E-03	.6862E-05	.4943E-05

## SHEAR STRAINS

EXY	.1033E-05	-.1917E-12	-.1033E-05	-.1231E-12	-.1760E-05
EXZ	.2384E-05	.2723E-05	.2384E-05	-.1194E-04	.1424E-05
EYZ	.4396E-04	.1906E-12	-.4396E-04	.0000E+00	-.1834E-03

## PRINCIPAL STRAINS

PE 1	.2842E-04	.2164E-04	.2842E-04	.1078E-04	.9002E-04
PE 2	-.1013E-03	-.1746E-04	-.1013E-03	-.2233E-05	-.1127E-04
PE 3	-.3476E-03	-.2858E-04	-.3476E-03	-.2202E-04	-.9390E-04

## PRINCIPAL SHEAR STRAINS

PSE 1	.3760E-03	.5021E-04	.3760E-03	.3280E-04	.1839E-03
PSE 2	.1297E-03	.3910E-04	.1297E-03	.1301E-04	.1013E-03
PSE 3	.2463E-03	.1111E-04	.2463E-03	.1979E-04	.8263E-04

**Scraper loading:****ELASTIC SYSTEM - maxscrap**

LAYER	ELASTIC MODULUS	POISSONS RATIO	THICKNESS
1	17350.	.350	12.000 IN
2	2800.	.350	2.000 IN
3	23063.	.350	38.000 IN
4	19675.	.350	60.000 IN
5	13237.	.350	SEMI-INFINITE

TEN LOAD(S) , EACH LOAD AS FOLLOWS

TOTAL LOAD.....	5100.00 LBS
LOAD STRESS.....	110.00 PSI
LOAD RADIUS....	3.84 IN

LOAD	LOCATED AT	
	X	Y
1	36.000	166.000
2	36.000	174.000
3	36.000	250.000
4	36.000	262.000
5	60.000	166.000
6	60.000	174.000
7	60.000	250.000
8	60.000	262.000
9	204.000	174.000
10	204.000	250.000

RESULTS REQUESTED FOR SYSTEM LOCATION(S)

DEPTH(S)	
Z=	12.31 14.00
X-Y POINT(S)	
X	Y
48.00	142.00
48.00	172.00
48.00	212.00
48.00	256.00
204.00	174.00
204.00	212.00
204.00	250.00

Z= 12.01 LAYER NO, 2

X	Y
48.00	142.00
48.00	172.00
48.00	212.00
48.00	256.00
204.00	174.00
204.00	212.00
204.00	250.00

#### NORMAL STRESSES

SXX	.3556E+00	-.7764E+01	-.7761E-01	-.6940E+01	-.3856E+01	-.1156E-01	.3856E+01
SYX	.7723E+00	-.5262E+01	-.3260E+00	-.5066E+01	-.3878E+01	-.1661E+00	.3878E+01
SZZ	.3604E+00	-.1274E+02	.7209E-01	-.1137E+02	-.1262E+02	.3020E-02	-.1262E+02

#### SHEAR STRESSES

SXY	.2405E-02	.1469E-02	-.1730E-08	-.1605E-02	-.5534E-02	-.1406E-03	.5273E-02
SXZ	.2239E-02	.2791E-02	.3093E-02	.2730E-02	-.1135E-01	-.1234E-01	-.1144E-01
SYZ	.1088E+01	-.6595E+00	-.2773E-01	-.5211E-01	.2098E-01	.4242E-04	-.2090E-01

#### PRINCIPAL STRESSES

PSI	.5407E+00	-.5205E+01	.7408E-01	-.5066E+01	-.3855E+01	.1007E-01	.3855E+01
PS2	.3556E+00	-.7764E+01	-.7767E-01	-.6940E+01	-.3879E+01	-.1860E-01	.3879E+01
PS3	-.1673E+01	-.1280E+02	-.3279E+00	-.1137E+02	-.1262E+02	-.1661E+00	-.1262E+02

#### PRINCIPAL SHEAR STRESSES

PSS1	.1107E+01	.3797E+01	.2010E+00	.3152E+01	.4383E+01	.8810E-01	.4383E+01
PSS2	.4481E+00	.1280E+01	.7588E-01	.9371E+00	.1204E-01	.1433E-01	.1201E-01
PSS3	.6589E+00	.2518E+01	.1251E+00	.2215E+01	.4371E+01	.7377E-01	.4371E+01

#### DISPLACEMENTS

UX	.1956E-03	.2115E-03	.2199E-03	.2098E-03	-.8377E-03	-.8675E-03	-.8404E-03
UY	.1313E-02	.1926E-02	.6860E-04	-.5225E-03	.2956E-03	.4796E-05	-.2867E-03
UZ	.1600E-01	.3420E-01	.1713E-01	.3273E-01	.2114E-01	.9851E-02	.2115E-01

#### NORMAL STRAINS

EXX	.1460E-04	-.5222E-03	.4015E-05	-.4242E-03	.6852E-03	.1626E-04	.6852E-03
EYY	-.1863E-03	.6838E-03	-.1157E-03	.4792E-03	.6748E-03	-.5827E-04	.6748E-03
EZZ	.1226E-04	-.2922E-02	.7619E-04	-.2560E-02	-.3541E-02	.2329E-04	-.3541E-02

#### SHEAR STRAINS

EXY	.2319E-05	.1416E-05	-.1668E-11	-.1547E-05	-.5337E-05	-.1356E-06	.5084E-05
EXZ	.2159E-05	.2691E-05	.2982E-05	.2633E-05	-.1095E-04	-.1190E-04	-.1103E-04
EYZ	.1049E-02	-.6360E-03	-.2674E-04	-.5024E-04	.2023E-04	.4091E-07	-.2015E-04

#### PRINCIPAL STRAINS

PE1	.4467E-03	.7116E-03	.7715E-04	.4794E-03	.6858E-03	.2669E-04	.6858E-03
PE2	.1460E-04	-.5222E-03	.3985E-05	-.4242E-03	.6742E-03	.1287E-04	.6742E-03
PE3	-.6208E-03	-.2950E-02	-.1166E-03	-.2560E-02	-.3541E-02	-.5827E-04	.3541E-02

#### PRINCIPAL SHEAR STRAINS

PSE1	.1068E-02	.3662E-02	.1938E-03	.3039E-02	.4227E-02	.8496E-04	.4227E-02
PSE2	.4321E-03	.1234E-02	.7317E-04	.9037E-03	.1161E-04	.1382E-04	.1158E-04
PSE3	.6354E-03	.2428E-02	.1206E-03	.2135E-02	.4215E-02	.7114E-04	.4215E-02

Z= 14.00 LAYER NO. 2

X	Y
48.00	142.00
48.00	172.00
48.00	212.00
48.00	256.00
204.00	174.00
204.00	212.00
204.00	250.00

#### NORMAL STRESSES

SXX	-.3442E+00	-.6854E+01	-.8189E-01	-.6179E+01	-.5452E+01	-.2833E-01	-.5452E+01
SYX	-.4376E+00	-.6471E+01	-.1526E+00	-.5882E+01	-.5464E+01	-.7917E-01	-.5464E+01
SZZ	-.5178E+00	-.1265E+02	-.3704E-02	-.1139E+02	-.1090E+02	-.2049E-01	-.1090E+02

#### SHEAR STRESSES

SXY	.1367E-02	.8723E-03	-.1252E-09	-.9489E-03	-.3219E-02	-.7684E-04	.3079E-02
SXZ	.2291E-02	.2866E-02	.3181E-02	.2803E-02	-.1189E-01	-.9671E-02	-.1198E-01
SYZ	.1242E+01	-.8566E+00	-.2927E-01	-.5390E-01	.2164E-01	.1374E-04	-.2155E-01

#### PRINCIPAL STRESSES

PS1	.7648E+00	-.6354E+01	.1960E-02	-.5881E+01	-.5451E+01	-.1397E-01	-.5451E+01
PS2	-.3442E+00	-.6854E+01	-.8200E-01	-.6179E+01	-.5465E+01	-.3485E-01	-.5465E+01
PS3	-.1720E+01	-.1276E+02	-.1581E+00	-.1139E+02	-.1090E+02	-.7917E-01	-.1090E+02

#### PRINCIPAL SHEAR STRESSES

PSS1	.1242E+01	.3204E+01	.8005E-01	.2753E+01	.2723E+01	.3260E-01	.2723E+01
PSS2	.5545E+00	.2503E+00	.4198E-01	.1489E+00	.6671E-02	.1044E-01	.6658E-02
PSS3	.6880E+00	.2954E+01	.3806E-01	.2604E+01	.2716E+01	.2216E-01	.2716E+01

#### DISPLACEMENTS

UX	.1873E-03	.2026E-03	.2107E-03	.2009E-03	-.8025E-03	-.8315E-03	-.8051E-03
UY	.2291E-03	.7910E-03	.2938E-04	-.5338E-03	.2975E-03	.4592E-05	-.2890E-03
UZ	.1594E-01	.2846E-01	.1723E-01	.2766E-01	.1502E-01	.9879E-02	.1503E-01

#### NORMAL STRAINS

EXX	-.3519E-05	-.5843E-04	-.9712E-05	-.4813E-04	.9784E-04	.2340E-05	.9786E-04
EYY	-.4853E-04	.1267E-03	-.4379E-04	.9515E-04	.9221E-04	-.2217E-04	.9217E-04
EZZ	-.8719E-04	-.2851E-02	.2799E-04	-.2559E-02	-.2527E-02	.6121E-05	-.2527E-02

#### SHEAR STRAINS

EXY	.1318E-05	.8411E-06	-.1208E-12	-.9150E-06	-.3104E-05	-.7410E-07	.2969E-05
EXZ	.2210E-05	.2764E-05	.3067E-05	.2703E-05	-.1147E-04	-.9325E-05	-.1155E-04
EYZ	.1197E-02	-.8260E-03	-.2822E-04	-.5197E-04	.2086E-04	.1325E-07	-.2078E-04

#### PRINCIPAL STRAINS

PE1	.5312E-03	.1829E-03	.3072E-04	.9541E-04	.9827E-04	.9262E-05	.9825E-04
PE2	-.3522E-05	-.5843E-04	-.9766E-05	-.4813E-04	.9184E-04	-.8011E-06	.9183E-04
PE3	-.6669E-03	-.2907E-02	-.4647E-04	-.2560E-02	-.2527E-02	-.2217E-04	-.2527E-02

#### PRINCIPAL SHEAR STRAINS

PSE1	.1198E-02	.3090E-02	.7719E-04	.2655E-02	.2625E-02	.3144E-04	.2625E-02
PSE2	.5347E-03	.2413E-03	.4048E-04	.1435E-03	.6433E-05	.1006E-04	.6420E-05
PSE3	.6634E-03	.2849E-02	.3670E-04	.2511E-02	.2619E-02	.2137E-04	.2619E-02

BERG-2 Freeze-Thaw Analyses

Sample layer data (VW-1):

```

LAYER NUMBER 1 OF 2
1:GRAVEL 2:SAND 3:SILT 4:ASPHALT 5:CONCRETE 6:INSULATION 7:USER MATERIAL
MATERIAL NUMBER----- 1
THICKNESS OF LAYER (FT)----- 1
----- THAW CYCLE-----
FROZEN % MOISTURE----- 4
FROZEN DENSITY OF LAYER (LB/FT^3)----- 130
FROZEN HEAT CAPACITY (BTU/FT^3 F°)----- 24.7
FROZEN CONDUCTIVITY (BTU/FT HR F°)----- 1.15
LATENT HEAT (BTU/FT^3)----- 749
THAWED % MOISTURE----- 4
THAWED DENSITY OF LAYER (LB/FT^3)----- 130
THAWED HEAT CAPACITY (BTU/FT^3 F°)----- 27.3
THAWED CONDUCTIVITY (BTU/FT HR F°)----- 1.37
----- FREEZE CYCLE-----
LATENT HEAT OF FUSION (BTU/FT^3)----- 749
FROZEN DENSITY (LB/FT^3)----- 130
FROZEN HEAT CAPACITY (BTU/FT^3 F°)----- 24.7
FROZEN CONDUCTIVITY (BTU/FT HR F°)----- 1.15
USE F1 - F8 TO SELECT A LAYER #, USE F10 TO SET TOTAL # OF LAYERS = LAYER #
OR MOVE CURSOR TO MODIFY DATA L-LOCATION R-RUN Q-QUIT

```

```

LAYER NUMBER 2 OF 2
1:GRAVEL 2:SAND 3:SILT 4:ASPHALT 5:CONCRETE 6:INSULATION 7:USER MATERIAL
MATERIAL NUMBER----- 6
THICKNESS OF LAYER (FT)----- .167
----- THAW CYCLE-----
FROZEN % MOISTURE----- 0
FROZEN DENSITY OF LAYER (LB/FT^3)----- 1.8
FROZEN HEAT CAPACITY (BTU/FT^3 F°)----- 3
FROZEN CONDUCTIVITY (BTU/FT HR F°)----- .02
LATENT HEAT (BTU/FT^3)----- 0
THAWED % MOISTURE----- 0
THAWED DENSITY OF LAYER (LB/FT^3)----- 1.8
THAWED HEAT CAPACITY (BTU/FT^3 F°)----- 3
THAWED CONDUCTIVITY (BTU/FT HR F°)----- .02
----- FREEZE CYCLE-----
LATENT HEAT OF FUSION (BTU/FT^3)----- 0
FROZEN DENSITY (LB/FT^3)----- 1.8
FROZEN HEAT CAPACITY (BTU/FT^3 F°)----- 3
FROZEN CONDUCTIVITY (BTU/FT HR F°)----- .02
USE F1 - F8 TO SELECT A LAYER #, USE F10 TO SET TOTAL # OF LAYERS = LAYER #
OR MOVE CURSOR TO MODIFY DATA L-LOCATION R-RUN Q-QUIT

```



**BERG-2 freeze-thaw output data for VW-1 location  
Case 1 ( $n_i = 1.7$ ,  $n_r = 0.5$ ):**

VW-1 (case 1)

Location	Thaw N	Frez N	MAAT	Thaw °F-day	Frez °F-day	Thaw Days	Frez Days
Fairbanks	1.70	0.50	26	2967	5303	161	204
T C H Y A C W L E	Frozen % Moisture	4.0	0	6.0	5.7	12.5	8.0
	Frozen Density	130.0	1.80	120.0	130.0	121.2	130.0
	Latent Heat	749	0	1037	1067	2181	1498
	Frozen Heat Capacity	24.70	3.00	24.00	25.81	28.18	27.30
	Frozen Conductivity	1.15	0.02	1.13	1.51	2.20	2.00
	Thawed % Moisture	4.0	0	6.0	5.7	12.5	8.0
	Thawed Density	130.0	1.80	120.0	130.0	123.6	130.0
	Thawed Heat Capacity	27.30	3.00	27.60	29.51	36.47	32.50
	Thawed Conductivity	1.37	0.02	1.25	1.54	1.68	1.72
	Initial Thickness	1.00	0.17	0.17	3.00	5.00	10.00
	Amount Thawed	1.00	0.17	0.17	3.00	0.93	0.00
	Consolidation	---	---	---	---	0.02	---
	Final Thickness	1.00	0.17	0.17	3.00	4.98	10.00
	F C R Y E C E L Z E E	Latent Heat	749	0	1037	1067	2225
Frozen Density		130.0	1.8	120.0	130.0	121.2	130.0
Frozen Heat Capacity		24.70	3.00	24.00	25.81	28.18	27.30
Frozen Conductivity		1.15	0.02	1.13	1.51	2.20	2.00
Initial Thickness		1.00	0.17	0.17	3.00	4.98	10.00
Amount Frozen		1.00	0.17	0.17	2.32	0.00	0.00
<b>Estimated Thaw = 5.26 ft.</b>		<b>Consolidation = 0.02 ft.</b>		<b>Freeze = 3.65 ft.</b>			

**BERG-2 freeze-thaw output data for VW-2 location  
Case 1 ( $n_i = 1.7$ ,  $n_r = 0.5$ ):**

VW-2 (case 1)

Location	Thaw N	Frez N	MAAT	Thaw °F-day	Frez °F-day	Thaw Days	Frez Days
Fairbanks	1.70	0.50	26	2967	5303	161	204
T C H Y A C W L E	Frozen % Moisture	4.0	0	6.0	6.6	15.0	8.5
	Frozen Density	130.0	1.80	120.0	130.0	115.0	130.0
	Latent Heat	749	0	1037	1236	2485	1591
	Frozen Heat Capacity	24.70	3.00	24.00	26.39	28.19	27.63
	Frozen Conductivity	1.15	0.02	1.13	1.70	2.11	2.10
	Thawed % Moisture	4.0	0	6.0	6.6	15.0	8.5
	Thawed Density	130.0	1.80	120.0	130.0	117.7	130.0
	Thawed Heat Capacity	27.30	3.00	27.60	30.68	37.66	33.15
	Thawed Conductivity	1.37	0.02	1.25	1.62	1.53	1.75
	Initial Thickness	1.00	0.17	0.17	3.00	5.00	10.00
	Amount Thawed	1.00	0.17	0.17	3.00	0.67	0.00
	Consolidation	---	---	---	---	0.02	---
	Final Thickness	1.00	0.17	0.17	3.00	4.98	10.00
	F C R Y E C E L Z E E	Latent Heat	749	0	1037	1236	2542
Frozen Density		130.0	1.8	120.0	130.0	115.0	130.0
Frozen Heat Capacity		24.70	3.00	24.00	26.39	28.19	27.63
Frozen Conductivity		1.15	0.02	1.13	1.70	2.11	2.10
Initial Thickness		1.00	0.17	0.17	3.00	4.98	10.00
Amount Frozen		1.00	0.17	0.17	2.04	0.00	0.00
<b>Estimated Thaw = 5.01 ft.</b>		<b>Consolidation = 0.02 ft.</b>		<b>Freeze = 3.38 ft.</b>			

**BERG-2 freeze-thaw output data for VW-4 location  
Case 1 ( $n_t = 1.7$ ,  $n_r = 0.5$ ):**

VW-4 (case 1)

Location	Thaw N	Frez N	MAAT	Thaw °F-day	Frez °F-day	Thaw Days	Frez Days
Fairbanks	170	050	26	2967	5303	161	204
			1	2	3	4	5
T C H Y A C W L E	Frozen % Moisture	4.0	0	6.0	18.0	11.0	
	Frozen Density	130.0	1.80	120.0	108.4	125.2	
	Latent Heat	749	0	1037	2811	1983	
	Frozen Heat Capacity	24.70	3.00	24.00	28.19	28.17	
	Frozen Conductivity	1.15	0.02	1.13	2.00	2.24	
	Thawed % Moisture	4.0	0	6.0	18.0	11.0	
	Thawed Density	130.0	1.80	120.0	111.3	127.5	
	Thawed Heat Capacity	27.30	3.00	27.60	38.95	35.70	
	Thawed Conductivity	1.37	0.02	1.25	1.38	1.77	
	Initial Thickness	1.00	0.17	0.17	10.00	10.00	
F C R Y E C E L Z E E	Amount Thawed	1.00	0.17	0.17	2.20	0.00	
	Consolidation	---	---	---	0.06	0.00	
	Final Thickness	1.00	0.17	0.17	9.94	10.00	
	Latent Heat	749	0	1037	2884	2020	
	Frozen Density	130.0	1.8	120.0	108.4	125.2	
	Frozen Heat Capacity	24.70	3.00	24.00	28.19	28.17	
	Frozen Conductivity	1.15	0.02	1.13	2.00	2.24	
	Initial Thickness	1.00	0.17	0.17	9.94	10.00	
	Amount Frozen	1.00	0.17	0.17	0.93	0.00	
	<b>Estimated Thaw = 3.54 ft. Consolidation = 0.06 ft. Freeze = 2.27 ft.</b>						

**BERG-2 freeze-thaw output data for VW-5 location  
Case 1 ( $n_t = 1.7$ ,  $n_r = 0.5$ ):**

VW-5 (case 1)

Location	Thaw N	Frez N	MAAT	Thaw °F-day	Frez °F-day	Thaw Days	Frez Days
Fairbanks	170	050	26	2967	5303	161	204
			1	2	3	4	5
T C H Y A C W L E	Frozen % Moisture	4.0	0	6.0	27.0	2.50	7.4
	Frozen Density	130.0	1.80	120.0	92.5	130.0	130.0
	Latent Heat	749	0	1037	3597	468	1385
	Frozen Heat Capacity	24.70	3.00	24.00	28.22	23.73	26.91
	Frozen Conductivity	1.15	0.02	1.13	1.72	0.84	1.87
	Thawed % Moisture	4.0	0	6.0	27.0	2.50	7.4
	Thawed Density	130.0	1.80	120.0	95.6	130.0	130.0
	Thawed Heat Capacity	27.30	3.00	27.60	42.08	25.35	31.72
	Thawed Conductivity	1.37	0.02	1.25	1.06	1.13	1.68
	Initial Thickness	1.00	0.17	0.17	6.00	5.00	9.00
F C R Y E C E L Z E E	Amount Thawed	1.00	0.17	0.17	1.79	0.00	0.00
	Consolidation	---	---	---	0.07	---	---
	Final Thickness	1.00	0.17	0.17	5.93	5.00	9.00
	Latent Heat	749	0	1037	3718	468	1385
	Frozen Density	130.0	1.8	120.0	92.5	130.0	130.0
	Frozen Heat Capacity	24.70	3.00	24.00	28.22	23.73	26.91
	Frozen Conductivity	1.15	0.02	1.13	1.72	0.84	1.87
	Initial Thickness	1.00	0.17	0.17	5.93	5.00	9.00
	Amount Frozen	1.00	0.17	0.17	0.77	0.00	0.00
	<b>Estimated Thaw = 3.13 ft. Consolidation = 0.07 ft. Freeze = 2.11 ft.</b>						

---

**Mass Transport Equations**
**General Equations for Conservation of Mass and Momentum Through Porous Media:**

The 3D conservation of mass (continuity) equation for steady state fluid transfer through a volume of unsaturated soil with uniform porosity is

$$\frac{\partial \rho}{\partial t} + \frac{\partial J_x}{\partial x} + \frac{\partial J_y}{\partial y} + \frac{\partial J_z}{\partial z} = 0 \quad [\text{E-1}]$$

where

$t$  = time (in seconds)

$\rho$  = fluid density (in lb/ft<sup>3</sup>)

$J = \rho v_{(x, y, z)}$  ; fluid flux (in lb/ft<sup>2</sup>-s)

$v_{(x, y, z)}$  = fluid linear velocity in the  $x$ ,  $y$ , and  $z$  directions (in ft/s)

In homogeneous, unsaturated soil, the general 3D mass transfer equation for non-sorbing chemicals that have not undergone biological or radioactive decay is

$$\frac{\partial(\theta C)}{\partial t} = -\frac{\partial J_s}{\partial x} - \frac{\partial J_s}{\partial y} - \frac{\partial J_s}{\partial z} \quad [\text{E-2}]$$

where

$$J_s = J_c + J_d + J_v$$

$$J_c = \left( -K \frac{\partial H}{\partial z} \right) C$$

$$J_d = -D_d \left( \frac{\partial C}{\partial x} + \frac{\partial C}{\partial y} + \frac{\partial C}{\partial z} \right)$$

$$J_v = -D_v \left( \frac{\partial C}{\partial x} + \frac{\partial C}{\partial y} + \frac{\partial C}{\partial z} \right)$$

$C$  = chemical (contaminant) concentration (in lb/ft<sup>3</sup>)

$\theta$  = soil moisture content

$D_d, D_v^*$  = diffusive and dispersive proportionality constants (in ft<sup>2</sup>/s)

If contaminant distribution in the  $xy$  plane is complete and, therefore, no appreciable change in solute concentrations, then equation [E-2] is reduced to the 1D equation

$$\frac{\partial(\theta C)}{\partial t} = -\frac{\partial J_s}{\partial z} = \frac{\partial}{\partial z} \left[ \theta D \left( \frac{\partial C}{\partial z} \right) + K \frac{\partial H}{\partial z} C \right] \quad [\text{E-3}]$$

where

$D^*$  = overall hydrodynamic dispersion coefficient (in ft<sup>2</sup>/s)

$K$  = soil hydraulic conductivity (in ft/s)

$H$  = total pressure head (ft)

The 1D form of Darcy's Law for fluid momentum is expressed as

$$v_z = -\frac{k_z}{\mu} \left( \frac{dP}{dz} + \gamma \frac{dz}{dz} \right) \quad [\text{E-4}]$$

---

\* The diffusivity and dispersion proportionality constants are empirically derived and are functions of porous media tortuosity, soil moisture content, soil structure variability. The overall hydrodynamic dispersion coefficient ( $D$ ) represents the additive effects of  $D_d$  and  $D_v^*$ , since both are macroscopically similar.

where

- $k_z$  = soil intrinsic permeability in the  $z$  (vertical) direction (in  $\text{ft}^2$ )
- $P$  = capillary pressure (in  $\text{lb}/\text{ft}^2$ )
- $\mu$  = fluid dynamic viscosity (in  $\text{lb}\cdot\text{s}/\text{ft}^2$ )
- $\gamma$  = fluid unit weight ( $\rho g$ ) (in  $\text{lb}/\text{ft}^3$ )
- $z$  = elevational difference (in ft)

The 3D form of the conservation of fluid momentum equation is

$$v_{(x,y,z)} = -\frac{k_{(x,y,z)}}{\mu} \left[ \left( \frac{dP}{dx} + \frac{dP}{dy} + \frac{dP}{dz} \right) + \gamma \left( \frac{dz}{dx} + \frac{dz}{dy} + \frac{dz}{dz} \right) \right] \quad [\text{E-5}]$$

---

**Surface Boundary Conditions**

**Calculation of the Surface Boundary Conditions for TDHC Analyses:**

From the Environmental Atlas of Alaska, for Fairbanks.

$$T_m = 25.6^\circ\text{F}, A_o = 35^\circ\text{F} \text{ and } \phi = 8 \text{ days}$$

The beginning and ending of the air thawing season are:

$$t_1 = \frac{365}{2\pi} \cos^{-1} \left( \frac{T_m - T_f}{A_o} \right)_{rad} + \phi_s = \frac{365}{2\pi} \cos^{-1} \left( \frac{25.6 - 32}{35} \right) + 8 = 110 \text{ days}$$

$$t_2 = \frac{365}{2\pi} \left[ 2\pi - \cos^{-1} \left( \frac{T_m - T_f}{A_o} \right)_{rad} \right] + \phi_s = \frac{365}{2\pi} \left[ 2\pi - \cos^{-1} \left( \frac{25.6 - 32}{35} \right) \right] + 8 = 271 \text{ days}$$

Next, the air thawing and freezing indices are calculated as

$$\begin{aligned} ATI &= (T_m - T_f)(t_2 - t_1) + \frac{365A_o}{\pi} \sin \left[ \frac{2\pi(t_1 - \phi)}{365} \right]_{rad} \\ &= (25.6 - 32)(271 - 110) + \frac{365(35)}{\pi} \sin \left[ \frac{2\pi(110 - 8)}{365} \right] = 2967 \text{ }^\circ\text{F-days} \end{aligned}$$

$$\begin{aligned} AFI &= 2(T_f - T_m)(t_1 - \phi) + \frac{365A_o}{\pi} \sin \left[ \frac{2\pi(t_1 - \phi)}{365} \right]_{rad} \\ &= 2(32 - 25.6)(110 - 8) + \frac{365(35)}{\pi} \sin \left[ \frac{2\pi(110 - 8)}{365} \right] = 5303 \text{ }^\circ\text{F-days} \end{aligned}$$

For case 1 (with snow), the n-factors for the D-1 sand-gravel surface are chosen as

$$n_i = 1.7, n_f = 0.5$$

The mean annual soil surface temperature is calculated and the amplitude of the ground surface temperature variation are now estimated (assuming  $\phi = \phi_s$ ):

$$T_{ms} = T_f + \frac{n_i(ATT) - n_f(AFI)}{365} = 32 + \frac{1.7(2967) - 0.5(5303)}{365} = 38.6^\circ F$$

$$A_{os} = \frac{\pi}{365 \sin \left[ \frac{2\pi(t_1 - \phi_s)}{365} \right]_{rad}} [n_i ATT - (T_{ms} - T_f)(t_2 - t_1)]$$

$$= \frac{\pi}{365 \sin \left[ \frac{2\pi(110 - 8)}{365} \right]} [1.7(2967) - (38.6 - 32)(271 - 110)] = 34.9^\circ F$$

New values of  $t_{1s}$  and  $t_{2s}$  are now found by substituting  $T_{ms}$  and  $A_{os}$  for the original  $T_m$  and  $A_s$ .

$$t_{1s} = \frac{365}{2\pi} \cos^{-1} \left( \frac{T_{ms} - T_f}{A_{os}} \right)_{rad} + \phi_s = \frac{365}{2\pi} \cos^{-1} \left( \frac{38.6 - 32}{34.9} \right) + 8 = 88 \text{ days}$$

$$t_{2s} = \frac{365}{2\pi} \left[ 2\pi - \cos^{-1} \left( \frac{T_{ms} - T_f}{A_{os}} \right)_{rad} \right] + \phi_s = \frac{365}{2\pi} \left[ 2\pi - \cos^{-1} \left( \frac{38.6 - 32}{34.9} \right) \right] + 8 = 293 \text{ days}$$

With these revised thaw season data  $A_{os}$  is further refined as

$$A_{os} = \frac{\pi}{365 \sin \left[ \frac{2\pi(88 - 8)}{365} \right]} [1.7(2967) - (38.6 - 32)(293 - 88)] = 32.4^\circ F$$

Finally, the approximate seasonal ground surface temperature variation is

$$T_s(t)_1 = T_{ms} - A_{os} \cos \left[ \frac{2\pi(t-\phi_s)}{365} \right]_{rad} = 38.6 - 32.4 \cos \left[ \frac{2\pi(t-8)}{365} \right]$$

$$T_s(t)_1 = 38.6 - 32.4 \cos [0.0172(t-8)]_{rad} \quad (\text{in } ^\circ\text{F})$$

Similarly, for case 2 (without snow cover) n-factors  $n_i = 1.7$  and  $n_f = 1.0$ , the following calculations provide the other seasonal ground surface temperature variation:

$$T_{ms} = 32 + \frac{1.7(2967) - 1.0(5303)}{365} = 31.3^\circ\text{F}$$

$$A_{os} = \frac{\pi}{365 \sin \left[ \frac{2\pi(110-8)}{365} \right]} [1.7(2967) - (31.3-32)(271-110)] = 45.2^\circ\text{F}$$

$$t_{1s} = \frac{365}{2\pi} \cos^{-1} \left( \frac{31.3 - 32}{45.2} \right) + 8 = 100 \text{ days}$$

$$t_{2s} = \frac{365}{2\pi} \left[ 2\pi - \cos^{-1} \left( \frac{31.3 - 32}{45.2} \right) \right] + 8 = 281 \text{ days}$$

$$A_{os} = \frac{\pi}{365 \sin \left[ \frac{2\pi(100-8)}{365} \right]} [1.7(2967) - (31.3-32)(281-100)] = 44.5^\circ\text{F}$$

$$T_s(t)_2 = 31.3 - 44.5 \cos [0.0172(t-8)]_{rad} \quad (\text{in } ^\circ\text{F})$$



---

**TDHC Input Files and Additional Thermal Comparison Plots**
**TDHC Input Data:****Zone I**

Zone I thermal input data for TDHC  
(Kf, Kt, Cf, Ct, L, Ti), in English units.  
1.15, 1.37, 24.7, 27.3, 749, 28  
0.0165, 0.0165, 0.54, 0.54, 0, 29  
0.25, 0.49, 16.1, 17.8, 490, 29.5  
1.51, 1.47, 25.6, 30.0, 1260, 30  
0.65, 0.67, 23.1, 27.5, 1267, 33.5  
1.16, 1.24, 24.0, 27.6, 1037, 35

Zone I problem definition portion of grid generated file for TDHC:

## TIME DATA

(time step, days) (start time, days from Jan.1) (run time, yrs.)  
1.013889 -61.25 2  
(print interval, # time steps)  
30

## HARMONIC NODE TEMPERATURES (surface boundary condition)

7 nodes

(node)	(Tm)	(Ao)	(phase lag)
454	38.6	32.4	8
455	38.6	32.4	8
452	38.6	32.4	8
449	38.6	32.4	8
445	38.6	32.4	8
440	38.6	32.4	8
434	38.6	32.4	8

## HARMONIC NODE TEMPERATURES (water table boundary condition)

7 nodes (avg. GW temp.)

260	36.5	3.5	8
254	36.5	3.5	8
248	36.5	3.5	8
242	36.5	3.5	8
236	36.5	3.5	8
230	36.5	3.5	8
224	36.5	3.5	8

### Zone II (1D analysis)

Zone II thermal input data for TDHC  
 (Kf,Kt,Cf,Ct,L,Ti), in English units.  
 1.15,1.37,24.7,27.3,749,28  
 0.0165,0.0165,0.54,0.54,0,29  
 0.25,0.49,16.1,17.8,490,29.5  
 1.51,1.47,25.6,30.0,1260,31  
 0.65,0.67,23.1,27.5,1267,33  
 1.16,1.24,24.0,27.6,1037,34

Zone II problem definition portion of grid generated file for TDHC:

TIME DATA

(time step, days)	(start time, days from Jan.1)	(run time, yrs.)
1.013889	-61.25	2

(print interval, # time steps)

30

HARMONIC NODE TEMPERATURES (surface boundary condition)

7 nodes

(node)	(Tm)	(Ao)	(phase lag)
216	38.6	32.4	8
217	38.6	32.4	8
214	38.6	32.4	8
211	38.6	32.4	8
207	38.6	32.4	8
202	38.6	32.4	8
196	38.6	32.4	8

HARMONIC NODE TEMPERATURES (water table boundary condition)

7 nodes (avg. GW temp.)

22	36.5	3.5	8
16	36.5	3.5	8
11	36.5	3.5	8
7	36.5	3.5	8
4	36.5	3.5	8
2	36.5	3.5	8
1	36.5	3.5	8

HEAT FLUX AT NODES (heat tape input @ t=0)

1 node (1/2 total heat flux)

190 4.71

### Zone III

Zone III thermal input data for TDHC  
 (Kf,Kt,Cf,Ct,L,Ti), in English units.  
 1.51,1.47,25.6,30.0,1260,28  
 0.65,0.67,23.1,27.5,1267,32  
 1.16,1.24,24.0,27.6,1037,32.8

Zone III problem definition portion of grid generated file for TDHC:

#### TIME DATA

(time step,days) (start time,days from Jan.1) (run time,yrs.)

1.013889 -61.25 2

(print interval, # time steps)

30

#### HARMONIC NODE TEMPERATURES (surface boundary condition)

7 nodes (Tm) (Ao) (phase lag)

412 38.6 32.4 8

413 38.6 32.4 8

410 38.6 32.4 8

407 38.6 32.4 8

403 38.6 32.4 8

398 38.6 32.4 8

392 38.6 32.4 8

#### HARMONIC NODE TEMPERATURES (water table boundary condition)

7 nodes (avg. GW temp.)

260 36.5 3.5 8

254 36.5 3.5 8

248 36.5 3.5 8

242 36.5 3.5 8

236 36.5 3.5 8

230 36.5 3.5 8

224 36.5 3.5 8

### Zone II (2D boundary analysis)

Zone II 2D boundary problem definition portion of grid generated file for TDHC:

TIME DATA

(time step, days) (start time, days from Jan.1) (run time, yrs.)  
 1.013889 -61.25 2

(print interval, # time steps)

30

HARMONIC NODE TEMPERATURES

45 nodes

(node)	(Tm)	(Ao)	(phase lag)
45	38.6	32.4	8
46	38.6	32.4	8
47	38.6	32.4	8
48	38.6	32.4	8
49	38.6	32.4	8
50	38.6	32.4	8
61	38.6	32.4	8
73	38.6	32.4	8
86	38.6	32.4	8
100	38.6	32.4	8
115	38.6	32.4	8
131	38.6	32.4	8
148	38.6	32.4	8
166	38.6	32.4	8
185	38.6	32.4	8
205	38.6	32.4	8
226	38.6	32.4	8
248	38.6	32.4	8
271	38.6	32.4	8
295	38.6	32.4	8
345	38.6	32.4	8
370	38.6	32.4	8
395	38.6	32.4	8
445	38.6	32.4	8
470	38.6	32.4	8
495	38.6	32.4	8
546	38.6	32.4	8
573	38.6	32.4	8
600	38.6	32.4	8
627	38.6	32.4	8
654	38.6	32.4	8
681	38.6	32.4	8
708	38.6	32.4	8
735	38.6	32.4	8
762	38.6	32.4	8
789	38.6	32.4	8
816	38.6	32.4	8
843	38.6	32.4	8
870	38.6	32.4	8
897	38.6	32.4	8
924	38.6	32.4	8
951	38.6	32.4	8
978	38.6	32.4	8
1004	38.6	32.4	8

HARMONIC NODE TEMPERATURES (water table boundary condition)  
 45 nodes (avg. GW temp.)

562	36.5	3.5	8
588	36.5	3.5	8
614	36.5	3.5	8
640	36.5	3.5	8
666	36.5	3.5	8
692	36.5	3.5	8
718	36.5	3.5	8
744	36.5	3.5	8
770	36.5	3.5	8
796	36.5	3.5	8
822	36.5	3.5	8
848	36.5	3.5	8
874	36.5	3.5	8
900	36.5	3.5	8
926	36.5	3.5	8
952	36.5	3.5	8
960	36.5	3.5	8
984	36.5	3.5	8
1008	36.5	3.5	8
1032	36.5	3.5	8
1077	36.5	3.5	8
1078	36.5	3.5	8
1079	36.5	3.5	8
1115	36.5	3.5	8
1133	36.5	3.5	8
1149	36.5	3.5	8
1164	36.5	3.5	8
1178	36.5	3.5	8
1191	36.5	3.5	8
1203	36.5	3.5	8
1214	36.5	3.5	8
1224	36.5	3.5	8
1233	36.5	3.5	8
1241	36.5	3.5	8
1248	36.5	3.5	8
1254	36.5	3.5	8
1259	36.5	3.5	8
1263	36.5	3.5	8
1266	36.5	3.5	8
1268	36.5	3.5	8
1269	36.5	3.5	8
320	38.6	32.4	8
420	38.6	32.4	8
520	38.6	32.4	8
1055	36.5	3.5	8
1096	36.5	3.5	8

```

HEAT FLUX AT NODES (heat tape input @ t=0)
20 nodes      (heat flux)
29             9.437
42             9.437
58             9.437
70             9.437
83             9.437
97             9.437
112            9.437
128            9.437
145            9.437
163            9.437
182            9.437
202            9.437
223            9.437
245            9.437
268            9.437
292            9.437
317            9.437
340            9.437
364            9.437
388            9.437

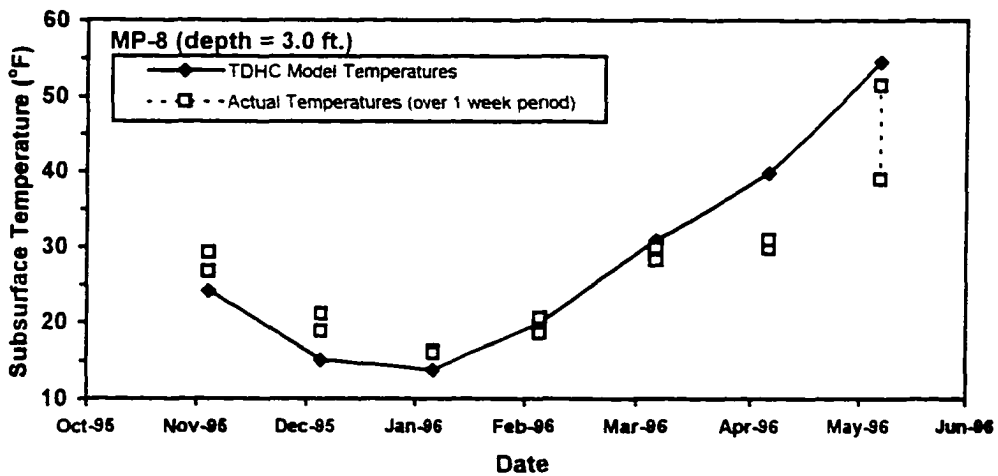
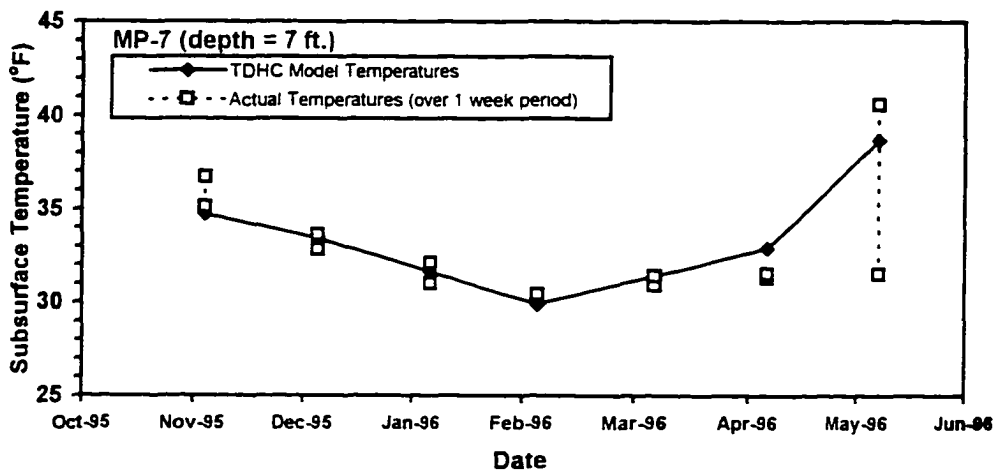
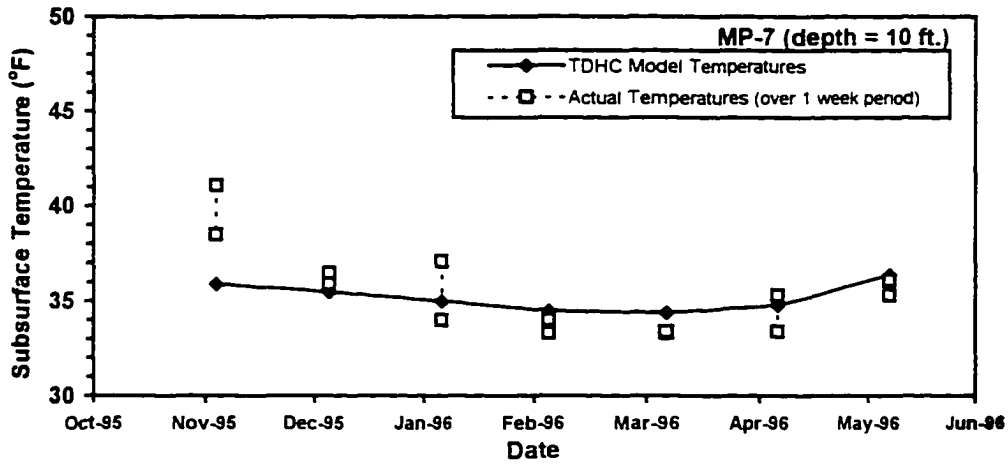
```

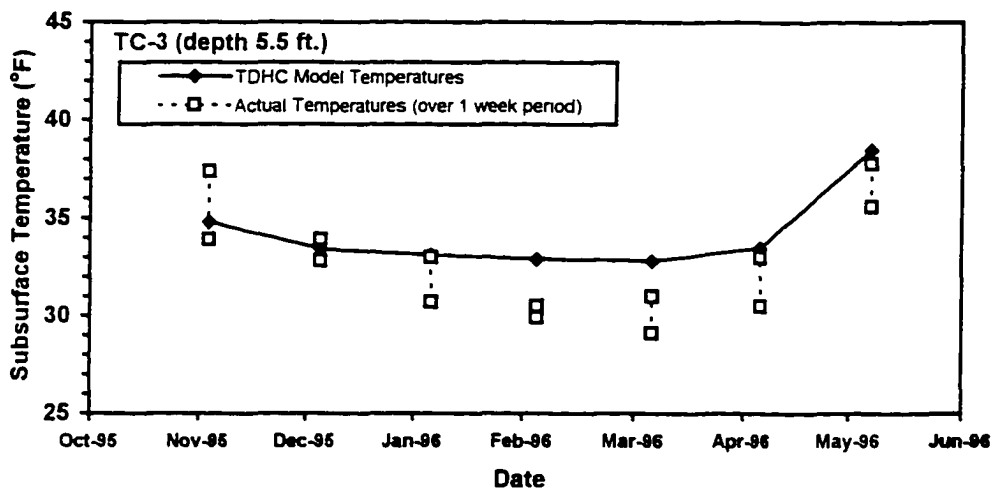
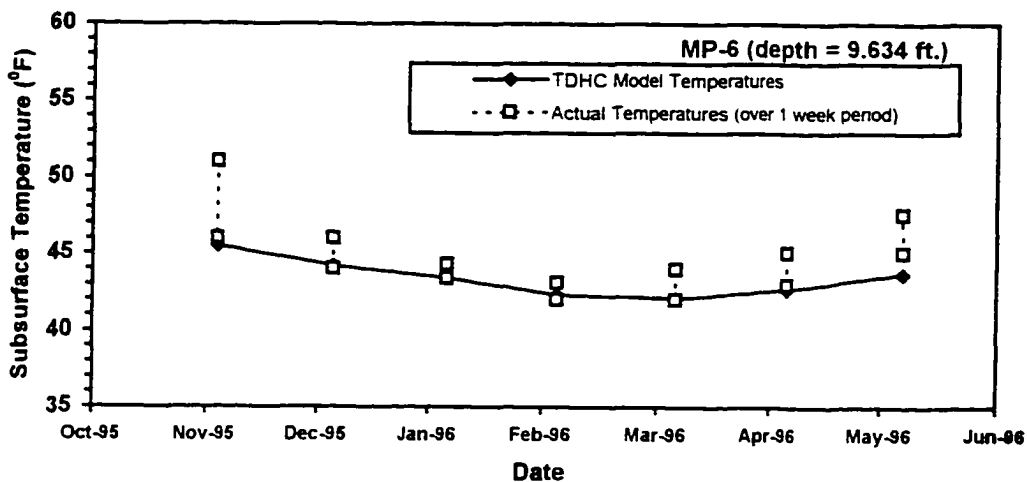
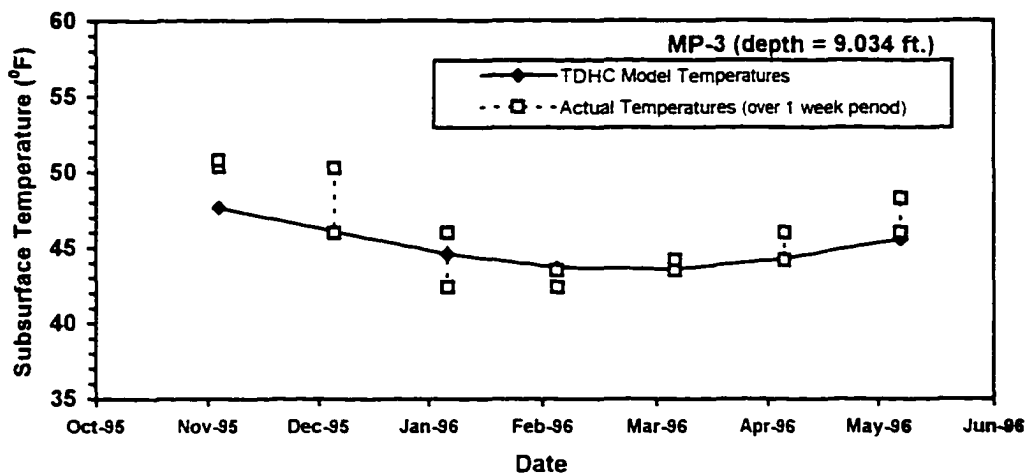
```

Zone II 2D thermal input data for TDHC:
(Kf,Kt,Cf,Ct,L,Ti), in English units.
1.15,1.37,24.7,27.3,749,28
1.15,1.37,24.7,27.3,749,28
1.15,1.37,24.7,27.3,749,28
0.0165,0.0165,0.54,0.54,0,29
0.25,0.49,16.1,17.8,490,29.5
1.51,1.47,25.6,30.0,1260,31
1.51,1.47,25.6,30.0,1260,29
1.51,1.47,25.6,30.0,1260,28
0.65,0.67,23.1,27.5,1267,33
0.65,0.67,23.1,27.5,1267,33
0.65,0.67,23.1,27.5,1267,33
1.16,1.24,24.0,27.6,1037,34
1.16,1.24,24.0,27.6,1037,34
1.16,1.24,24.0,27.6,1037,34

```

**Additional Thermal Comparison Plots:**







**APPENDIX H**

**Table H-1. Summary of soil analytical results (concentrations in ppm).**

<b>Well or Boring</b>	<b>Sample Depth (ft.)</b>	<b>Date</b>	<b>Benzene</b>	<b>Toluene</b>	<b>Ethylbenzene</b>	<b>Xylenes</b>	<b>Total BTEX</b>	<b>GRPH</b>	<b>DROs</b>
PW-105	12.5-13.3	Jun-90	5	79	29	200	313	1200	NT
PW-107	5-6.5	Jun-90	ND	0.03	0.02	0.11	0.16	1	NT
	15-16.5	Jun-90	0.08	1.1	0.44	2.6	4.22	20	NT
PW-110	10-11.5	Jul-90	ND	0.06	0.07	0.7	0.83	9	NT
	12.5-14	Jul-90	ND	71	65	410	546	2400	NT
	15-16.5	Jul-90	ND	71	15	82	168	930	NT
PW-111	5-6.5	Jul-90	0.5	0.04	0.02	0.06	0.62	ND	NT
	10-11.5	Jul-90	0.95	27	12	64	104	370	NT
	12.5-14	Jul-90	14	210	85	420	729	2000	NT
MW-201	5	Jun-91	ND	ND	ND	0.006	0.006	ND	NT
	10	Jun-91	ND	0.051	0.014	0.11	0.175	0.7	NT
B-104	5-6.5	Jun-90	ND	ND	4.5	28	32.5	300	NT
	15-16	Jun-90	ND	ND	ND	ND	ND	ND	NT
B-108	15-15.9	Jun-90	ND	ND	ND	ND	ND	ND	NT
Shemp	8-10	Jul-95	ND	ND	ND	ND	ND	ND	NT
	11-13	Jul-95	ND	ND	0.02	0.03	0.05	ND	NT
	13-15	Jul-95	ND	ND	ND	ND	ND	ND	NT
Larry	8-9.5	Jul-95	ND	ND	0.03	ND	0.03	ND	NT
	9.5-11.5	Jul-95	ND	ND	ND	0.05	0.05	ND	NT
	11.5-13.5	Jul-95	ND	ND	ND	ND	ND	ND	NT

Table H-1 continued.

Well or Boring	Sample Depth (ft.)	Date	Benzene	Toluene	Ethylbenzene	Xylenes	Total BTEX	GRPH	DROs
Curly	5-7.5	Jul-95	0.04	0.28	0.26	0.11	0.69	27	NT
	10-12.5	Jul-95	0.1	0.5	0.9	0.9	2.4	3.9	NT
	12.5-14.5	Jul-95	0.36	5.67	4.43	23.6	34.06	150	NT
Moe	7-8.5	Jul-95	ND	ND	ND	ND	ND	ND	NT
	10-12	Jul-95	ND	ND	ND	ND	ND	ND	NT
	12-14	Jul-95	ND	ND	ND	ND	ND	ND	NT
Joe	7-9	Jul-95	ND	ND	ND	ND	ND	ND	NT
	9-11	Jul-95	ND	ND	ND	ND	ND	ND	NT
	11-13	Jul-95	ND	0.04	ND	ND	0.04	2.4	NT
H	4.5-6	Jun-96	0.0033	0.0068	0.0034	0.0088	0.0223	ND	91.2
	6.5-8	Jun-96	0.0054	0.01	ND	0.014	0.0294	ND	24.3
	13-15	Jun-96	0.24	0.66	0.12	0.66	1.68	4.8	ND
Z	4.5-6	Jun-96	ND	0.01	ND	0.01	0.02	ND	ND
	6.5-8	Jun-96	ND	0.01	0.01	0.04	0.06	ND	ND
	13-15	Jun-96	0.02	0.02	0.03	0.8	0.87	2.4	ND
G	6.5-8	Jun-96	0.01	0.11	0.02	0.3	0.44	1.3	ND
	12.5-14	Jun-96	ND	0.27	7.38	21.7	29.35	160	13.6
C	7-8.5	Jun-96	0.01	0.06	0.01	0.08	0.16	0.7	34.5
	11.5-13.5	Jun-96	0.005	0.019	0.004	0.023	0.051	0.3	ND

GRPH = gasoline range petroleum hydrocarbon  
 ND = none detected

DROs = diesel range organics  
 NT = not tested for

**Sample Theoretical Temperature Calculations** for whiplash curves in Figures 6-1(a) and (b):

For Figure 6-1(b):

Case 1 data (Table 4-7):

$$T_{ms} = 38.6^\circ\text{F}$$

$$A_{os} = 32.4^\circ\text{F}$$

$$\phi_s = 8 \text{ days}$$

D-1 Layer data (Table 4-3):

$$\alpha_t = K_t/C_t = 1.37/27.3$$

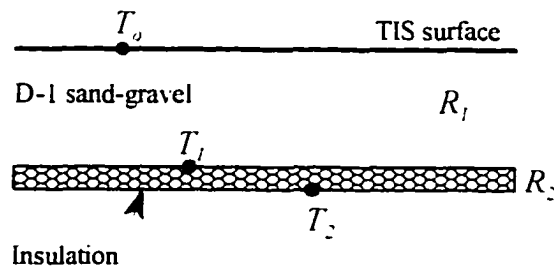
$$= 0.05 \text{ ft}^2/\text{hr} = 438 \text{ ft}^2/\text{yr}$$

$$\alpha_f = K_f/C_f = 1.15/24.7$$

$$= 0.0465 \text{ ft}^2/\text{hr} = 407 \text{ ft}^2/\text{yr}$$

Surface temperature ( $T_o$ ) calculation on Jan. 16, 1995:

$$T_o(t) = 38.6 - 32.4 \cos[0.0172 (t - 8)]_{\text{rad}} = 6.5^\circ\text{F}$$



The surface heat flux can be approximated by substituting the general sinusoidal surface temperature variation into Fourier's Law and setting  $x = 0$  for the TIS surface:

$$q = -K \left. \frac{\partial T_s}{\partial x} \right|_{x=0} = -K \frac{\partial(\text{general surf. temp. variation})}{\partial x}$$

where the general surface temperature variation can be expressed as a function of the mean surface temperature ( $T_{ms}$ ), the geothermal gradient, and mathematical expressions for the decay and oscillatory motion of a typical whiplash curve as:

$$T_s(t) = T_{ms} - A_{os} e^{\left(-x \sqrt{\frac{\pi}{\alpha}}\right)} \left( \cos \left[ 2\pi \frac{(t - \phi_s)}{365} \right] - \sin \left[ 2\pi \frac{(t - \phi_s)}{365} \right] \right) + Gx$$

In the previous equation, the exponential decay term is essentially 1 for small (shallow) depths, and the TIS materials effectively negate any geothermal influence above the insulation. Therefore, the resulting surface heat flux approximation is:

$$q|_{x=0} = K A_{os} \sqrt{\frac{\pi}{\alpha}} \left( \cos \left[ 2\pi \frac{(t-\phi_s)}{365} \right] - \sin \left[ 2\pi \frac{(t-\phi_s)}{365} \right] \right)_{rad}$$

Again, for Jan. 16, 1995, and  $T_o = 6.5^\circ F$ :

$$q|_{x=0} = 1.15 \frac{BTU}{hr-ft^2-^\circ F} (32.4^\circ F) \sqrt{\frac{\pi}{407 \frac{ft^2}{yr}}} \cdot \left( \cos \left[ 2\pi \frac{(16-8)}{365} \right] - \sin \left[ 2\pi \frac{(16-8)}{365} \right] \right)_{rad}$$

$$q|_{x=0} = 2.79 \frac{BTU}{hr-ft^2}$$

$$q_1 = 2.79 \frac{BTU}{hr-ft^2} = \frac{T_1 - T_o}{R_1} = \frac{T_1 - T_o}{x/K_1} = \frac{T_1 - 6.5^\circ F}{\left( 1 ft / 1.15 \frac{BTU}{hr-ft^2-^\circ F} \right)}$$

Solving for  $T_1$ :

$$T_1 = 8.9^\circ F$$

$$q_2 = q_1 = 2.79 = \frac{T_2 - T_1}{R_2} = \frac{T_2 - 8.9}{5}$$

Solving for  $T_2$ :

$$T_2 = 22.9^\circ F$$

---

## A “How To” Guide to Bioventing in Cold Regions

The scope of a cold regions bioventing project is easily conceptualized through use of an organization chart (Figures I-1 through I-3). Project tasks can be grouped into three main phases: I) the initial subsurface investigation, II) the bioventing system installation, and III) site monitoring and system maintenance. This chart, and the topic discussions that follow, can serve as a guide for engineers, environmental specialists, and biologists in bioremediation practice.

### I.1. Bioventing Organization Chart

*Phase I* (Figure I-1):

- This initial phase consists of exploratory borings and soil and groundwater sampling and testing. A few Standard Penetration Test (SPT) borings are strategically placed around the site for general subsurface characterizations. Soil density information and split-spoon sampling (for both geotechnical and microbiological sampling protocols) are accomplished with SPT drilling. Contaminant assessment can then be further delineated through a combination of cheaper auger borings, soil gas probing (with portable equipment), and on-site organic vapor analysis of soils. The number of borings, soil gas probes, and samples collected for testing should be determined by the project engineer.
- Groundwater sampling should also be performed at this time, for smear zone characterizations, baseline contaminant levels, and to assess the site groundwater gradient.
- Because microbiological analyses often requires soil testing be initiated within 72 hours, a preliminary determination should be made by the site engineer regarding

remedial methodology. If bioventing is a likely option, and this soil testing can be performed in-house, then additional sampling for microbiological testing should be incorporated.

- A [remedial alternatives] feasibility study is then undertaken as soil testing occurs in the laboratory. If microbiological analyses must be performed at an outside laboratory, the additional sampling should wait until the system installation process (Phase II).

### Phase I: Subsurface Investigation

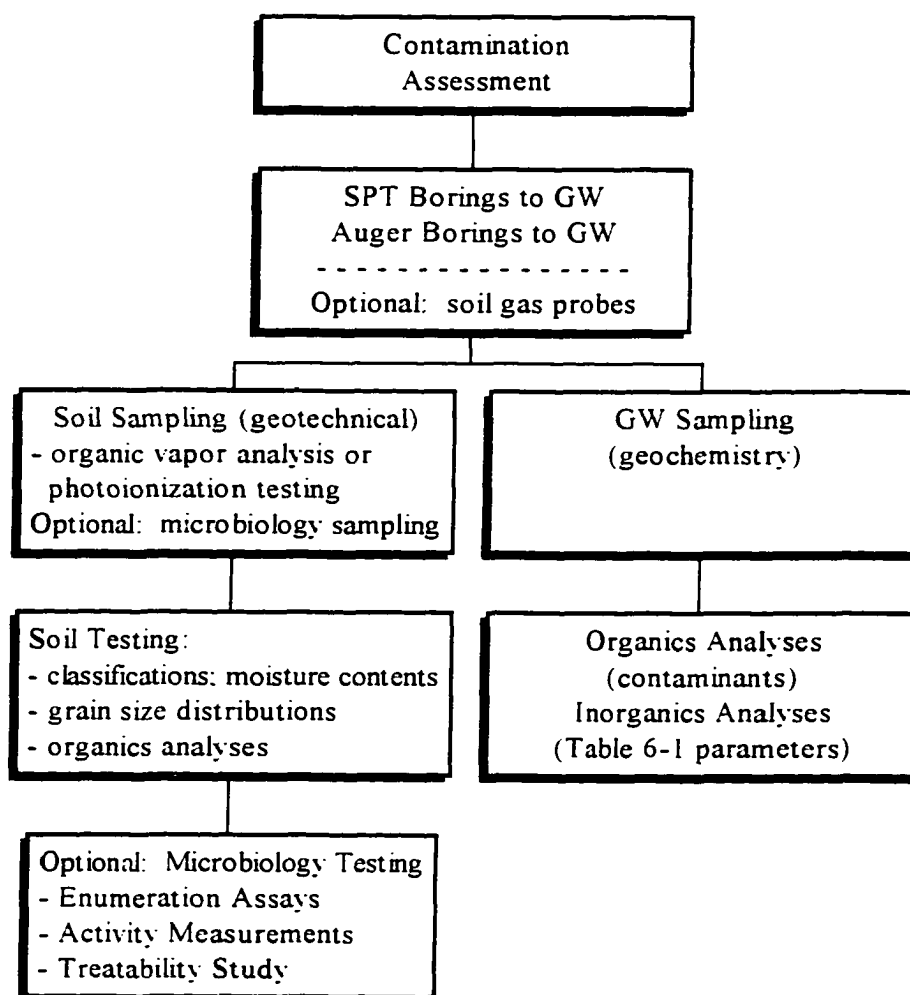


**Figure I-1.** The initial subsurface investigation.

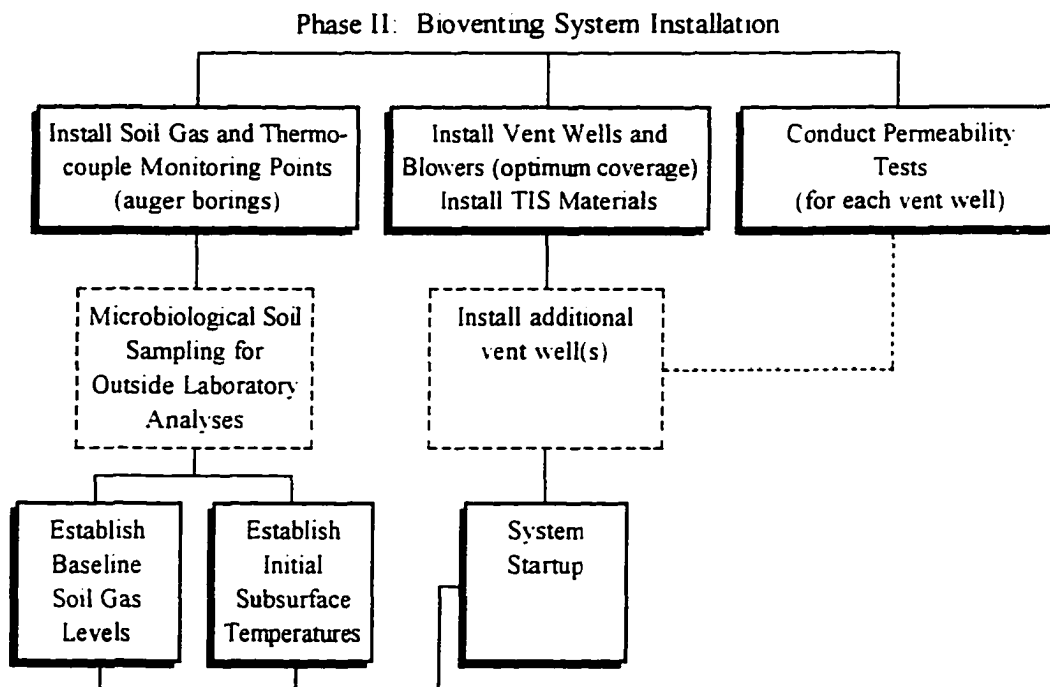


**Figure I-2.** Bioventing system installations.

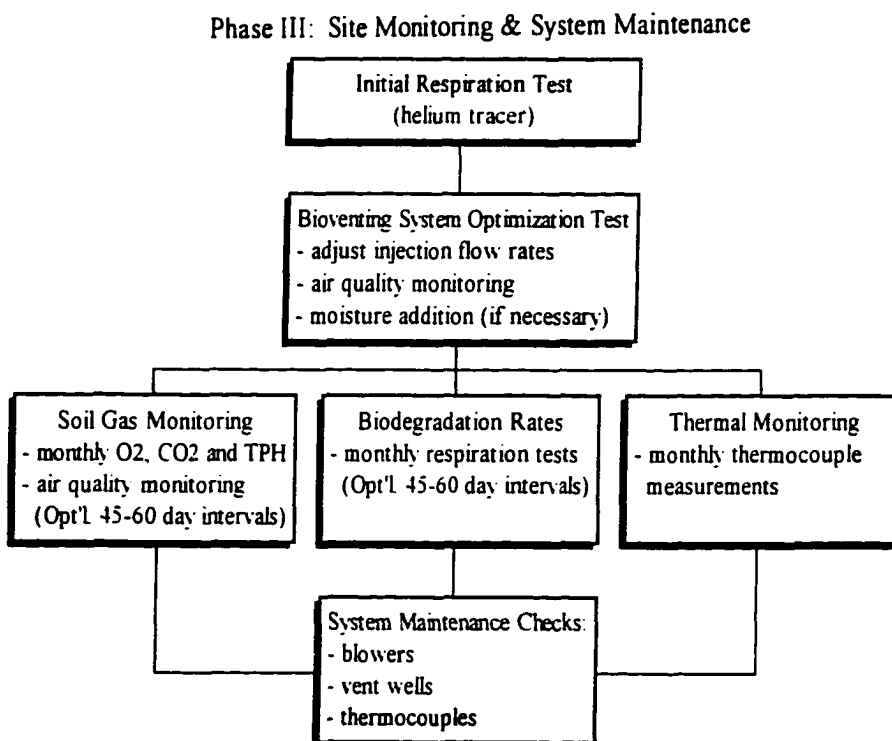


**Figure I-3.** Site monitoring and system maintenance.

*Phase II (Figure I-2):*

- Phase II is implemented only after a feasibility study has been performed, a contaminant assessment report (CAR) has been submitted, and a remedial action plan (RAP) has been approved by the client and/or governing regulatory agency.
- Bioventing system installations include joint soil gas and thermocouple [cluster] monitoring points, development of the air-injection [vent] wells and their connection to blowers, and the installation of surface TIS materials. Once the vent wells are operational, discrete air permeability tests can be performed. Site characteristic permeability(s) and radii of influence are subsequently determined. From this information the engineer can determine if additional vent wells are needed.
- After permeability testing, baseline soil gas levels (O<sub>2</sub>, CO<sub>2</sub>, and TPH) and initial subsurface temperature (to the water table) measurements are collected. The vent wells and active warming equipment (heat tape in this case) are brought on-line.
- For most state and federally funded remediation projects, a Quality Assurance Project Plan (QAPP) and Quality Assurance/Quality Control (QA/QC) report are required. Their approval typically precedes system startup. The QAPP establishes quality assurance guidelines for data collection, handling, manipulation, and reporting. These guidelines must satisfy EPA requirements for precision, accuracy, representation, completeness, and comparability between soil, water, soil gas, and thermal data.
- A brief one week startup period is usually sufficient to identify and eliminate any operational problems with system equipment.

*Phase III (Figure I-3):*

- This is a good time to perform the initial respiration test and assess initial biodegradation rate(s).
- It typically takes three weeks to one month to obtain and analyze all microbiological and geochemistry results from the initial Phase I sampling effort. Combined with the site specific geotechnical information, these results can lead to system refinements and increased bioactivity. By varying injection flow rates and periodically adding moisture



to the subsurface (if necessary), all the while monitoring air quality for hydrocarbons. system optimization can be accomplished. Little consideration is given to nutrient enhancement because of cost and potential high risk for additional regulatory concern.

- Once the bioventing system is operating at its static mode, monthly soil gas and thermal monitoring and respiration tests are performed. This frequency can be decreased to 45 or 60 day intervals with reduced surface condition variability.
- System maintenance checks should be performed as often as monitoring occurs. Weekly site visits for maintenance checks is recommended where economically feasible (Gast™ and Fuji™ venting/soil vapor extraction blowers are designed for low maintenance and remote application).

## **I.2. Soil and Groundwater Sampling**

SPT and hollow-stem auger drilling in the U.S. generally follows American Society for Testing and Materials (ASTM) guidelines. The purpose for SPT borings is to collect samples for soil density (blow counts; ASTM D-1586-67) and geotechnical information. Two-inch diameter split-spoon samplers are sufficient to collect undisturbed samples for USCS (Unified System of Soil Classification) classification (ASTM, Part 19), moisture contents (ASTM D-2216), grain size distribution (ASTM D-421), and organic analyses. Geotechnical soil samples are typically sealed in glass jars with Teflon-lined caps. Sample collection, storage, identification, logging, transport, chain of custody, and equipment decontamination procedures typically follow EPA guidelines and are typically delineated in the QA/QC report. A number of EPA analytical methods are used to identify and quantify volatile and nonvolatile organics at a typical bioventing site (Table I-1).

During initial soil testing, volatile organic compounds (VOCs) should be tested for in the samples using a portable organic vapor analyzer (OVA) or photoionization instrument (Photovac™ TIP typical). These measurements are first-line indicators of contaminants in soil and help to direct the subsurface investigation.

The groundwater sampling protocol is also included in the QA/QC report. Generally, groundwater sampling requires Teflon™ bailers, Teflon-sealed glass jars, labels, a chain-of-

custody sheet, a trip blank, and a well insulated cooler (with ice). A peristaltic vacuum pump, Teflon™ tubing, a 5-gallon purge bucket, and a portable conductivity meter are also needed to retrieve samples. A discussion of the groundwater sampling protocol is reported in Section 5.4.4.

A discussion about the more stringent protocol for microbiological sampling is presented in Section 5.4.

**Table I-1.** Common soil and groundwater analytical testing methods for organics.

<b>EPA Method</b>	<b>Analyte</b>	<b>Description</b>
8020	Aromatic Volatile Organics (purgeable aromatics)	Gas Chromatography: (benzene, toluene, ethylbenzene, xylenes, TPH, and benzene derivatives)
8015M	Gasoline Range Organics	Gas Chromatography: (leaded and unleaded gasoline constituents and derivatives)
8100	Polynuclear Aromatic Hydrocarbons	Gas Chromatography: (wide range of constituents)
8100M	Diesel Range Organics (polynuclear aromatic hydrocarbons)	Gas Chromatography
8010	Halogenated Volatile Organics (purgeable halocarbons)	Gas Chromatography: (wide range of chlorides and ethanes; TCE, chloroform, methylene chloride, TCFM)
160.3	% Solids	For estimating natural organic conc's.

### **I.3. Monitoring Points**

Typical soil gas monitoring points require suction vapor strainers (1-1/4" x 8" filters), 1/4-inch polyethylene tubing in three colors, heat-shrink tape, and tubing end caps. Plastic ties anchor the [2 or 3] discrete points to a 1/2-inch schedule 80 CPVC pipe. The pipe is placed in the excavated hole, backfilled with intermittent layers of clean tailings or pea gravel and bentonite seals (above each strainer), and surface-protected with a riser. Soil gas

sampling requires a small vacuum pump (0.3 hp Gast or Fuji typical), Tedlar bags, and portable vapor detector monitors (GasTechtor™ TraceTechtor for TPH; model 3252-OX for O<sub>2</sub> and CO<sub>2</sub>, typical).

Similarly, two or three Type T, K or J subminiature connectors, wired to Neoflon™ thermocouple wire, are tied to the CPVC anchor pipe. A compatible digital thermometer (Omega™ HH models typical) is used to record temperatures.

#### I.4. Vent Well Construction

A 6-inch diameter hollow-stem auger is suitable to drill the vent well borings. The 2-inch diameter PVC bioventing well has a 10 slot PVC screened bottom section, the length of which extends through the contaminated zone and into the groundwater table (Figure I-4). A medium grade silica sand is generally used as a filter pack around this section of the well. Bentonite is then used to plug the remaining annular space around the upper well section. Concrete

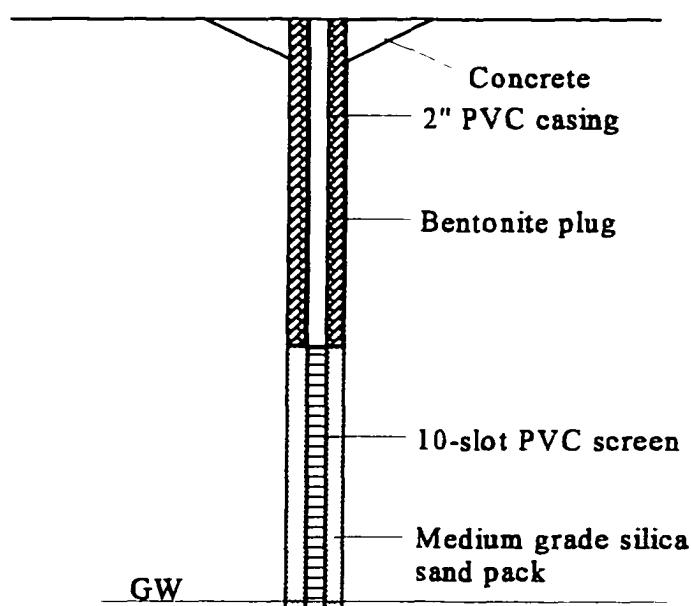


**Figure I-4.** 2-inch diameter PVC bioventing well installed.

The 2-inch PVC casing is extended twelve inches above the surface and permanently capped. The well is then sealed into the ground with a concrete pour. Rubber flex-tubing then connects the well to the blower exhaust.

### **I.5. Blowers**

Pressure (venting) or vacuum (extraction) regenerative blowers (Fuji™, Gast™, Rotron™, Siemens™, and Spencer™ typical) can be used to inject air into the vadose zone. Single or three phase, 50-60 Hz, 0.37 to 1 hp, insulated, and thermally protected compressors are sufficient for most bioventing applications. For shallow vadose zones vented at low operating flow rates (less than 5cfm), 0.37 to 0.51 hp units will suffice. If a larger volume of soil is contaminated at depth, higher flow rates may be desirable. One to two horsepower blowers will satisfy these demands. Approximate 1994 costs for 0.37 hp, 0.51 hp, 1 hp, and 2.3 hp blowers were \$506, \$556, \$632, and \$802, respectively. The corresponding efficiency ratings for the 0.37 hp to the 2.3 hp blower were 0.7 to 0.85 (Fuji, 1994). Energy savings realized with the optimum blower over time may offset capital costs associated with purchasing a larger blower.

Acrylic with stainless steel float constructed flowmeters and magnehelic pressure gages were used to monitor injection rates and to measure pressures during permeability and respiration tests. Flowmeters graduated from 0 to 3 scfm (standard cubic feet per minute) and from 3 to 25 scfm are needed for low and higher venting rates. Magnehelic gages capable of measuring pressure from 0 to 1, 0 to 10, and 0 to 100 inches of water are needed for the various tests and monitoring requirements.

There are advantages to injecting warmed air into cooler soils. With sub-freezing air temperatures and sufficient moisture contents, vent well screening can ice over and clog. Additionally, some convective soil warming is occurring within a few feet radially outward from the well. Heat generated from blowers housed in enclosed, standard plastic animal carriers, was shown to increase injection air temperature by 20°F at the UAF site. However, at subarctic and arctic sites where ambient air temperatures drop below -20°F regularly in winter, a heat tape strip should be ventically installed inside the vent well casing.

### **I.6. Air Quality Monitoring**

At low venting rates (less than 3 cfm) air-stripping of VOCs is minimized. Air quality monitoring is not likely to be required for such cases. However, where off-gases are anticipated to exceed EPA, state, or local minimum acceptable levels, surface emissions testing will be required. Leeson et al. (1995) present a schematic design of a dynamic surface emissions system. The system requires compressed [pure] air be passed through an enclosure over an area of biovented soil. The inert Teflon box is thereby purged of ambient air, and then allowed to fill with emissions from the subsurface. A heater box, equipped with a sorbent tube and a small vacuum pump, then draws an emission sample from the box. The sorbent retains hydrocarbons screened from the emissions sample. The sample tube is then thermally desorbed, with the organics quantified by gas chromatography (Leeson et al. 1995). Portable air monitoring equipment can also be used, but meters are more expensive.

### **I.7. TIS Materials**

The cost of materials and energy demands will likely govern bioventing TIS design. Some design configurations are presented (Table I-2) for specific active warming applications. Considerations for vadose zone thickness, contamination levels, capital costs, and power demands are incorporated into the designs. Polystyrene is the choice of insulation. These TIS schemes are applicable to the bioremediation of petroleum-based contaminants in unsaturated soils. The remediation times (RT) are estimates based on subarctic case studies to date. Where two or three choices are checked, remediation times may vary. The final decision of choice will likely weigh cost against remediation time.

In some cases, shallow vadose zone contamination (to 5 ft.) may be remediated quicker and cheaper with excavation and incineration or some other treatment method, especially if the site is small. The shallow cases identified in Table I-2 pertain to urban or remote sites where incineration is not available and *in-situ* treatment is required. Other cheaper insulation materials (sawdust, plywood, etc.) may be effective for shallow contaminated soils in warmer coastal cold regions.

**Table I-2.** Bioventing TIS design configurations for active warming.

Case	TIS Configuration							
	Heat tape/Insulation/Spacing (in W/lf./in./ft.)							
	3/2/5	3/3/5	3/2/10	3/3/10	5/2/10	5/3/10	8/3/8	8/3/12
VZ: to 5 ft. CL: ≤ 5,000 ppm RT: ≤ 1.5 yrs.	✓			✓				
VZ: to 5 ft. CL: ≤ 5,000 ppm RT: ≤ 2 yrs.			✓		✓			
VZ: to 20 ft. CL: ≤ 5,000 ppm RT: 2-3 yrs.		✓				✓		✓
VZ: to 30 ft. CL: ≤ 3,000 ppm RT: ≤ 3 yrs.						✓	✓	

VZ = vadose zone; CL = maximum contaminant level; RT = remediation time.

The amount of protective covering (D-1 sand and gravel material) for the heat tape and insulation is a function of site operations. If a bioventing site must remain open (useable), a thicker and compacted D-1 layer is warranted for traffic or storage use. Additionally, physical barriers and signage may be required to protect equipment. For closed sites, insulation can be weighted with a thin D-1 layer; compaction is not necessary. Cover layers from one inch to one foot thick should be sufficient for most thermally enhanced bioventing applications.

### 1.8. Maintenance Items

Maintenance requirements are also site specific. If a bioventing site remains open, maintenance requirements will be greater than for a closed site. The implementation of TIS enhancement implies a shorter remediation time. Consequently, no large-scale maintenance requirements (TIS and blower repairs or replacements) are anticipated. Some common maintenance items associated with any bioventing system are:

- Riser de-icing
- Power connections
- Air-flow connections/seals
- Blower socks
- Surface rutting
- Thermocouple connections
- Flow checks
- TIS impact assessments
- Monitoring equipment calibrations
- Tedlar™ sample bag leak checks